DOCTORAL DISSERTATION

Under international joint-supervision

Lodz University of Technology

UNIVERSITÉ DE STRASBOURG

EDSC
École Doctorale des Sciences Chimiques

Politechnika Łódzka
Wydział Chemiczny

Université de Strasbourg
École Doctorale des Sciences Chimiques

In Partial Fulfillment of the Requirements for the Degree

Doktor Nauk Chemicznych
Chemia

Docteur
Chimie

Ru/TiO_2-based catalysts for the hydrogenation of levulinic acid using formic acid as internal hydrogen source

By

Joanna WOJCIECHOWSKA

Thesis Supervisors:

Dr. hab. inż. Agnieszka Ruppert, prof. PŁ, Lodz University of Technology, Poland

Dr. hab. Nicolas Keller, CNRS Directeur de Recherche, Université de Strasbourg, France

Łódź, 14 December 2018

Composition of the Jury

Dariusz BIELIŃSKI	Professor	Poland	Chairman
Michele BESSON	Directeur de Recherches CNRS	France	Thesis Reviewer
Lucjan CHMIELARZ	Professor	Poland	Thesis Reviewer
Agnieszka RUPPERT	Professor	Poland	Thesis Supervisor
Nicolas KELLER	Directeur de Recherches CNRS	France	Thesis Supervisor

Invited member

Jacek GRAMS	Professor	Poland	Invited Member

Thesis title in French (Titre de thèse en français):

Catalyseurs à base de Ru/TiO_2 pour l'hydrogénation de l'acide lévulinique avec l'acide formique comme source interne d'hydrogène.

Thesis title in Polish (Tytuł rozprawy po polsku):

Katalizatory rutenowe naniesione na TiO_2 w reakcji uwodornienia kwasu lewulinowego z wykorzystaniem kwasu mrówkowego jako wewnętrznego źródła wodoru.

I would like to thank my thesis supervisors

dr. hab. inż. Agnieszka Ruppert and dr. hab. Nicolas Keller

for their support.

Besides, this work would have not been possible without the involvement of so many wonderful people –

THANK YOU!

Jakubowi,

który niestrudzenie
mnie podnosił,
gdy upadałam...

Table of contents

Abstract

Value added platform molecules issued from the conversion of lignocellulosic biomass feedstock are expected to play a pivotal role in the future 'renewable-based' biorefinery schemes. Especially γ-valerolactone (GVL) has attracted a significant attention in the recent decade due to its versatile applications. GVL can be obtained by the catalytic hydrogenation of levulinic acid (LA) issued from the hydrolytic conversion of lignocellulosic biomass using a pressurized external source of hydrogen. However, a more sustainable approach is to utilize hydrogen originating from the decomposition of formic acid (FA) that is formed in an equimolar mixture with levulinic acid during the acidic hydrolysis of lignocellulosic biomass. This is more challenging, since the strategy requires that both the hydrogenation of LA to GVL and the FA dehydrogenation can be catalyzed by a single material in similar reaction conditions.

Therefore, the main objective of this PhD work is to develop active and selective catalysts based on titania supports for the one-pot hydrogenation of levulinic acid to γ-valerolactone with internal hydrogen supply *via* the *in-situ* decomposition of formic acid, as well as to define the properties/activity relationship driving the performance of the catalysts in the studied reactions.

In this work, a modification of the titanium oxide support was proposed in order to increase the reaction selectivity in the decomposition of formic acid towards hydrogen. In addition, an alternative method of dispersion of the active metallic phase on the support has been proposed, which allows to obtain very small ruthenium particle size with a narrow size distribution, and additionally permits to precisely tune the particle size of Ru.

The bibliographic part presents the context of this PhD work and the biomass-derived molecules such as levulinic acid and γ-valerolactone, the catalytic systems used for LA hydrogenation and dehydrogenation of formic acid. A large part of this chapter is also devoted to the role of the support, the influence of the basic sites and the effect of the metal particle size on the catalytic activity in the studied reactions, as well as to different methods for controlling the size of Ru particles.

The experimental part is devoted to the catalysts' preparation protocols and the details regarding the analytical techniques employed for the investigation: X-ray diffraction, N_2 physisorption, isoelectric point measurements, FTIR-CO chemisorption, inductively-coupled plasma atomic emission spectroscopy, temperature programmed reduction, transmission electron microscope, scanning electron microscope, X-ray photoelectron spectroscopy and time of flight secondary-ion mass spectrometry. Moreover high-performance liquid chromatography and gas chromatography were used for the analysis of the reaction products, and the reaction protocols are described.

In the first part of the work, titanium oxide was modified by doping with calcium ions during the sol-gel synthesis method for elaborating titania-based mixed supports. Materials with different calcium content (0, 1, 5, 10 and 20 wt. % in respect to TiO_2) were obtained, and were analyzed by X-ray diffraction analysis and N_2 physisorption. It was found that the modification of the TiO2 support with Ca resulted in an increase in the specific surface area of the carrier, together with the appearance of a new crystallographic phase of calcium titanate $CaTiO_3$, more pronounced as the Ca content increases. In addition, the change in the anatase cell parameters and volume suggested that calcium ions were also incorporated into the crystal lattice of TiO_2.

A significant part of the work was focused on the development of an innovative photo-assisted synthesis method for obtaining heterogeneous catalysts with the use of sunlight. This method, although already used for different metals, was not usually implemented to support ruthenium nanoparticles. The mechanism of photodeposition was studied for two ruthenium precursors, $RuCl_3$ and $Ru(acac)_3$, some parameters of the process like the nature and the concentration of the precursor, the reaction time or the pH were optimized in terms nanoparticle size distribution and the synthesis kinetics. In addition, it was demonstrated that this method allows a precise control of the size of the ruthenium particles depending on the reaction conditions. Those catalysts were compared to the materials prepared by a conventional wet impregnation method the photo-assisted method led to prepare much smaller Ru particles, uniformly dispersed on TiO_2 with a very narrow, sub-nanometric particle size distribution.

The next step of the work consisted in the evaluation of the catalytic behavior of the Ru/TiO_2-based materials in the hydrogenation of levulinic acid using formic acid as internal source of hydrogen. The influence of the Ca modification and of the preparation method was investigated by additionally

implementing separately the LA hydrogenation reaction using molecular hydrogen and the FA decomposition in both the liquid and the gas phase. It has been shown that the controlled modification of the TiO_2 support by calcium addition improved the catalytic performance in both the FA dehydrogenation step and the LA hydrogenation reaction and as a result in the one-pot combined FALA reaction. With the formation of a new calcium titanate phase, through the introduction of Ca, smaller ruthenium particles were stabilized on the support, as well as the optimal Ru size has been found to be 1.5 nm. Stronger interaction of ruthenium with the support was observed, which affected the strength of CO adsorption on the surface of the Ca-modified catalyst, thus facilitating the reaction performance. The role of calcium was also related to the increased basicity of the catalyst surface, which positively influenced the catalytic activity in the studied reactions. In addition, much higher catalytic performance in both combined and separated reactions were achieved by the photo-assisted synthesis method was possible owing to the formation of uniform, small and well-dispersed metal nanoparticles as well as the optimal interactions between the metal and the carrier. The interest of using Ca-modified TiO_2 supports has been also evidenced in the gas phase formic acid decomposition by favoring the dehydrogenation pathway through the suppression of CO formation.

In summary, Ca-modified TiO_2 supported Ru catalysts exhibited improved activity in the levulinic acid hydrogenation using formic acid as internal hydrogen source, when compared to Ca-free samples, thanks to enhanced activity in the formic acid decomposition and levulinic acid hydrogenation This was caused by stronger interaction of the ruthenium with the support and consequently weaker adsorption of CO on the active sites, as well as by the increased basicity of the material. In addition, significant improvement in catalytic performance was achieved by using an alternative catalyst preparation method that was optimized for dispersing sub-nanometric size ruthenium nanoparticles at large loadings, while stabilizing uniformly dispersed ruthenium nanoparticles of much smaller size than those obtained by the incipient wet impregnation method.

Streszczenie

Związki o ważnych znaczeniu przemysłowym (z ang. *platform molecules*) otrzymane z konwersji biomasy lignocelulozowej odgrywają kluczową rolę w strategii rozwoju przyszłych biorafinerii opartych na stosowaniu odnawialnych źródeł energii oraz surowców. Szczególnie gamma-walerolakton (GVL) w ostatnich latach cieszy się znacznym zainteresowaniem ze względu na swoje wszechstronne zastosowanie. GVL można uzyskać poprzez katalityczne uwodornienie kwasu lewulinowego (LA) używając do tego celu zewnętrznego źródła wodoru. Jednak bardziej zrównoważone podejście polega na wykorzystaniu wodoru pochodzącego z rozkładu kwasu mrówkowego (FA), który powstaje w równomolowej mieszaninie z kwasem lewulinowym podczas kwaśnej hydrolizy biomasy lignocelulozowej. Ta strategia jest dużo trudniejsza, ponieważ wymaga ona, aby zarówno uwodornienie LA do GVL, jak i rozkład FA zachodziły w obecności tego samego katalizatora, w podobnych warunkach reakcji.

Dlatego głównym celem niniejszej rozprawy doktorskiej jest opracowanie aktywnych i selektywnych katalizatorów na bazie dwutlenku tytanu do reakcji uwodornienia kwasu lewulinowego do γ-walerolaktonu z użyciem kwasu mrówkowego jako wewnętrznego źródła wodoru, jak również określenie właściwości wpływających na wydajność katalizatorów w badanych reakcjach.

W niniejszej pracy zaproponowano modyfikację nośnika tlenku tytanu w celu zwiększenia selektywności katalizatora w reakcji rozkładu kwasu mrówkowego do wodoru. Ponadto zaproponowano alternatywną metodę nanoszenia metalicznej fazy aktywnej na nośnik, która pozwalaja otrzymać bardzo małe rozmiary cząstek rutenu na nośniku o wąskim zakresie rozmiarów krystalitów, dodatkowo umożliwia precyzyjne kontrolowanie rozmiaru cząstek metalu.

W części bibliograficznej przedstawiono informacje dotyczące właściwości fizykochemicznych kwasu lewulinowego i γ-walerolaktonu, oraz układów katalitycznych stosowanych do uwodorniania LA i rozkładu kwasu mrówkowego. Znaczna część tego rozdziału poświęcona jest także roli nośnika, wpływowi centrów zasadowych oraz wielkości cząstek metalu na aktywność katalityczną w badanych reakcjach, a także różnym metodom pozwalającym na kontrolę wielkości cząstek metalu

W części eksperymentalnej umieszczone są informacje dotyczące preparatyki katalizatorów oraz opis technik analitycznych stosowanych w badaniach właściwości fizykochemicznych katalizatorów: dyfrakcji promieni rentgenowskich (XRD), adsorpcji fizycznej azotu, pomiaru punktów izoelektrycznych, chemisorpcji CO, spektrometrii mas sprzężonej z plazmą wzbudzaną indukcyjnie (ICP-MS), temperaturowo programowanej redukcji (TPR), transmisyjnego i skaningowego mikroskopu elektronowego (TEM i SEM), spektrometrii mas jonów wtórnych z analizatorem czasu przelotu (ToF-SIMS) oraz spektroskopii fotoelektronów w zakresie promieniowania X (XPS). Ponadto zawarte są informacje dotyczące wysokosprawnej chromatografiicieczowej (HPLC) oraz chromatografii gazowej (GC), które stosowane były do analizy produktów reakcji.

W pierwszym etapie pracy badano modyfikację tlenku tytanu jonami wapnia. Otrzymano materiały o różnej zawartości wapnia (0, 1, 5, 10 i 20% masowych w stosunku do TiO_2), które poddano m.in. analizie dyfraktometrii rentgenowskiej oraz badaniu powierzchni właściwej. W oparciu o otrzymane wyniki stwierdzono, że w wyniku modyfikacji zwiększono powierzchnię właściwą nośników oraz w przypadku wyższych zawartości wapnia zaobserwowano obecność nowej fazy krystalograficznej tytanianu wapnia $CaTiO_3$. Dodatkowo zmiany parametrów komórki elementalnej anatazu pozwoliły wnioskować o częściowej interkalacji jonów Ca^{2+} do struktury tlenku tytanu.

Zasadnicza część pracy dotyczy badań nad opracowaniem nowatorskiej metody otrzymywania katalizatorów heterogenicznych z użyciem światła słonecznego. Metoda fotodepozycji była znana już wcześniej jednak w literaturze istnieje tylko kilka przykładów jej użycia do otrzymywania katalizatorów rutenowych. Zoptymalizowano warunki procesu, określając mechanizm fotodepozycji zachodzący przy użyciu dwóch prekursorów rutenu ($RuCl_3$ oraz $Ru(acac)_3$), określono wpływ prekursora, jego stężenie na szybkość fotodepozycji oraz na właściwości otrzymanego katalizatora. Ponadto opracowano metodę pozwalającą na precyzyjną kontrolę wielkości otrzymanych cząstek rutenu w zależności od warunków prowadzenia procesu depozycji. Otrzymane katalizatory porównano do materiałów otrzymanych konwencjonalną metodą mokrej impregnacji i stwierdzono, że stosując alternatywną metodę preparatyki można uzyskać dużo mniejsze rozmiary Ru, jednorodnie rozdyspergowanych na TiO_2 o bardzo wąskim rozkładzie wielkości cząstek na powierzchni. Ponadto, w przeciwieństwie do metody impregnacyjnej, metoda fotodepozycji nie wymaga zastosowania obróbek wysokotemperaturowych.

Kolejnym etapem pracy było określenie aktywności katalitycznej otrzymanych katalizatorów w reakcji uwodornienia kwasu lewulinowego z użyciem kwasu mrówkowego jako wewnętrznego źródła wodoru, a także osobno w reakcjach uwodornienia LA z użyciem cząsteczkowego wodoru oraz samego rozkładu kwasu mrówkowego w fazie ciekłej jak i gazowej. Wykazano, że modyfikacja nośnika TiO_2 poprzez wprowadzenie jonów wapnia zwiększyła wydajność katalityczną zarówno w rozkładzie kwasu mrówkowego, jak i w reakcji uwodornienia kwasu lewulinowego. Modyfikacja ta umożliwiła otrzymanie mniejszych krystalitów anatazu, oraz utworzenie nowej fazy- tytanianu wapnia, co stabilizowało mniejsze cząstek rutenu na nośniku. Dla tych materiałów zaobserwowano silniejsze oddziaływanie rutenu z nośnikiem, co wpłynęło na zmianę siły adsorpcji CO na powierzchni modyfikowanego katalizatora. W konsekwencji modyfikacja ta pozwoliła na otrzymanie większej wydajność GVL w badanej reakcji. Rola wapnia jest również związana ze zwiększoną zasadowością katalizatora, co wpłynęło pozytywnie na aktywność katalityczną w badanych reakcjach. Ponadto dużo wyższą aktywność katalityczną w obu reakcjach osiągnięto z użyciem katalizatorów otrzymanych przy pomocy fotodepozycji, co było spowodowane między innymi mniejszym rozmiarem cząstek rutenu na powierzchni TiO_2, a także zmianą oddziaływań pomiędzy metalem a nośnikiem.

Podsumowując, katalizatory rutenowe oparte na zmodyfikowanym jonami wapnia tlenku tytanu charakteryzowały się dużo większą aktywnością w reakcjach rozkładu kwasu mrówkowego oraz uwodornienia kwasu lewulinowego w porównaniu do próbek nie zawierających wapnia. Było to spowodowane między innymi silniejszym oddziaływaniem metal-nośnik, a w konsekwencji słabszą adsorpcją CO na centrach aktywnych katalizatora oraz zwiększoną zasadowością materiału. Dodatkowo znaczą poprawę wydajności katalitycznej do GVL udało się osiągnąć stosując alternatywną, zoptymalizowaną w niniejszej pracy metodę osadzania fazy aktywnej na nośniku – metodę fotodepozycji, dzięki której otrzymano jednolicie rozdyspergowane nanocząstki rutenu o dużo mniejszym rozmiarze niż uzyskane na drodze mokrej impregnacji.

General introduction and aim of the work

The depletion of fossil fuel reserves associated to the necessity of limiting the worldwide CO_2 release has been the driving force over the last decades in the search for alternative value chains for producing sustainable fuels and chemicals. Value added platform molecules issued from the conversion of lignocellulosic biomass feedstock are expected to play a pivotal role in the move towards future renewable-based biorefinery schemes.

In this frame, γ-valerolactone (GVL) has attracted a significant attention since it is used in many potential versatile applications, as biofuel additive thanks to a low volatility, a minimum toxicity and a good stability, as well as solvent or precursor in chemical syntheses. GVL can be obtained by the catalytic hydrogenation of levulinic acid (LA) issued from the hydrolytic conversion of lignocellulosic biomass.

Ruthenium remains often a metal of choice for LA hydrogenation in water solvent due to its outstanding performance, which is related to the decrease of its energetic span in the presence of a protic solvent. The nature of the catalyst support was also reported to be of high importance, and TiO_2 was proved to be a promising candidate for supporting Ru nanoparticles for producing GVL.

So far, most of the studies used externally supplied H_2 for performing the hydrogenation of LA into GVL. However, a step forward in the design of sustainable biomass hydrogenation processes can be achieved by using formic acid (FA) as an internal source of H_2. Indeed, the acidic hydrolysis of lignocellulosic biomass forms a LA/FA equimolar mixture, while FA can be further selectively decomposed into H_2. So far the latter approach in LA hydrogenation was not investigated to such extend as the use of high pressure H_2, as it is more challenging. The aforementioned strategy requires that both the hydrogenation of LA to GVL and the FA dehydrogenation can be catalyzed by a single material in similar reaction conditions. FA can decompose either *via* dehydrogenation into H_2 and CO_2 or *via* dehydration into CO_2 and CO - and possible side reactions like the water-gas-shift reaction or Fischer-Tropsch with methane production can take part. Therefore, the H_2 formation from FA is often considered as a limiting factor.

Although being very active for LA hydrogenation, Ru catalysts are known to also catalyze side reactions of FA decomposition that affect strongly the selectivity to hydrogen, so the implementation of adequate modification of Ru catalysts remains actually an approach of high interest in this respect. In consequence, designing selective and robust catalysts still remains a crucial challenge.

Therefore, **the main objective of this PhD work** is to develop active and selective catalysts based on titania supports for the one-pot hydrogenation of levulinic acid to γ-valerolactone with internal hydrogen supply *via* the *in-situ* decomposition of formic acid. Additionally the aim was to define the properties/activity relationship driving the performance of the catalysts in the studied reactions.

Two strategies have been chosen to achieve those goals. The first one concerns titania support modification in order to introduce the basic sites into its network. It has been reported that the presence of bases such as amines in the reaction system could facilitate the selective decomposition of formic acid into hydrogen. The design of heterogeneous catalysts with basic sites is an elegant and more sustainable approach for avoiding separation issues resulting from the continuous supply of the reaction media with high amounts of amine additives. Moreover, according to the literature, it appeared noteworthy to obtain a deeper insight in the influence of the support character and of its preparation way, on the catalytic behavior of titania-based materials. Therefore, a large part of the work is devoted to the design of innovative materials based on titania for use as supports of metal catalytic nanoparticles.

The second strategy concerns the development of a flexible and sustainable approach allowing synthesizing metal nanoparticle catalysts at the surface of the support material. It is critical to have a good control over the size of the metal nanoparticles remaining at the same time narrow size distribution. The preparation of supported metal catalysts with suitable particle sizes and in turn increased dispersion for a given metal loading is desired for improved catalytic performance. Moreover, it would allow for more detailed structure-properties relationship studies.

This PhD thesis is therefore divided into seven chapters. **Chapter 1** consists in a bibliographic overview on the context of this study, the role played by lignocellulosic biomass and the biomass derived substrates such as levulinic acid and γ-valerolactone, the catalytic systems used for LA hydrogenation and dehydrogenation of formic acid. A large part of this chapter is also devoted to the role of the support, the influence of the basic sites and the effect of the metal particle size on the catalytic activity in the

studied reactions as well as to the different methods for controlling the size of Ru particles. In **Chapter 2** all the catalysts' preparation protocols and the details regarding the analytical techniques employed for the investigation can be found. The reaction protocols are also described.

The results and discussion part of the thesis begins with **Chapter 3** where the characterization of the support materials used in this work is presented.

Then, a large part of this thesis is included in **Chapter 4** and concerns the development of an innovative photo-assisted synthesis method for the preparation of highly dispersed Ru nanoparticles supported on TiO_2. A mechanistic study is presented together with the influence of different process parameters on the nanoparticle size distribution. A comparison with catalysts prepared by a conventional incipient wet impregnation method is shown.

Chapter 5 presents the study of the catalytic performance of the Ru/TiO_2–based catalysts in the one-pot levulinic acid hydrogenation with formic acid as internal H_2 source. The behavior of the catalysts in separate reactions of formic acid decomposition and levulinic acid hydrogenation was also evaluated. In addition, the influence of several factors (Ru particle size, support modification, novel synthesis method) on the reaction yield was investigated and the optimal catalyst was proposed.

Chapter 6 presents a short study on the catalytic activity of the $5\%Ru/TiO_2$-based catalysts in the gas phase formic acid decomposition. The parameters such as the presence of Ca, the Ru particle size and the preparation method were investigated.

Finally, in **Chapter 7,** the conclusions from this thesis and the perspectives for further work can be found.

Résumé de thèse

L'épuisement des réserves de combustibles fossiles associé à la nécessité de limiter les émissions mondiales de CO2, a été l'un des principaux domaines de recherches durant ces 10 dernières années dans la quête d'alternatives pour la production de carburants et de produits chimiques durables. Les résultats obtenus sur des molécules issues de la conversion de la matière première de la biomasse lignocellulosique devraient jouer un rôle central dans la transition vers de futurs systèmes de bioraffinage à base d'énergie renouvelable.

Dans ce contexte, la γ-valérolactone (GVL) a attiré une attention particulière car elle est utilisée dans de nombreuses applications polyvalentes potentielles, comme additif pour biocarburant grâce à une faible volatilité, une toxicité minimale et une bonne stabilité, ainsi que comme solvant ou précurseur en synthèse chimique. Les GVL peuvent être obtenues par hydrogénation catalytique de l'acide lévulinique (LA) issu de la conversion hydrolytique de la biomasse lignocellulosique à l'aide d'une source externe d'hydrogène sous pression (Figure 1).

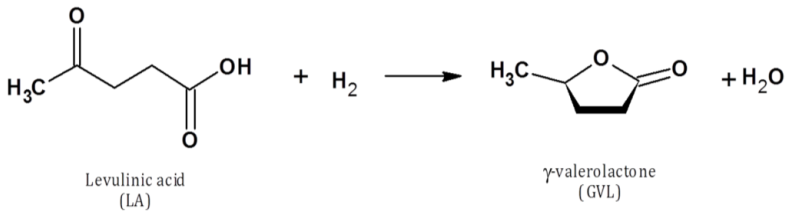

Figure 1. Reaction scheme of LA hydrogenation with internal hydrogen source.

Le ruthénium reste souvent un métal de choix pour l'hydrogénation de LA dans un solvant à base d'eau en raison de ses performances remarquables, liées à la diminution de sa durée énergétique en présence d'un solvant aprotique. La nature de catalyseur en guise de support a montré d'importants résultats bénéfiques et il a été prouvé que le TiO2 était un candidat prometteur pour y déposer/décorer les nanoparticules de Ru afin de produire des GVL.

Jusqu'à présent, la plupart des études utilisaient du H2 fourni par une source externe pour effectuer l'hydrogénation de LA en GVL. Cependant, l'utilisation d'acide formique (FA) comme source interne de H2 permet d'obtenir une étape supplémentaire dans la conception de procédés durables d'hydrogénation

de la biomasse. En effet, l'hydrolyse acide de la biomasse lignocellulosique forme un mélange équimolaire LA/FA, tandis que le FA peut être davantage décomposé de manière sélective en H2. Jusqu'à présent, la dernière approche de l'hydrogénation de LA n'a pas été étudiée dans des conditions difficiles telles que l'utilisation de H2 à haute pression. La stratégie susmentionnée nécessite que l'hydrogénation de LA en GVL et la déshydrogénation de FA puissent être catalysées par un seul matériau dans des conditions de réaction similaires. Le FA peut se décomposer soit par déshydrogénation en H2 et CO2, soit par déshydratation en CO2 et CO. Il est également possible que des réactions secondaires, telles que la réaction *shift* eau-gaz ou la réaction de Fischer-Tropsch avec production de méthane soient impliquées. Par conséquent, la formation de H2 à partir de FA est souvent considérée comme un facteur limitant.

Bien que très actifs pour l'hydrogénation de LA, les catalyseurs à base de Ru sont également connus pour catalyser des réactions secondaires de décomposition en FA qui affectent fortement la sélectivité en hydrogène. La mise en œuvre d'une modification adéquate des catalyseurs au Ru demeure donc une approche très intéressante à cet égard. En conséquence, la conception de catalyseurs sélectifs et robustes reste un défi crucial.

Par conséquent, **l'objectif principal de cette thèse** a été de développer des catalyseurs actifs et sélectifs à base d'un support en titane pour l'hydrogénation *one-pot* d'acide lévulinique en γ-valérolactone avec un apport d'hydrogène interne *via* la décomposition *in situ* de l'acide formique. De plus, l'objectif était aussi de définir les propriétés/activité des catalyseurs dans les réactions étudiées

Deux stratégies ont été choisies pour atteindre ces objectifs. La première concerne la modification d'un support de dioxyde de titane afin d'introduire les sites alcalins dans son réseau. Il a été rapporté que la présence de bases telles que des amines dans le système réactionnel pourrait faciliter la décomposition sélective de l'acide formique en hydrogène. La conception de catalyseurs hétérogènes avec des sites alcalins constitue une approche élégante et plus durable pour éviter les problèmes de séparation résultant de l'alimentation continue du milieu réactionnel avec de grandes quantités d'additifs d'amine. De plus, selon la littérature, il est serait judicieux de mieux comprendre au préalable l'influence du caractère de support et de son mode de préparation sur le comportement catalytique des matériaux à base d'oxyde de titane. Par conséquent, une grande partie du travail a été consacrée à la conception de matériaux innovants

à base de dioxyde de titane destinés à être utilisés comme supports de nanoparticules métalliques catalytiques.

La deuxième stratégie concerne le développement d'une approche flexible et durable permettant la synthèse de catalyseurs à base de nanoparticules métalliques à la surface du matériau support. Il est essentiel d'avoir un bon contrôle sur la taille des nanoparticules métalliques tout en maintenant une distribution granulométrique étroite. La préparation de catalyseurs métalliques avec des tailles de particules appropriées, couplé à une bonne dispersité, est souhaitée pour améliorer les performances catalytiques. De plus, cela permettrait des études plus détaillées sur les relations structure/propriétés.

Cette thèse est donc divisée en sept chapitres. Le **chapitre 1** consiste en une vue d'ensemble bibliographique sur le contexte de cette étude, le rôle joué par la biomasse lignocellulosique et les substrats dérivés de la biomasse tels que l'acide lévulinique et le γ-valérolactone, les systèmes catalytiques utilisés pour l'hydrogénation et la déshydrogénation de l'acide formique. Une grande partie de ce chapitre est également consacrée au rôle du support, à l'influence des sites alcalins et à l'effet de la taille des particules métalliques sur l'activité catalytique dans les réactions étudiées, ainsi qu'aux différentes méthodes de contrôle de la taille des particules de Ru. Le **chapitre 2**, regroupe et décrit en détail les protocoles de préparation des catalyseurs et les détails concernant les techniques analytiques utilisées pour cette étude. Les protocoles de réaction sont également inclus dans ce chapitre.

La partie résultats et discussion de la thèse commence dans le **chapitre 3**, qui présente la caractérisation des supports utilisés dans ce travail. De l'oxyde de titane a été modifié par dopage avec des ions calcium durant le procédé de synthèse sol-gel pour l'élaboration de supports mixtes à base de dioxyde de titane. Des matériaux avec différentes teneurs en calcium (0, 1, 5, 10 et 20% en poids par rapport au TiO_2) ont été obtenus et analysés par diffraction des rayons X, physisorption de N_2, par mesures de potentiel zêta et d'analyse MEB. De plus, en guise de référence générale, du TiO_2 P25 commercial a été utilisé. Les profils de diffraction des rayons X sur la poudre des supports à base de TiO_2 ont montré, pour du TiO_2 modifié avec du Ca ou non, des pics de diffraction correspondant au TiO_2 anatase (Figure 2). De plus, il a été constaté que la modification du support TiO_2 avec du Ca entraînait une diminution de la taille des cristaux d'anatase en raison de l'inhibition de la croissance des cristallites de TiO_2 en présence de Ca^{2+}, se traduisant donc par une augmentation de la surface spécifique du support.

Le résultat le plus intéressant a toutefois été l'apparition d'une nouvelle phase cristallographique de titanate de calcium $CaTiO_3$, plus prononcée à mesure que la teneur en Ca augmente. La présence d'une nouvelle phase de titanate de calcium a également été confirmée par imagerie TEM sur la base du calcul de l'espacement entre les plans. En outre, la modification des paramètres et du volume des mailles de l'anatase suggère que des ions calcium ont également été incorporés dans le réseau cristallin de TiO_2. De plus, la charge de surface des matériaux a été évaluée sur la base des mesures du potentiel zêta et des valeurs ponctuelles isoélectriques. Dans le cas des matériaux de support synthétisés, la modification de TiO_2 avec Ca^{2+} a entraîné une diminution du point isoélectrique des supports. Il a été proposé que cette diminution du point isoélectrique soit liée à la formation de nouveaux sites basiques à la surface du support. En effet, il a été rapporté que le dopage de l'oxyde métallique par le promoteur de Ca peut entraîner une augmentation du nombre et de la force des sites basiques, sous la forme d'ions oxygène insaturés de manière coordonnée O^2.

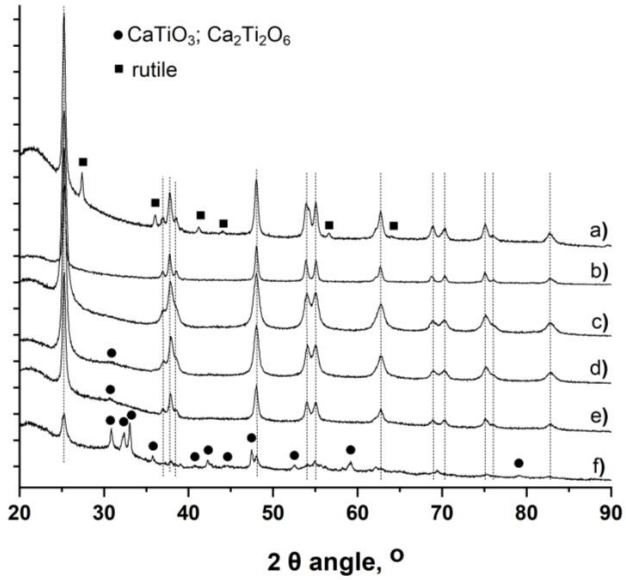

Figure 2. Powder XRD pattern of the support materials a) TiO_2 P25; b) T500; c) 1Ca-T500; d) 5Ca-T500; e) 10Ca-T500; f) 20Ca-T500. (vertical lines) diffraction peaks corresponding to the anatase TiO_2 phase; (●) most intense peaks corresponding to the titanate phases.

Ensuite, une partie importante du travail a été consacrée au développement d'une méthode innovante de synthèse photo-assistée permettant d'obtenir des catalyseurs hétérogènes avec l'utilisation de la lumière solaire (**chapitre 4**). Cette méthode, bien que déjà utilisée pour différents métaux, n'était

généralement pas mise en œuvre pour y ajouter des nanoparticules de ruthénium. Ansi, une synthèse photo-assistée en une seule étape à température ambiante a été mise en œuvre en phase liquide et sous lumière solaire pour la préparation de catalyseurs à base de TiO_2 hautement dispersés, sans traitement thermique final, sans hydrogène externe, ni réducteur chimique. L'acétylacétonate de Ru (III) et le chlorure d'hydrate de Ru (III) ont été utilisés comme précurseurs. Tout d'abord, l'influence de la nature du précurseur métallique de Ru et de la teneur réelle en Ru ciblée a été étudiée (Figure 3) et l'efficacité de la méthode de préparation a été caractérisée par analyse chimique, microscopie et analyse de surface. Il a été montré qu'à une teneur en Ru donnée, une dégradation plus rapide était observée avec le chlorure comparé à l'acétylacétonate. Pour les deux précurseurs de Ru, l'augmentation de la concentration en Ru entraînait une augmentation du temps de réaction nécessaire, l'effet étant plus prononcé avec l'acétylacétonate. En effet, essayer d'obtenir 2 m.% en Ru conduit seulement à un rendement de photodéposition de 35%, où aucune photodéposition n'a été observée pour une concentration en Ru de 5 m.%. Même dans le cas du précurseur de chlorure pour lequel une cinétique plus rapide a été observée, la préparation d'un catalyseur hautement chargé en Ru/TiO_2 avec des charges supérieures à 2 m.% ne pourrait pas être atteint pour un temps raisonnable sous irradiation.

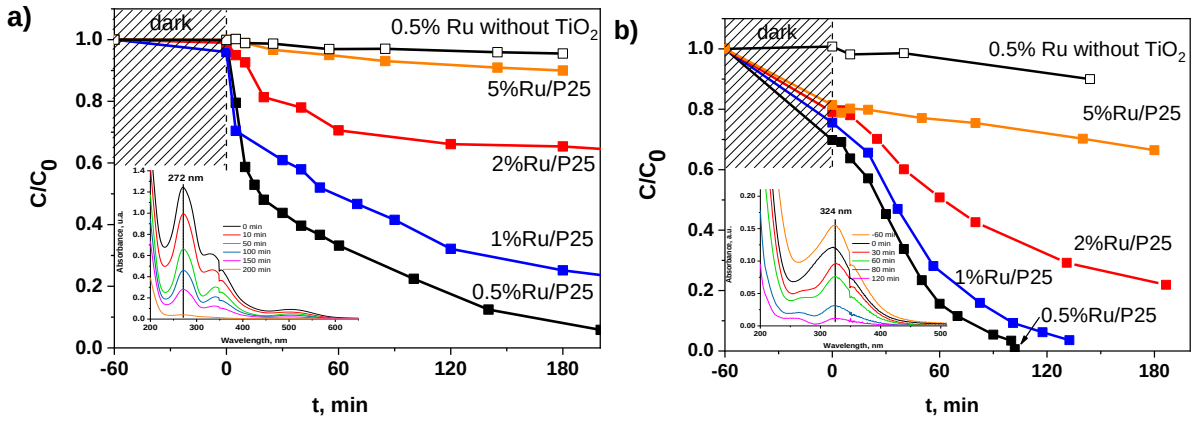

Figure 3. Disappearance of the Ru precursor in the presence of TiO_2 P25 as a function of the illumination time for a) $Ru(acac)_3$ and b) $RuCl_3$ precursors, with a Ru content of 0.5, 1, 2 and 5 wt. %. Inset: Examples of UV-vis absorbance spectra evolution as a function of the illumination time during the photo-assisted synthesis.

Les analyses MET ont montré qu'il est possible d'obtenir des tailles de particules moyennes similaires, que l'on utilise de l'acétylacétonate ou la forme de chlorure du précurseur de Ru, malgré la différence de nature chimique. Dans les deux cas, de petites nanoparticules de ruthénium ont été synthétisées sur le support de TiO_2 avec une distribution granulométrique nette et sub-nanométrique centrée sur 0.6-0.7 nm avec 0,5-1% de Ru (Figure 4).

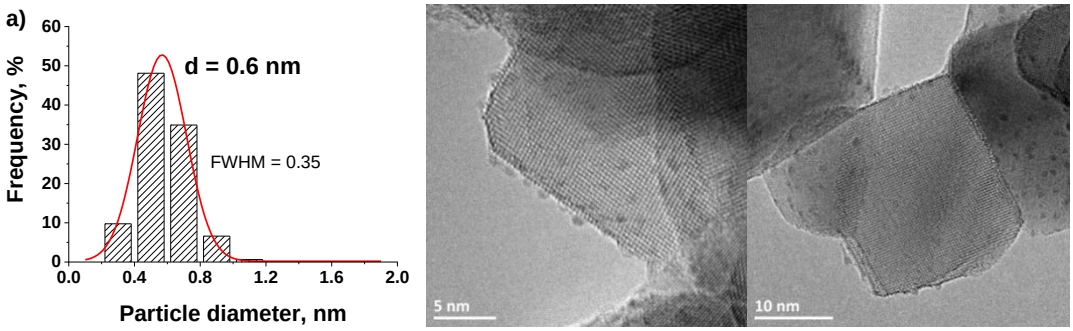

Figure 4. TEM images and the corresponding histograms of the Ru nanoparticle size distribution for 0.5%Ru_acac P25 catalyst.

La distribution granulométrique obtenue diffère fortement de celle obtenue sur un échantillon de référence Ru/TiO2 P25, préparé par imprégnation humide classique à partir de $Ru(acac)_3$ en solution méthanolique et réduction thermique finale sous hydrogène, pour laquelle une distribution granulométrique considérablement plus large a été obtenue conjointement avec une plus grande taille moyenne de particules de 1,3 nm. De plus, la nature métallique des nanoparticules de Ru synthétisées sur le support de TiO_2 a été confirmée par TEM et par analyse de surface XPS.

Des études supplémentaires ont révélé une différence dans le mécanisme de photodéposition se produisant à la surface de TiO_2 en fonction du précurseur de Ru utilisé. Le mécanisme de synthèse photo-assistée a été discuté concernant l'implication des électrons seuls photogénérés dans le cas du chlorure, alors que les trous photogénérés et les électrons seraient impliqués dans les étapes d'oxydation et de réduction, respectivement, dans le cas du précurseur d'acétylacétonate, le premier l'étape étant l'oxydation photocatalytique du ligand acétylacétonate. La vitesse de photodéposition la plus faible dans le cas de l'acétylacétonate par rapport au précurseur de chlorure pourrait résulter directement du mécanisme de réaction différent mis en place et, par conséquent, il a été proposé que $RuCl_3$ conviendrait mieux à la préparation de catalyseurs au Ru. De plus, l'acétylacétonate de Ru pourrait avoir une adsorption plus

faible à la surface du TiO_2, très probablement en raison de sa nature non ionique. En revanche, la photodéposition de Ru à partir du précurseur de $RuCl_3$ tire parti de l'adsorption privilégiée des produits hydrolytiques du sel de $RuCl_3$ dans l'eau, comme le montre la forte pré-adsorption se déroulant pendant la période d'équilibre dans le noir.

De plus, il a été démontré qu'un contrôle précis de la taille des nanoparticules métalliques de Ru sur le support de TiO_2 était possible via une croissance contrôlée des nanoclusters de Ru sous irradiation, obtenue en augmentant la durée de l'irradiation après la conversion complète du sel précurseur de Ru. Cela a mis en évidence la possibilité de fournir à la demande des catalyseurs Ru/TiO_2 avec une distribution granulométrique monomodale et une taille de particule moyenne bien calibrée pour étudier et optimiser la réactivité de catalyseurs hétérogènes dans différentes réactions dépendant de la taille ou sensibles à la structure.

Par ailleurs, l'influence du pH de la solution de précurseur dans le cas du précurseur de chlorure a été étudiée et a suggérer l'éventualité d'augmenter la teneur en Ru pour la préparation de catalyseurs à 5 m.% de Ru. L'augmentation du pH a conduit à une augmentation significative de l'adsorption d'espèces précurseurs de Ru sur le support de TiO_2 dans le noir, ce qui a par la suite de réduire considérablement le temps nécessaire pour obtenir une disparition complète du précurseur de Ru (Figure 5). Ce comportement s'explique par l'attraction électrostatique entre la surface de TiO_2 chargée négativement aux valeurs de pH supérieures à son point isoélectrique et les espèces de Ru chargées positivement présentes dans la solution dans les conditions données.

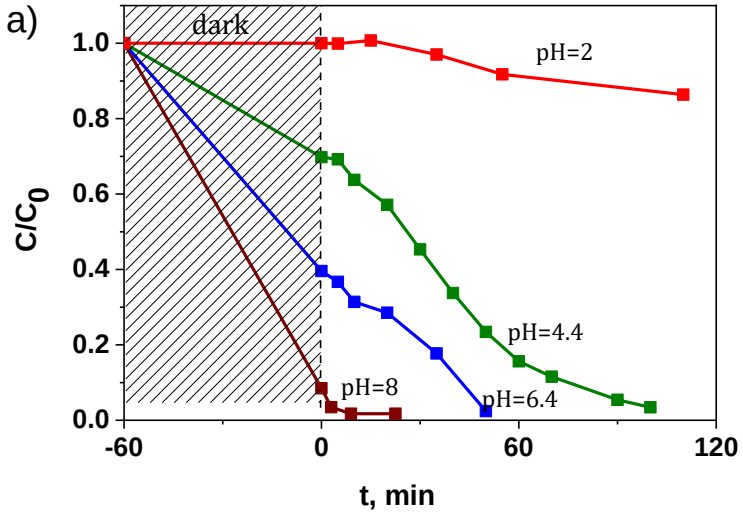

Figure 5. Influence of the pH of the precursor solution on the disappearance of the $RuCl_3$ precursor in the presence of TiO_2-P25 as a function of the illumination time for a Ru content of 0.5 wt. %;

La forte influence du pH sur le comportement d'adsorption, et par conséquent sur la cinétique de photodéposition, a suggéré la possibilité de préparer des catalyseurs Ru/TiO_2 avec une teneur élevée de 5 m.% en Ru métallique. Lors de la réaction à pH élevé (pH 8), il a été constaté que l'augmentation de la teneur en Ru d'un ordre de grandeur (de 0,5 m.% à 5 m.%) n'ait pas entraîné une forte augmentation de la taille moyenne des particules, ni dans polydispersité en taille, vu que des particules de Ru d'environ 1 nm ont encore été obtenus. Enfin, le procédé de préparation a été mis à l'échelle pour préparer l'ensemble de catalyseurs Ru/TiO_2 (sur supports modifiés avec TiO_2 et Ca) à utiliser dans les études catalytiques. Les nanoparticules supportées ont été dispersées de manière homogène dans chaque cas et aucun grand agrégat de nanoparticules de ruthénium n'a été observé (Figure 6).

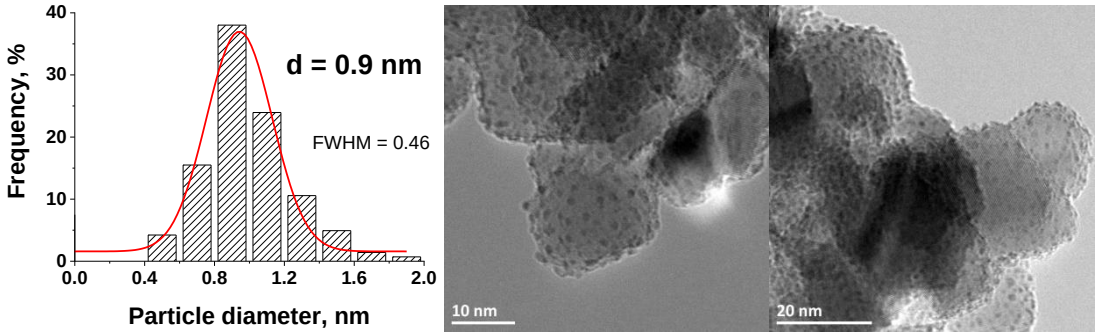

Figure 6. TEM images and the corresponding histogram of the Ru nanoparticle size distribution for the Ru(5 wt.%)/TiO_2-P25 catalyst obtained by the photdeposition method at the large scale at pH 8.

De petites nanoparticules de Ru ont été synthétisées sur les supports, avec des distributions de taille centrées sur des particules de petite taille. Il a été observé que la présence de Ca dans le support diminuait la taille moyenne des particules de Ru. De plus, en guise de comparaison, un ensemble des catalyseurs à 5% en poids de Ru a été préparé au moyen du procédé d'imprégnation classique. Il a été observé que des nanoparticules de Ru encore plus petites, présentant une distribution de taille plus nette, étaient synthétisées par photodéposition par rapport aux catalyseurs préparés par imprégnation humide suivis d'une réduction thermique finale sous hydrogène.

L'étape suivante de cette étude consistait à évaluer le comportement catalytique des matériaux à base de Ru/TiO_2 préparés par photodéposition ainsi que les méthodes d'imprégnation par voie humide pour l'hydrogénation de l'acide lévulinique en utilisant l'acide formique comme source interne d'hydrogène appelée la réaction FALA (**Chapitre 5**). Dans le cas des deux types de catalyseurs, les catalyseurs à base de Ru modifiés au Ca ont donné de bien meilleurs résultats que le Ru supporté sur du TiO_2 sol-gel et la P25 commercial, montrant donc un effet positif de la modification par le Ca (Figure 7).

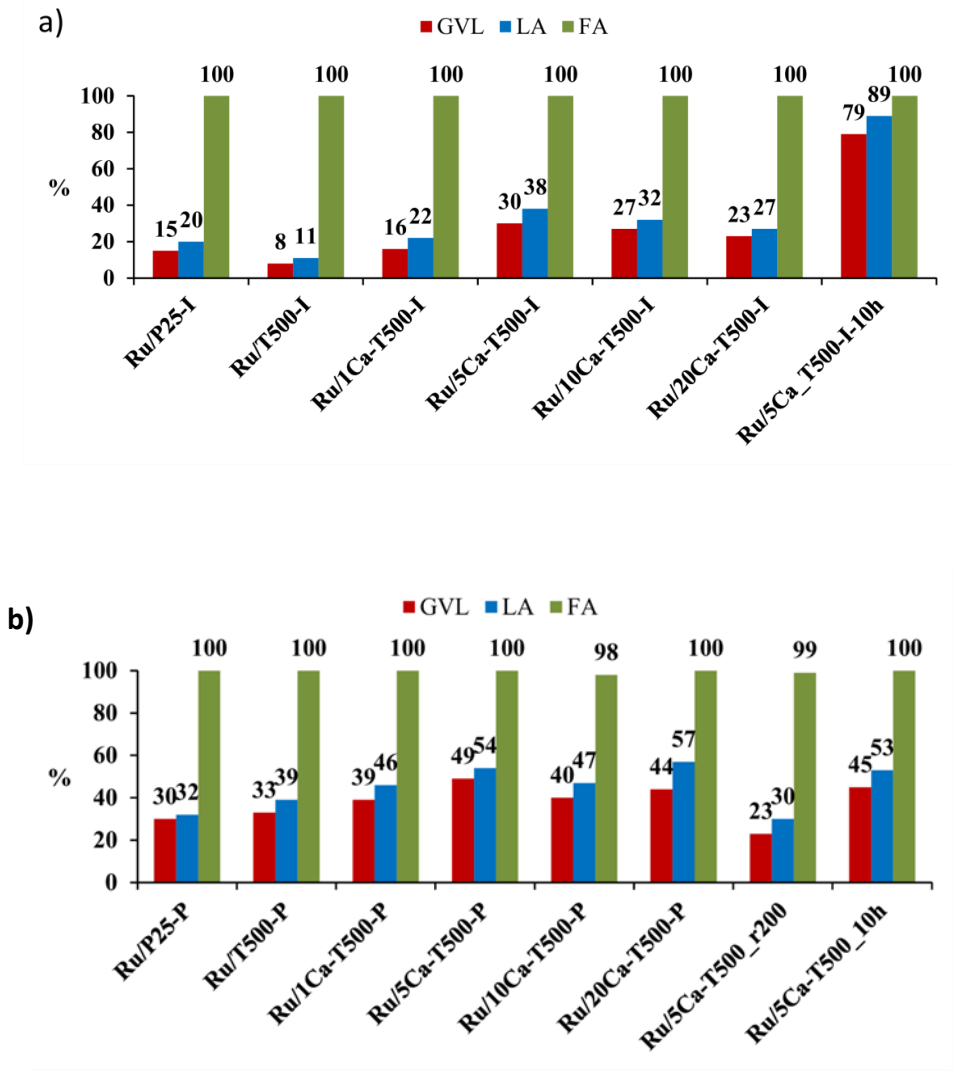

Figure 7. Catalytic activity of the Ru catalysts a) prepared by wet impregnation and b) prepared by photodeposition method in the FALA reaction.

L'activité catalytique maximale a été obtenue pour un échantillon contenant 5% de calcium. Une concentration croissante en ions calcium dans l'échantillon n'améliore pas la capacité catalytique des catalyseurs au Ru et provoque en fait une légère diminution du niveau de conversion de LA et du

rendement en GVL. Les catalyseurs préparés par la méthode de photodéposition ont montré de meilleurs résultats pour la réaction FALA, tout en présentant des profils similaires pour la conversion en LA et le rendement GVL obtenus pour les catalyseurs préparés par imprégnation. Il est important de mentionner que les échantillons préparés par la méthode de photodéposition ont été testés dans la réaction sans aucune étape supplémentaire de réduction thermique. L'influence de la modification par le Ca et de la méthode de préparation a été étudiée en mettant en œuvre séparément la réaction d'hydrogénation de LA utilisant de l'hydrogène moléculaire et la décomposition du FA en phase liquide et en phase gazeuse. Il a été montré que la modification contrôlée du support de TiO_2 par addition de Ca améliorait les performances catalytiques à la fois dans l'étape de déshydrogénation de FA et dans la réaction d'hydrogénation de LA et, par conséquent, dans la réaction combinée de FALA *one-pot*. Les catalyseurs préparés par photodéposition ont également montré des performances catalytiques supérieures à celles de leurs homologues préparés par imprégnation dans les deux réactions séparées. Afin de mieux comprendre les caractéristiques des catalyseurs jouant un rôle dans l'amélioration des performances du processus, les catalyseurs ont été caractérisés par analyses TPR, CO-FTIR et ToF-SIMS.

Il a été mis en évidence que la modification contrôlée du support de TiO_2 par addition de calcium améliorait les performances catalytiques dans la réaction FALA combinée, avec l'amélioration à la fois de l'étape d'hydrogénation de FA et de la réaction d'hydrogénation de LA. Une telle modification a entraîné une diminution de la taille des cristallites d'anatase, ainsi que la formation d'une nouvelle phase de titanate de calcium, conduisant à la stabilisation de plus petites particules de ruthénium sur le support.

Par la suite, il a été montré que la méthode de préparation de catalyseur photo-assisté permettait de renforcer l'activité catalytique en vue de la production de GVL avec du FA comme source d'hydrogène par rapport aux homologues de référence préparés par imprégnation. Cela a été possible grâce à la formation de cristallites métalliques uniformes, petites et bien dispersées. Une courbe en forme de volcan a été obtenu en faisant le lien entre la taille moyenne des nanoparticules de Ru et l'activité catalytique, avec une taille de Ru optimale de 1,5 nm donnant le catalyseur le plus actif dans toutes les réactions (Figure 8).

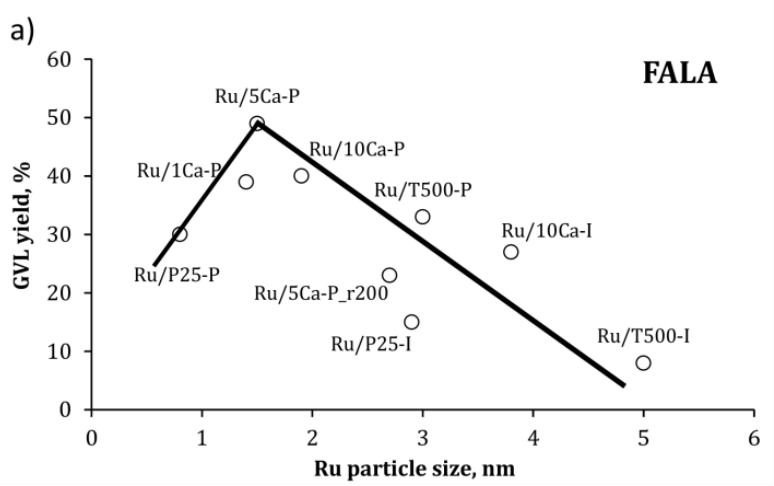

Figure 8. Influence of the Ru nanoparticle size on the GVL yield in FALA.

Cette courbe en forme de volcan a été associée à la proportion appropriée d'atomes de faible coordination (petites particules) et de haute coordination (grosses particules).

Cependant, le rôle du calcium ne s'est pas limité qu'à l'effet de la taille des nanoparticules. Des ions Ca^{2+} ont été incorporés dans le réseau cristallin de TiO_2 au moment de la formation de la nouvelle phase de titanate de calcium. Cela a eu un effet sur les nanoparticules de Ru sur support qui interagissaient plus fortement avec le support lorsque la teneur en calcium augmentait. Ceci a été confirmé sur les analyses TPR des catalyseurs préparés par la méthode d'imprégnation ainsi que sur les spectres CO-FTIR avec présence de la bande à 1980 cm^{-1} affectée à l'adsorption de CO sur Ru interagissant fortement avec le support.

Les caractérisations par ToF-SIMS ont fourni d'autres preuves concernant l'interaction directe de Ru avec le support modifié par Ca. La présence d'ions $CaRuO^{2+}$ a été identifiée pour des catalyseurs contenant plus de Ca^{2+}. Des changements de la force d'interaction métal-support ont entraîné une modification de la nature de l'adsorption des molécules de CO. Cela suggèrerait que pour les matériaux à base de Ca, l'adsorption de CO était plus faible, ce qui pourrait expliquer en partie leur performance généralement meilleure où le CO pourrait agir comme un poison pour les centres de métaux actifs. Outre le fait que le CO et le H_2 s'absorbent sur les mêmes sites, cela expliquerait pourquoi l'activité catalytique n'augmente pas avec la quantité croissante de Ca.

De plus, le rôle de la modification avec les ions Ca^{2+} était également fortement associé à la formation de nouveaux sites alcalins. La présence de sites alcalins expliquerait l'amélioration des

performances catalytiques des catalyseurs à base de Ca dans les réactions de décomposition de FA et d'hydrogénation de LA malgré le procédé de préparation du catalyseur. La déshydrogénation de FA était aidée par la présence de sites alcalins qui agissent comme pièges à protons dans l'étape de clivage de la liaison O-H. D'autre part, le mécanisme d'amélioration des performances catalytiques dans l'hydrogénation du LA pourrait être lié à l'activation du composé carbonyle où les sites basiques interagiraient avec l'orbitale π* des groupements C=O.

En raison de l'intérêt croissant porté à ces sujets de recherche, il était également intéressant d'évaluer le potentiel de catalyseurs à base de 5% de Ru/TiO2 dans la réaction de décomposition de l'acide formique en phase gazeuse dans un réacteur flux continue (**chapitre 6**). La phase gazeuse a été choisie étant donné que la majorité des rapports publiés dans la littérature ont été élaborés au cours de cette phase et que le réacteur à flux fournit l'apport constant en hydrogène qui est important du point de vue industriel pour maintenir le processus en continu. Par conséquent, les catalyseurs à base de 5% de Ru/TiO_2 préparés par des procédés d'imprégnation en voie humide et de photodéposition ont été testés dans la décomposition de l'acide formique en phase gazeuse.

Tout d'abord, les matériaux de support « nus » ont été testés dans la réaction pour examiner leur influence sur les performances finales des catalyseurs. En effet il a été rapporté dans la littérature que le TiO_2 présentait une activité vis-à-vis de la déshydratation de l'acide formique dans la phase gazeuse formant CO et H_2O. Il a été observé que les deux supports de TiO_2 sans Ca ont montré une activité dans la déshydratation de FA à 190 ° C, avec une conversion de FA de 37% et 21%, respectivement. Le CO était le seul produit de réaction détecté, ni H2 ni CO2 n'étant formés. D'autre part, la conversion en FA a chuté de manière significative lorsque les ions Ca ont été introduits dans le support. Pour un taux plus élevée en Ca, telle que 20%, aucune activité n'a été observée. De plus, l'activité d'une série de matériaux de TiO_2 disponibles dans le commerce, différant notamment en termes de taille moyenne de cristallite, et couvrant donc une large plage de surface spécifique BET, a été évaluée (Figure 9).

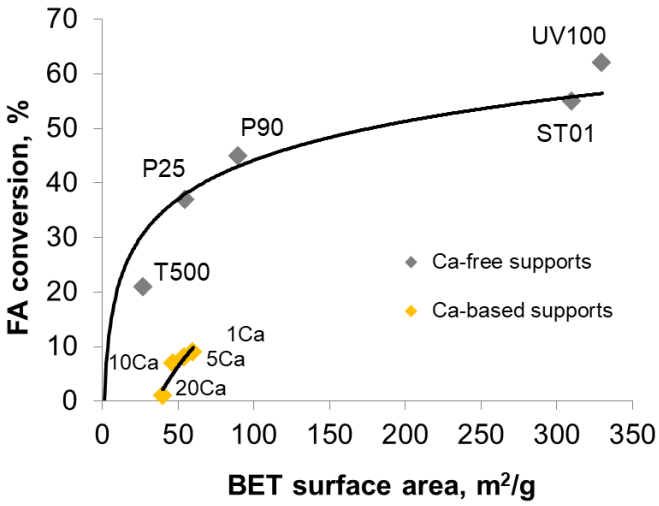

Figure 9. FA conversion obtained on the TiO_2 and the Ca-modified TiO_2 support materials in the gas phase formic acid decomposition at 190^{o}C as a function of the BET specific surface area.

Les résultats ont confirmé que pour les supports de TiO_2 non modifiés, la surface spécifique était plus élevée, la conversion du FA était plus élevée, mais uniquement pour la voie de déshydratation (formation de CO). Par conséquent, la surface spécifique est certainement l'un des paramètres qui influent directement sur l'activité des oxydes dans la décomposition de FA. D'autres effets jouent cependant un rôle lorsque des échantillons à base de Ca sont pris en compte. Quelle que soit la teneur en Ca, la conversion en FA a chuté de manière significative jusqu'à un niveau proche de zéro. Plus la teneur en Ca est élevée, plus la conversion en FA est faible. Il a été proposé que la présence de Ca^{2+} puisse bloquer efficacement la majorité des sites actifs sur du matériel de support « nu ». Par conséquence, la modification du TiO_2 par le calcium constituait donc un moyen intéressant de supprimer l'activité intrinsèque du support lui-même, et donc d'inhiber la formation de CO, connu pour agir en tant que poison potentiel dans le cas des catalyseurs à base de nanoparticules de Ru.

Ensuite, les matériaux à base de Ru/TiO_2 préparés par la photodéposition ainsi que les procédés d'imprégnation par voie humide ont été testés dans la décomposition de FA en phase gazeuse. Des conversions élevées en FA ont été obtenues à 190 ° C et une certaine activité a également été observée à des températures plus basses telles que 150 ° C ou même à 100 ° C dans quelques cas. Bien qu'il soit clairement démontré que les sites actifs pour cette réaction sont situés sur des sites métalliques de Ru, il existe toujours une contribution potentielle de l'activité de support car la décomposition de FA se fait par

déshydratation mais aussi par voie de déshydrogénation. Cependant, une augmentation significative de la quantité de H_2 produite pour les matériaux de référence de Ru par rapport aux supports de TiO_2 « nu » a été observée. Cela pourrait résulter du fait que la surface de TiO_2 est partiellement recouverte de nanoparticules de Ru et que des sites moins actifs du support lui-même sont disponibles pour la voie de déshydratation. Il a été observé qu'avec une quantité croissante de Ca, la distribution des produits gazeux est davantage orientée positivement vers l'hydrogène (plus de H_2 et moins de CO sont produits). Malheureusement l'amélioration de la sélectivité avec l'ajout de Ca^{2+} s'accompagne par la décroissance de la conversion en FA.

Il a été observé que les catalyseurs préparés par le procédé de photodéposition donnaient un taux de conversion en FA plus élevé, ce qui a été attribué à la taille généralement plus petite des nanoparticules de Ru produites avec le procédé de photo-réduction, par rapport à celle des échantillons préparés par imprégnation. Il a toutefois été suggéré que d'autres paramètres que la taille des particules de Ru, jouent un rôle plus important dans l'amélioration des performances catalytiques, tels que la présence de Ca^{2+} dans les supports. La modification du support avec 1% de Ca entraîne une amélioration à la fois de la conversion et de la sélectivité en H_2, principalement à 190 °C pour les deux types d'échantillons. Cependant, une nouvelle baisse de l'activité (avec une amélioration simultanée de la sélectivité vis-à-vis de H_2) a été attribuée au fait que la contribution de la voie de déshydratation, provenant de TiO_2 non modifié, est considérablement réduite sur les matériaux à base de Ca.

Pour résumer (**Chapitre 7**), comparée aux catalyseurs de référence Ru/TiO_2 préparés traditionnellement par une imprégnation humide, la production de GVL a été améliorée avec succès en combinant deux méthodes de synthèses complémentaires, jouant à la fois sur le matériau de support et sur la phase active supportée. Au niveau du support, la modification contrôlée d'une synthèse sol-gel de TiO_2 par des ions calcium, a entraîné la formation d'un nouveau support de TiO_2 modifié par le calcium. Il a été proposé que la TiO_2 anatase incorpore des ions Ca dans le réseau cristallin, ce dernier permettant de limiter la croissance des cristallites anatase au cours de la synthèse, tandis que la phase de titanate de calcium $CaTiO_3$, nouvellement formée, est d'autant plus mise en évidence que la teneur en Ca augmentait. Cette modification du support a amélioré les performances catalytiques des catalyseurs à base de Ru lors de l'hydrogénation combinée de l'acide lévulinique en γ-valérolactone en utilisant de l'acide

formique comme source d'hydrogène interne. Cette amélioration résulte à la fois en de meilleures performances dans l'étape de décomposition de l'acide formique et dans l'hydrogénation de l'acide lévulinique indépendamment. De plus, des particules de ruthénium plus petites ont été stabilisées sur les supports modifiés au Ca. Une interaction plus forte du ruthénium avec le support a été observée, ce qui a affecté la force d'adsorption de CO à la surface du catalyseur modifié au Ca, facilitant ainsi les performances de la réaction. De plus, il a été proposé que l'ajout de Ca se traduise par une basicité accrue des matériaux en raison de la présence d'ions oxygène insaturés de façon coordonnée, O^{2-}. La présence de sites alcalins pourrait faciliter la déshydrogénation de l'acide formique et améliorer également l'étape d'hydrogénation en aidant à l'activation des fonctions carbonyles.

Travailler au niveau de la phase active a abouti au développement d'une élégante méthode de synthèse photo-assistée en une seule étape (*one-pot*) à basse température. Cette méthode serait une alternative durable comparée à l'imprégnation humide naissante classique pour la synthèse de nanoparticules de métal hautement dispersées sur des supports TiO_2 et CaO modifiés. Cette méthode tire parti de la photoactivité redox développée par les supports à base de TiO_2 sous lumière solaire. Que l'acétylacétonate de Ru (III) ou le chlorure d'hydrate de Ru (III) ait été utilisé comme précurseurs, des nanoparticules sub-nanométriques de Ru métallique ont été synthétisées avec succès sur le support avec une distribution de taille monodisperse (uniforme). Des nanoparticules de Ru beaucoup plus petites, présentant une distribution de taille plus nette, ont été synthétisées *via* le procédé de synthèse photo-assistée par rapport aux catalyseurs homologues préparés *via* une imprégnation à l'état humide avec réduction thermique finale sous hydrogène. Par conséquent, l'amélioration des performances catalytiques dans les deux réactions séparées a également permis d'améliorer la production de γ-valérolactone dans la réaction combinée *one-pot* par rapport à celles obtenues sur les catalyseurs de contrepartie préparés par imprégnation humide classique. Les performances catalytiques ont encore été plus exaltées grâce à la modification contrôlée du support *via* l'introduction de calcium dans le support en titane. Une relation de type « volcan » a été obtenue en fonction de la taille des nanoparticules de Ru, avec une taille optimale de 1,5 nm.

En ce qui concerne la décomposition de l'acide formique en phase gazeuse, il a été démontré que la modification du support de TiO_2 avec du calcium était un moyen de supprimer l'activité de

déshydratation négative en CO du support lui-même, ce qui irait à l'encontre de la mise en oeuvre de support à base de TiO_2 dans cette réaction.

This work was done under the French Government Scholarship –

BGF Doctorat en cotutelle 2015-2018.

CHAPTER 1

1. LITERATURE REVIEW

1.1. Biomass as an alternative source of energy, chemicals and fuels

Consumption of fossil fuels, which still remain a main source of current world energy, is dramatically increasing along with improvements in the quality of life, industrialization of developing countries, and increase of the world population.[1] Figure 1 shows the world total energy consumption in the years 1990-2017 and it is expected that by the year 2050, world-wide energy demand will be at least twice of today's level.

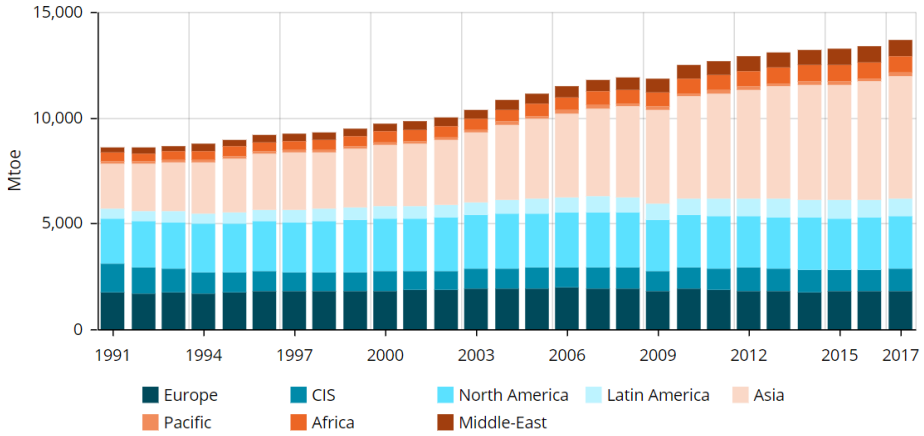

Figure 1. Total energy consumption in the world.[2]

The excessive fossil fuel consumption leads not only to the diminishing fossil fuel reserves, but it also has a significant negative impact on the environment, resulting in increased health risks and the threat of global climate change.[3,4,5] The depletion of fossil fuel reserves associated with the necessity of limiting the worldwide CO_2 release has been the driving force over the last decades in the search for alternative value chains for producing sustainable fuels and chemicals.

[1] N.L. Panwar, S.C. Kaushik, S. Kothari, Renewable and Sustainable Energy Reviews 2011, 15, 1513
[2] Enerdata. "Total energy consumption." Global Energy Statistical Yearbook 2018. https://yearbook.enerdata.net/total-energy/world-consumption-statistics.html
[3] D. M. Alonso, S. G. Wettstein, J. A. Dumesic, Green Chem 2013, 15, 584
[4] W. Luo, M. Sankar, A. M. Beale, Q. He, C. J. Kiely, P. C. A. Bruijnincx, B. M. Weckhuysen, Nat. Commun. 2015, 6, 6540
[5] A. M. Ruppert, K. Weinberg, R. Palkovits, Angew. Chem. Int. Ed. 2012, 51, 2564; Angew. Chem. 2012, 124, 2614

One alternative is to develop novel chemical processes based on renewable feedstocks, typically mixed streams of waste biomass.[6] Biomass generally refers to organic materials such as wood, grass, algae, agricultural crops and their residues and wastes, including some animal waste.[7] All of these materials originally result from biological photosynthesis from readily available atmospheric CO_2, water and sunlight making biomass a sustainable and green feedstock. Biomass can serve as a source and of sustainable energy and organic, renewable carbon for our industrial society.[8] Moreover, production of energy from biomass has the potential to generate lower greenhouse gas emissions compared to the combustion of fossil fuels, because the CO_2 released during energy conversion is consumed during subsequent biomass regrowth.[9]

Lignocellulosic biomass is considered as a second generation of biomass since it does not compete with food industry and have received intensive attention over the past decades. Many studies have shown that lignocellulosic biomass offers great potential to be used as a renewable feedstock due to its availability and abundance.[10, 11] Already today the use of biomass contributes to 10% of the total energy consumption (Figure 2) and it is expected that this value would increase to 15% by 2050.[12]

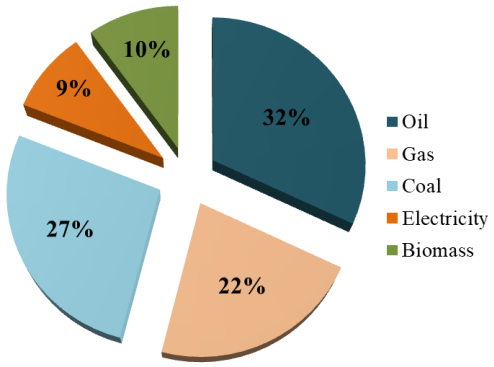

Figure 2. Worldwide consumption of energy in 2017 with breakdown by the type of energy. Adapted from[2].

[6] G. W. Huber, S. Huber, S. Iborra, A. Corma, Chem. Rev. 2006, 106, 4044
[7] Biomass Gasification and Pyrolysis, ed. P. Basu, Elsevier, 2011, 325-326
[8] J. N. Chheda, G. W. Huber, J. A. Dumesic, Angew. Chem. Int. Ed. 2007, 46, 7164
[9] K. Osamu, H.W. Carl, Biomass Handbook, Gordon Breach Science Publisher, 1989
[10] P. Gallezot, Chem Soc. Rev. 2012, 41, 1538
[11] K. Wu, Y. Wu, Y. Chen, H. Chen, J. Wang, M. Yang, ChemSusChem 2016, 9, 1355
[12] P. Azadi, O. R. Inderwildi, R. Farnood, D. A. King, Renew. Sus. En. Rev. 2013, 21, 506

However, due to the relatively low calorific value of biomass[13] an emphasis is put on its chemical processing aimed at obtaining highly specialized value added chemicals so called platform molecules rather than using biomass as a direct energy source. [14] A bio-based platform molecule is a chemical compound originating wholly from biomass that can be utilised as a building block for the production of other high-value chemicals and materials – the analogues for chemicals and materials obtained from fossil feedstock.[15] First selection of a set of value added chemicals from biomass was performed by US Department of Energy's (US DOE) in 2004.[16] This list however has been revisited several times in the recent years due to the dynamic development of the biomass industry and therefore the changing interest in certain molecules[17,18,19] Platform molecules have an advantage over the fossil-based compounds (hydrocarbons) to be already highly functionalized and therefore fewer steps are necessary to transform them into the desired products. However production of platform molecules and their selective transformation with minimum waste remains a great challenge due to the large number of functional groups (carboxyl, carbonyl and hydroxyl, double bonds) present in chemical compounds obtained from biomass and therefore the possibility of significant number of side reactions.[14] Many occurring hydroxyl and carbonyl groups can be subjected to both oxidation as well as reduction processes. Moreover the carboxyl groups can also undergo decarboxylation with the release of CO_2 reducing the number of carbon atoms in a molecule. In addition, the compounds with the proper functional groups are also subject to esterification and etherification reactions, coupling or dehydration. Therefore, to limit the number of possible side reactions it is necessary to use an appropriate catalyst.[20]

Catalysts currently used for chemicals and fuel production in petroleum industry are characterized by resistance to high temperatures and organic solvents necessary for the conversion of hydrocarbons. However for biomass processing reactions, water is often used as a green solvent as in the example of

[13] A. Özyuğuran, S. Yaman, Energy Procedia, 2017, 107, 130.
[14] R. A. Sheldon, Green Chemistry, 2014, 16, 950.
[15] T. J. Farmer, M. Mascal, "Platform Molecules," in Introduction to Chemicals from Biomass, 2014.
[16] T. Werpy, G. Petersen, Top Values Added Chemicals from Biomass: Volume I - Results of Screening for Potential Candidates from Sugars and Synthesis Gas, 2004.
[17] A. Corma, S. Iborra, A. Velty, Chem. Rev. 2007, 107, 2411.
[18] J. J. Bozell, G. R. Petersen, Green Chem, 2011, 12, 539.
[19] F. H. Isikgor, C. R. Becer, Polymer Chem. 2015, 6, 4497.
[20] M. J. Climent, A. Corma, S. Iborra, Green Chem. 2014, 16, 516.

acidic hydrolysis of cellulose (Figure 3) and therefore the existing catalysts used in petroleum industry are not suitable anymore.

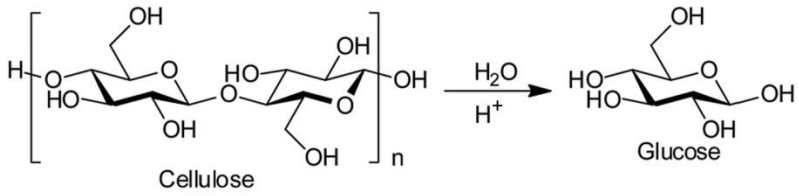

Figure 3. Scheme of acid catalyzed hydrolysis of cellulose.

When using bio-based feedstock the catalysts have to be stable in hydrothermal conditions and varying pH in order to prevent structural changes unfavorably affecting the activity and selectivity of the catalytic systems. Another problem that involves the use of aqueous solutions during lignocellulose processing is the leaching of the catalyst active phase to the reaction media. This results not only in the deactivation of the catalyst, but also contamination of the end product solution with heavy metals. In addition, hydrolytic mixtures of lignocellulosic biomass contain very often small amounts of elements like Cl, F, P, S or Mg which are able to poison active centers of the catalyst causing its complete deactivation.[21]

Therefore it is clear that the design of new, active and selective catalysts, stable in the reaction conditions and resistant to the impurities present in biomass is the key aspect of modern research using lignocellulose as a source of chemicals.

1.2. Levulinic acid and γ-valerolactone as platform molecules

1.2.1. Production, properties and applications of levulinic acid

Levulinic acid LA ($C_5H_8O_3$), also known as 4-oxopentanoic acid, β-acetylpropionic acid or γ-ketovaleric acid is a non-toxic organic compound soluble in water, ethanol and ether with a ketone and carboxylic group (Figure 4).

[21] J.C. Serrano-Ruiz, R. Luque, A. Sepulveda-Escribano, Chem. Soc. Rev. 2011, 40, 5266.

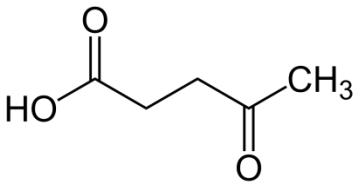

Figure 4. Chemical structure of levulinic acid.

These two functional groups make levulinic acid a versatile chemical intermediate that can be used for the production of a wide range of chemicals such as in solvents, polymers, pesticides and herbicides, pharmaceuticals, and even gasoline or diesel components.[22] For that reason the levulinic acid has been classified as one of the Top Value Added Chemicals from Biomass by the US Department of Energy (DOE) in 2004.[23]

The most common pathway to obtain levulinic acid is through acid-catalysed depolymerization and dehydration of cellulosic biomass to isomeric mixture of glucose and fructose (Figure 5). Then, through the dehydration of glucose hydroksymetylofurfural (HMF) is formed which further after hydration gives levulinic acid.

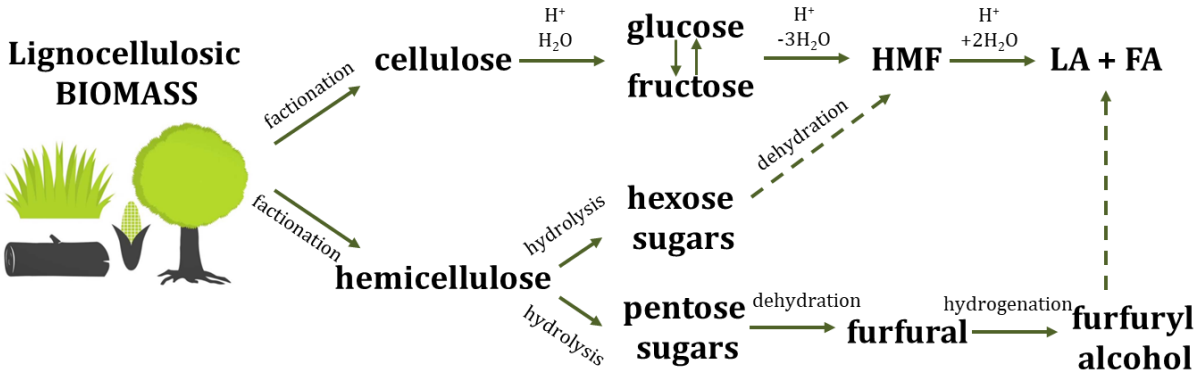

Figure 5. Simplified scheme of the formation of levulinic acid from lignocellulosic biomass.

In this conversion of hexose sugars to levulinic acid, formic acid (FA) is also produced in equimolar amount. Formic acid is a chemical used in the production of formaldehyde, rubber, plasticizers, pharmaceuticals and textiles. Furthermore there is an increasing interest of using FA as hydrogen storage

[22] F. H. Isikgor, C. R. Becer, Polym. Chem. 2015, 6, 4497.
[23] T. Werpy, G. Petersen, Top Values Added Chemicals from Biomass: Volume I - Results of Screening for Potential Candidates from Sugars and Synthesis Gas, 2004.

material for automotive applications or as internal hydrogen source for bio-based reactions.[24][25] Levulinic acid could be also produced from hemicellulose either from hexose sugars (with HMF as intermediate) or starting from pentose sugars *via* the furfural route.[26]

Today, levulinic acid is already produced commercially and involves petrochemical conversion from maleic anhydride[27] or hydrolysis of furfuryl alcohol[28] to achieve the final product of analytical grade purity. However since these methods are more complex than the acid hydrolysis of biomass resulting in the high market price of LA, the processes using lignocellulosic biomass which is at <5% of the cost compared to maleic anhydride is of high importance.

Fitzpatrick developed a Biofine technology where levulinic acid is produced[29] in a two-stage acid-catalyzed reaction process. In the first flow reactor the lignocellulosic feedstock is dehydrated to HMF at between 210–230°C (>3 MPa) for less than 30 s. Levulinic acid is produced in the second reactor at 195–215°C (~1.5 MPa) for 15 to 30 min. The reaction conditions in the second reactor are such that formic acid and furfural are kept in the vapour phase to allow simple separation of these products. The maximum yield of LA obtained from cellulose through the Biofine process is 50%.[30]

GF Biochemicals company, founded in 2008, produces LA on the industrial scale using a wide range of biomass including cellulosic waste. A company developed unique technologies for reactor as well as for the recovery and purification of levulinic acid. The continuous process produces formic acid and char which are recovered. Commercial production started in the summer of 2015 producing currently 10,000 MT of LA per year and intending to increase the capacity to 50,000 MT per year in 2020-2025.[31] Levulinic acid is an ideal platform chemical that can be utilized to produce a number of high –value bio-based chemicals. The most important applications of LA are presented in the Figure 6 and they include the production of solvents, fuels, fragrances, resins, polymers, herbicides, pharmaceuticals, anti-freeze agents, plasticisers or chemical intermediates.

[24] J. Q. Bond, D. M. Alonso, D. Wang, R. M. West, J. A. Dumesic, Science 2010, 327, 1110.
[25] H. Heeres, R. Handana, D. Chunai, C. B. Rasrendra, B. Girisuta, H. J. Heeres, Green Chem 2009,11, 1247.
[26] K.J. Zeitsch, The Chemistry and Technology of Furfural and its many by-products, Elsevier, London 2000.
[27] L. Moens, Sugar cane as a renewable feedstock for the chemical industry: Challenges and opportunities. Sugar Processing Research Conference; New Orleans, USA 2002, 26-41.
[28] B. V. Timokhin, V. A. Baransky, G. D. Eliseeva, Russian Chem Rev 1999, 68, 73.
[29] S.W. Fitzpatrick, Production of levulinic acid from carbohydrate-containing materials, US patent 5608105, 1997.
[30] D. J. Hayes, S. W. Fitzpatrick, M. H. B. Hayes, J.R.H. Ross, The Biofine process - Production of levulinic acid, furfural, and formic acid from lignocellulosic feedstocks, 2006.
[31] http://www.gfbiochemicals.com

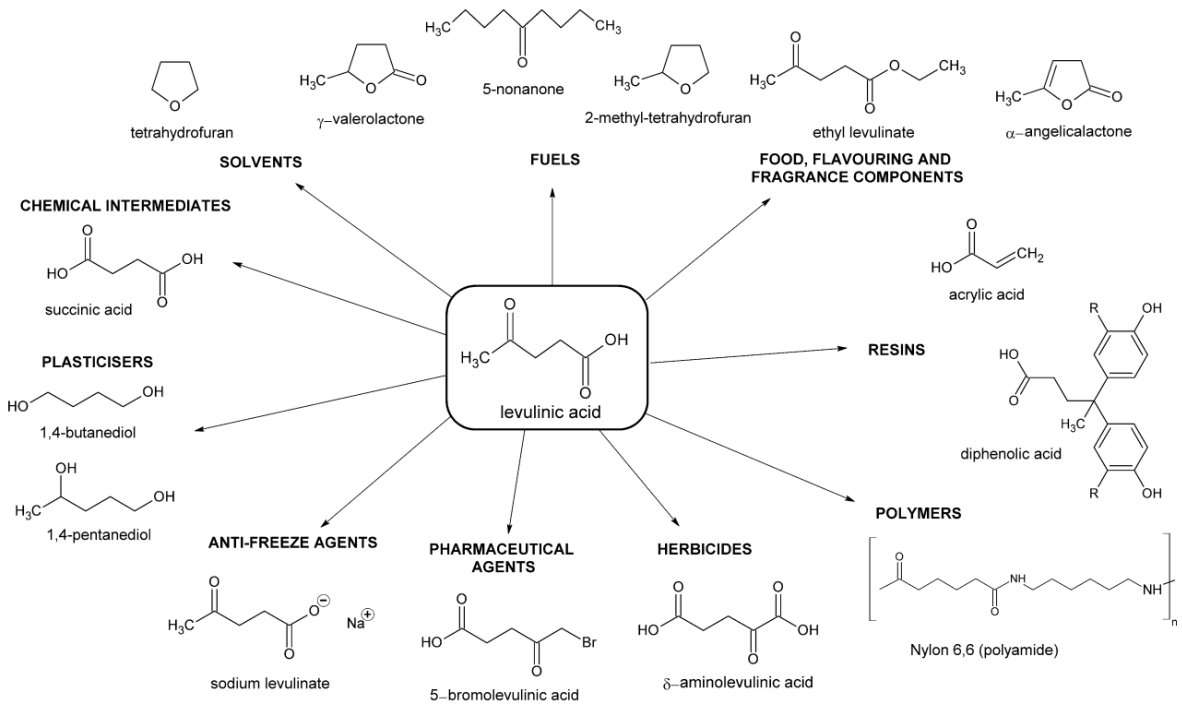

Figure 6. Applications of levulinic acid as a platform chemical.[32]

As can be seen LA could be a precursor for many valuable chemicals that have potential to replace petrochemical building blocks. For instance, bisphenol A (BPA) which has a pseudo-hormonal effect on the body[33] and which use in certain products is not authorised by The Food and Drug Administration (FDA) anymore[34] could be replaced with fully renewable and sustainable diphenolic acid (DPA), depending on its cheaper production from lignocellulosic biomass.[35]

Levulinic acid platform is particularly interesting for the production of biofuel derivatives such as 2-methyl-tetrahydrofuran (2-MTHF) and γ-valerolactone (GVL) which can be directly mixed with petrol gasoline creating cleaner-burning fuels. Their advantage over other fuel additives such as ethanol is that they do not suffer from phase separation and therefore are not readily contaminated with water.[32] Levulinic acid could also undergo a thermal de-oxygenation process to be converted into energy dense (low oxygen to carbon ratio) cyclic and aromatic products that may be easily upgraded to hydrocarbon

[32] D.W. Rackemann, W.O.S. Doherty, Biofuels Bioprod. Bioref. 2011, 5, 198.
[33] J. Ertl, E. Cerri, M. Rizzuto, D. Caretti, AIP Conf. Proc. 2014, 1599, 326.
[34] The U.S. Food and Drug Administration (FDA), http://www.fda.gov/food/newsevents/constituentupdates/ucm360147.htm, Accessed June 18, 2014
[35] F.H. Isikgor, C.R. Becer, Polym. Chem. 2015, 6, 4497.

fuels.[36] However especially interesting product obtained from LA with a high potential for the fuel industry is γ-valerolactone. As mentioned it could be used a fuel additive as such but it could be also transformed further into bio-based fuels. GVL could undergo esterification to pentenoate ester forming valeric biofuels or hydrogenation to pentanoic acid that in turn could be upgraded to 5-nonanone by ketonization and hydrogenated to alkanes or alcohols (depending on the catalyst employed). The alcohols can be subsequently dehydrated to alkenes and oligomerized enabling the production of C_6-C_{27} hydrocarbon fuels.[37] Properties and production of γ-valerolactone are described in the next chapter.

1.2.2. Production, properties and applications of γ-valerolactone

γ-Valerolactone GVL ($C_5H_8O_2$), also known as γ-methyl-γ-butyrolactone or 4-hydroxypentanoic acid lactone is a non-toxic, biodegradable organic compound with a pleasant smell naturally occurring in fruits (Figure 7).

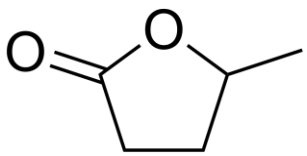

Figure 7. Chemical structure of γ-valerolactone.

Horvath et al. in 2007 proposed GVL for the first time as a sustainable liquid for the production of fuels and carbon-based products.[38] GVL could be produced from lignocellulosic biomass and due to its attractive properties is one of the most promising platform molecule. GVL has low melting point and high boiling and flash points and it is well soluble in water. Moreover its distinct smell allows for easy detection of any leaks or spills. Very important especially from the industrial point of view is that GVL is also easy and safe for storing and transporting since it is not reacting with water or air under ambient conditions and its very low vapour pressure helps to minimize the emission.[38]

GVL could be obtained by the hydrogenation of levulinic acid or its esters alkyl levulinates and therefore, the same like in case of LA, both cellulose and hemicellulose fractions could be used as the

[36] T.J. Schwartz, A.R.P. van Heiningen, M.C. Wheeler , Green Chem. 2012, 12, 1353.
[37] D.W. Rackemann, W.O.S. Doherty, Biofuels Bioprod. Bioref. 2011, 5, 198.
[38] I.T. Horvath, Green Chem. 2008, 10, 238.

starting materials. The literature reports on two possible pathways for LA hydrogenation towards GVL when using heterogeneous catalyst (Figure 8): *via* 4-hydroxy-pentanoic acid (HPA) or angelica lactone as intermediates.[39,40]

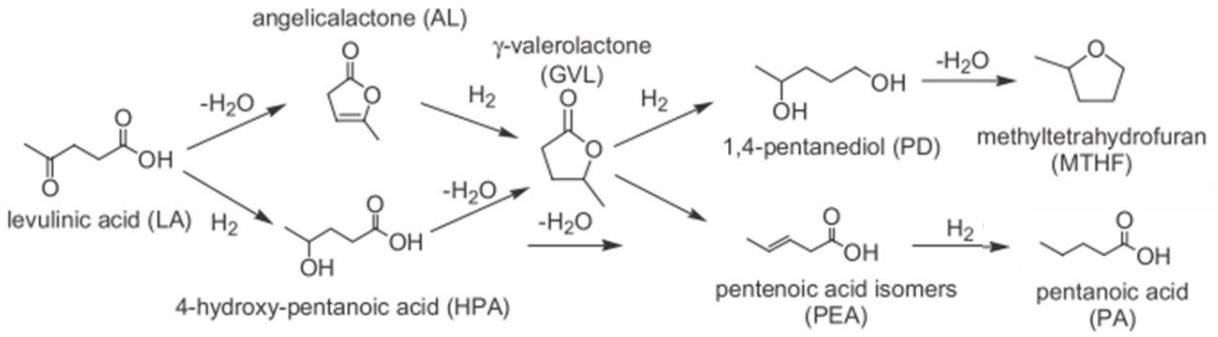

Figure 8. Hydrogenation of levulinic acid based on heterogeneous catalyst.[41]

Although there is still debate in the literature what are the factors responsible for the each pathway. The pathway *via* HPA is favored in mild reaction conditions whereas *via* angelicalactone occurs when harsh temperatures and pressures are applied.[42,43] It has been proposed by Galletti et al.[44] that with supported metal catalysts LA hydrogenation to GVL follows the reaction pathway *via* the 4-hydroxy pentanoic acid which takes place at rather mild conditions and in a protic solvent.[45] As presented in Figure 9, the first step during the hydrogenation reaction is the adsorption and dissociation of molecular hydrogen on the surface of metal active sites forming the bond between metal and hydrogen.[46] Then the molecule of levulinic acid is adsorbed on the surface of metal through the carbonylic C and O atoms and the first hydrogen atom is added to the LA generating an intermediate to link to the surface of metal by an o-bond formed between carbon and metal. Further adding another H atom would result in the formation of 4-hydroxypentanoic acid.[47] Finally, the produced 4-hydroxypentanoic acid undergoes the ring closure,

[39] O.A. Abdelrahman, A. Heyden, Q. Bond, ACS Catal. 2014, 4, 1171.
[40] Q. Bond, D. Martin Alonso, R.M. West, .A. Dumesic, Langmuir, 2010, 26, 16291.
[41] W. Luo, P.C.A. Bruijnincx, B. M. Weckhuysen, J Catal. 2014, 320, 33
[42] V. Mohan, C. Raghavendra, C. V. Pramod, B. D. Raju, K. S. R. Rao, RSC Adv. 2014, 4, 9660.
[43] P. P. Upare, J.-M. Lee, D. W. Hwang, S. B. Halligudi, Y. K. Hwang, J.-S. Chang, J. Ind. Eng. Chem., 2011, 17, 287.
[44] A. M. R. Galletti, C. Antonetti, V. De Luise, M. Martinelli, Green Chem., 2012, 14, 688
[45] C. Michel, J. Zaffran, A. M. Ruppert, J. Matras-Michalska, M. Jędrzejczyk, J. Grams, P. Sautet, Chem. Commun., 2014, 50, 12450.
[46] K. Yan, T. Lafleur, C.Jarvis, G. Wu, J. Clean. Prod. 2014, 72, 230.
[47] R.H. H. Heeres, D. Chunai, C. Borromeus, R. Buana, G. Hero,J. Heeres, Green Chem. 2009, 11, 1247

dehydration and dehydrogenation steps to form GVL. Metallic active sites are necessary for the reduction step, while the acid sites are required usually for the dehydration. However in the work of Galletti et al. where 5%Ru/C with resin Amberlyst 70 was used, the authors emphasized the positive effect of the acid co-catalyst on both steps, keto group hydrogenation and successive intramolecular lactonization.[48] On the other hand Ruppert et al. using 1%Ru/TiO_2 mentioned that the presence of metallic ruthenium sites could be more important as the formation of HPA is most probably the rate-limiting step and the closure of the GVL ring proceeds more easily.[49]

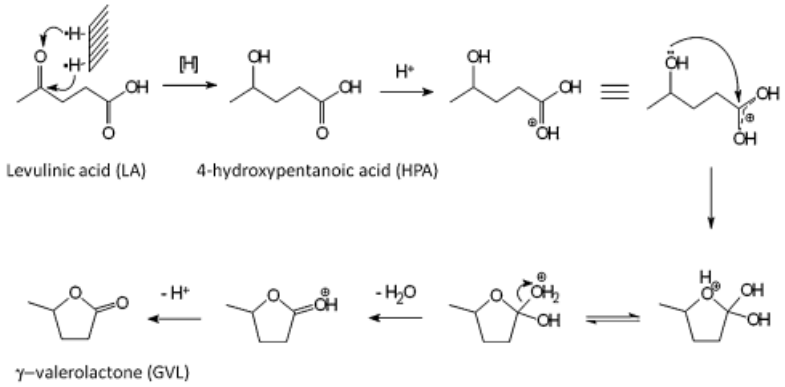

Figure 9. Proposed mechanism of the levulinic acid hydrogenation via HPA intermediate.[49]

The mechanism *via* second possible pathway (Figure 10) was proposed by Mohan et al.[50] Starting with the cyclising dehydration of the enolic form of LA a pseudo levulinic acid is formed.[51] Subsequently, the angelicalactone would be formed from the endothermic dehydration of LA.[52] In the presence of metal nanoparticles and continuous H_2 supply, the C=C bond of the intermediary angelicalactone is then rapidly hydrogenated leading to GVL. As it was reported in the literature, this mechanism operates at higher temperatures > 200°C. In their study Mohan et al. used Ni/H-ZSM-5, that contains Brønsted as well as Lewis acid sites on which angelica lactone was formed with further hydrogenation on Ni active sites to give GVL.[50]

[48] A. M. Raspolli Galletti, C. Antonetti, V. De Luise and M. Martinelli, Green Chem., 2012, 14, 688
[49] A.M. Ruppert, J. Grams, M. Jedrzejczyk, J. Matras-Michalska, N. Keller, K. Ostojska, P. Sautet, ChemSusChem 2015, 8, 1538.
[50] V. Mohan, C. Raghavendra, C. V. Pramod, B.D. Raju, K. S. R. Rao, RSC Adv. 2014, 4, 9660
[51] K. Yan, T. Lafleur, G. Wu, J. Liao, C. Ceng, X. Xie, Appl. Catal. A 2013, 468, 52.
[52] G.M. Gonzalez Maldonado, R.S. Assary, J. Dumesic, L.A. Curtiss, Energy Environ. Sci. 2012, 5, 6981.

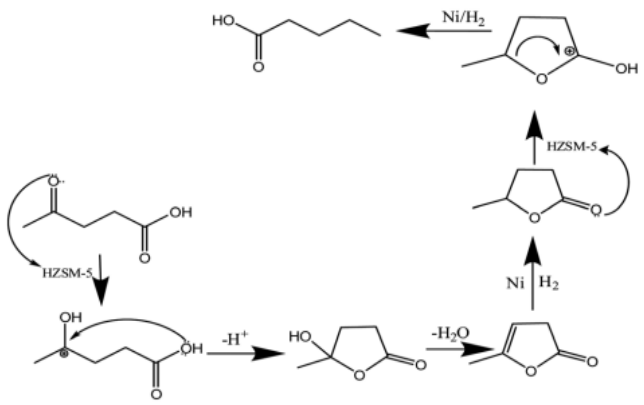

Figure 10. Proposed mechanism of the hydrogenation of levulinic acid over NHZ catalyst via angelicalactone intermediate.[50]

GVL can be further hydrogenated especially when the harsh reaction conditions are used, which can lead to the decrease in selectivity (Figure 8). GVL can be further reduced to 1,4-pentanediol (PD) and subsequently dehydrated to 2-methyltetrahydrofuran (MTHF) over a PtRe/C catalyst.[53] The other possibility is that GVL would undergo the ring-opening to yield pentanoic acid. This process requires the combination of acid sites and hydrogenation function (similarly like during the LA hydrogenation step) as was shown by Dumesic et al. where GVL was converted to pentanoic acid over a bifunctional metal/acid catalyst, such as Pd/Nb_2O_5. The group of Weckhuysen further proved that having strong acidic sites especially in a close proximity with the metal particles (hydrogenation sites) would facilitate the direct conversion of LA to PA and thus avoiding the most difficult step of both sequences i.e. GVL ring-opening.

In most of the reactions described above externally supplied high pressure of hydrogen was used. Therefore a step forward in the design of sustainable biomass hydrogenation processes can be achieved by using formic acid (FA) as internal source of hydrogen. Indeed, the acidic hydrolysis of lignocellulosic biomass produces an equimolar mixture of LA and FA, while FA can be further selectively decomposed to form hydrogen. This one-pot process would allow utilizing directly the crude mixture obtained from biomass for avoiding the costly separation of acids and further purification of LA.[54]

[53] J.J. Bozell, L. Moens, D.C. Elliott, Y. Wang, G.G. Neuenscwander, S.W. Fitzpatrick, R.J. Bilski, J.L. Jarnefeld, Resour. Conserv. Recyc. 2000, 28, 227.
[54] Z. Zhang, ChemSusChem 2016, 9, 156.

γ-Valerolactone is a versatile biomass-derived platform molecules that finds many applications in the production of fuels and chemicals (Figure 11). Horvath et al showed that GVL can be used as a fuel additive by comparing the properties of a mixture of 10 vol% GVL or EtOH with 90 vol% 95-octane gasoline.[55] Study revealed the similar properties of both mixtures with the apparent advantages of GVL over ethanol – first the fact that GVL does not form the azeotrope with water therefore could be removed by distillation results in less energy-demanding process and second the mixture of gasoline and GVL had a low vapour pressure, which improves the combustion at similar octane numbers.

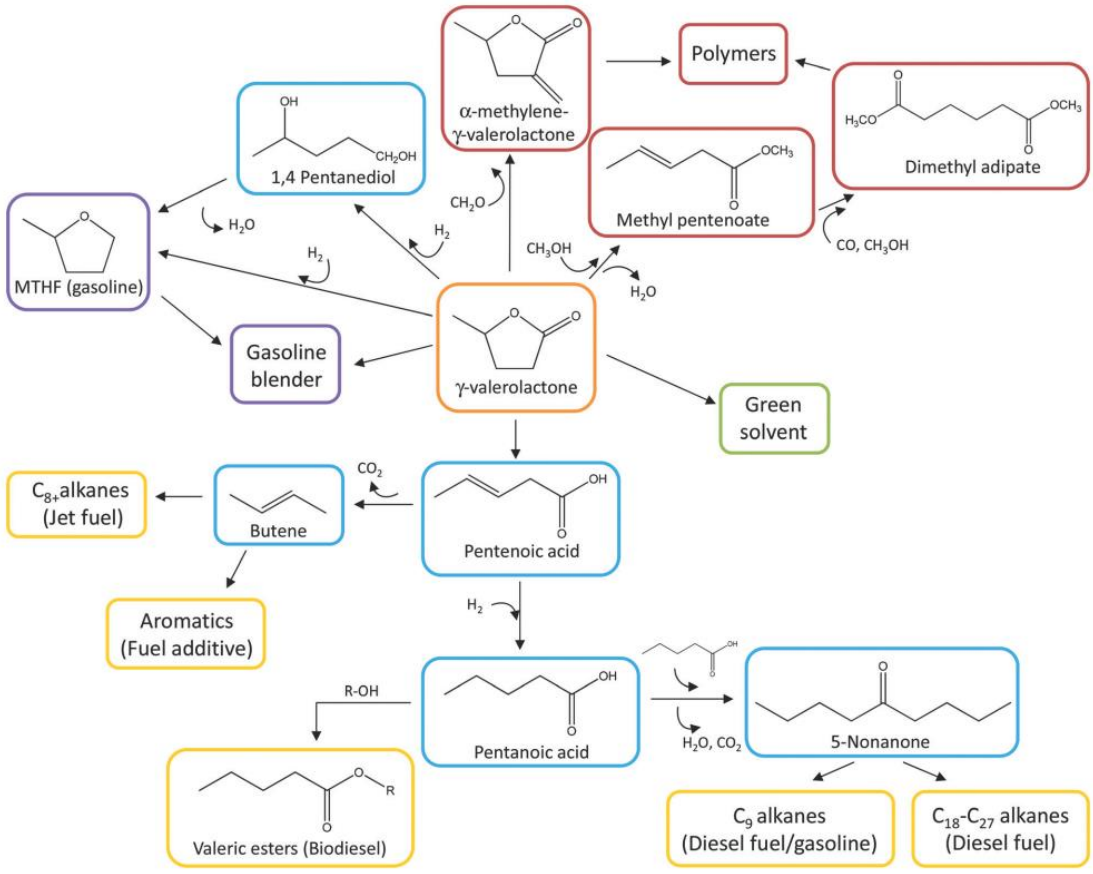

Figure 11. Reaction pathways for the conversion of GVL into fuels, fuel additives and chemicals.[56]

However direct use of GVL in a transportation sector is limited due to its high solubility in water, smaller cetane number and lower energy density as compared with fossil-based fuels.[57] Those limitations are overcome by upgrading GVL to other products with better characteristics.

[55] I. T. Horvath, H. Mehdi, V. Fabos, L. Boda, L. T. Mika, Green Chem. 2008,10, 238.
[56] D.M. Alonso, S.G. Wettstein, J.A. Dumesic, Green Chem., 2013, 15, 584.

For instance, methyl tetrahydrofuran (MTHF) which could be formed by catalytic hydrogenolysis of GVL[58,59] is regarded as promising product since it could be blended up to 70% with gasoline and has a high octane number of 87.[60] Moreover MTHF can also be converted into fuels (C_4–C_9 alkanes with high energy density) in the presence of an acid and metal catalyst at high pressure and moderate temperatures.[61]

Valeric esters could also be used as an excellent additive for gasoline and diesel fuel without the need for modifying the current engine technology.[62] The pioneering work of Lange and co-workers reported on the performance of regular gasoline blended with 15 vol. % of ethyl valerate evaluated in a road trial run based on ten vehicles with a cumulative distance of 250000 km. The authors observed no measurable impact on engine wear, oil degradation, vehicle durability, engine deposits, or regulated tailpipe emissions.

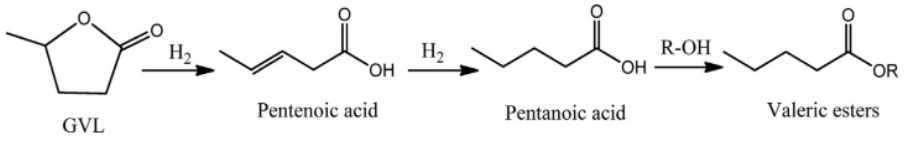

Figure 12. Conversion of GVL to valeric esters.

The first step in the synthesis of valeric esters from γ-valerolactone (Figure 12) is its ring opening to form pentenoic acid which in turn is hydrogenated to pentanoic acid. Next step is the esterification of pentanoic acid with alcohols or glycols to form the corresponding esters. The process requires a bifunctional acid-metal catalyst.[61]

Unfortunately either MTHF or valerates cannot be used as a pure fuel due to their relatively lower energy densities compared to petroleum-derived products. To increase the energy density, the GVL could be converted into liquid hydrocarbon fuels meaning an increase in carbon chain length and a decrease in oxygen content. Figure 13 shows two routes for transforming GVL into liquid hydrocarbon fuels that

[57] X. Tang, X. Zeng, Z. Li, L. Hu, Y. Sun, S. Liu, T. Lei, L. Li, Renewable and Sustainable Energy Reviews 2014, 40, 608.
[58] I.T. Horváth, H. Mehdi, V. Fábos, L. Boda L, L.T. Mika, Green Chem. 2008, 10, 238.
[59] M.G. Al-Shaal, A. Dzierbinski, R. Palkovits, Green Chem. 2014, 16, 1358.
[60] G.W. Huber, S. Iborra, A. Corma, Rev 2006, 106, 4044.
[61] Z. Zhang, ChemSusChem 2016, 9, 156.
[62] J.-P Lange, R. Price, P. M. Ayoub, J. Louis, L. Petrus, L. Clarke, H. Gosselink, Angew. Chem. 2010, 122, 4581.

currently used. In the first route the pentenoic acid obtained from GVL is upgraded to butane and further oligomerized to C_8 or C_{12} alkanes.[63] The second route involves pentanoic acid which is ketonized to 5-nonanone and upgraded further to C_9 alkanes or C_9 branched alkanes or C_{18} alkanes.[64]

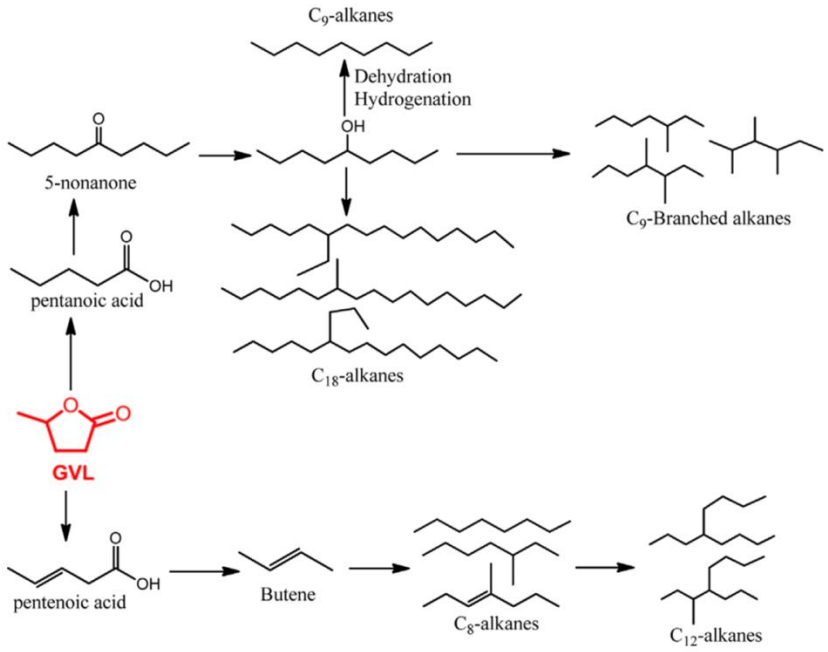

Figure 13. Routes for the transformation of GVL into liquid alkanes.[65]

Unique properties of GVL makes it ideal candidate for sustainable polar aprotic solvent. Compared to many conventional solvent, GVL is not toxic, renewable and can be easily recycled by distillation. Zhang in his comprehensive study showed the overview of GVL used as a solvent in many reactions such as lignocellulosic pre-treatment and depolymerization, synthesis of furans or even some biocatalytic reaction catalysed by enzymes.[66]Other very important applications of γ-valerolactone include synthesis of polymers or aromatic hydrocarbons.[67]

[63] J.Q. Bond, D.M. Alonso, R.M. West, J.A. Dumesic. Langmuir 2010, 26, 16291.
[64] J.C. Serrano-Ruiz, D. Wang, J.A. Dumesic, Green Chem 2010, 12, 574.
[65] K. Yan, Y. Yang, J. Chai, Y. Lu, Appl. Catal. B: Environ. 2015, 179, 292
[66] Z. Zhang, ChemSusChem 2016, 9, 156.
[67] K. Yan, Y. Yang, J. Chai, Y. Lu, Appl. Catal. B: Environ. 2015, 179, 292

1.3. Catalytic systems for levulinic acid hydrogenation using external H_2 source

The LA hydrogenation is usually performed using molecular H_2 due to its easy separation in liquid reaction systems.[68] Various heterogeneous catalysts for GVL production have been already successfully developed using commercial or biomass-derived LA and external molecular H_2 as hydrogen source. Supported metal particles exhibit usually good catalytic performance in the hydrogenation reactions due to their large surface area and the synergic effect between metal NP and support. [69] Both noble and non-noble metals have been reported for the GVL production.

Nickel and copper are the most common non-noble metal catalysts used in the LA hydrogenation. For instance, Ni nanoparticles supported on different supports (such as Al_2O_3, SiO_2, ZnO, ZrO_2, TiO_2 and MgO) were studied in LA hydrocyclization by Mohan et al. They studied the effect of the support and concluded that both Lewis as well as Brønsted acid sites which were responsible for the dehydration of the intermediate 4-hydroxy pentanoic acid to yield GVL.[70] The highest yield ca. 90% of GVL was obtained on Ni/SiO_2 at atmospheric pressure and 250^{o}C in a fixed-bed reactor. Hengne and Rode have studied the hydrogenation of LA and its ester over $Cu–ZrO_2$ and $Cu–Al_2O_3$ nanocomposites and a complete conversion of LA with 90-100% selectivity to GVL in methanol and water respectively was noticed. In addition Cu supported on ZrO_2 exhibited reduced metal leaching in water due to the formation of stable tetragonal phase ZrO_2, , which facilitates the strong binding with Cu.[71]

An alternative solution to improve the overall performance of the material or its stability is to use bimetallic catalysts. For example Ni was used as a promoting agent for Cu catalysts supported on SiO_2 in order to overcome deactivation problem during the time on stream hydrogenation of LA at 265 °C and with 25 bars of H_2. High yield of GVL up to 96% was obtained using Ni—Cu bimetallic catalysts.[72] Another study reported an excellent GVL yield of 97% under solvent-free and mild reaction conditions (8 bar H_2, 140^{o}C, 5 h) of $Ni–MoO_x/C$ bimetallic catalyst. Better performance of $Ni-MoO_x/C$ in relation to

[68] X. Tang, X. Zeng, Z. Li, L. Hu, Y. Sun, S. Liu, T. Lei, L. Li, Renewable and Sustainable Energy Reviews 2014, 40, 608.
[69] K. Yan, Y. Yang, J. Chai, Y. Lu, Appl. Catal. B: Environ. 2015, 179, 292
[70] V. Mohan, V. Venkateshwarlu, C. V. Pramod, B.D. Raju, K.S.R. Rao, Catal. Sci. Technol., 2014,4, 1253.
[71] A. M. Hengnea, C.V. Rode, Green Chem., 2012, 14, 1064.
[72] P.P Upare, ChemSusChem 2011, 4, 1749.

other noble-metal-free catalysts was attributed to the co-presence of metallic Ni and partially reduced MoO_2 species.[73]

Nonetheless, the noble metals still outperform non-noble ones in terms of their activity and selectivity. Yan et al. studied Pd nanoparticles supported on silica which showed 96% yield of GVL at full conversion of LA in water solvent. The catalysts were also stable over several catalytic runs which is very promising in terms of industrial scale use.[74,75] Use of gold catalysts in the LA hydrogenation was proved promising by Mustafin et al. The authors studied the Au NPs supported on various oxides (Al_2O_3, CeO_2 and TiO_2) and achieved 100% GVL yield in the continuous gas phase system at 220-300^oC.[76] Iridium nanoparticles were reported by Du et al. exhibiting excellent GVL yield at mild conditions. Iridium and other metals such Pt, Pd and Ru were supported on various carriers – carbon nanotubes CNT, C, CeO_2, TiO_2, Al_2O_3, ZnO, SiO_2, MgO and tested in liquid phase hydrogenation at 50^oC for 1 h using 20 bar H_2. Ir/CNT tested in water gave full LA conversion, GVL yield and selectivity.[77]

Among noble metals ruthenium-based catalysts have been however reported as the most active for the LA hydrogenation. Therefore ruthenium remains often a metal of choice for LA hydrogenation in water solvent due to its outstanding performance, which is related to the decrease of its energetic span in the presence of a protic solvent. This was shown in the study of Michel et al. where three noble metal catalysts, Ru, Pt and Pd supported on TiO_2 having similar metal crystallite size were tested. The LA hydrogenation was carried out in two different environments: water and THF as an aprotic solvent. Ru catalyst exhibited very high activity in water while it was not active in THF. The activities of Pd and Pt were not dependent on the solvent. The explanation of this effect was supported by the DFT calculations where LA hydrogenation was modeled using Ru (0001) surface and the acetone as a model of the ketone. It was found that the effective activation barrier of the hydrogenation reaction was decreased by 35% in

[73] K. Shimizu, S. Kannoa, K. Kon, Green Chem., 2014, 16, 3899.
[74] K. Yan, T. Lafleur, G. Wu, J. Liao, C. Ceng, X. Xie, Appl. Catal. A: General 2013, 468, 52.
[75] K. Yan, T. Lafleur, C. Jarvis, G. Wu, Journal of Cleaner Production 2014, 72, 230.
[76] K. Mustafin, F. Cárdenas-Lizana, M. A. Keane, J. Chem. Technol. Biotechnol 2017, 92, 2221.
[77] X. Du, Y. Liu, J. Wang, Y. Cao, K. Fan, Chinese Journal of Catalysis 2013, 34, 993.

case of ruthenium in the presence of water leading to its strong increase of the activity in a protic solvent.[78]

Initially, carbon supported ruthenium catalysts were proven to exhibit an outstanding performance. Manzer et al. screened various C-supported metals (Ir, Rh, Pd, Ru, Pt, Re and Ni) all noble metal based catalysts revealed very high activity, 5%Ru/C was clearly the most selective one. Under moderate conditions of 150^{o}C and 34.5 bar H_2 over 4 h in dioxane they obtained 100% of GVL with >97% selectivity.[79] This observation was further confirmed by Yan and co-workers where 5%Ru/C performed better than Pd and Ni and gave 92% GVL yield and 99% selectivity in methanol media under milder reaction conditions tat130^{o}C, with 12 bar of H_2 during 160 min.[80] Those conditions were considerable milder than the ones needed to ensure a high GVL yield using Pd-NPs (180^{o}C, 6 h and 90 bar H_2) based on another studies.[81] Even milder conditions were achieved by Galletti et al. where an acid co-catalyst was used in a combination with Ru NPs. The addition of ion exchange resin Amberlyst A70 allowed to obtain 99 % GVL yield after 3 h reaction carried out at 70^{o}C and 5 bar H_2 in water phase.[82]

It was reported that the dispersion of Ru NPs could be one of the key parameter in controlling the catalytic activity.[83] The catalytic performance of Ru, Pt and Pd was tested in the hydrogenation of LA under vapour phase in a continuous down flow fixed-bed reactor system at 265^{o}C for 3 h. Ru/C catalyst gave GVL with 100% LA conversion and 100% selectivity over 10 days without losing the activity. The higher catalytic activity and selectivity of Ru catalyst has been attributed to the higher dispersion of metallic Ru over carbon in nano-sizes compared to Pt and Pd catalysts.[83] Moreover it was proved by Primo et al. that the GVL yield could be increased by improving the Ru NPs dispersion. This was achieved by lowering the loadings of active metal from 5% to 0.6%, which resulted in a higher GVL yield of 93% over 0.6% Ru/TiO_2 than that over 5% Ru/C (90%) at the same reaction conditions.[84]

[78] C. Michel, J. Zaffran, A. M. Ruppert, J. Matras-Michalska, M. Jędrzejczyk, J. Grams, P. Sautet, Chem. Commun., 2014, 50, 12450.
[79] L.E. Manzer, Appl. Catal. A: General 2004, 272, 249.
[80] Yan Z, Lin L, Liu S., Energy Fuels 2009, 23, 3853.
[81] K. Yan, T. Lafleur, G. Wu, J. Liao, C. Ceng, X. Xie, Appl Catal A 2013, 468, 52.
[82] A.M.R. Galletti, Green Chem. 2012, 14, 688.
[83] P.P. Upare, J.M. Lee, D.W. Hwang, S.B. Halligudi, Y.K. Hwang, J.S. Chang, J Ind Eng Chem 2011, 17, 287.
[84] A. Primo, P. Concepcion, A. Corma, Chem Commun 2011, 47, 3613.

1.4. Levulinic acid hydrogenation using internal H_2 source

Although majority of the work on LA hydrogenation has been done using molecular hydrogen, due to the wide availability, this approach possesses many safety concerns.[85,86] Handling highly flammable hydrogen gas at high pressures and temperatures usually required in the process carries a considerable risk as well as a need for expensive infrastructure which in turn could be an economic barrier for developing a sustainable biomass-upgrading industry.[87] A very promising and renewable alternative is to use organic molecules such alcohols or formic acid as hydrogen donors for the reduction with the assistance of catalysts. This approach called often catalytic transfer hydrogenation would alleviate described above hazardous aspects and would allow reducing the costs of the experimental setup. Catalytic transfer hydrogenation was introduced already some time ago[88] however it gained popularity in the recent years with the development of homogenous and heterogeneous catalysts that helped to overcome the drawback of low reaction rates and product yields. . Although the employment of internal H_2 source has been practiced far less frequently, it has been proved to be efficient and potentially economically viable pathway in the production of biofuels and renewable chemicals.[89]

Especially using formic acid as an internal H_2 source is of high interest. As it was mentioned in a previous chapter formic acid is formed in an equimolar mixture with levulinic acid from hydrolysis of carbohydrates and therefore the perspective of its utilization as an in-situ hydrogen donor is highly attractive from the green chemistry point of view.[90,91] Formic acid has been regarded as a promising source of renewable, high purity H_2.[92,93]

[85] L. C. Demailly, B. K. Ly, D. P. Minh, B. Tapin, C. Especel, F. Epron, A. Cabiac, E. Guillon, M. Besson, C. Pinel, ChemSusChem 2013, 6, 2388.
[86] Y. Yang, C.-J. Sun, D. E. Brown, L. Zhang, F. Yang, H. Zhao, Y. Wang, X. Ma, X. Zhang, Y. Ren, Green Chem. 2016, 18, 3558.
[87] M. J. Gilkey, B. Xu, ACS Catal. 2016, 6, 1420.
[88] G. Brieger, T.J. Nestrick, Chem. Rev. 1974, 74, 567.
[89] M. J. Gilkey, B. Xu, ACS Catal. 2016, 6, 1420−1436
[90] L. Deng, J. Li, D. M. Lai, Y. Fu, Q. X. Guo, Angew. Chem. 2009, 121, 6651.
[91] L. Deng, Y. Zhao, J. Li, Y. Fu, B. Liao, Q. X. Guo, ChemSusChem 2010, 3, 1172.
[92] T.C. Johnson, D.J. Morris, M. Wills, Chem Soc Rev 2010, 39, 81.
[93] G. Laurenczy, M. Grasemann, Energy Environ Sci 2012, 5, 8171.

1.4.1. Mechanisms of formic acid decomposition and the role of basic additives

In the process of levulinic acid hydrogenation with formic acid as H_2 source the decomposition of formic acid is a limiting factor as this reaction occurs in the first step due to very strong affinity of FA to the surface, additionally very strong adsorption of formate on the surface prevents the start of other process. Therefore it is of high interest to focus on some aspects influencing the decomposition of formic acid.

Considerable effort has been paid to the development of high performance homogeneous catalyst for the formic acid decomposition with ruthenium and iridium complexes. However due to the obvious advantages of heterogeneous catalysts such as separability and reusability the main research focus should focus in the development of heterogeneous materials.[94] The decomposition of FA in presence of heterogeneous catalysts has been reported already in 1930s.[95] Many heterogeneous systems have been investigated in the gas phase over catalysts including metals, metal oxides, and metal supported on carbon or metal oxides.[96,97] Nowadays, the dominant catalysts are based on the noble metals such as palladium[98,99], gold[100], and platinum.[101]

Formic acid could decompose in two different directions: through dehydrogenation (Equation 1) or through dehydration (Equation 2).

$$HCOOH \rightarrow H_2 + CO_2 \qquad \Delta G = -35.0\ kJ{\cdot}mol^{-1} \tag{1}$$

$$HCOOH \rightarrow H_2O + CO \qquad \Delta G = -14.9\ kJ{\cdot}mol^{-1} \tag{2}$$

Selective dehydrogenation is pivotal for the production of pure H_2 utilized in the hydrogenation. Undesired dehydration produces toxic CO poisoning the active metal sites of the catalyst. Almost exclusively the dehydrogenation reaction takes place on metals, while the situation is more complex on

[94] X. Wang, Q. Meng, L. Gao, Z. Jin, J. Ge, C. Liu, W. Xing, Int. J Hydr. En. 2018, 43, 7055.
[95] H.H. Storch, J Am Chem Soc 1935, 57, 1395.
[96] Z. Li, Q. Xu, Acc Chem Res 2017, 50, 1449.
[97] A.K. Singh, S. Singh, A. Kumar, Catal Sci Technol 2016, 6, 12.
[98] M-H. Jin, D. Oh, J-H. Park, C-B. Lee, S-W. Lee, J-S. Park, Sci Rep 2016, 6, 33502.
[99] M. Zacharska, L.G. Bulusheva, A.S. Lisitsyn, S. Beloshapkin, Y. Guo, A.L. Chuvilin, Chemsuschem 2017, 10, 720.
[100] A. Gallas-Hulin, J. Mielby, S. Kegnaes, Chemistry 2016, 1, 3942.
[101] D.A. Bulushev, M. Zacharska, A.S. Lisitsyn, O.Y. Podyacheva, F.S. Hage, Q.M. Ramasse, ACS Catal 2016, 6, 3442.

metal oxides.[102] The mechanism of the FA dehydrogenation on metals and metal oxides was proposed by Mars.[102] In the initial step formic acid is adsorbed on the metal surface and donates a proton to the catalyst leading to the formation of formate intermediate[103,104] (Equation 3).

$$HCOOH + O\text{-}M \rightarrow HCOO^- + H\text{-}O\text{-}M \quad (3)$$

Then the metal-formate species undergo β-hydride elimination producing CO_2 and the H^- that forms H_2 with previously adsorbed H^+ on the catalyst.[105,106] In view of this mechanism it could be proposed that the dehydrogenation of FA is catalyzed by the basic sites which would facilitate the formate formation.[107]

Indeed the role of basic sites has been well illustrated in several studies. Many researchers reported that the dehydrogenation of FA is facilitated by the presence of various organic amines and sodium or potassium formate acting as a proton scavenger in O-H bond cleavage step leading to the formation of a metal-formate species during the initial step of the overall dehydrogenation process.[108] However such additives could lower the gravimetric energy density of FA[109] and therefore the development of a solid catalyst without any additives would be of great importance to maximize the overall kinetic properties of dehydrogenation of FA.[110]

Instead of adding free amines Mori et al. presented an interesting alternative of using macromolecular basic resin possessing $–N(CH_3)_2$ groups as a support for Pd and Cu NPs to catalyze the FA dehydrogenation. The catalyst gives a high TOF of 810 h^{-1} in FA/SF mixture at 75°C with 100% selectivity. Improved activity of this bimetallic material compared to the monometallic ones as well as to the one supported on resin with $-SO_3H$ groups could be explained by two effects: $–N(CH_3)_2$ groups facilitate the O–H bond dissociation as a proton scavenger and promoting effect of Cu particles that

[102] P. Mars, J.J.F. Scholten, P. Zwietering, Adv Catal. 1963, 14, 35.
[103] A. Masami, K. Kosaku, I.Toshinobu, T. Shiichiro, Bull Chem Soc Japan, 1966, 40, 1290.
[104] M. Adachi, T. Imanaka, S. Teranishi, Nippon Kagaku Kaishi. 1968, 89, 446; Nippon Kagaku Kaishi 1969, 90, 348; Nippon Kagaku Kaishi 1970, 91, 400.
[105] M. Ojeda, E. Iglesia, Angew Chem Int Ed 2009, 48, 4800.
[106] S. Fukuzumi, T. Kobayashi, T. Suenobu, ChemSusChem 2008,1, 827.
[107] M. Ai, J. Catal. 1977, 50, 291
[108] Q-Y. Bi, X-L. Du, Y-M. Liu, Y. Cao, H-Y. He, K-N. Fan, JACS 2012, 134, 8926
[109] X. Zhou, Y. Huang, W. Xing, C. Liu, J. Liao, T. Lu, Chem. Commun. 2008, 3540
[110] Q. Y. Bi, J. D. Lin, Y. M. Liu, X. L. Du, J. Q. Wang, H. Y. He, Y. Cao, Angew. Chem. Int. Ed. 2014, 53, 13583; Angew. Chem. 2014, 126, 13801

transfer electrons to the active Pd sites due to the difference in ionization potential.[111] The proposed mechanism for the basic sites facilitating the selective FA dehydrogenation is presented in Figure 14. A key role of basic sites is to promote the O-H bond cleavage by acting as a proton scavenger and thus leading to the formation of metal-formate species during the first step. Then the metal-formate complex undergoes a dehydrogenation to produce a molecular hydrogen and CO_2 molecule. In the final step this molecular hydrogen together with the proton bonded to the base form H_2 molecule which desorb from the catalyst surface.

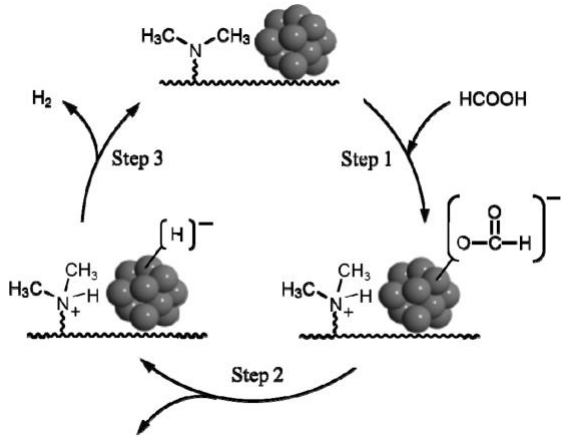

Figure 14. Possible reaction pathway for the H_2 production from FA decomposition by the Pd/resin with basic groups.[112]

Very similar approach was utilized by the group of Bulut where Pd-MnO_x nanoparticles were dispersed on aminopropyl functionalized silica (Pd-MnO_x/SiO_2-NH_2). High TOF value was achieved (1300 h^{-1}) at high selectivity (>99%) and conversion (>99%) under mild conditions (at 50◦C and under air).The higher reactivity of the amine-grafted catalyst compared to the non-grafted was assigned to the presence of –NH_2 groups allowing a basic environment around Pd-MnOx particles which facilitates O-H bond dissociation forming metal-formate species. On the other hand a drop in activity at high amine concentration was explained by the NP surface coverage. Moreover it was proposed that the CO poisoning resistance of Pd is significantly enhanced by the existence of separately nucleated MnO_x NPs, which acts as CO-sponge around the active sites of Pd NPs.[113]

[111] K. Mori, H. Tanaka, M. Dojo, K. Yoshizawa, H. Yamashita, Chemistry 2015, 21, 12085.
[112] K. Mori, M. Dojo, H. Yamashita, ACS Catal. 2013, 3, 1114
[113] A. Bulut, Appl Catal B: Environ 2015, 164, 324.

Bi et al. effectively modulated the surface electronic and acid-base properties of the Pd catalysts by incorporating pyridinic-N into the carbon support achieving impressive turnover frequency of 3625 h^{-1}. This result was the effect of described already above promotion of O-H bond cleavage by the modified basic surface. Moreover it was found that the electron transfer from the modified support to Pd particles takes place enhancing its activity in the C-H bond cleavage steps.[114] The electronic effect was also the reason for the improved activity of AuPd-La_2O_3/CNT described by Jiang et al. La_2O_3 modified AuPd alloys gave TOF = 589 h^{-1} at 50^{o}C and TOF = 280 h^{-1} at 25^{o}C and the XPS measurement illustrated that the addition of La and Au transfers electrons to Pd, proving that the alloy effect significantly improves the catalytic activity.[115]

Except amines and nitrogen, other modifiers have been used to design the proper catalyst for FA dehydrogenation. Recently, the work of Bulushev et al. showed a great improvement in terms of hydrogen production from formic acid in vapour phase with a very high selectivity thanks to the addition of K to Au/Al_2O_3 and Pd/C catalysts through incipient wetness impregnation. As it was explained by the authors the presence of K causes the significant increase in the formate ions concentration and thus the production of H_2 and CO_2 is facilitated.[116,117]

Although great efforts have been made in selective formic acid decomposition using heterogeneous catalysts their performance is still lower than the homogenous ones and therefore a long journey is still ahead before FA can be successfully used as the hydrogen source in industrial application.

1.5. Catalytic systems in levulinic acid hydrogenation with formic acid as an internal H_2 source

Performing levulinic acid hydrogenation with formic acid as an external hydrogen source is much more challenging in comparison to reaction with external hydrogen source, since the catalyst has to be active in both reactions and stable in the reaction conditions. Different examples have been shown in the literature including also some non-noble metals.

[114] Q.-Y. Bi, J.-D. Lin, Y.-M. Liu, H. Y. He, F-Q. Huang, Y. Cao, Angew. Chem. Int. Ed. 2016, 55, 1.
[115] Y. Jiang, X. Fan, X. Xiao, X. Huang, M. Liu, S. Li, H. Ge, L. Chen, Int J Hydrogen Energy, 2017, 1.
[116] D. A. Bulushev, M. Zacharska, Y. Guo, S. Beloshapkin, A. Simakov, Catalysis Comm 2017, 92, 86.
[117] D. A. Bulushev, L. Jia, S. Beloshapkin, J. R. H. Ross, Chem Comm 2012, 48, 4184.

Lomate et al. has been studying recently Cu NPs in a vapour phase LA hydrogenation supported on various carriers having different acid-base properties- Al_2O_3, SiO_2, TiO_2, ZSM-5 and SiO_2 –Al_2O_3. They reported 6wt.%Cu/SiO_2 as the best catalyst in this study giving 48% of LA conversion with 80% selectivity towards GVL at 250^{o}C when using 1:2 LA/FA molar ratio and slightly better results (56% LA conversion and 87% selectivity) when the molar ratio was increased to 1:3. Relatively strong support interactions with the copper species in Cu/SiO_2 due to the formation of copper silicates were responsible for its good performance.[118] The same authors in another study focused on Cu supported on several SiO_2 supports with different pore diameters. Under optimized conditions they achieved higher LA conversion of 66% with lower selectivity of 81% than previously. They concluded that the active species in this reaction were partially oxidized Cu species in strong interaction with the support having high number of medium strength acid sites.[119] SiO_2 was also used as a support for Ni particles by Varkolu and co-workers who investigated the effect of the catalyst preparation method on its performance. They found that 30%Ni/SiO_2 prepared by citric acid assisted impregnation-combustion method gave almost 90% of GVL yield and 100% LA conversion. The reaction was carried out in vapour phase at 250^{o}C with LA/FA molar ratio being 1:5, and the high dispersion of Ni with optimal porosity of the support played a crucial role in its performance. Unfortunately the material lost its activity due to the low stability in the reaction conditions after long reaction time.[120] Such high loadings of Ni were also tested on different supports such as Al_2O_3, MgO and hydrotalcite in similar conditions (vapour phase, 250^{o}C, FA/LA ratio of 1:5) by Mohan et al.[121] Ni/Al_2O_3 performed the best due to the presence of highly dispersed small size Ni particles formed after reduction of largely available and weakly interacting with the support NiO species. Although Ni supported on MgO initially gave similar results as on Al_2O_3, both catalysts dispersed of MgO and hydrotalcite underwent deactivation due to the phase transformation of MgO with water. Nickel and copper were also tested together as a bimetallic catalyst supported on SiO_2 in vapour phase hydrogenation by Upare et al. The addition of Ni to the catalytic system improved its thermal stability and prevented Cu sintering even after 200h of reaction. Very good LA conversion was achieved, 98%, with

[118] S. Lomate, A. Sultana, T. Fujitani, Catal Lett, 2018, 148, 348.
[119] S. Lomate, A. Sultana, T. Fujitani, Catal. Sci. Technol. 2017, 7, 3073.
[120] M. Varkolu, D. Raju Burri, S.R. Rao Kamaraju, S.B. Jonnalagadda, W.E. van Zyl, Chem. Eng. Technol. 2017, 40, 719.
[121] V. Mohan, V. Venkateshwarlu, B.D. Raju, K.S. Rama Rao., New J. Chem. 2016, 40, 3261.

92% selectivity at 265°C using 1:2 LA/FA molar ratio, however the authors used extremely high metal loadings, 20% of Ni and 60% of Cu.[122]

So far all the examples of hydrogenation were carried out in the vapour phase which requires a high energy input due to the vaporization of levulinic acid (245°C). Therefore liquid phase reaction should in principle be simpler and more economic. Al-Naji et al. studied a bimetallic system of Ni-Ru and Ni-Pt supported on zirconia and alumina in a liquid phase at 150°C in a microwave reactor for 90 min. Although they obtained 100% selectivity in case of all tested materials, Ru-Ni catalyst gave 71% of LA conversion and its high activity was assigned to a high concentration of Ru^0 with a weak interaction with the support favoring their activation. The same NPs supported on ZrO_2 were less active but much more stable in contract to alumina supported ones as they deactivated already in the second catalytic run.[123]

It could be seen, similarly to the case when using external H_2, that Ru remains the metal of choice thanks to its high hydrogenation capability. However, in the hydrogenation of levulinic acid with formic acid as a hydrogen source, one difficulty is to find a catalyst capable of performing equally well for both reactions: FA dehydrogenation and LA hydrogenation. Unfortunately, the main challenge with using Ru is related with lack of selectivity in the formic acid decomposition. Taking into account that FA can decompose either *via* dehydrogenation into H_2 and CO_2 or *via* dehydration into CO_2 and CO - with possible side reactions like the water-gas-shift reaction or Fischer-Tropsch with methane production, the first step H_2 formation from FA is often considered as a limiting factor. Indeed, FA dehydration and side reactions negatively impact on the H_2 selectivity while CO acts as a poison for the active sites, so that designing selective and robust catalysts still remains a crucial challenge. Ru catalysts are known to also catalyze side reactions that affect strongly the selectivity to hydrogen of the FA decomposition, so the implementation of adequate modification of Ru catalysts remains actually an approach of high interest in this respect. Another serious difficulty concerns the fact that the catalyst surface is fully covered by formate until a high enough conversion is reached in formic acid dehydrogenation, liberating catalytic sites for H_2 and levulinic acid. It can be said that the formate acts as an inhibitor for the LA hydrogenation

[122] P. P. Upare, M.-G. Jeong, Y. K. Hwang, D. H. Kim, Y. D. Kim, D.W. Hwang, U.-H. Lee, J.-S. Chang, Appl Catal A: General 2015, 491,127.
[123] M. Al-Naji, A. Yepez, A. M. Balu, A. A. Romero, Z. Chen, N. Wilde, H. Li, K. Shih, R. Gläser, R. Luque, J Mol Catal A: Chemical 2016, 417, 145.

and therefore it has to be fully decomposed in order for the next step to take place.[124] Moreover it was also proved that the presence of CO_2 in the batch reactor could considerably reduce the catalytic efficiency of ruthenium catalysts.[124]

It was recently shown in our laboratory that 5%Ru/C performed better than Pd or Pt catalysts in a water phase at 190^{o}C and it gave further, under carefully optimized conditions, 57% of GVL yield and 81% of LA conversion. The reaction however was carried out with excess of formic acid (LA/ FA = 1:5).[124] To increase the GVL yield, Jing et al. used trimethylamine together with a commercial 5%Ru/C catalyst. Indeed, they achieved higher than in a previous case LA conversion of 87% and GVL yield of 81% in a liquid phase hydrothermal conditions at 160^{o}C. It was reported that the addition of base could promote the LA hydrogenation[125], however this study did not offer any particular explanation. Trimethylamine was also used by Ortiz-Cervantes and García to stabilize the Ru NPs generated in situ in the reaction from $[Ru_3(CO)_{12}]$. The addition of Et_3N allowed to obtain 1 nm Ru particles compared to 2-3 nm without any additives. After 24 h reaction at 130^{o}C and LA/FA molar ratio of 1:4 100% GVL yield was reached. The authors however reported the drop in activity in a third run due to the metal particle agglomeration.[126] To further address the problem of catalyst stability, Gao and co-workers encapsulated Ru nanoparticles by entrapping the metal within the pores of the support using a sol-gel process in order to minimize the leaching and prevent particles agglomeration. Indeed such prepared 2.5%Ru/ZrO_2 performed better than its impregnated reference material giving 73% of LA conversion (compared to 63%) due to the smaller Ru NPs size and reduced leaching. The reaction was carried out in water solvent at 150^{o}C for 12 h. Interestingly, the authors used a mixture of formic acid and potassium formate to avoid the formation of CO which can poison the active sites. The presence of formate would facilitate the formation of bicarbonate as the co-product rather than CO. The molar ratio of LA/(FA+formate) was kept at 1:1 and the ruthenium catalyst outperformed the other metals such Ni, Cu, Ag and Pd. The drop in

[124] A.M. Ruppert, M. Jędrzejczyk, O. Sneka-Płatek, N. Keller, A.S. Dumon, C. Michel, P. Sautet, J. Grams, Green Chem. 2016,18, 2014.
[125] L. Deng, J. Li, D.M. Lai, Y. Fu, Q.X. Guo, Angew. Chem. Int. Ed. 2009, 48, 6529.
[126] C. Ortiz-Cervantes, J.J. García, Inorg. Chim. Acta 2013, 397, 124.

activity was reported in the second run due to the ZrO_2 phase transformation from tetragonal to monoclinic, however the incorporation of 0.1% SiO_2 effectively stabilized the support.[127]

As could be seen from above examples there is plenty of room for improvement in terms of designing heterogeneous catalyst for process of LA hydrogenation with FA as H_2 donor. Very often to improve the conversion high metal loadings or very long reaction times are used and those solutions are not economically feasible. It is also crucial to work with the equimolar ratio of formic to levulinic acid as it would allow utilizing directly the crude mixture obtained from biomass avoiding the costly separation of acids and further purification of LA and therefore developing more sustainable process on the industrial scale. Most often stability of the catalytic materials remains a critical issue and it is the main reason for their quick deactivation. The researchers try to overcome this obstacle through the employment of more sophisticated preparation methods which usually require additional steps and more chemicals that might cause increase in the costs of final process.

1.6. Catalytic support in levulinic acid hydrogenation reactions

1.6.1. Role of the support in the catalytic system

Today there are no doubts that the role of the support in heterogeneous catalysis reaches beyond the increasing of the specific surface area of the metal phase and maintaining its high dispersion in order to decrease the amount of costly metal being utilized. It is well known that the type of the support affects the catalytic activity and selectivity that the catalyst gives in a certain reaction due to the formation of new active centers formed through the interactions of metal phase and the support or due to the presence of support acid and basic sites. Those new active sites could appear through several different pathways: formation of alloys or intermetallic compounds between the components of the support and the metallic phase; transfer of the electric charge between the metal particles and the support and finally through the exposure of different crystallographic planes of metal crystallite depending on the support used.[128]
Therefore, the selection of an appropriate catalyst's support material has been of huge interest. The morphology and pores size, surface area of the support materials play an important role in enhancing the

[127] Y. Gao, H. Zhang, A. Han, J. Wang, H-R. Tan, E-S. Tok, S. Jaenicke, G.-K. Chuah, Chem. Select 2018, 3, 1343.
[128] B. Grzybowska-Świerkosz, Elementy katalizy heterogenicznej, Warszawa 1993.

heterogeneous catalyst's stability and performance.[129] Importantly, it is possible to improve the heterogeneous catalyst performance over various type of support modification.[130],[131],[132]

1.6.2. TiO_2 as a support material in the levulinic acid hydrogenation

As shown in previous chapters various support materials have been tested in levulinic acid hydrogenation with the activated carbons being the most common[133,134] due to their good performance and availability[135] Ru/C catalysts are considered as a reference for this reaction however they get deactivated due to the formation of carbonaceous deposit that blocks the active sites and reduces the specific surface area. The regeneration of such materials is limited because it requires the removal of the coke deposit at elevated temperatures at which carbon support is also decomposed.[136] Other materials such SiO_2, Al_2O_3, Nb_2O_5, ZrO_2, TiO_2, with higher mechanical and thermal stability have been therefore tested as supports for Ru particles[137,138,139] for LA hydrogenation. Even though it is possible to regenerate those materials at high temperatures, their stability under hydrothermal conditions, at which LA hydrogenation is carried out, could be limited as shown recently by Lange on Pourbaix diagrams.[140] Based on the estimation of oxide support stability in pressurized water at 200 °C at different pH values only TiO_2 and ZrO_2 were stable over the entire pH range, although in case of the latter one hydrated $Zr(OH)_4$ was found to be the thermodynamically most stable phase in water. The better performance of TiO_2 and ZrO_2 over other supports was further proven by Lange et al. in a screening study where 50 catalysts were tested in a flow reactor in LA hydrogenation.[141]

Especially TiO_2 is considered as an excellent candidate for a heterogeneous catalytic support due to its nontoxicity, good mechanical resistance, stability in alkaline and acidic media as well as a possibility

[129] D. Astruc, F. Lu, J. R. Aranzaes, Angew. Chem. Int. Ed, 2005, 44, 7852.
[130] P. Cong, R. D. Doolen, Q. Fan, Angew. Chem. 1999, 38, 484.
[131] B. Uysal, B. S. Oksal, Research on Chemical Intermediates, 2013.
[132] K. Yamaguchi, C. Yoshida, S. Uchida, N. Mizuno, J Am Chem Soc 2005, 127, 530.
[133] Z.P. Yan, L. Lin, S. Liu, Energy Fuels 2009, 23, 3853.
[134] A.M. Raspolli Galletti, C. Antonetti, V. De Luise, M. Martinelli, Green Chem. 2012, 14, 688.
[135] D. Ding, J. Wang, J. Xi, X. Liu, G. Lu, Y. Wang, Green Chem 2014, 16, 3846.
[136] J.C. Serrano-Ruiz, D. Wang, J.A. Dumesic, Green Chem. 2010, 12, 574.
[137] A.M. Raspolli Galletti, C. Antonetti, E. Riberchini, M.P. Colombini, N. Di Nasso, E. Bonari, Appl. Energy 2013, 102, 157.
[138] W. Luo, U. Deka, A.M. Beale, E.R.H. van Eck, P.C.A. Bruijnincx, B.M. Weckhuysen, J. Catal. 2013, 301, 175.
[139] M.G. Al-Shaal, W.R.H. Wright, R. Palkovits, Green Chem. 2012, 14, 1260.
[140] J.-P. Lange, Angew. Chem. Int. Ed. 2015, 54, 13186.
[141] J.-P. Lange, R. Price, P.M. Ayuob, J. Louis, L. Petrus, L. Clarke, H. Gosselink, Angew. Chem. 2010, 122, 4581.

to modify its bulk and surface properties to improve the activity and selectivity of the catalysts.[142] Moreover in contrast to acidic supports it does not catalyse the direct formation of pentanoic acid from LA through the ring opening reaction of GVL.

The positive role of titania support was also explained in the levulinic acid hydrogenation.[143] In TiO_2 being a reducible support after the reduction at high temperature the formation of Ti^{3+} sites and oxygen vacancies occur. Moreover the migration of reduced titania species could take place which creates the additional sites at the metal–support interface. Due to the presence of oxygen vacancies on titania the transfer of electrons from the support to nobel metal atoms located in their close vicinity occurs.[144]

The reduction of the carbonyl group could take place at the metal–support interface where titania Lewis acid sites could coordinate the oxygen of the ketones group, weakening the C=O bond and rendering it more susceptible to hydrogenation (Figure 15).

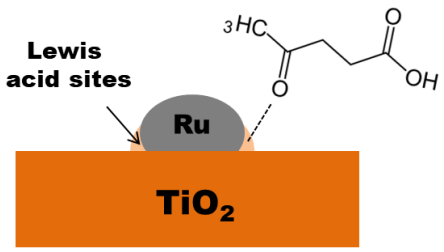

Figure 15. The adsorption of levulinic acid on Lewis acid sites at the Ru-TiO_2 interface.

Many literature reports confirm an excellent performance of TiO_2 as a support for Ru particles in LA hydrogenation reaction. Tan et al. compared commercial titania and zirconia materials as supports for Ru catalyst for performing the reaction in water phase at 70°C. They claimed that titania is more suitable than ZrO_2, as the strong metal–support interaction between Ru and TiO_2 facilitates the metal dispersion and therefore increases the catalyst stability.[145]

Moreover it was evidenced that the phase composition of the TiO_2 support directly influenced the catalytic performance of the Ru catalysts. The highest activity was observed for an anatase/rutile mixed phase titania when compared to the counterpart catalysts on the pure anatase or rutile phase supports.

[142] S. Bagheri, N. M. Julkapli, S. B.A. Hamid, The Scientific World Journal 2014, Article ID 727496.
[143] A.M. Ruppert, J. Grams, M. Jedrzejczyk, J. Matras-Michalska, N. Keller, K. Ostojska, P. Sautet, ChemSusChem 2015, 8, 1538.
[144] P. Panagiotopoulou, D. I. Kondarides, J Catal, 2009, 267, 57.
[145] J. Tan, J. Cui, T. Deng, X. Cui, G. Ding, Y. Zhu, Y. Li, ChemCatChem 2015, 7, 508–512

This was related with the presence of the optimum size of the Ru particles.[146] On rutile the deposition of Ru was facilitated due to the presence of the same crystallographic structures of RuO and rutile and therefore formation of small particles strongly interaction with the support. By contrast, large Ru aggregates were formed on anatase, which led to low catalytic activity. It was also found that the activity of the anatase-based Ru catalyst could be improved by implementation of either a calcination step of the anatase support before impregnation to reduce the micropore volume or by avoiding a high temperature reduction step during catalyst synthesis by using a mild chemical reduction step.

Similar results were also reported by Al-Shaal et al. where Ru/TiO_2 (P25, 75:25 mixture of anatase-rutile) showed much better performance than rutile supported particles in the LA hydrogenation in ethanol and ethanol–water mixtures.[147] In addition, Li et al. showed that the high activity and selectivity achieved on anatase TiO_2 supported Ru catalysts were attributed to enhance metal-support interaction thanks to intimate contact between Ru and anatase nanoparticles and to the Ru nano-size. A stronger electron donation from TiO_2 to Ru and an easier reducibility of Ru species were proposed to modify both activity and selectivity patterns and to boost Ru for the selective transformation of substrates.[148]

Kuwahara et al. studied the catalytic transfer hydrogenation of levulinate esters with alcohols as hydrogen donors using $Ru(OH)_x/TiO_2$ catalysts, and evidenced that high surface area anatase TiO_2 supported highly-dispersed $Ru(OH)_x$ nano-clusters were the most active catalyst.[149] Optimum dispersion and distribution of Ru on the TiO_2 support was recently proposed for explaining the high activity and stability displayed by a $5\%Ru/TiO_2$ catalyst in the continuous flow hydrogenation of methyl levulinate when compared to commercial Ru/C and Ru/Al_2O_3 reference catalysts.[150]

1.6.3. Influence of basic sites on the catalytic performance

Many different strategies exist for improving the performance of heterogeneous catalysts and one of them is a modification of the support such as changing its morphology, porosity, increasing the specific

[146] A.M. Ruppert, J. Grams, M. Jedrzejczyk, J. Matras-Michalska, N. Keller, K. Ostojska, P. Sautet, ChemSusChem 2015, 8, 1538.
[147] M.G. Al-Shaal, W.R.H. Wright, R. Palkovits, Green Chem. 2012, 14, 1260.
[148] G. Li, H. Yang, M. Cheng, W. Hu, L. Tian, W. Mao, R. Nie, Mol. Catal. 2018, 455, 95.
[149] Y. Kuwahara, W. Kaburagi, T. Fujitani, RSC Adv. 2014, 4, 45848.
[150] C. Xu, W. Ouyang, M. J. Muñoz-Batista, M. Fernández-García, R. Luque, ChemSusChem 2018, 11, 2604.

surface area or creating new active sites. It has been reported in the literature that acid-base properties of the support could significantly change the catalytic activity and selectivity in many different reactions using various types of the catalytic materials. Indeed, one of the strategies for selectivity improvement is related with the introduction of bases to the reaction system, either by addition of free bases to the reaction mixture or by introducing directly basic sites to the catalyst surface through material modification. Although majority of cases concern homogenous catalysis and simply the addition of amines, the design of heterogeneous catalysts with basic sites would be an elegant and more sustainable approach for avoiding separation issues resulting from the continuous supply of the reaction media with high amounts of amine additives.

The importance of catalyst basic sites in hydrogenation reactions has been already proposed in the literature. The presence of both acidic and basic sites was proved to be responsible for the preferential hydrogenation of C=O group in cinnamaldehyde using Au catalysts.[151] Another study by Liu et al. reported high performance of well-dispersed Cu/MgO catalyst in the hydrogenation of furfural (>90% conversion and >90% selectivity). The authors explained the improved catalytic performance by the activation of the carbonyl compound where basic sites would interact with π* orbital of C=O group and weaken the double bond.[152]

The role of base was also investigated in the LA hydrogenation for reactions performed with FA used as hydrogen source. Ruthenium although being very active for LA hydrogenation, is known to also catalyze side reactions that affect strongly the selectivity to hydrogen in FA decomposition, so it becomes an issue when carrying out the reaction with this internal H_2 source. Therefore the implementation of adequate modification of Ru catalysts remains of particularly high interest in this respect.

A proof of concept for using ruthenium catalysts with basic sites in LA hydrogenation was already shown in a few studies. Java et al.[153] presented Ru supported on Mg-LaO mixed oxide obtained from hydrotalcite as an efficient catalyst for producing GVL. Although 92% conversion and >99% selectivity was achieved at low temperature of 80^{o}C after 4h, the reaction was carried out under the hydrogen pressure of 0.5 MPa in toluene as the solvent. However, no explanation for the role of basic sites in this

[151] Y. Zhang, S. Zhang, X. Pan, M. Bao, J. Huang, W. Shen, Catal lett 2017, 147, 102.
[152] H. Liu, Q. Hu, G. Fan, L. Yang, F. Li, Catal. Sci. Technol., 2015, 5, 3960.
[153] V.S. Jaya, M. Sudhakar, S.N. Kumar, A. Venugopal, RSC Adv, 2015, 5, 9044.

system was proposed. In another study the same group proposed hydroxyapatite $Ca_5(PO_4)_3(OH)$ as a support for ruthenium metal. Catalyst gave 99% of GVL yield with 99% selectivity after 4 h of reaction in water phase at 70°C under 50 bar of H_2 showing also good stability up to 4 recycles. This good performance the authors ascribed to the presence of both acidic and basic sites on the surface of the catalyst.[154]

Another, very complex work was presented by Cao et al.[155] where Ru/C and Ru/Al_2O_3 with different metal loadings were tested in the LA hydrogenation at 220°C for 6 h using 200 psi of H_2 and 1,4-dioxane as a solvent. A beneficial effect of potassium introduced to the catalysts in a form of KNO_3 by impregnation was reported. K doping (3 wt.%) caused over 2.5 times and 6 times higher activity of Ru/C and Ru/Al_2O_3 respectively which the authors explained by the electronic effect and therefore higher ratio of Ru^0/Ru^{n+} as well as decreased CO adsorption on K-doped materials. In their follow-up study the researchers examined in more details the effect of alkali metals on Ru activity in LA hydrogenation. This time they tested Na^+, K^+ and Cs^+ with different loadings (1-5%) and in all cases they observed increased TOF values (even up to 10 times) compared to the unpromoted catalyst. Similarly to the previous report the promotional effect was assigned to the electron transfer from alkali metal to ruthenium. With the same atomic ratio the promotion follows the order $Na^+ < K^+ < Cs^+$ which is explained by the higher electron density enrichment with higher polarizability of the element. While the TOF value was increasing with the increase of the Na^+ loading in the catalyst, interestingly in case of K^+ and Cs^+ doping the volcano-type tendency was observed with the highest activity for potassium and cesium at 3% content. This effect could be attributed to the balance between under-promotion where not all sites are promoted and over-promotion where the active sites are blocked by the excess of the promoter.[156]

Another study by Song et al. showed the promoting effect of La on Ru/carbon fibres (CF) catalysts. The materials were obtained by the coprecipitation of Ru and La precursors on CF support with varying amount of La and tested in the LA hydrogenation using 50 bar of H_2. It was found that the activity improved with the increasing La content reaching maximum at 0.5 La/Ru molar ratio and then declined

[154] M. Sudhakar, M.L. Kantam, V.S. Jaya, R. Kishore, K.V. Ramanujachary, A. Venugopal, Catal Comm 2014, 50, 101.
[155] S. Cao, J. R. Monnier, C. T. Williams, W. Diao, J.R. Regalbuto, J Catal 326, 2015, 69.
[156] S. Cao, J.R. Monnier, J. R. Regalbuto, J Catal 2017, 347, 72.

with the further increase in La concentration forming volcano-type dependence which was explained by the blocking of Ru active sites. The characterization revealed that the La promoter could increase the electron density of Ru species, which led the back donation of electrons from Ru to carbonyl, meaning that LA was adsorbed stronger on RuLa/CF catalysts which in turn facilitated the hydrogenation reaction. Therefore it was shown that reaction rate was a consequence of the amount of Ru active site and the promoting effect of Ru-La interaction.[157]

Very interesting study where no noble metal was used was shown by Hussain et al. who tested the calcined Mg-Al hydrotalcites (HTC) with various Mg/Al ratios in the gas phase conversion of LA into GVL with FA as an internal hydrogen donor. All samples gave the same selectivity towards GVL (95-98%) with the samples having ratio of Mg/Al 1:1 and 3:1 showing the best catalytic activity. By performing several experiments: with pure MgO, with mechanical mixture of MgO and Al_2O_3 and with HTC supported Cu and Ni, the authors proved that large number of active basic sites present in hydrotalcites play a crucial role in determining their catalytic performance. The superior catalytic activity in calcined sample can be explained based on the strong interaction of Mg and Al oxides known as synergetic effect, thus physically mixed samples did not show this effect. The lower activity of Cu and Ni catalysts was explained by the coverage of basic sites in the HTC samples by incorporation of metals.[158]

1.7. Size of the metal nanoparticles

1.7.1. Effect of nanoparticles size in formic acid dehydrogenation

There are many aspects that influence the dehydrogenation efficiency of formic acid such as type of active metal and promoters, supports, modifiers or additives used. Undoubtedly, the particle size of the active metals also has crucial effect on the catalytic performance of the catalyst. Generally it is known that the catalytic activity increases with the decrease in metal NP size, as smaller particles possess higher

[157] W. Song, Z. Chen, W. Lai, I. Rodríguez-Ramos, X.Yi, W. Weng, W.Fang, Appl. Catal. A: General, 540, 2017, 21.
[158] S.K. Hussain, V. Kumar Velisoju, N. Pethan Rajan, B. Putra Kumar, .K.V. R. Chary, Chem. Select 2018, 3, 6186.

surface areas and therefore more active sites are available. The influence of the metal particles size on their activity in formic acid decomposition has been observed by many researchers.[159,160,161,162]

The detailed systematic investigation of the effect of NPs size has been done based on Pd particles as very attractive catalysts for FA decomposition. Yamashita et al. studied Pd NPs with different particle sizes ranging from 2.7 to 5.5 nm prepared by the polyol method and impregnated on carbon in a closed liquid phase system for 3 h. A volcano-type relationship has been observed with the particles of 3.9 nm having the highest activity which authors related to the proper balance between high-coordinated (HC) and low-coordinated (LC) Pd atoms with respect to total number of surface atoms.

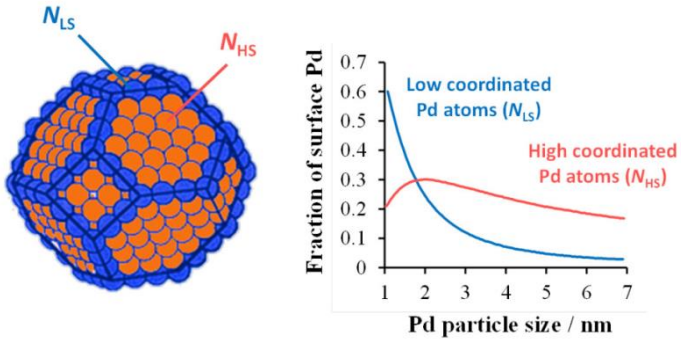

Figure 16. Schematic illustration of high-coordinated and low-coordinated atoms and their fraction of surface area.[163]

It is well-known that the smaller NPs with higher surface area have a larger proportion of unsaturated surface atoms (edge and corners) while the larger ones have more terrace surface atoms (
Figure *16*).[164] TOF values calculated based on both LC and HC atoms as a function of particles size as well as kinetic isotope effect studies revealed that the formic acid decomposition is a structure sensitive reaction and that terrace surface atoms act as active sites. This fact can be explained by the adsorption mode of the formic acid on Pd NPs. Bridging (bidentate) formate species exist on high-coordinated atoms directing the reaction towards CO_2 and H_2 while linear (monodentate) forms are found on unsaturated defect atoms enabling stronger chemisorption and giving rise to CO and H_2O *via* the dehydration

[159] K. Mori, M. Dojo, H. Yamashita, ACS Catal. 2013, 3, 1114.
[160] F.-Z. Song, Q.-L. Zhu, N. Tsumori, Q. Xu, ACS Catal. 2015, 9, 5141.
[161] Z. Li, X. Yang, N. Tsumori, Z. Liu, Y. Himeda, T. Autrey, Q.Xu, ACS Catal. 2017, 4, 2720.
[162] Q.-Y. Bi, J.-D. Lin, Y.-M. Liu, F.-Q. Huang, Y. Cao,International Journal of Hydrogen Energy, 41, 2016, 21193.
[163] M. Navlani-Garcıa, K. Mori, A. Nozaki, Y. Kuwahara, H. Yamashita Chem Select 2016, 1, 1879.
[164] K. Mori, T. Hara, T. Mizugaki, K. Ebitani, K. Kaneda, J. Am. Chem. Soc. 2004, 126, 10657.

pathway. Yamashita et al. explains further the volcano-type behavior of Pd NPs in view of the adsorption-desorption steps from metal surface. The adsorption energy of $HCOO^-$ is favoured on small NPs but due to the space exclusion repulsive interactions take place decreasing the total coverage of formate species. On larger NPs the high surface coverage could be achieved but the adsorption energy is decreased. Therefore a proper balance between highly reactive small NPs and high coverage of intermediate species on larger NPs is necessary to obtain the optimum catalytic performance in the formic acid dehydrogenation. Moreover since the dehydration reaction prefers to take place at low coordination sites the formation of poisonous CO could lower the activity which would explain decreased TOF for the smallest Pd NPs.[165] Another explanation could be given by the increased adsorption affinity on smaller NPs which in turn impedes the C-H bond cleavage considered as the rate-determining step in FA dehydrogenation process.

Interestingly, Lu et al. did not observe any volcano-shaped dependence of TOF on Pd NP size as in their study the activity was continuously increasing with lowering the metal particles size. XPS results revealed increasing fraction of $Pd^{\delta+}$ for smaller particles and thus enhanced interactions between $Pd^{\delta+}$-$HCOO^-$ species promoting the reaction. The authors also reported that according to TOF calculations based on HC and LC atoms all surface atoms act as active sites in the reaction.[166]

1.7.2. Effect of nanoparticle size in levulinic acid hydrogenation

The effect of metal nanoparticles size on their catalytic activity in levulinic acid hydrogenation has not been studied as thoroughly as in formic acid decomposition. In fact it is still not fully clear whether this reaction is "structure sensitive" as contradicting data has been published []. For instance a study of support screening for Ru nanoparticles performed by Piskun et al. suggested that for C, Al_2O_3 and TiO_2 supports LA hydrogenation is structure insensitive. However this work considered rather narrow particles size range (0.9-1.5 nm) and ruthenium was supported on different materials which undoubtedly has an effect on their activity.[167]

[165] S. Zhang, B. Jiang, K. Jiang, W.B. Cai, ACS Appl Mat 2016, 9, 24678.
[166] J. Li, W. Chen, H. Zhao, X. Zheng, L. Wu, H. Pan, J. Zhu, Y. Chen, J. Lu, J Catal, 2017, 352, 371.
[167] A. Piskun, J. G. M. Winkelman, Z. Tang, H. J. Heeres, Catalysts 2016, 6, 131.

On the other hand, the researchers report the importance of preparation of stable small metal particles and very often assign the improved catalytic performance to the presence of smaller NPs. Tao et al. prepared series of Ru nanoparticles supported on few-layer graphene (Ru/FLG) with the Ru particles size between 1.33 nm and 2.82 nm controlled by manipulating the Ru loading. The catalyst 3.78%Ru/FLG with the average NPs size of 1.68 nm gave 96.7% of GVL yield with 100% selectivity in a reaction performed for 2 h at 80^{o}C and with 60 bar of H_2. This result was enhanced compared with the previously reported by the same team Ru/graphene which they explained by the presence of larger fraction of Ru particles with sizes in the range of 1.4-1.8 nm (~ 50%) compared with the graphene-based material (Ru sizes: 2-6 nm).[168]

Li and coworkers by utilizing the hydrothermal method synthetized TiO_2 crystallites, which size could be controlled by varying the amount of hydrofluoric acid during the preparation step. TiO_2 were used as the supports for Ru metal and tested in LA hydrogenation at mild conditions (30^{o}C, 10 bar H_2, 30 min). Small TiO2 particles size facilitated the preparation of small Ru particles and the best results were achieved for Ru particles of 1.7 nm (97.4% LA conversion, 99% selectivity to GVL). Based on XPS and H_2 -TPR results it was concluded that strong electron donation from TiO_2 to Ru and easier reducibility of Ru species due to its smaller size was responsible for such high catalytic performance.[169]

The most systematic investigation on the influence of metal nanoparticles on their performance in LA hydrogenation has been carried out by the Regalbuto and coworkers. They examined the effect of the Ru particles size (0.92 – 4.82 nm) for two supports C and Al_2O_3 in the 6 h reaction at 220°C under 13.8 bars of H_2 using 1,4-dioxane as solvent. They proposed that LA hydrogenation is structure sensitive and depends on the Ru particle size, with an activity maximum at about 1.5 nm.[170]

1.7.3. Methods for controlling Ru nanoparticles size

According to the literature the most common approach for controlling Ru nanoparticles size and maintaining their high dispersion is the preparation of colloidal catalyst solutions that is further deposited on a support. In order to control size and shape of metallic nanoparticles in solution, organic stabiliser

[168] H. Tao, J. Ding, C. Xie, Y. Gao, J. Song, Z. Sun, Nanotechnology 2018, 29, 75708.
[169] G. Li, H. Yang, M. Cheng, W. Hu, L. Tian, W. Mao, R. Nie, Molecular Catalysis 2018, 455, 95.
[170] S. Cao, J. R. Monnier, C. T. Williams, W. Diao, J. R. Regalbuto, J Catal 2015, 326, 69.

with terminal functional groups interacting with the metal NPs is commonly used as it prevents excessive growth of NPS during their synthesis Once the particles are deposited on the support, the stabilizer agent is removed *via* thermal, chemical, UV-ozone or plasma treatments, as otherwise it would block the surface active sites. This removal is however not easy due to the strong interaction of the metal NPs and stabilizing molecules otherwise, aggregation of metal NPs may occur. Moreover often during the removal process, mostly oxidative heat treatment, the size and the morphology of the synthetized NPs changes drastically.

Bock et al. reported on a facile method to control the size of Ru-Pt bimetallic nanoparticles based on the preparation of colloid NPs solution in ethylene glycol and mixing it with a carbon support. Ethylene glycol acts as a reducing agent for the Pt and Ru precursor salts while itself it gets oxidized to glycolic acid which could interact with metal colloids forming chelate-type complexes *via* its carboxyl groups and therefore preventing the NPs from aggregation. Depending on the pH of the colloid solution glycolic acid is present in its deprotonated form as the glycolate anion A^- (basic pH) or in its protonated form HA (acidic pH). Therefore, pH of the solution during synthesis is a key factor for controlling catalyst particle size since the interactions between the metal particles and glycolic acid are smaller, meaning HA would be poor stabilizer while stronger interactions are formed between the glycolate anion and its stabilizing force is higher. Since the changes in the glycolate and glycolic acid concentrations take place within the pH range between 6 and 2, the metal particles are expected to be the smallest at pH > 6 and the largest when pH < 2. The authors showed that they obtained Ru-Pt/C with particles size between 0.7 nm and 4 nm depending on the initial NaOH concentration during the synthesis step (Figure 17). The remaining stabilizer can be oxidatively removed either electrochemically or by oxidative heat treatment already at 160°C.[171]

In another study of Morawa Eblagon et al. Ru nanoparticles were synthetized in a solution using polyaromatic amine-containing compounds (aminoethylcarbazole, aminoanthracene and aminoanthraquinone) as stabilizers by means of three different methods: modified polyol reduction, borohydride reduction and phase-transfer method. All of the obtained ruthenium nanoparticles displayed a very small diameter between 1–3 nm.

[171] C. Bock, C. Paquet, M. Couillard, G. A. Botton, B. R. MacDougall, J.A.C.S. 2004, 126, 8028.

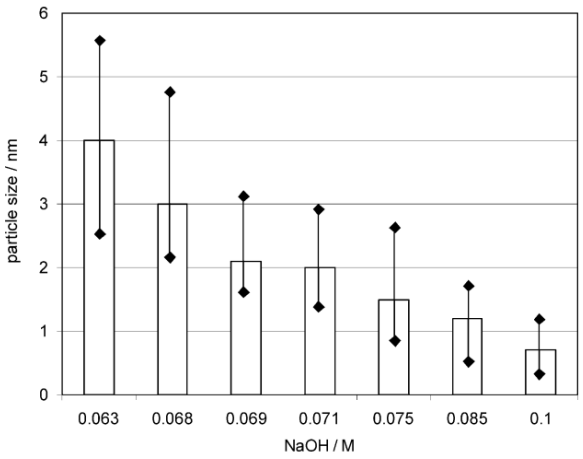

Figure 17. Average particle size dependence on the NaOH concentration in the ethylene glycol synthesis solution.[171]

Further the authors investigated the influence of different parameters such as temperature, stirring speed and ageing time on particle size using modified polyol process and biphasic method. Generally, the later one allowed achieving smaller nanoparticles with a very narrow distribution. The particle size was found to be strongly dependent on the amount of stabiliser used where the smaller NPs are obtained for higher concentrations of amines. In case where no stabilizer was used the particles with no well-defined shape and with broad size distribution centred at 6.33 nm were formed. Temperature in the polyol process was also found to affect the NPs size despite the type of stabilizer used as the higher the temperature used, the higher the nucleation rate and therefore the smaller the nanoparticles obtained. Moreover the higher the stirring speed the smaller particles since the growth of particles seem to be restricted. The authors also tested the obtained catalysts in the hydrogenation of cinnamaldehyde and showed that the material prepared in polyol process showed outstanding performance giving >90% conversion and selectivity.[172]

Many studies have focused also on using polymers or dendrimers to stabilize metal nanoparticles by taking advantage of their binding affinity as well as the steric bulk of their 3D framework. For example Jones at el. Prepared Ru/C catalysts *via* sol-immobilisation method using poly vinyl alcohol (PVA) to prevent aggregation of Ru and $NaBH_4$ as chemical reducing agent. High GVL yield was

[172] K. Morawa Eblagon, T. Valdes-Solis, K.M. Kerry Yu, A. J. Ramirez-Cuesta, S. Chi Tsang, Int. J. Nanoparticles, 3, 2010, 104.

reported (90%) when using such prepared catalyst in the LA hydrogenation (100°C, 5 bar H_2, 1 h) in contrast to the catalysts obtained without the PVA (50% of GVL yield). Possibility to maintain high dispersion of Ru on carbon support when using a stabilizer was the reason for improved performance, however it was also noted that the excess of PVA caused blocking the active sites.[173]

Nemanashi and co-workers on the other hand used hydroxyl-terminated dendrimers as templating agent for the synthesis of dendrimer-encapsulated Ru and Pt nanoparticles which were subsequently deposited on TiO_2 and SiO_2 supports *via* the wet-impregnation method. Also in this case $NaBH_4$ was utilized to reduce the Ru and Pt. The NPs were characterized by a very small average particles size of 1.2 nm and 1.7 nm for Pt and Ru, respectively, and narrow size distribution. The catalysts were used for LA hydrogenation (150 °C, 10 bar H_2, 5 h) and gave nearly 100% of LA conversion and selectivity to GVL.[174]

As a "greener" response for using dendrimers which are toxic and which the synthesis is rather complicated was offered by Chen et al. who used water-soluble cyclodextrin polymer prepared through cross-linking of β-cyclodextrin (β-CD) and polyethylene glycol diglycidyl ether (PEGDE). Ru nanoparticles incorporated to the synthetized co-polymer (PEG-CD) were reduced using $NaBH_4$ and importantly, no organic solvent was used in the catalyst preparation process. The authors reported the formation of highly dispersed particles with the average size of 1.7 nm which was smaller than the Ru obtained when using PVP or PEGDE as stabilizers (2.3 nm and 3.9 nm respectively). Among all these catalysts, Ru/PEG-CD exhibited the highest activity and selectivity, leading to 97% LA conversion and 99% selectivity to GVL after 4.0 h (80°C, 40 bar H_2). Importantly high dispersion was maintained even after 4th run of the LA hydrogenation.[175]

A slightly different but an interesting and simple approach was also used by Lee et al. who synthetized bimetallic Fe-Ru oxide nanoparticles by the liquid phase plasma (LPP) method. In this process aqueous solutions composed of Fe and Ru chlorides and cetyltrimethylammonium bromide (CTAB) as an anticoagulant were put into the LPP reactor to generate the Fe-Ru oxide nanoparticles. It was shown that using this facile method allows controlling the size of bimetallic oxide particles by adjusting the LPP

[173] D. R. Jones, S. Iqbal, P. J. Miedziak, D. J. Morgan, J. K. Edwards, Q. He, G. J. Hutchings, Topics in Catalysis 2018, 61, 833.
[174] M. Nemanashi, J.-H. Noh, R. Meijboom, Appl Catal A, General 2018, 550, 77.
[175] M. Chen, Q. Dong, W. Ni, X. Zhao, Q. Gu, G. Tang, D. Li, W. Ma, and Z. Hou, Chemistry Select 2017, 2, 10537.

reaction time. The particles of 5 nm were obtained after 10 min and they grew up to 50-80 nm for the reaction time of 60 min.[176]

So far all the presented methods used some type of organic molecules as stabilizer for spatial-isolation of metal particles. The main disadvantage of this approach is the risk of blocking the active sites by those molecules and therefore decreasing substantially the catalytic activity of the prepared catalyst. Another drawback is that very often removal of the stabilizer is related to some kind of treatment that might change the final size and dispersion of the particles. Competitive approach for dispersing and stabilizing metal NPs is to immobilize them within mesoporous support materials of well-defined pores. An interesting example of this strategy was presented by Kuwahara et al. who prepared Ru NPs supported on Zr-containing spherical mesoporous silica. Zr sites embedded within the mesoporous SiO_2 that was prepared by the sol-gel process have an ability to disperse and stabilize Ru nanoparticles. Highly dispersed NPs were obtained with the average size of 1.24 nm. The materials containing different amount of Zr were prepared and tested in methyl levulinate hydrogenation (70 ^{o}C, 5 bar H_2, 4 h) and the best catalyst gave 67% of GVL yield with almost 100% selectivity which was much better than for Ru particles supported on the material without Zr sites or conventional silica for which Ru NPs size was also higher. The authors explained the formation of such small metal particles by the presence of smaller silica particles size in the prepared material and the short mesopore channels facilitating the incorporation of Ru species inside them as well as by the anchoring effect of Zr sites which prevent the Ru from growing into big agglomerates.[177]

As was shown only very few studies proposed a way to precisely control the Ru particles size by varying some process parameters. Most of the work concerns rather methods for achieving a high dispersion of small NPs and they lack of any information if the obtained size could be tuned in any way. But even those methods that offer size control possess many drawbacks in a form of using toxic organic molecules that could block the active sites or many step, complicated preparation process involving high temperature heat treatment which would prevent using such prepared materials in an industrial scale.

[176] S.-J. Lee, H. Lee, K.-J. Jeon, H. Park, Y.-K. Park, S.-C. Jung, Nanoscale Research Letters 2016, 11, 344.
[177] Y. Kuwahara, Y. Magatani, H. Yamashita, Catal. Today 2015, 258, 262.

1.8. Photodeposition method

1.8.1. Concept of the preparation method

The most widely used methods for preparing supported metal catalysts combine the implementation of consecutive elemental operations, with first the introduction of the metal precursor onto the support carrier, achieved usually *via* incipient wetness or wet impregnation, ion exchange, precipitation, co-precipitation, deposition–precipitation or deposition of a colloidal precursor, further a drying/calcination step, and finally an activation/reduction step to get the supported metallic nanoparticles.[178] The reduction treatment usually consists in a thermal treatment with the use of external hydrogen, or in a chemical reduction in solution with reducing agents such as $NaBH_4$, hydrazine or formaldehyde. Depending on the method, the supported catalysts can suffer from heterogeneous and/or broad metal particle size distributions, from detrimental temperature-activated side-reactions between the metal precursor and the support and from limitations in terms of metal loadings.

The photon-assisted synthesis of supported nanoparticles - often reported commonly as photodeposition synthesis method by simplification, is an elegant and sustainable alternative to classical methods for the controlled preparation of small size supported metal nanoparticles, provided that the support carrier is a semi-conductor material. Following a study of Kraeutler and Bard in 1978[179] where the authors showed that well-dispersed nanoparticles of Pt could be obtained on anatase TiO_2 by illuminating a slurry composed of anatase powder, hexachloroplatinic acid, hydrochloric acid, sodium carbonate and acetic acid, the interest in photodeposition has expanded significantly.

The underlying strategy of the photodeposition method is to use the redox photo-activity of the host semi-conductor activated under appropriate irradiation for promoting electrons to the conduction band of the semi-conductor, further able to reduce metal ions adsorbed at the surface of the semi-conductor support (Figure 18).

[178] F. Pinna, Catal. Today 1998, 41, 129.
[179] B. Kraeutler, A. J. Bard, J. Am. Chem. Soc. 1978, 100, 4317.

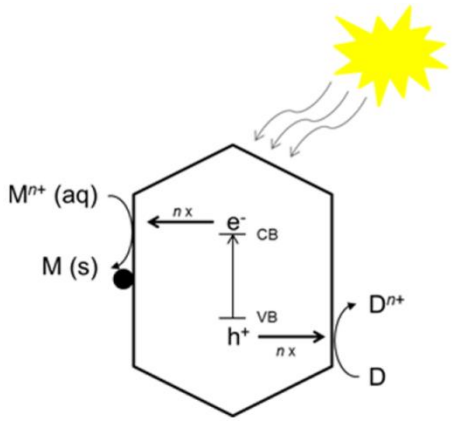

Figure 18. Schematic overview of a reductive photodeposition;VB- valence band; CB - conduction band; M -metal; D - electron donor; n - number of electrons (or holes) involved.

This can result in the synthesis of well-defined metal nanoparticles on the support material, offering a potential control over the supported nanoparticle size, their distribution and their oxidation state.[180] The method is usually implemented by irradiating a suspension of the semi-conductor support containing the metal precursor salt.

Several conditions are required for the photodeposition to take place[180]:

a) the photon energy of the irradiation light has to be equal or larger than the energy band gap of the semiconductor;

b) the reduction potential of the metal ion has to be more positive than the conduction band of the semiconductor;

c) the efficient separation and migration of photogenerated electron-hole pairs is necessary;

d) the semiconductor needs to provide sufficient active surface sites.

Photodeposition is a one-step and low-temperature synthesis method that does not require any final thermal treatment, any external hydrogen, or any chemical reductant and therefore is a very attractive alternative to more conventional methods such as impregnation. The photodeposition method has been mainly used for synthesizing metallic nanoparticles on a semi-conductor photocatalyst with controlled metal/semi-conductor interface for improving the overall photocatalytic activity of the material, in both gas- and liquid-phase environmental remediation oxidation/reduction reactions, as well as in hydrogen production-related reactions such as water-splitting or alcohol reforming. The investigated metals mainly

[180] K. Wenderich, G. Mul, Chem. Rev. 2016, 116, 14587.

included Ag[181], Au[182], Pd[183], Pt[184], Cu[185] and Rh[186], using usually nitrates, chlorides, acetylacetonates and chloric acids as metallic salts, and TiO_2 as semi-conductor support, although materials such as $BiVO_4$, ZnO, WO_3 or CdS were also used. The materials prepared by means of this photo-assisted method include core – shell particles[187], bimetallic co-catalysts[188] or even trimetallic co-catalysts.[189]

The photodeposition method was used also for preparing thermal catalysts with enhanced performances when compared to those prepared *via* classical impregnation or coprecipitation methods, for instance in the case of mono- and bi-metallic catalysts (Pt, Pt-Ag) on ceria and titania support.[190,191]

1.8.2. Examples of comparative studies

Encouraged by the advantages of the photodeposition method over the ones requiring several steps and additional reducing agent (thermal or chemical), researchers have compared the activity of the catalysts prepared by the photodeposition to that obtained on catalysts prepared by the most common conventional impregnation methods.

One of the exemplary study is done by Jiang et al. who prepared Pt/TiO_2 *via* the photodeposition with glycerol as sacrificial agent under anaerobic conditions using solar light and the impregnation followed by the reduction either in H_2 at 400°C or using $NaBH_4$/NaOH solution. It was found that the Pt particle size was on the order of 2 nm for all preparation methods; however the oxidation state of the Pt nanoparticles varied between the methods. Photo-assisted synthesis method allowed obtaining exclusively Pt in the metallic state while using the classical impregnation resulted in a formation of Pt^0, Pt^{II} and Pt^{IV} species which significantly lowered the catalytic activity of those materials in the photocatalytic glycerol

[181] S. Parastar, S. Nasseri, S.H. Borji, M. Fazlzadeh, A.H. Mahvi, A.H. Javadi, M. Gholami, Desalin. Water Treat. 2013, 51, 7137.
[182] A. Tanaka, S. Sakaguchi, K. Hashimoto, H. Kominami, Catal. Sci. Technol. 2014, 4, 1931.
[183] R. Camposeco, S. Castillo, I. Mejia-Centeno, J. Navarrete, J. Marin, Mater. Charact. 2014, 95, 201.
[184] M. Maicu, M.C. Hidalgo, G. Colón, J.A. Navío, J. Photochem. Photobiol. A Chem. 2011, 217, 275.
[185] A.J.J. Lennox, P. Bartels, M.M. Pohl, H. Junge, M. Beller, J. Catal. 2016, 340, 177.
[186] K. Maeda, D. Lu, K. Teramura, K. Domen, Energy Environ. Sci. 2010, 3, 471.
[187] A. Tanaka, K. Fuku, T. Nishi, K. Hashimoto, H. Kominami, J. Phys. Chem. C 2013, 117, 16983.
[188] J.M. Herrmann, J. Disdier, P. Pichat, A. Fernandez, E. Gonzalez, G. Munuera, C.J. Leclercq, J Catal. 1991, 132, 490.
[189] P. Qiao, S. Zou, S. Xu, J. Liu, Y. Li, G. Ma, L. Xiao, H. Lou, J. Fan, J. Mater. Chem. A 2014, 2, 17321.
[190] S. Scirè, C. Crisafulli, S. Giuffrida, C. Mazza, P.M. Riccobene, A. Pistone, G. Ventimiglia, C. Bongiorno, C. Spinella, Appl. Catal. A Gen. 2009, 367, 138.
[191] S. Scirè, C. Crisafulli, S. Giuffrida, G. Ventimiglia, C. Bongiorno, C. Spinella, J. Mol. Catal. A Chem. 2010, 333, 100.

reforming. It was however also mentioned that metallic Pt could be obtained only in dilute suspension of P25 and at low glycerol concentration otherwise oxidized Pt was formed.[192] Arsana et al. on the other hand prepared silver and copper doped zinc oxide photocatalysts by means of photodeposition and impregnation methods. The metal doped ZnO synthetized by photodeposition proved to be more effective in photocatalytic degradation of acid red 142 dye than the ones prepared by the impregnation method. The difference in activity was explained in terms of oxidation state of the metals. The photodeposition yields Ag and Cu directly in their metallic form (adsorbed ions are reduced by photogenerated electrons) on the surface of ZnO while oxidized Ag^{+} and Cu^{2+} are produced after impregnation. Those oxidized Ag^{+} and Cu^{2+} consume electrons during the photocatalytic process leading to the overall decrease in photocatalytic activity.[192]

Very interesting examples of using photodeposition for the preparation of thermal catalysts have been provided by Scirè et al. who studied Ag/TiO_2 and Ag/CeO_2 in methanol combustion. Catalysts prepared through the photochemical approach exhibited much higher catalytic activity comparing to the ones prepared by the incipient wetness impregnation (Ag/TiO_2) or coprecipitation (Ag/CeO_2) methods. In case of titania supported catalysts, no significant differences were found in terms of the Ag particle size. Further TEM analysis showed however the presence of spherical, multiple twinned, highly defective Ag crystallites for the sample prepared by the photodeposition that were concluded to be responsible for the higher activity of this sample compared to the one prepared by the impregnation (presence of more faceted, defect-free aggregates). In case of ceria supported system, it was impossible to perform TEM analysis due to the very low contrast however the XRD data revealed a different mean particle size between the sample prepared by the photochemical approach and that prepared by the conventional coprecipitation technique with estimated mean diameters of <3–4 nm and 6.5 nm, respectively. Therefore better performance in methanol combustion was explained with the formation of smaller Ag nanoparticles.[193] Similar observations were further reported by the same group regarding the Pt catalysts supported on titania and ceria in acetone and toluene combustion. Higher activity of the materials prepared by photodeposition was due to the formation of homogeneously distributed, small Pt NPs with

[192] X. Jiang, X. Fu, L. Zhang, S. Meng, S. Chen, J Mat Chem A, 2015, 3, 2271.
[193] S. Scirè, C. Crisafulli, S. Giuffrida, C. Mazza, P.M. Riccobene, A. Pistone, G. Ventimiglia, C. Bongiorno, C. Spinella, Appl. Catal. A Gen. 2009, 367, 138.

diameters in the range of 1.6–2 nm and narrow size distribution. In contrast, the catalysts prepared by the impregnation exhibited both local massive Pt aggregates and very small Pt particles giving non homogenous distribution.[194]

Another interesting example when the photodeposition method proved to be beneficial for achieving improved catalytic performance was reported by Han et al. In this study, photochemical approach led to site specific deposition of Ag on the Pt surface to form a core-shell (Pt@Ag) like structure supported on TiO_2. Therefore, for the same Ag loadings, Pt-Ag/TiO_2 prepared by photodeposition displays higher surface Ag enrichment than the one prepared by impregnation and having only Pt-Ag ensemble. Presence of core-shell structures enhanced the catalyst stability and the selectivity towards ethylene in the hydrodechlorination of 1,2-dichloroethane.[195]

As seen based on the presented examples, photodeposition method could be beneficial for the preparation of highly active or selective catalysts in many various reactions. The simplicity of this method and the possibility to produce small size of metal particles with homogenous distribution make photodeposition a very attractive and reliable alternative to the classical catalyst preparation method such as impregnation.

1.8.3. Photodeposition of ruthenium nanoparticles

Using a photodeposition method for synthesizing Ru nanoparticles dispersed on a support remained scarce till now. Using TiO_2, CeO_2, CdS, $CuInS_2$ quantum dots and very recently also $KTaO_3$ as host semiconductors, most of the studies were targeting the enhancement of the photocatalytic activity of the prepared materials in liquid phase reactions such as phenol degradation, water splitting or during photoelectrochemical reactions. Deposition in those cases was achieved using $(NH_4)_3RuCl_6$ or $RuCl_3$ as ruthenium salts, by applying UV-vis or visible light irradiation. An overview of the photocatalysts consisting in ruthenium nanoparticles supported on various semiconductors prepared for different applications as well as the preparation conditions used for the photodeposition method is presented in Table 1.

[194] S. Scirè, C. Crisafulli, S. Giuffrida, G. Ventimiglia, C. Bongiorno, C. Spinella, J. Mol. Catal. A Chem. 2010, 333, 100.
[195] Y. Han, J. Zhou, W. Wang, H. Wan, Z. Xu, S. Zheng, D. Zhu, Appl. Catal. B: Environ. 2012, 125, 172.

Table 1. Overview of the ruthenium nanoparticles photodeposited on various semiconductors.

Catalyst	Photodeposition conditions	Reaction	Comments	Ref.
Ru/TiO_2	30 W Hg lamp, pH 4, anaerobic, 40 °C or 55°C, in water	Photocatalytic dehydrogenation of 2-propanol	improved photoactivity of TiO_2	196
0.4% Ru/TiO_2	UV-irradiation, in water/methanol	Photocatalytic H_2SO_3 oxidation	improved photoactivity of TiO_2	197
0.75% Ru/TiO_2	180 W Hg lamp, $RuCl_3$, anaerobic, in water/methanol (10:1)	hydrogen photoevolution from water-methanol	simultaneous Ru^{3+} reduction and H_2 photoproduction	198
Ru/CdS	1000 W tungsten-halogen lamp, $RuCl_3$, pH 4.5	-	Improved performance of CdS photoanode	199
$CdS/0.3\%Ru/TiO_2$ three-component nanojunction system	150-W Xe lamp, anaerobic, in water/ethanol	photocatalytic degradation of methylene blue	improved photoactivity of CdS/TiO_2	200
RuO_2/TiO_2	Xe or Hg arc lamp, $KRuO_4$, in water	UV light driven water splitting	improved photoactivity of TiO_2	201
$0.1\%Ru/CeO_2$	400 W high-pressure mercury arc, anaerobic, in water with oxalic acid, 25°C	photocatalytic decomposition of acetic acid	improved photoactivity of CeO_2	202
0.5% $Ru/CuInS_2$ quantum dots	450 W high-pressure mercury lamp, $(NH_4)_2RuCl_6$	H_2 evolution from water	Improving the photoactivity of quantum dots	203
Ru/decahedral TiO_2	250 W Xe lamp, $RuCl_3$, anaerobic, in ethanol	photocatalytic phenol degradation	Enhanced phenol degradation rate under UV-vis light	204
2% $Ru/KTaO_3$	250 W Xe lamp, $RuCl_3$, anaerobic, in ethanol	Photocatalytic pollutant decomposition (phenol, toluene, formic acid)	improved photoactivity of $KTaO_3$	205

Up to date there are very few studies that focused in more details on the ruthenium particles themselves rather than on the activity of the resulting metal/semiconductor photocatalysts. In early study published by Sobczynski et al. the hydrogen evolution from a methanol/water mixture was monitored

[196] S. Teratani, J. Nakamichi, K. Taya, K. Tanaka, Bull Chem Soc Japan, 1982, 55, 1688.
[197] K.-H. Stadler, H. P. Boehm, Zeitschrift für Physikalische Chemie Neue Folge, Bd. 1985, 144, 9.
[198] A. Sobczynski, T. Jakubowska, S. Zielinski, Monatshefte Fur Chemie Chem. Mon. 1989, 120, 101.
[199] I. B. Rufus, V. Ramakrishnan, B. Viswanathan, J.C. Kuriacose, J Mat Sci Lett 1996, 15, 1921.
[200] S. Shen, L. Guo, X. Chen, F. Ren, C. X. Kronawitter, S. S. Mao, J Green Nanotech: Mat Sci & Eng, 2010, 1, 94.
[201] A. Mills, P.A. Duckmanton, J. Reglinski, Chem. Commun., 2010, 46, 2397.
[202] A. Tanaka, K. Hashimoto, H. Kominam, Chem. Lett. 2011, 40, 354.
[203] T.-L. Li, C.-D. Cai, T-F. Yeh, H. Teng, J Alloys and Compounds 2013, 550, 326.
[204] E. Grabowska, M. Diak, T. Klimczuk, W. Lisowski, A. Zaleska-Medynska, Mol Catal 2017, 434, 154.
[205] A. Krukowska, G. Trykowski, M. Jerzy Winiarski, T. Klimczuk, W. Lisowski, A. Mikolajczyk, H.P. Pinto, A. Zaleska-Medynska, Appl Surf Sci, 2018, 4, 56.

during the photodeposition synthesis of Ru particles on anatase TiO_2 using $RuCl_3$ as precursor salt.[206] The authors observed enhanced hydrogen evolution despite a non-homogeneous particle distribution was observed over the support.

Very recent study of Krukowska and coworkers reported on a preparation of mono and bimetallic catalysts supported on $KTaO_3$. Ruthenium as well as a series of other metals (Au, Ag, Pd, Pt and Rh) was deposited and bimetallic systems were prepared by either simultaneous or subsequent photodeposition. The authors performed very detailed physicochemical characterisation of all the materials and investigated the influence of both the type and the amount of noble metal precursor as well as photodeposition method using techniques such UV-vis spectroscopy, N_2 physisorption, TEM, SEM, powder XRD, Raman spectroscopy and XPS. In general it was found that the morphology, structure and size of mono and bimetallic catalysts are corresponded to individual type, surface energy, reduction potential and photodeposition method of noble metal. Moreover, improved visible light activity in phenol and toluene degradation as well as enhanced photocatalytic H_2 generation from formic acid over all prepared materials were observed.[207]

[206] A. Sobczynski, T. Jakubowska, S. Zielinski, Monatshefte Fur Chemie Chem. Mon. 1989, 120, 101.

[207] A. Krukowska, G. Trykowski, M. Jerzy Winiarski, T. Klimczuk, W. Lisowski, A. Mikolajczyk, H.P.

CHAPTER 2

2. EXPERIMENTAL PROCEDURES

In this chapter, the material preparation protocols have been described as well as the details regarding the analytical techniques employed for the investigation and the catalytic tests conditions and procedures.

2.1. Preparation of the TiO_2 based supports using sol-gel technique

Ca-modified TiO_2 was synthesized according to a sol-gel method in basic conditions using titanium tetraisopropoxide (TTIP, 97%, Sigma–Aldrich) and calcium nitrate ($Ca(NO_3)_2 \cdot 4H_2O$, 99%, Sigma–Aldrich) as precursors. First, TTIP was added to a 40 mL ethanolic solution of calcium nitrates, with calcium contents corresponding to 1, 5, 10 and 20 wt. % relatively to TiO_2, before a similar volume of water was added dropwise to solution. After rectification of the pH to 9 by adding ammonia (Carlo Erba, 30% aqueous solution), the solution was left under agitation at room temperature until dry paste was obtained. The resulting powder was further dried at 100°C for 8 h and finally calcined at 500°C in static air for 3 h with a heating rate of 5°C/min to form the Ca-TiO_2 supports. The prepared materials were labelled as 1Ca-T500, 5Ca-T500, 10Ca-T500 and 20Ca-T500. A reference TiO_2 support was synthesized according to a similar sol-gel method in the absence of any calcium nitrate, and the resulting material after calcination at 500°C was labelled as T500. Aeroxide© P25 TiO_2 (Evonik) has been used as a commercial TiO_2 reference.

2.2. Preparation of the Ru catalysts

2.2.1. Incipient wet impregnation

Ruthenium catalysts were prepared by incipient wet impregnation from aqueous $RuCl_3$ (Sigma-Aldrich, min 40% Ru content) solutions on commercial TiO_2 (Aeroxide© P25, Evonik), TiO_2 prepared by sol-gel method (T500) and Ca modified TiO_2 supports to obtain the 5 wt. % of the Ru loading. To 30 mL of the aqueous solutions of $RuCl_3$, 1 g of the support was added and stirred for 5 min. Then, the dispersion was left without mixing in order for the solution to penetrate the pores of the supporting material and after 24

h the remaining solvent was evaporated under vigorous stirring. The catalysts were then dried for 2 h at 120°C and reduced for 1 h in hydrogen flow at 200°C and labelled as 5%Ru/P25-I, 5%Ru/T500-I, 5%Ru/1Ca-T500-I, 5%Ru/5Ca-T500-I, 5%Ru/10Ca-T500-I and 5%Ru/20Ca-T500-I.

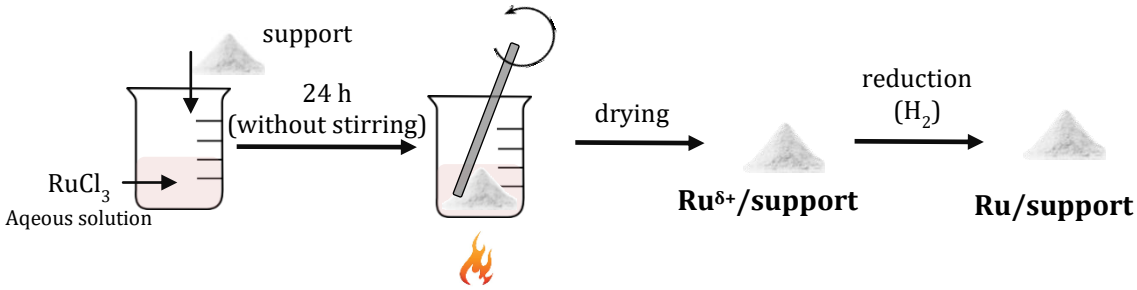

Figure 19. Scheme of the catalyst preparation by incipient wet impregnation method.

2.2.2. Photodeposition

Aeroxide© P25 TiO_2 (Evonik) as well as prepared by sol-gel method TiO_2 and Ca-modified TiO_2 have been used as supports for synthesizing the Ru/TiO_2 catalysts under solar light irradiation. Ruthenium (III) acetylacetonate $(Ru(acac)_3$, 97%, Sigma-Aldrich) and ruthenium (III) chloride hydrate ($RuCl_3 \bullet xH_2O$, min 40% Ru content, Sigma-Aldrich) were used as ruthenium precursors. Dissolution of the $Ru(acac)_3$ precursor was achieved in distilled water under stirring at 50°C for 2 days, whereas the $RuCl_3$ precursor was dissolved under stirring in 10 ml of methanol for 12 h, prior to the addition of 90 ml of distilled water to give a methanol:water ratio of 1:9 v/v. Methanol was used as a co-solvent to ensure the presence of well resolved signal in UV-VIS spectrometer. In each experiment, 100 mg of TiO_2 support was dispersed under stirring in 100 mL of ruthenium solution in a beaker-type glass reactor, with a precursor concentration depending on the targeted Ru content to be achieved in the Ru/TiO_2 material. Prior to irradiation, the suspension was stirred in the dark for 1 h to ensure the establishment of the adsorption-desorption equilibrium. In the case of $Ru(acac)_3$, pH value of the suspension was adjusted with NaOH to pH 10. In case of $RuCl_3$ and the deposition of 5 wt. % Ru, after stirring the suspension for 1 h in the dark, pH value was adjusted with NaOH to pH 8 and the stirring was continued for another 1 h in the dark. A typical photodeposition synthesis was performed at a TiO_2 concentration of 1 g/L by exposing the suspension under stirring to a 500 W/m^2 solar light irradiation within an ATLAS Suntest XLS+ reaction

chamber (Xenon arc lamp NXE 2201). The deposition was followed by UV-vis spectrophotometry using a Cary 100Scan Varian spectrophotometer monitoring the disappearance of the main absorption peak at λ = 272 nm and λ = 324 nm for $Ru(acac)_3$ and $RuCl_3$ precursors, respectively. After completion of the process, the suspended catalysts were recovered by filtration and dried at 100°C for 1 h. The prepared catalysts were labelled as Ru/P25-P, Ru/T500-P, 5%Ru/1Ca-T500-P, 5%Ru/5Ca-T500-P, 5%Ru/10Ca-T500-P and 5%Ru/20Ca-T500-P.

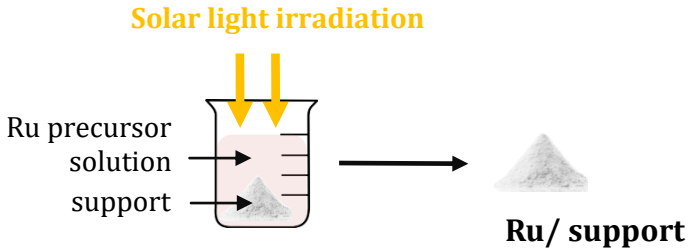

Figure 20. Scheme of the catalyst preparation by photodeposition method.

2.3. Characterization techniques

2.3.1. X-ray diffraction

X-ray powder diffraction (XRD) is a non-destructive analytical technique to identify crystal phase, phase composition and crystallite average size of crystallized materials. The principle of X-ray diffraction is based on constructive interference occurring when monochromatic X-rays are diffracted by a crystalline sample. The X-rays generated by a metallic anode are filtered to produce monochromatic radiation, collimated to concentrate, and directed toward the sample. The interaction of the incident rays with the sample then produces constructive interference when the diffracted rays satisfy Bragg's Law:

$$n\lambda = 2d\sin\theta$$

Where n is a positive integer, λ is the wavelength of incident wave, θ is the scattering angle and d is the interplanar distance for lattice planes.

The crystallographic structure of the powders has been characterized by X- ray diffraction patterns (XRD) recorded on a D8 Advance Bruker diffractometer in a θ/θ mode and using the $K_{\alpha 1}$ radiation of a Cu anticathode (λ = 1.5406 Å). The anatase mean crystallite size was calculated from the Scherrer equation applied with the usual assumption of spherical crystallites. The database of patterns is from International

Center for Diffraction Data's JCPDS files. Anatase cell parameters and cell volume were calculated through the Rietveld refinement method using the FullProf software.[208]

2.3.2. N_2 physisorption

Gas sorption among other methods is routinely used in heterogeneous catalysis to characterize porous materials. Brunauer–Emmett–Teller (BET) theory can be used to derive the specific surface area of a solid material from the physical adsorption of gas molecules on a solid surface. In this model, the specific surface area is obtained by experimentally building the adsorption isotherm of an adsorbate gas at its boiling temperature (in case of N_2 of −196°C). The specific surface area in m^2/g is determined by calculating the amount of adsorbate gas corresponding to a mono-molecular layer on the surface as a function of the relative pressure, using the so-called BET equation:

$$\frac{1}{V_a(\frac{P_0}{P}-1)} = \frac{C-1}{V_m C} \times \frac{P_0}{P} + \frac{1}{V_m C}$$

where:

P - Partial vapor pressure of adsorbate gas in equilibrium with the surface at boiling point of liquid nitrogen, in Pa

P_0 - Saturated vapor pressure of adsorbate gas at given temperature, in Pa

V_a - Volume of gas adsorbed per gram of solid at standard temperature and pressure, in mL/g

V_m - Volume of a monolayer of gas adsorbed per gram of solid, in mL/g

C – adsorption constant

The measurements have been carried out on a Micrometrics Tristar 3000 using N_2 as adsorbent at −196°C with a prior outgassing at 200°C over-night in order to desorb the impurities or moisture. The Brunauer-Emmett-Teller (BET) specific surface area has been calculated from the N_2 adsorption isotherm. Pore volume was determined using Barrett-Joyner-Halenda (BJH) model from the desorption branch of the isotherm.

[208] H. M Rietveld. J Appl Crystallography, 1967, 22, 151.

2.3.3. Isoelectric point measurements

In order to determine the changes in the surface charge in the Ca-modified titanias, the isolectric point was measured for the samples. The isoelectric point is the pH value at which the zeta potential is approximately zero and therefore can be determined by performing the zeta potential titration. Zeta potential measurements were conducted on a Malvern Zetasizer NanoZS system with irradiation from a 632.8 nm He-Ne laser. The ζ-potential was determined from the measured electrophoretic mobility using the Smoluchowski approximation.[209] The measurements were performed at different pH values starting from basic pH 9 adjusted with NaOH and gradually decreasing pH with HCl by means of the autotitrator.

2.3.4. FTIR-CO chemisorption

Fourier-transform infrared spectroscopy (FTIR) was used to study the adsorption forms of CO on the catalyst surface. CO adsorption and desorption measurements were carried out with Nicolet 6700 FTIR spectrometer equipped with MCT detector made by Thermo Scientific, using transmission cell. Number of scans was chosen as 64 and spectral resolution was set as 4 cm^{-1}. Each sample was prepared by grinding the exact mass (20 mg) and pressing to obtain tablets. Before the measurements, samples were reduced in H_2 flow at 200°C for 1h. After this time samples were cooled down to 40°C in argon. Then carbon monoxide sorption was performed for 20 min and during this process spectra were collected every 5 minutes. After that time CO desorption was performed for 20 min in Ar flow. During desorption, spectra was collected every 2 min. Gas flow was set every time as 20 ml/min.

2.3.5. Inductively coupled plasma atomic emission spectroscopy

The ruthenium content in the catalysts was determined by inductively coupled plasma atomic emission spectroscopy (ICP – AES). This method is based on the measurement of the intensity of light emitted by

[209] N. G. Van Kampen, Stochastic processes in Physics and Chemistry. NorthHolland, Amsterdam, 1961.

atoms or ions at specific wavelengths using atomic emission spectroscopy. The argon plasma (temp. 6000 - 10000°C) is used for atomization and excitation of the sample atoms.

2.3.6. Temperature programmed reduction

The temperature-programmed reduction (TPR) is one of the basic techniques used for the physicochemical characterization of the catalysts, mainly for studying their reduction susceptibility and the various reduction stages. In the described method, reducing gas (most often a mixture of hydrogen and argon or hydrogen and nitrogen) flows continuously through the catalyst bed, whose temperature changes linearly over time. The TPR profiles indicate the hydrogen consumption as a function of temperature. Temperature-programmed reduction was performed on AMI1 system (Altamira Instruments) equipped with a thermal conductivity detector (TCD) and was used for examining the catalyst reducibility. The TPR profiles were recorded after performing a slight in-situ oxidative treatment in air (200°C for 30 min) on the impregnated supports after a drying step, allowing the decomposition of the chloride precursor. The catalysts were submitted to H_2/Ar (5:95 v/v) flow of 20 cm^3/min using a heating rate of $10^oC\ min^{-1}$. Each time, precisely 0.100 g of the sample was used.

2.3.7. Transmission electron microscope

The transmission electron microscope (TEM) is a microscopy technique using an electron beam as “light source”, generated and accelerated under ultrahigh vacuum in the column of the microscope. This microscope operates in a bright field recording mode, meaning that the image is produced by the non-diffracted electron beam transmitted through a thin sample. Interaction between the electrons and the material leads to the recording of the image, possibly with nanometric resolution. The TEM technique provides information on size, morphology and structure of materials. Thicker regions of the sample or regions with a higher atomic number will appear dark, whilst regions with no sample in the beam path will appear bright.

The Ru nanoparticle size distribution of Ru/TiO_2 samples was determined by transmission electron microscopy using a JEOL 2100F with a point resolution of 0.2 nm. The samples were sonically dispersed in an ethanol solution before a drop of the solution was deposited onto a copper grid covered by a holey

carbon membrane for observation. The size distributions were calculated for each nanoparticle sample by averaging 300 particles from the TEM images using ImageJ software.

2.3.8. Scanning electron microscope

Scanning electron microscope (SEM) produces images of a sample by scanning the surface with a focused beam of electrons. The principle is based on the interactions of electrons with atoms at various depths within the sample producing various signals containing information about the sample surface topography and composition. Scanning electron microscopy and elemental mapping were performed in secondary electron mode on a JEOL JSM-6700 F FEG microscope.

2.3.9. X-ray photoelectron spectroscopy

X-Ray photoelectron spectroscopy (XPS) is a non-destructive and semi-qualitative analysis method that can provide essential information such as elemental composition, empirical formula, chemical state and electronic state of the elements within the surface layer of materials. The XPS principle is based on the measurement of the kinetic energy of photoelectrons emitted by the sample when irradiated by a low energy monochromatic X-ray beam under ultrahigh vacuum.

X-Ray Photoelectron Spectroscopy (XPS) characterization was performed on a ThermoVGMultilabESCA3000 spectrometer (Al Kα anode at hλ = 1486.6 eV). Deconvolutions of the obtained spectra were performed using CasaXPS Software. The energy shift due to electrostatic charging was subtracted using the adventious sp^2 carbon C 1s band at 284.6 eV. Contributions with Doniach–Sunjic shape[210] and a' S-shaped' Shirley type background[211] were used. Surface atomic ratios were derived using the appropriate experimental sensitivity factors.[212]

2.3.10. Time of flight secondary-ion mass spectrometry

Time-of-flight secondary ion mass spectrometry (ToF-SIMS) is a method of mass spectrometry in which an ion's mass-to-charge ratio is determined *via* a time of flight measurement. TOF-SIMS is used to

[210] S. Doniach, M. Sunjic, J. Phys. C Solid State Phys. 1970, 3 285
[211] D.A. Shirley, Phys. Rev. B. 1972, 5, 4709
[212] C.D. Wagner, L.E. Davis, M.V. Zeller, J.A. Taylor, R.M. Raymond, L.H. Gale, Surf. Interface Anal. 1981, 3, 211

characterize surface of solid materials and allows analysing composition and distribution of elements and ions on the surface of tested sample. ToF-SIMS measurements were performed using ION-TOF GmbH instrument (ToF-SIMS IV) equipped with a 25 kV pulsed Bi^+ primary ion gun in the static mode. The samples were pressed into pellets before the measurements and attached to the sample holder using double-sided tape. The analysed area corresponded to a 500 μm × 500 μm size square. For each sample, three spectra were collected. Charge, which accumulates during measurement, is neutralized by flood gun – electron beam with low energy. Depth of the analysis did not exceed 1 nm, mass resolution at m/z=29 was in the range of 4000-7000. The samples were stored and transported in disposable containers for avoiding any contamination.

2.3.11. Thermogravimetric analysis

Thermogravimetric analysis (TGA) was carried out with a 20% (v/v) O_2/N_2 mixture at a flow rate of 40 mL/min at a heating rate of 10°C/min from 25°C to 600°C using a Q 5000 TA Instrument thermoanalyzer.

2.4. Evaluation of the catalytic performances and test procedures

2.4.1. Liquid phase reactions of levulinic acid hydrogenation and formic acid decomposition

Liquid phase reactions of levulinic acid (LA) hydrogenation and formic acid (FA) decomposition were carried out in a Teflon-lined stainless steel autoclave (Berghof, Germany), equipped with a Teflon insert allowing a reaction volume of 45 ml (Figure 21).

Figure 21. Berghof BR-25 reactor used for the liquid phase catalytic tests. (berghof-instruments.com)

Levulinic acid hydrogenation (Figure 22) was performed with two different sources of hydrogen:

a) externally H_2 supplied from a gas cylinder;

b) formic acid as an internal H_2 source (FALA reaction).

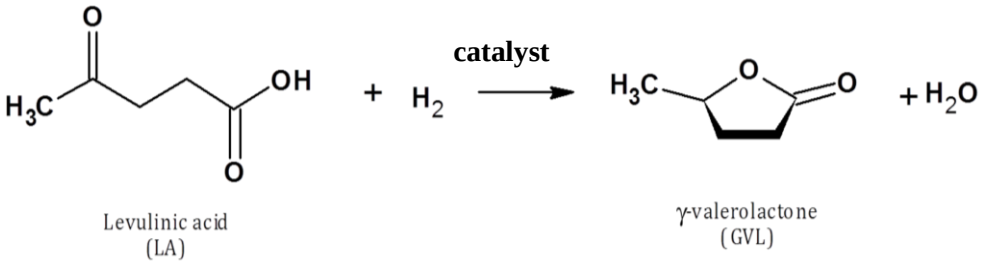

Figure 22. Reaction scheme of LA hydrogenation with internal hydrogen source.

In a typical LA hydrogenation experiment with external H_2 source, 1 g of LA, 0.15 g of catalyst and 30 ml of water were mixed in a Teflon-lined stainless steel autoclave (Berghof). The reactor was pressurized with H_2 to 5 bar and the temperature was maintained at 190 °C for 30 min. At the end of the reaction, the reactor was cooled down and the gas products were analysed using GC chromatography. Then, the remaining pressure was released and the reaction mixture was centrifuged to separate the solid catalyst and the product solution.

In a typical LA hydrogenation experiment with formic acid as internal H_2 source, 1 g of LA, 0.4 ml of FA, 0.6 g of a catalyst and 30 ml of water were mixed in a Teflon-lined stainless steel autoclave

(Berghof). The reactor was flushed with H_2 for 30 s and Ar for 15 s. Then, the temperature was raised and maintained at 190°C for 5 h. At the end of the reaction, the reactor was cooled down and the gas products were analysed using GC chromatography. Then, the remaining pressure was released and the reaction mixture was centrifuged to separate the solid catalyst and the product solution.

In a typical experiment of **formic acid decomposition (**Figure 23**)**, 0.4 ml of formic acid, 0.15 g of reduced catalyst, and 30 ml of distilled water were mixed in a Teflon-lined stainless steel autoclave (Berghof). The reactor was flushed with H_2 for 30 s and Ar for 15 s. The reactor was then heated to 190°C for 2 h. At the end of the reaction, the reactor was cooled down and the gas products were analysed using GC chromatography. Then, the remaining pressure was released and the reaction mixture was centrifuged to separate the solid catalyst and the product solution.

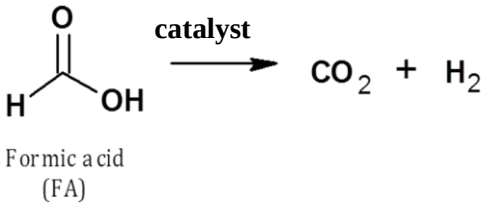

Figure 23. Reaction scheme of selective formic acid decomposition.

Reaction products were analysed by means of high-performance liquid chromatography (HPLC) and gas chromatography (GC).

2.4.2. High-performance liquid chromatography

Reaction residues were tested using high-performance liquid chromatography (HPLC). Chromatograph (Agilent Technologies 1260 Infinity) was equipped with Refractive Index Detector (RID). Samples were filtrated, diluted 10 times and injected to the instrument equipped with a REZEX ROA-Organic Acid column with polymer fulfilment (grain with sulfonic copolymer styrene –divinylbenzene). Temperature of the column was 60°C and 0.0025 M H_2SO_4 was used as an eluent with a flow of 0.6 ml/min.

Calculations for conversion of formic acid:

Based on a calibration curve: $y = ax + b$

where:

x – concentration of analysed compound, g/mL

y – peak area in chromatograph, -

$$x \cdot Z \cdot V_{H_2O} = m_{FA_i}$$

where:

m_{FAi} – mass of formic acid after reaction, in g,

Z – dilution factor (for HPLC measurement)

V_{H2O} – volume of water used in the reaction,

$$C_{FA} = \frac{m_{FA_i} - m_{FA_0}}{m_{FA_i}} \times 100\%$$

where:

C_{FA} – conversion of formic acid, in %,

m_{FAi} – mass of formic introduced to the reaction, in g,

m_{FA0} – mass of formic acid after the reaction, calculated using the calibration curve, in g.

Calculations for conversion of levulinic acid:

$$C_{FA} = \frac{m_{LA_i} - m_{LA_0}}{m_{LA_i}} \times 100\%$$

where:

C_{LA} – conversion of levulinic acid, in %,

m_{LAi} – mass of levulinic acid introduced to the reaction, in g,

m_{LA0} – mass of levulinic acid after the reaction, calculated using the calibration curve (analogous to the formic acid calculations), in g.

Calculations for yield to gamma-valerolactone:

$$Y_{GVL} = \frac{n_{GVL}}{n_{LA}} \times 100\%$$

where:

Y_{GVL} – yield to gamma-valerolactone, in %

n_{GVL} – number of mol of produced gamma-valerolactone, calculated using the calibration curve (analogous to the formic acid calculations), in mol

n_{LA} – number of mol of levulinic acid introduced to the reaction, in mol

2.4.3. Gas chromatography

Gaseous products were analyzed by gas chromatography (GC) equipped with a Thermal-Conductivity Detector (TCD).

The analysis is based on the transfer of the analyzed sample in gaseous state by a carrier gas towards a column where the analyzed gases are separated. The gases are detected according to their retention time that is strictly defined for each chemical compound. For the analysis argon was used as a carrier gas with a flow of 15 ml/min, a sensitivity of the TCD detector was set to 128 and each injection included 1 cm^3 volume of gaseous mixture.

Calculations for gaseous products distribution* (example of H_2):

$$S_{H_2} = \frac{n_{H_2}}{\sum gases\ in\ reaction} \times 100\%$$

where:

n_{H2} – number of mol of H_2 (height of H_2 peak in chromatogram devided by the slope of the calibration curve), in mol

∑gases in reaction – sum of numbers of mol of all tested gases, in mol

Calculations for other gaseous products were done analogically.

*The term ‘products distribution’ is used instead of selectivity because of the fact that in case of fully selective decomposition of FA towards H_2 and CO, the maximum calculated selectivity would be only 50%.

2.4.4. Gaseous phase reaction of formic acid decomposition

The reaction of formic acid decomposition in gas phase was carried out in a quartz flow reactor (Figure 24). Formic acid is given from the saturator to the catalyst bed in a flow of argon gas. Constant partial pressure of formic acid in the reaction mixture was maintained by keeping constant temperature at 1.7^{o}C using a cooling apparatus, which corresponds to the volume concentration of formic acid of 17000 ppm. In order to avoid the condensation of the reactants, the flow line was kept at 90^{o}C. The catalysts were reduced in situ before the reaction.

In a typical experiment of formic acid decomposition, 0.02 g of catalyst is placed in the quartz reactor and reduced in situ before the reaction. Then the reaction is carried out for 1 h at given temperature: 50^{o}C, 100^{o}C, 150^{o}C and 190^{o}C with the argon flow of 30 ml/min. Reaction products were analysed after each hour using Gas Chromatograph HP 5890 equipped with a Porapak Q column and TCD detector.

Calculations for conversion of formic acid and gaseous products distributions were done analogically to the liquid phase reaction using the calibration curve.

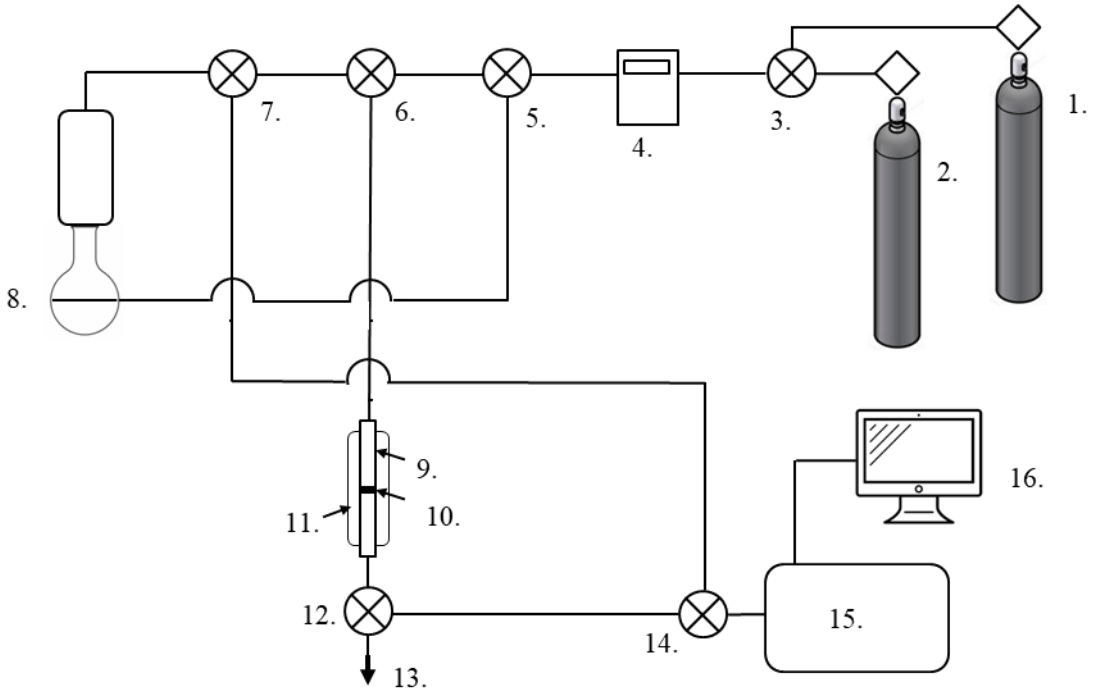

Figure 24. Flow reaction system joint with gas chromatograph. 1. H_2 gas bottle, 2. Ar gas bottle, 3,5,6,7,12. Valves, 4. Flow-meter, 8. Formic acid saturator, 9. Quartz reactor, 10. Catalyst bed, 11. Oven, 13. Outlet, 14. Six-way valve, 15. Gas chromatograph, 16. Computer.

CHAPTER 3

3. CHARACTERIZATION OF THE CATALYTIC SUPPORTS

This chapter presents the main physicochemical characterisation of the TiO_2-based materials further used for supporting the Ru nanoparticles. Emphasis has been put on the modification of the support through calcium modification.

All prepared catalytic supports (synthesis details can be found in Chapter 2.1.) were characterized by X-ray diffraction, N_2 physisorption, zeta potential measurements and SEM analysis. Figure 25 shows the powder XRD patterns of the TiO_2-based supports. Whether TiO_2 was modified with Ca or not, they exhibited diffraction reflexes corresponding to anatase TiO_2 (JCPDS card 21-1272), with the characteristic most intense peak at 25.3° corresponding to the diffraction of (101) planes, no rutile phase being observed, except in the case of the TiO_2 P25 commercial reference. For low Ca content, no phase related to the presence of Ca such as oxides or hydroxides was observed, in agreement with previous works on the modification of sol-gel TiO_2 by Ca ions.[213,214] Increasing the Ca content resulted in the progressive appearance of a weak and broad diffraction signal at $2\theta = 31.0°$ assigned to the $Ca_2Ti_2O_6$ phase (JCPDS card 40-0103), and in the observation of clear diffraction peaks corresponding to both $CaTiO_3$ (JCPDS cards 78-1013) and $Ca_2Ti_2O_6$ phases) for the 20Ca-T500. It is however difficult to distinguish between those two phases of calcium titanate due to signal overlaps. This was accompanied with a strong decrease in the intensity of the anatase diffraction peaks, in agreement with the work of Al-Salim et al. that showed that increasing the content of alkaline earth ion such as Ca^{2+} in the sol-gel synthesis of TiO_2 strongly increased the amorphous content.[214]

[213] U.G. Akpan, B.H. Hameed, J Col Interface Sci 2011, 357, 168.
[214] N. I. Al-Salim, S. A. Bagshaw, A. Bittar, T. Kemmitt, A. J. McQuillan, A. M. Mills, M. J. Ryan, J. Mater. Chem. 2000, 10, 2358.

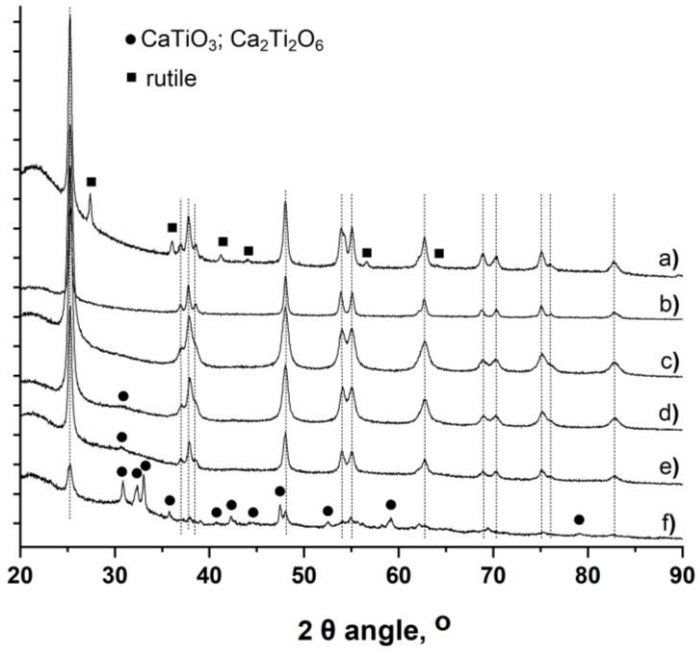

Figure 25. Powder XRD pattern of the support materials a) TiO_2 P25; b) T500; c) 1Ca-T500; d) 5Ca-T500; e) 10Ca-T500; f) 20Ca-T500. (vertical lines) diffraction peaks corresponding to the anatase TiO_2 phase; (●) most intense peaks corresponding to the titanate phases.

Whether calcium titanate phases were observed or not, the modification of titania with Ca^{2+} ions caused also some distortion in the TiO_2 lattice, as a result of the intermediate ionic radius of Ca^{2+} at 1.06 Å being larger than that of Ti^{4+} (0.64 Å) and smaller than that of O^{2-} (1.31 Å), so that Ca^{2+} ions could be either isomorphously substituted or interstitially introduced into the TiO_2 lattice with the corresponding formation of oxygen vacancies or of Ti^{3+} centers, respectively. In agreement with Al-Salim et al.[215] and Hameed et al.[216] this was experimentally visualized by an increase in the a cell parameter and a decrease in the c parameter, resulting in an overall change in the anatase cell volume (Table 2). Both commercial TiO_2 P25 and sol-gel TiO_2 T500 displayed the largest anatase mean crystallite size at 21 and 25 nm, respectively, whereas the Ca-modified TiO_2 materials exhibited a lower mean crystallite size at 13-16 nm, with no significant differences between the different Ca contents. This indicated that the modification with Ca^{2+} can inhibit the TiO_2 crystallite growth.

[215] N. I. Al-Salim, S. A. Bagshaw, A. Bittar, T. Kemmitt, A. J. McQuillan, A. M. Mills, M. J. Ryan, J. Mater. Chem. 2000, 10, 2358.
[216] U.G. Akpan, B.H. Hameed, J Col Interface Sci 2011, 357, 168.

Table 2. Physicochemical characterization of the TiO_2-based supports

Sample	P25	T500	1Ca-T500	5Ca-T500	10Ca-T500	20Ca-T500
Amount of Ca, %	0	0	1	5	10	20
Anatase average crystallite size, nm[a]	21[b]	24	13	15	15	16
BET surface area, m^2g^{-1}	50	27	60	54	47	40
Pore volume, cm^3g^{-1}	0.23	0.14	0.12	0.10	0.09	0.13
Isoelectric point	4.5	3.4	2.6	2.4	3.0	-
Cell parameter a, Å[c]	-	3.7816	3.7831	3.7828	3.7830	3.7839
Cell parameter c, Å[c]	-	9.5020	9.4840	9.4650	9.4820	9.4770
Cell volume, $Å^3$	-	135.88	135.73	135.44	135.70	135.69

[a] The mean TiO_2 crystallite size, i.e. the average size of the coherent diffracting domains, was derived from XRD measurement through the Scherrer equation applied to the (101) peak of anatase at 25.7° with the usual assumption of spherical crystallites; [b] calculated on the anatase phase; [c] Derived from XRD patterns (recorded for 12 h) by the Rietveld refinement method using the FULLPROF software.[16]

This TiO_2 crystal size decrease upon doping with alkaline earth ions was previously reported by Fu et al. and Al-Salim et al.[217,218] as well as in the case of the cationic modification of TiO_2 and more generally of transition metal oxides nanomaterials. The smaller mean anatase crystallite size of Ca-modified samples compared to that of the Ca-free reference correlated well with their higher non-microporous BET specific surface area (SSA) in the 40-60 m^2/g range vs. 27 m^2/g for the TiO_2 T500 (Table 2). The decrease in surface area when increasing the Ca content could be explained by the slight increase in the mean crystallite size of anatase. It is worth noting that the surface area and the pore volume of Ca-TiO_2 materials remained lower than those of the TiO_2 P25, probably due to the existence of grain boundaries between crystallites in the samples that lower the overall specific surface area.

The surface charge of the materials was evaluated based on the zeta potential measurements. The samples were dispersed in water and the zeta potential values were measured by changing pH values starting from basic or neutral and consequently lowering the pH until the zero surface charge was obtained. Example of the measurement for TiO_2 P25 is presented in Figure 26.

[217] N. I. Al-Salim, S. A. Bagshaw, A. Bittar, T. Kemmitt, A. J. McQuillan, A. M. Mills, M. J. Ryan, J. Mater. Chem. 2000, 10, 2358.
[218] W. Fu, S. Ding, Y. Wang, L. Wu, D. Zhang, Z. Pan, R. Wang, Z. Zhang, S. Qiu, Dalton Trans 2014, 43, 16160.

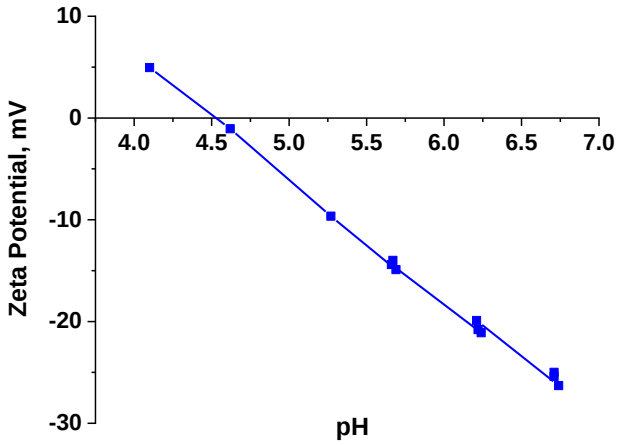

Figure 26. Zeta potential measurements of P25 nanoparticles as a function of pH.

The pH at which zeta potential is equal zero is called isoelectric point and gives the information about the surface charge of the material. In case of negatively-charged surfaces, this charge can be reduced to zero by adding more H^+ to the dispersion (lowering the pH) as is illustrated in Figure 27. Therefore the samples with higher concentration of negative surface groups (or negatively-charged oxygen ions in the case of oxide network) will be characterized by the lower isoelectric points, since more protons would be required to compensate the negative charge.

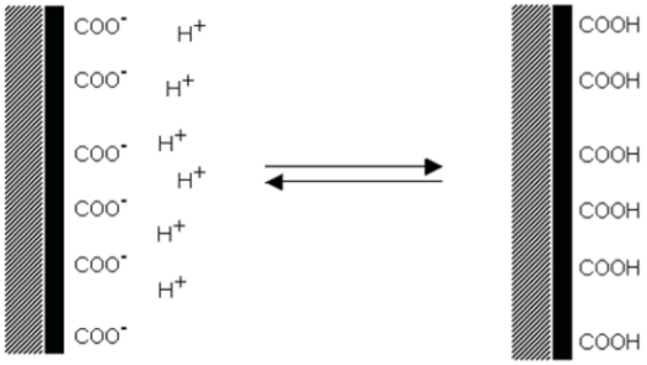

Figure 27. Scheme of a negatively-charged surface compensated by the H^+.

In case of the synthetized support materials one could note that modifying TiO_2 with Ca^{2+} led to a decrease in the isoelectric point of the supports, with values within the 2.4-3.0 range for Ca-modified TiO_2 materials compared to 3.4 for the and 4.5 for the TiO_2 T500 reference and the TiO_2 P25. This decrease in isoelectric point might be related to the formation of new basic sites at the support surface. Indeed, it has been reported that the doping of metal oxide by Ca promotor can cause an increase in the number and strength of basic sites,

in the form of coordinately unsaturated oxygen ions O^{2-}.[219] For instance, the nature of alumina supports has been reported to be strongly shifted from acidic to basic by addition of growing amount of Ca. Therefore the Ca-modified samples required the addition of a higher amount of H^+ during the zeta potential measurement for neutralizing the more negative surface by charge compensation, so resulting in the measurement of a lower isoelectric point.

Figure 28 shows N_2 adsorption-desorption isotherms as well as BJH desorption pore size distribution of the prepared sol-gel materials. First it could be clearly seen, that P25 exhibits typical type II isotherm with basically no hysteresis loop, which is characteristic for non-porous materials. This is in agreement with the pore size distribution where the flat curve proves no presence of mesopores but rather macropores. Macropores in this case is considered as the space between the grains of P25. The sol-gel TiO_2-based samples displayed type IV isotherm (Figure 28a) associated with the existence of mesopores in the materials together with a more or less marked type II contribution at high relative pressure. In case of sol-gel TiO_2 T500, the formation of some mesopores (7-10 nm) can be observed and therefore can be concluded that the preparation method allowed to introduce some porosity to the material. Then, the addition of Ca ions to the titania structure further increased the amount of mesopores (broad hysteresis). The differences in the isotherm shapes could be discussed in terms of the type of the hysteresis loop. Sample T500 exhibits typical H3 type which does not give any plateau at high p/p^0 suggesting no well-defined mesopore volume and non-rigidity of the aggregate structure. Then with the addition of Ca^{2+} to the titania structure, the hysteresis of H2 type becomes more pronounced meaning the existence of more regular and rigid pore structure. The differences between the materials are represented also by the pore size distribution profiles (Figure 28b). It was observed that the narrowest pore size distribution (mesopores of 4 nm) was observed for 10Ca-T500 with the contribution of larger (10-20 nm) pores. Very similar profiles were recorded for samples with 1% and 5% of Ca having pores only with the size range of 4-6 nm. On the other hand the sample 20Ca-T500 possesses a very broad range of pore diameters starting from as small as 4 nm and reaching up to 20 nm.

[219] S. Scirè, C. Crisafulli, R. Maggiore, S. Minicò, S. Galvagno, Appl Surf Sci. 1998, 136, 311.

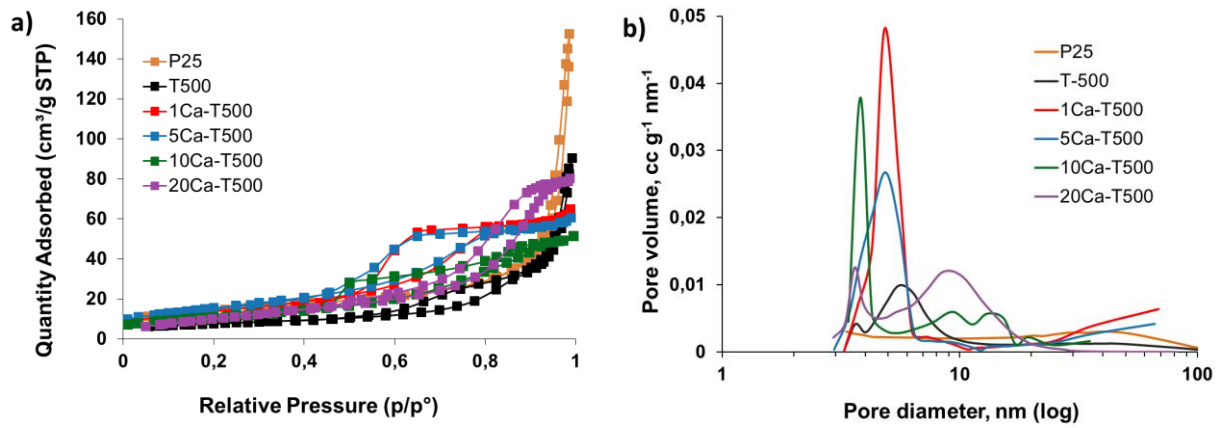

Figure 28. a) N_2 adsorption-desorption isotherms and b) pore size distribution of the prepared sol-gel materials.

The SEM images shown in Figure 29 revealed the morphological changes observed when modifying the TiO_2 with calcium. While the Ca-free TiO_2 reference displayed the classical morphology of sol-gel TiO_2 materials, the incorporation of calcium into the support increased the heterogeneity of the material surface. This property may be assigned to the smaller TiO_2 crystallite size and the progressive appearance of the calcium titanate phases when increasing the calcium content. Sample with 1 wt.% of Ca appears as larger blocks of coarse material with smaller particles of very irregular shape although some small regular particles like in TiO_2 are still visible. 5Ca-T500 displays very similar features as 1Ca-T500 but with higher amount of small irregular powder chunks and larger blocks of coarse parts that seem to be fused together. The sample with 20 wt.% of Ca revealed the most altered morphology with the appearance of melted-like small size particles. Whatever the Ca content, the Ti, Ca and O elemental mapping evidenced the homogeneous distribution of the calcium heteroatoms in the TiO_2-based supports, whether the Ca ions distributed within the TiO_2 lattice or the Ca ions from the titanate phase are concerned. In addition, the Ca contents derived from the EDS analysis were in good agreement with the theoretical values from the modified sol-gel syntheses, confirming that the Ca species were evenly distributed in the samples.

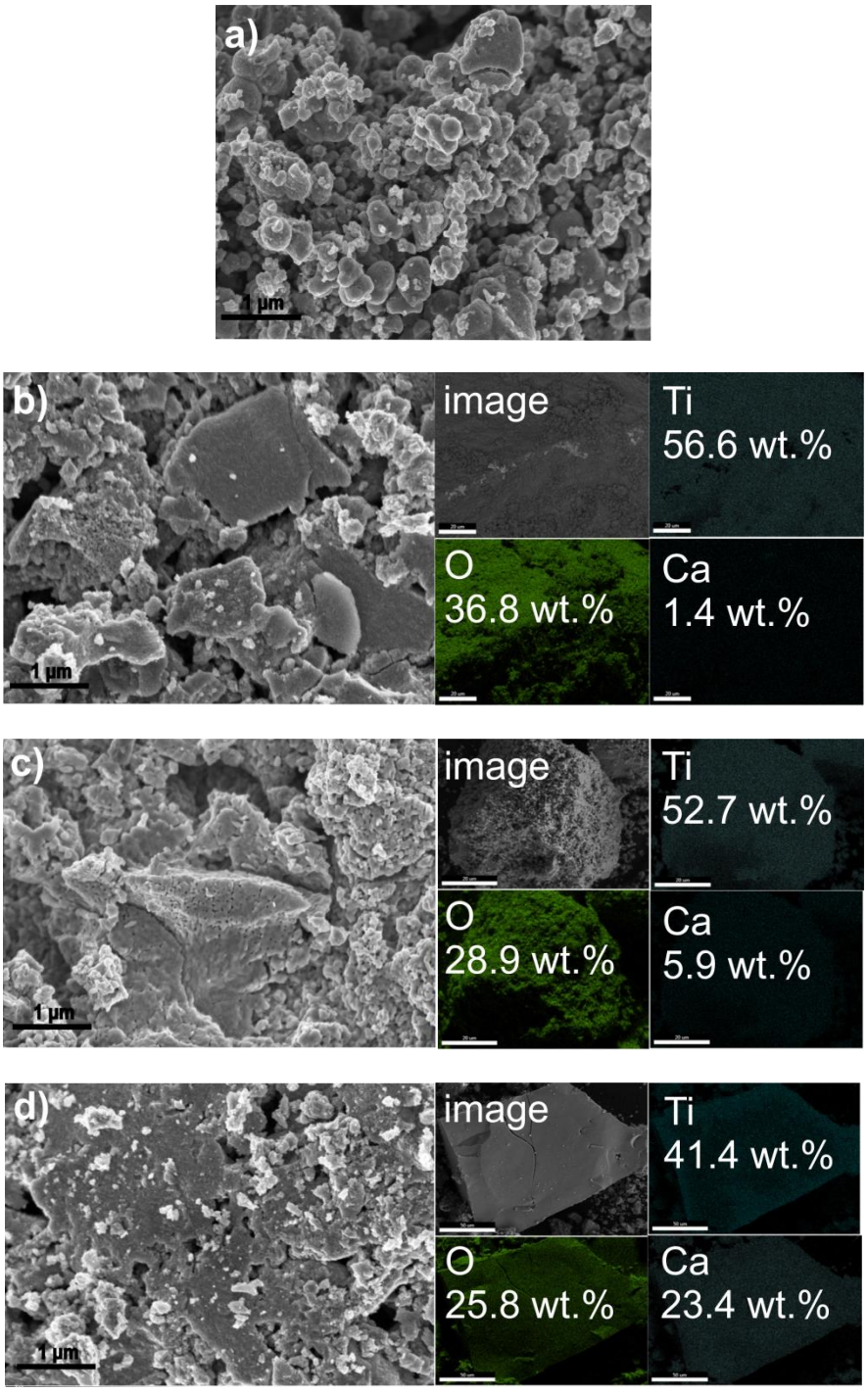

Figure 29. SEM images and the corresponding O, Ti and Ca element mapping images of selected support materials: a) T500; b) 1Ca-T500; c) 5Ca-T500; d) 20Ca-T500.

In addition, the presence of new calcium titanate phase was also confirmed by means of high resolution TEM image. Figure 30 presents the Ru/5Ca-T500-P catalyst with the visible presence of two different interplanar spacings attributed to the anatase TiO_2 and the calcium titanate phase inside the

support. In this image, the nanosized metallic Ru nanoparticles are also visible, which the preparation is described in the next chapter.

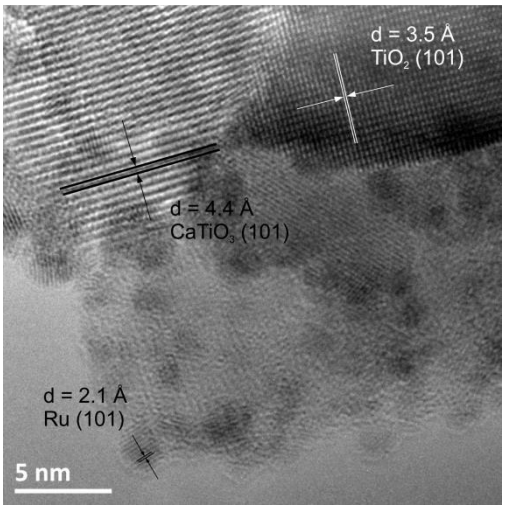

Figure 30. High resolution TEM images of the Ru/5Ca-T500-P catalysts, with the interplane distances of (101) planes of metallic Ru, of (101) planes for anatase TiO_2 and of (101) planes for $CaTiO_3$.

In this chapter, the characterization of the support materials prepared by the sol-gel method and of the commercial P25 was presented, and the effect of the Ca modification on the material properties was evaluated. The sol-gel preparation method with calcium introduction led to form the anatase TiO_2 anatase phase whatever the Ca content, together with a distortion of the crystal lattice of TiO_2 due to the doping of Ca^{2+} in the TiO_2 network. This was also accompanied by as amorphisation of the material and by the formation of new calcium titanate phase $CaTiO_3$, all the more marked that the Ca content was increasing. Moreover the addition of Ca results in the decrease in the anatase crystal size due to an inhibited TiO_2 crystalline growth, with the consequent increase in the BET surface area. Eventually, the increased basicity of the materials due to the presence of coordinatively unsaturated oxygen ions O^{2-} in the Ca-modified materials was observed.

CHAPTER 4

4. PHOTO-ASSISTED SYNTHESIS METHOD FOR PREPARING Ru/TiO_2 CATALYSTS

A one-step room temperature photo-assisted synthesis has been implemented in liquid phase and under solar light for preparing highly dispersed TiO_2 supported metallic Ru catalysts, with no need of final thermal treatment, external hydrogen, or chemical reductant. Both Ru (III) acetylacetonate and Ru (III) chloride hydrate have been used as precursors, as they are the most common precursors used for preparing supported Ru catalysts on a wide variety of supports *via* the impregnation method with final reduction in temperature under hydrogen. First, the influence of the nature of the Ru metallic precursor and of the targeted Ru content has been studied, and the efficiency of the preparation method has been characterized through chemical analysis, microscopy and surface analysis. Further, the influence of the pH of the precursor solution in the case of the chloride precursor has been studied and opened the possibility of increasing the Ru content for preparing catalysts with 5 wt. % of Ru. Finally, the preparation method has been scaled-up for preparing the set of Ru/TiO_2 catalysts (on TiO_2 and Ca-modified supports) to be used in the catalytic studies. The synthesis protocols are extensively described in Chapter 2.2.

4.1. Influence of the Ru metallic precursor and of the targeted Ru content

A series of ruthenium catalysts has been prepared using both hydrated $RuCl_3$ and $Ru(acac)_3$ as metallic precursors targeting a nominal Ru concentration from 0.5 wt. % to 5 wt. %. The deposition was followed by UV-vis spectrophotometry monitoring the disappearance of the main absorption peak at λ=272 nm and λ=324 nm for $Ru(acac)_3$ and $RuCl_3$ precursors in their solvent, respectively. The disappearance with time of both Ru precursors using TiO_2 P25 as semi-conductor support is shown in Figure 31.

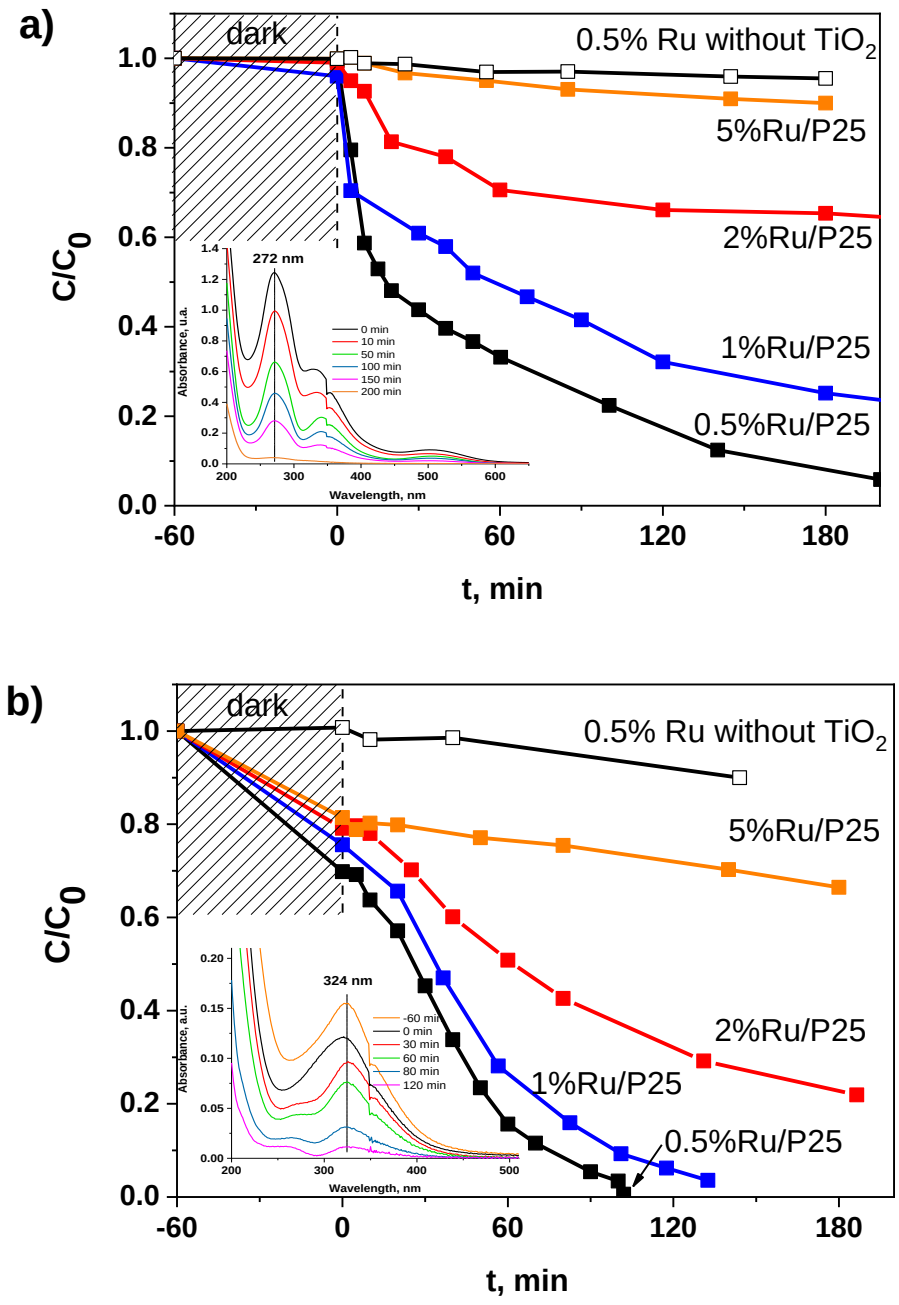

Figure 31. Disappearance of the Ru precursor in the presence of TiO_2 P25 as a function of the illumination time for a) $Ru(acac)_3$ and b) $RuCl_3$ precursors, with a Ru content of 0.5, 1, 2 and 5 wt. %. Inset: Examples of UV-vis absorbance spectra evolution as a function of the illumination time during the photo-assisted synthesis.

First, whatever the precursor used, no significant degradation of the ruthenium precursor has been observed under solar light in the absence of catalyst, indicating that the photolysis of the ruthenium precursor can be neglected in the experimental conditions. The evolution with time of the relative

concentration demonstrated that the photocatalytic degradation of the $Ru(acac)_3$ and $RuCl_3$ species occurred on the TiO_2 material. It evidenced the influence of both the ruthenium concentration and the ruthenium precursor nature on the degradation kinetics. At a given Ru content, a faster degradation was observed with chloride when compared to acetylacetonate, a reaction time of 100 min and over 200 min being necessary for achieving a full disappearance of the Ru precursor at a content of 0.5 wt. % using the chloride and acetylacetonate precursors, respectively. For both Ru precursors, increasing the Ru concentration led to an increase in the necessary reaction time, the effect being more pronounced using acetylacetonate. Indeed, targeting a Ru content of 2 wt. % led only to a photodeposition yield of 35%, where no photodeposition was observed for a Ru concentration of 5 wt. %. Even in the case of the chloride precursor for which faster kinetics have been observed, the preparation of highly loaded Ru/ TiO_2 catalyst with loadings higher than 2 wt. % could not be achieved within a reasonable time under irradiation.

4.2. Characterization of the Ru/TiO_2 P25 catalysts with Ru loading from 0.5 wt. % to 2 wt. %.

Table 3 shows the real metal content of the materials after the photo-assisted deposition.

Table 3. Ru content in Ru/TiO_2 P25 materials analyzed by ICP-OES.

Sample name	Ru content, wt.%
0.5%Ru/TiO_2_acac [a]	0.45 ± 0.01
1%Ru/TiO_2_acac	0.76 (0.8) [b]
0.5%Ru/TiO_2_acac	0.36 (0.4) [b]
0.5%Ru/TiO_2_Cl	0.46
1%Ru/TiO_2_Cl	0.96
1.6%Ru/TiO_2_Cl	1.29 (1.30) [b]
2%Ru/TiO_2_Cl	1.23 (1.37) [b]

[a] accuracy determined by performing twice the photoassisted synthesis of the Ru/TiO_2 sample.

[b] theoretical Ru content deposited calculated from the conversion of the Ru acetylacetonate or chloride precursors derived from the UV-vis absorption spectra, when stopping the photodeposition experiment before the full disappearance of the UV-vis absorption signal corresponding to the Ru species.

By stopping some photodeposition experiments before the full disappearance of the UV-vis absorption signal corresponding to the Ru species, a good agreement was obtained between the measured Ru content and the theoretical one derived from the evolution of the UV-vis absorption signal, with a relative difference being at the maximum of about 10%. So, the results obtained showed that the direct monitoring of the Ru species disappearance by UV-Vis spectrophotometry was a suitable and fast method for determining the Ru content of the Ru/TiO_2 materials prepared, with no need of implementing additional time-consuming analytical techniques.

Figure 32 shows TEM images with the corresponding histograms of the Ru nanoparticle size distribution for Ru/TiO_2 P25 catalysts prepared with $RuCl_3$ and $Ru(acac)_3$ as metallic precursors with a Ru concentration of 0.5 wt. % and 1 wt. %. First, similar mean particle sizes were obtained whether the acetylacetonate or the chloride form of the Ru precursor was used, despite the difference in terms of chemical nature. In both cases, small ruthenium nanoparticles were synthesized on the TiO_2 support with a sub-nanometric and sharp particle size distribution centered at 0.6-0.7 nm. The supported nanoparticles were homogeneously dispersed and no ruthenium nanoparticle aggregates were formed. Beside the mean particle size, the size distribution, characterized by the Full Width at Half Maximum (FWHM), is another important parameter characterizing the particle size distribution. Although the distribution remained in both cases very narrow, the supported Ru nanoparticles prepared with acetylacetonate displayed a slightly broader particle size distribution when compared to that obtained with the chloride counterpart, with a FWHM of 0.35-0.40 *vs.* 0.25. However, it was remarkable that increasing the Ru content did not result neither in an increase in the mean particle size, nor in its broadening.

Further, performing the TEM image analysis through different operators allowed us to rule out the critical operator influence in the establishment of reliable particle size distributions, similar mean particle size and FWHM being obtained whatever the operator for two acetylacetonate and chloride precursors derived samples. The nanoparticle size distribution obtained differed strongly from that achieved on a Ru/TiO_2 P25 reference sample, prepared by classical incipient wet impregnation from $Ru(acac)_3$ in methanol solution and final thermal reduction in hydrogen, for which a considerably broader size

distribution was achieved (FWHM of 1.0 nm) together with a larger mean particle size of 1.3 nm (Figure 33).[220]

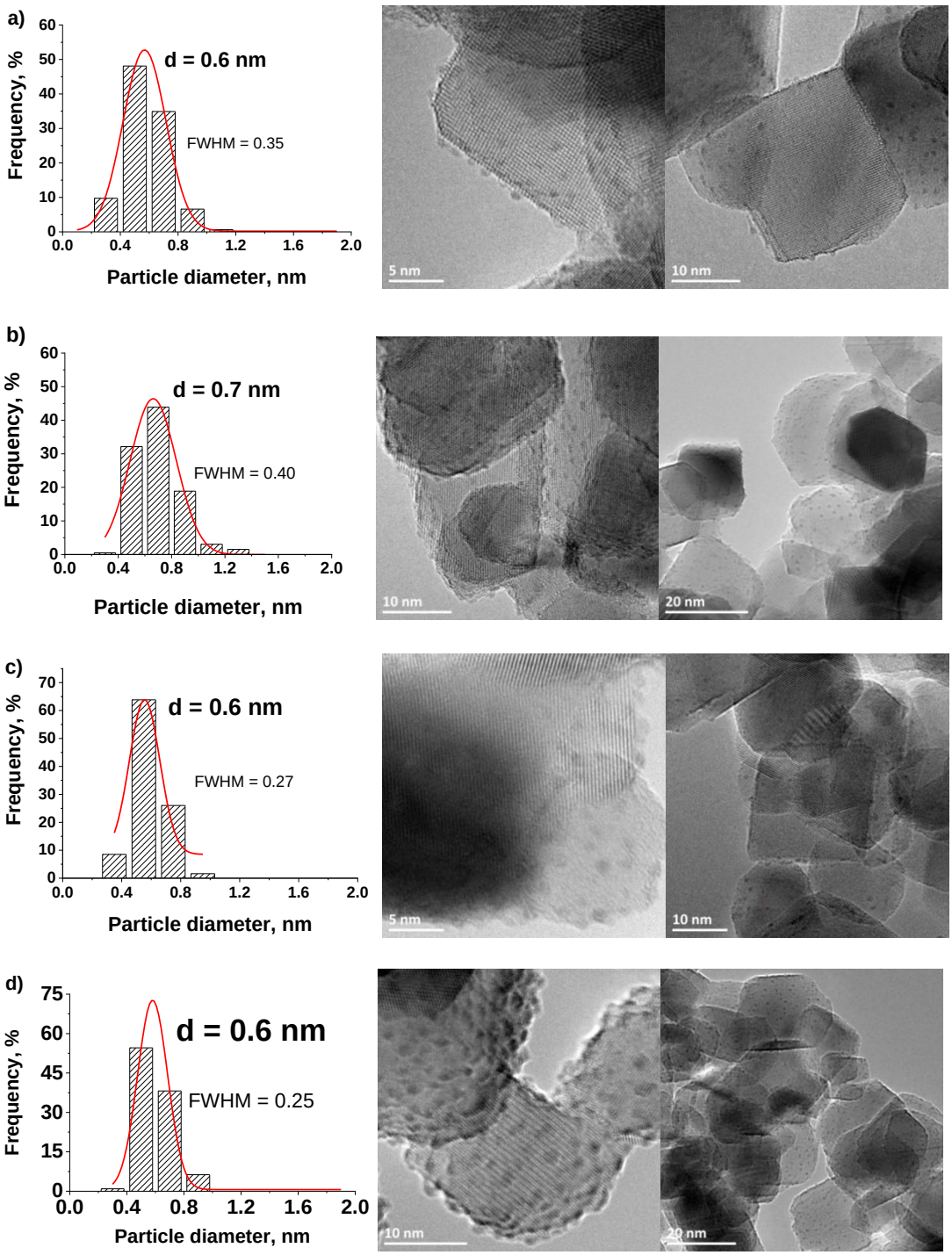

[220] A.M. Ruppert, J. Grams, M. Jędrzejczyk, J. Matras-Michalska, N. Keller, K. Ostojska, P. Sautet, ChemSusChem. 2015, 8, 1538.

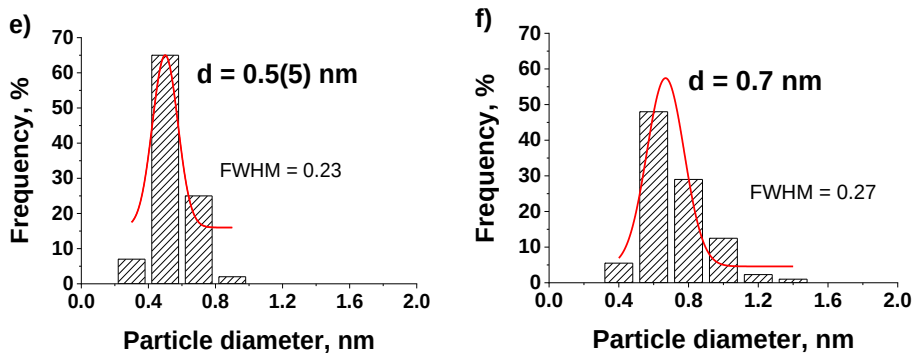

Figure 32. TEM images and the corresponding histograms of the Ru nanoparticle size distribution for Ru/TiO$_2$ P25 catalysts: a) 0.5%Ru_acac, b) 1%Ru_acac, c) 0.5%Ru_Cl, d) 1%Ru_Cl, e) 1%Ru_Cl derived from TEM image analysis by another operator, f) 1%Ru_acac derived from TEM image analysis by another operator.

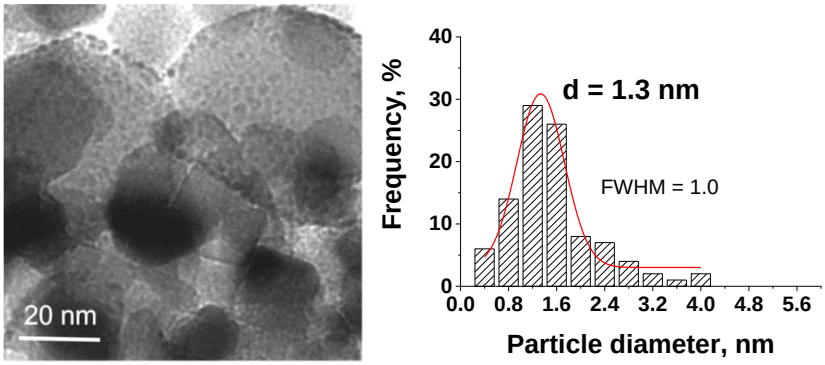

Figure 33. TEM image and the corresponding Ru particle size distribution of 1%Ru/TiO$_2$ prepared by classical impregnation with final reduction in hydrogen at 200°C using Ru(acac)$_3$.

The metallic nature of the Ru nanoparticles synthesized on the TiO_2 support was confirmed by TEM analysis and XPS surface characterization (Figure 34). TEM image evidenced an interplane distance of 2.1 Å in the Ru nanoparticles, that corresponds to the interplane distance of (101) planes of metallic Ru.[221] Whatever the Ru precursor used, the Ru $3p_{1/2}$ orbital XPS spectra shown for the Ru(0.5 wt.%)/TiO_2 samples prepared with both Ru precursors, revealed the presence of both metallic Ru^0 (484.1 eV) and Ru^{4+} (488.7 eV) species at the surface.[222] Despite a more complex multi-contribution profile due to the binding energy overlap between both C 1s and Ru 3d XPS spectra, the Ru 3d spectra confirmed the

[221] B. Coşkuner Filiz, E.S. Gnanakumar, A. Martínez-Arias, R. Gengler, P. Rudolf, G. Rothenberg, N.R. Shiju, Catal. Letters. 2017, 147, 1744.
[222] A.M. Ruppert, M. Jędrzejczyk, O. Sneka-Płatek, N. Keller, A.S. Dumon, C. Michel, P. Sautet, J. Grams, Green Chem. 2016, 18, 2014.

presence of two Ru species (280.2 eV for Ru^0 and 281.9 eV for Ru^{4+}), with the presence of two Ru $3d_{5/2}$ - Ru $3d_{3/2}$ orbital doublet contributions with spin orbit coupling splitting of 4.1 eV, in addition to the contributions resulting from the contamination carbon.[222]

By combining both Ru 3p and the Ru 3d spectra results, the ratio of atomic concentrations between Ru^0 and Ru^{4+} has been estimated at 70/30 ± 7, and it was observed that the oxidation state of ruthenium species at the TiO_2 surface was not influenced by the precursor used. Also, the Ru(0.5 wt.%)/TiO_2 material had a Ru/Ti surface atomic ratio of *ca.* 0.02 in both cases, confirming that the Ru nanoparticle size distribution was not affected by the choice of the metallic precursor. Given an average Ru particle size derived from TEM images of 0.6 nm and the interlayer distance between the atomic (101) planes of metallic Ru, we could in a first approximation consider that the ruthenium nanoparticles supported on TiO_2 consisted in average in about 3-4 atomic layers only. Taking into account the Ru^0/Ru^{4+} ratio derived from XPS and the fact that Ru undergoes oxidation very easily when exposed to the air, we suppose that the Ru^{4+} species evidenced by XPS corresponded to the presence of one monolayer resulting from a natural surface oxidation. In addition, the Cl 2p XPS spectra did not reveal the presence of any residual chlorine species at the surface when the sample was prepared from the chloride precursor (not shown).

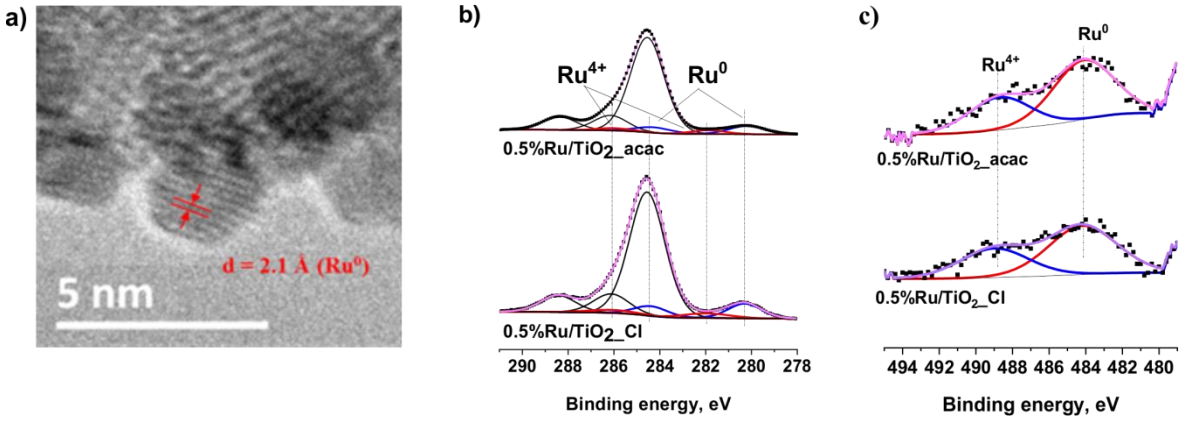

Figure 34. a) TEM image of Ru/TiO_2 P25 with the measured interplane distance of (101) planes of metallic Ru; b) Ru 3p and c) Ru 3d + C 1s XPS profiles of the Ru(0.5 wt.%)/TiO_2 P25 catalysts.

4.3. **Mechanistic studies**

The different behaviour in terms of degradation kinetics observed on the TiO_2 support depending on the nature of the Ru metallic precursor used led to propose that the photo-assisted synthesis of Ru nanoparticles supported on TiO_2 occurred *via* two different mechanisms.

Based on the study of Naya et al. on the preparation of Cu/$BiVO_4$ photocatalysts from Cu acetylacetonate[223] the following mechanism involving both photogenerated holes and electrons can be proposed for the synthesis of metallic Ru nanoparticles on the TiO_2 support in the case of the Ru acetylacetonate precursor:

$$TiO_2 + Ru(acac)_3 \leftrightarrow Ru(acac)_{3ad} \cdot\!\!-\!\!\cdot TiO_2 \quad (1)$$

$$TiO_2 + hv \rightarrow e^- + h^+ \quad (2)$$

$$Ru(acac)_{3ad} + 3h^+ \rightarrow Ru^{3+} + (acac)_{ox} + H^+ \quad (3)$$

$$Ru^{3+} + 3e^- \rightarrow Ru^0 \quad (4)$$

According to this mechanism, the first step is the adsorption of the Ru acetylacetonate precursor at the titania surface. The adsorbed Ru acetylacetonate can be oxidized, either directly by the photogenerated holes from the valence band or indirectly by the OH° hydroxyl radicals resulting from the oxidation by the holes of adsorbed water or surface -OH groups. The adsorbed Ru^{3+} ions generated by the ligand oxidation can be further reduced into metallic Ru by the photogenerated electrons from the conduction band. In the case of copper, the reduction of Cu^{2+} into metallic Cu was reported to be easier than the direct reduction of $Cu(acac)_2$.[223]

By contrast to the mechanism proposed for the acetylacetonate that involves both holes and electrons charge carriers in oxidation and reduction steps, respectively, we propose that only electrons would be involved in the case of the $RuCl_3$ precursor, since the $RuCl_3$ precursor is present in aqueous solution as a mixture of various ruthenium chlorohydroxides.[224]

[223] S.I. Naya, M. Tanaka, K. Kimura, H. Tada, Langmuir 2011, 27, 10334.
[224] M.M. Taqui Khan, G. Ramachandralah, A. Prakash Rao, Inorg. Chem. 1986, 25, 665.

In the attempt to support the above hypothesis, a series of complementary experiments was carried out, on one hand by voluntarily reducing the oxidative photoactivity of the TiO_2 support by synthesizing Ca-modified TiO_2 photocatalysts, and on another hand by adding to the reaction media controlled amounts of hole and electron scavengers, methanol and potassium persulfate ($K_2O_2S_8$), respectively.[225] Methanol is considered as indirect hole scavenger, by reacting rapidly with OH° radicals formed from holes.[226] The reactions in which the electron scavenger is involved are presented in the following equations:

$$S_2O_8^{2-} + e^- \rightarrow SO_4^{\bullet-} + SO_4^{2-} \quad (5)$$

$$SO_4^{\bullet-} + e^- \rightarrow SO_4^{2-} \quad (6)$$

In parallel to the photo-assisted synthesis of Ru nanoparticles, the well-known degradation of the Diuron herbicide (3-(3,4-dichlorophenyl)-1,1-dimethyl-urea) has been used as test reaction of oxidation photocatalysis in aqueous phase under simulated solar light.[227]

Protocol of the Diuron herbicide degradation experiments. In each experiment, 100 mg of the photocatalyst (TiO_2 or Ca-modified TiO_2) was dispersed under stirring in 100 mL Diuron aqueous solution at 10 mg/L and exposed to a 250 W/m^2 solar light irradiation within an ATLAS Suntest XLS+ reaction chamber. Prior to irradiation, the suspension was stirred in the dark for 1 h to ensure the establishment of the adsorption-desorption equilibrium. The Diuron concentration was monitored by UV-visible spectrophotometry via the disappearance of the absorption peak at λ = 248 nm.[228]

[225] A. Syoufian, K. Nakashima, J. Colloid Interface Sci. 2007, 313, 213.
[226] M. Pelaez, P. Falaras, V. Likodimos, K. O'Shea, A. A. de la Cruz, P. S.M. Dunlop, J. A. Byrne, D. D. Dionysiou, J Mol Catal, 2016, 425, 183
[227] S. Malato, J. Caceres, A.R. Fernandez-Alba, L. Piedra , M.D. Hernando, A. Aguera, J. Vial, Environ. Sci. Technol. 2003, 37, 2516.
[228] A. Fkiri, M.R. Santacruz, A. Mezni, L.-S. Smiri, V. Keller, N. Keller, Environ. Sci. Pollut. Res. 2017, 24, 15622.

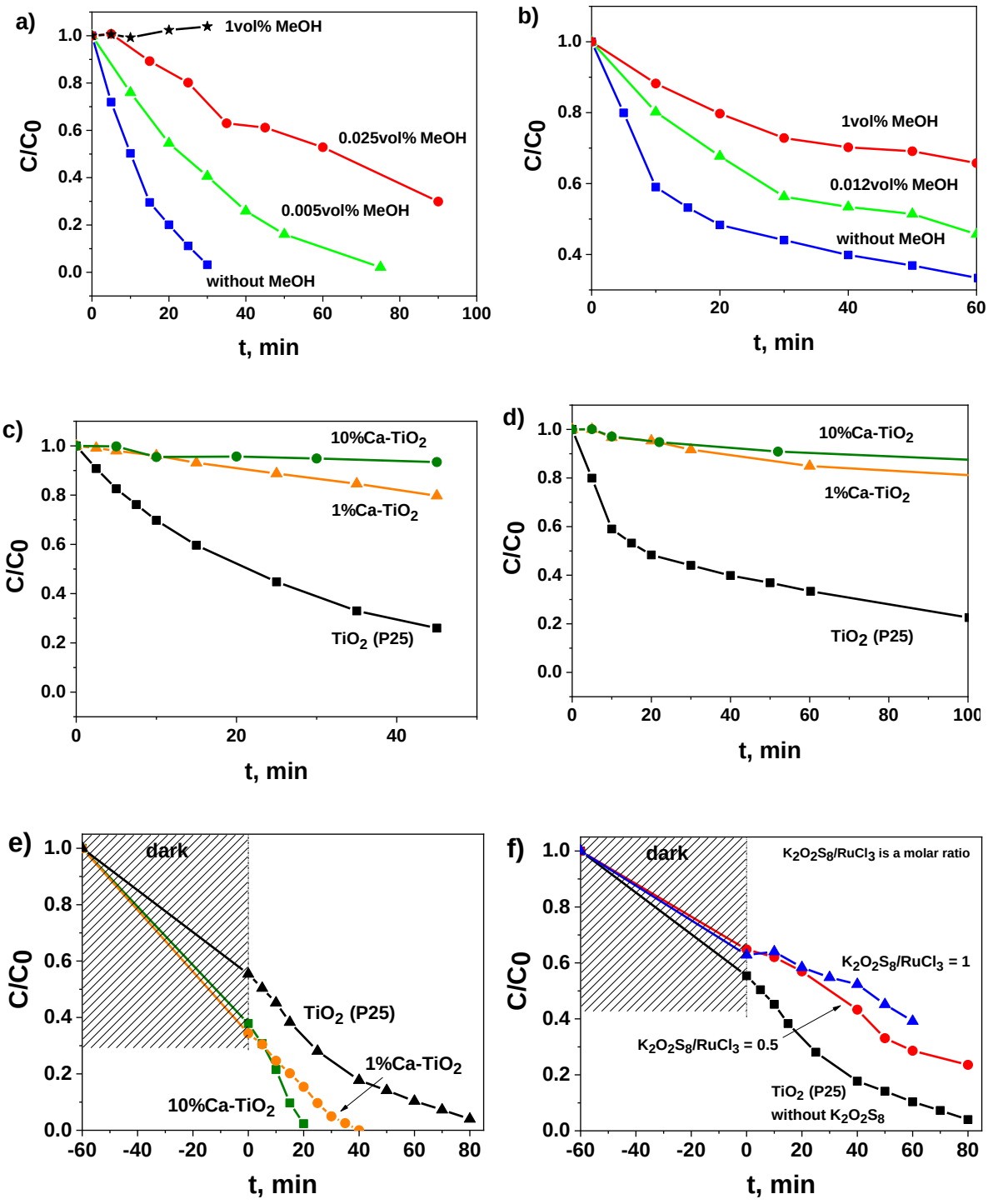

Figure 35. Photodegradation kinetics for (a) Diuron and (b) Ru(acac)$_3$, on TiO$_2$ P25 as a function of the MeOH concentration; (c) Diuron and (d) Ru(acac)$_3$, on Ca-modified TiO$_2$ photocatalyst; (e) Photo-degradation kinetics for hydrated RuCl$_3$ on Ca-modified TiO$_2$ photocatalyst; (f) Influence of the K$_2$O$_2$S$_8$ concentration on the photodegradation kinetics for hydrated RuCl$_3$ on TiO$_2$ P25. In the case of RuCl$_3$ (e-f), the photodeposition experiments were started after the adsorption/desorption dark equilibrium was

reached. No strong adsorption being observed using Diuron and Ru(acac)$_3$, the dark equilibrium period has not been reported (a-d).

Figure 35a and b shows respectively the influence of the addition of methanol on the Diuron degradation and on the Ru photodeposition from Ru(acac)$_3$ using TiO_2 P25. Adding methanol as hole scavenger slowed down strongly the degradation of the Diuron molecule, as expected, the methanol scavenger reacting with holes or hydroxyl radicals at the TiO_2 surface. A similar behaviour was observed in the case of Ru(acac)$_3$ degradation, with a slowdown of the Ru photodeposition. In both cases, higher the concentration of methanol, more pronounced the effect. This confirmed that the photodeposition of Ru was controlled by oxidation reactions when acetylacetonate was used as reactant, and that photogenerated holes were involved in the photodeposition mechanism, either directly or indirectly by generating oxidative hydroxyl radicals, in a similar way than for the photocatalytic degradation of carbon-containing pollutants in water.

We further tested this hypothesis by performing the Diuron degradation and the photodeposition with Ru(acac)$_3$ on deactivated TiO_2 photocatalysts, synthesized by modifying TiO_2 with calcium ions (see synthesis and characterisation in Chapter 2 and 3, respectively). First, Figure 35c evidenced that the oxidative degradation of the Diuron reactant was strongly reduced on Ca-modified TiO_2 photocatalysts compared to the Ca-free TiO_2 reference, with a decrease in the apparent kinetic rate constant from $5.7\ 10^{2}$ min^{-1} on TiO_2 P25 down to $1.7\ 10^{-3}$ min^{-1} on Ca(10%)-modified TiO_2 according to a pseudo first-order kinetics in a Langmuir-Hinshelwood model. So, higher the Ca content, weaker the oxidation ability of the photocatalyst, almost no degradation being observed on the photocatalyst containing 10% of calcium for 45 min of reaction. In the case of the photodeposition with Ru(acac)$_3$, it has been observed that weaker the oxidation ability of the photocatalyst, slower the Ru photodeposition process (Figure 35d). The similarity of behaviour observed for both reactants confirmed the involvement of photogenerated holes and more globally of oxidation reactions at the TiO_2 support surface in the photodeposition mechanism when acetylacetonate was used as reactant.

By contrast, Figure 35e shows that TiO_2 photocatalysts with weak oxidation ability were still able to perform the Ru photodeposition using chloride as reactant. Further, increasing the amount of calcium in

the Ca-modified TiO_2 photocatalyst resulted in a strongly accelerated Ru photodeposition, although it reduced drastically the Diuron degradation. This behaviour was attributed to the extended lifetime of the photogenerated electron charge carrier that would lead to a better availability of electrons at the surface of the photocatalyst for reducing the Ru chloride precursor into metallic Ru. This enhanced lifetime would result from an extended consumption of the photogenerated holes by the deactivated Ca-TiO_2 material itself. Further, performing the Ru photodeposition with chloride in the presence of potassium persulfate used as electron scavenger showed that increasing the concentration of $K_2S_2O_8$ strongly slowed down the photodeposition process on TiO_2 P25, evidencing the direct involvement of the photogenerated electrons in the degradation of the $RuCl_3$ precursor (Figure 35f).

TOC measurements have been implemented for confirming further the proposed mechanism in the case of the $Ru(acac)_3$ precursor. A photodeposition experiment targeting the synthesis of Ru nanoparticles at a loading of 0.5 wt.% on TiO_2 P25, corresponding to an initial TOC value of 15 ppm in the reactional media, has been stopped at a photodeposition efficiency of 80%. At this point, the aqueous reaction media contained 8 ppm of TOC, while a complete mineralization of the acetylacetonate ligands into CO_2 would correspond to the residual presence of 3 ppm of TOC. This result means that both partial oxidation of the acetylacetonate ligands and mineralization to CO_2 occurred during the photodeposition process. The TiO_2 photocatalyst could consequently suffer from competitive adsorption between the Ru acetyacetonate reactant and the partially oxidized ligands that could either block the TiO_2 surface or adsorb for being further photocatalytically degraded into CO_2. This adsorption competition effect could explain the strong slowing down of the photodeposition process observed when increasing the starting concentration of the $Ru(acac)_3$ reactant. In addition, the presence of small amounts of carbon-containing reaction intermediate species at the surface of the Ru/TiO_2 resulting from the ligand oxidation was confirmed by TGA analysis, with a higher weight loss attributed to the desorption and the combustion of those species when using acetylacetonate compared to that observed on the material prepared with chloride (Figure 36).

The lower photodeposition rate in the case of the acetylacetonate *vs.* chloride precursor was then proposed to directly result from the different reaction mechanism taking place, with the establishment of competitive adsorption and oxidation phenomena between the Ru acetyacetonate reactant and the partially oxidized acetyacetonate ligands that are formed during the oxidative steps of the photodeposition

process. This led to a partial deactivation of the TiO_2 photocatalyst, and then to lower photodeposition rates. Also the Ru acetylacetonate could suffer from a lower adsorption at the TiO_2 surface, most probably due to its non-ionic character. By contrast, the Ru photodeposition from the $RuCl_3$ precursor was taking advantage of the favored adsorption of the hydrolytic products of the $RuCl_3$ salt in water, as visualized by the strong pre-adsorption taking place during the initial dark equilibrium period.

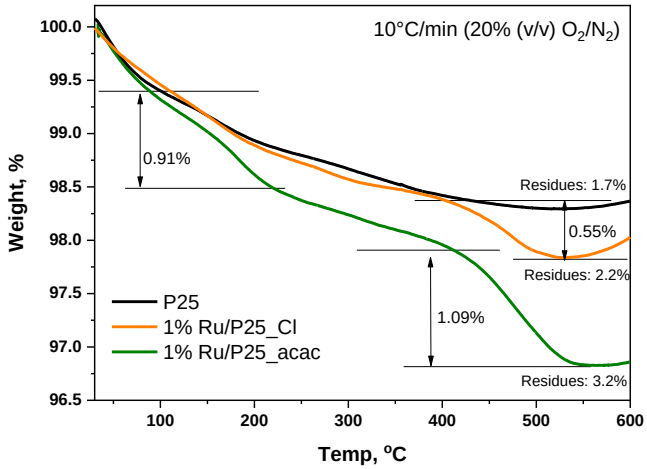

Figure 36. TGA curves of TiO_2 P25 and 1%Ru/TiO_2 P25 materials prepared from $Ru(acac)_3$ and hydrated $RuCl_3$ precursors. The weight loss observed on the reference TiO_2 sample, corresponded to the low temperature desorption of molecularly adsorbed water and to the surface dehydroxylation (dehydration) at higher temperature. The additional weight loss observed on the 1%Ru/TiO_2 material prepared from $RuCl_3$ precursor, was attributed to the combustion of carbonaceous residues issued from the partial oxidation of methanol during the photodeposition process.

4.4. **Fine control of the Ru particle size distribution**

It has been further demonstrated that a fine monitoring of the metal Ru nanoparticle size on the TiO_2 support was possible *via* a controlled growth of the Ru nanoclusters under irradiation, achieved by extending the duration of the irradiation after the full conversion of the Ru precursor salt was achieved. Indeed, Figure 37 shows that the mean Ru particle size progressively and slightly increased from 0.6 nm to 0.9 nm and further to 1.1 nm, when 2 h and 6 h of supplementary irradiation time was provided to the

system, respectively. Simultaneously, the FWHM values slightly increased from 0.25 nm to 0.52 nm and further to 0.62 nm, evidencing a slight broadening of the particle size distribution. Whatever the irradiation time, it was worth noting that the nanoparticles remained homogeneously dispersed on the support with a small mean particle size and without the formation of large ruthenium nanoparticle aggregates. This highlighted the possibility to provide on-demand Ru/TiO$_2$ catalysts with a monomodal particle size distribution and a well-calibrated mean particle size for studying and optimizing the reactivity of heterogeneous catalysts in different size-dependent or structure-sensitive reactions.[229,230]

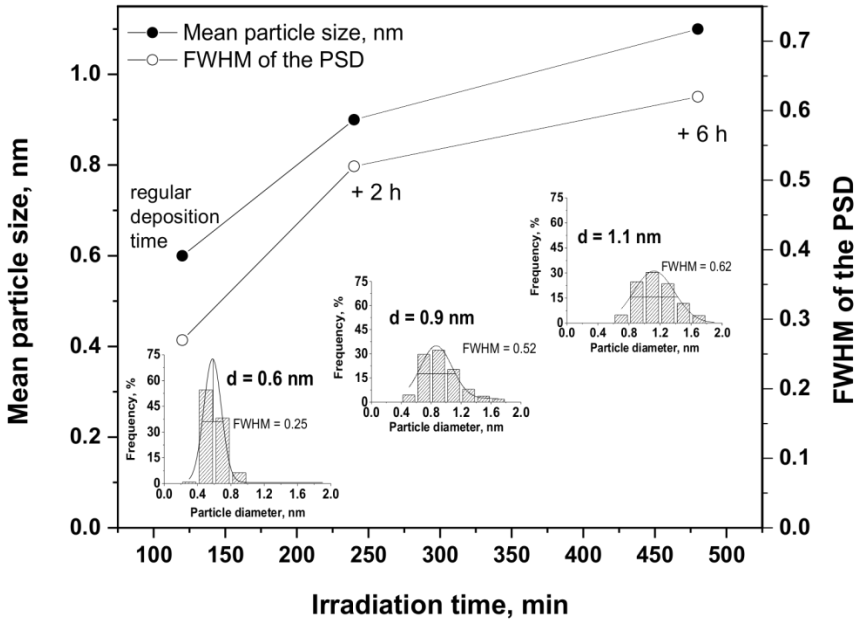

Figure 37. Evolution of the mean Ru particle size and of the distribution FWHM as a function of the irradiation time for the 1%Ru/TiO$_2$ P25 catalyst prepared with the chloride precursor. Inset: Ru particle size distributions obtained for 2 h, 4 h and 8 h of irradiation, corresponding to the regular irradiation time, and 2 h and 6 h of extra-time irradiation in the absence of new Ru species, respectively.

4.5. Influence of the pH of the precursor solution - towards the preparation of the Ru(5 wt. %)/TiO$_2$ catalyst

Figure 39a shows the influence of the pH of the aqueous ruthenium precursor solution on the photodeposition kinetics on 0.5 wt. % Ru on TiO$_2$ P25. It was worth noting that increasing the pH led to

[229] Z. Xu, F.S. Xiao, S.K. Purnell, O. Alexeev, S. Kawi, S.E. Deutsch, B.C. Gates, Nature 1994, 372, 346.
[230] M. Boudart, G. Djega-Mariadassou, Kinetics of Heterogeneous Catalytic Reactions. Princeton University Press, 1994.

significantly enhance the adsorption of the Ru precursor species on the TiO_2 support in the dark, while this subsequently reduced strongly the time necessary for achieving a complete disappearance of the Ru precursor, and consequently for preparing the Ru(0.5 wt. %)/TiO_2 material. This behavior with increasing the pH of the solution has been attributed to the amphoteric nature of the TiO_2 support, for which the surface is negatively-charged for pH higher that the zero-charge point (ie. 4.5 for TiO_2-P25 as it has been measured in Chapter 3), and positively-charged for pH lower that the zero-charge point.[231] Thus, the TiO_2 surface is considered to be negatively-charged when the photodeposition was performed at pH 8 and at pH 6.4, whereas the TiO_2 surface charge gradually increased with decreasing the pH of the solution, so that the reaction was implemented on almost a zero charge surface at pH 4, and consequently on a positively-charged surface at pH 2.

In water, $RuCl_3$ species are very complex systems and co-exist in the form of various aqueous chloro-complexes, for which the thermodynamic equilibrium depends on parameters such as the pH, the temperature and the concentration.[232] The determination of Ru forms in solution remains however very challenging, due to the multiple degrees of polymerization of the Ru chloro-complexes as well as the co-existence of different oxidation states for Ru.[233] Considering the aqueous Ru chloro-complexes distribution diagrams (Figure 38) with the chloride concentration evolution, it could be proposed to rule out the existence of negatively-charged Ru complexes such as $RuCl_6^{3-}$, $RuCl_5(H_2O)^{2-}$ and $RuCl_4(H_2O)^{2-}$ in the TiO_2 suspension in the range of pH 2-8 (10^{-8}-10^{-2} M HCl). Thus it was assumed that the Ru species are most probably present as a mixture of $RuCl_3(H_2O)_3$, and of positively-charged $RuCl_2(H_2O)_4^{+}$ and $RuCl(H_2O)_5^{2+}$ species.[234,235]

[231] A.M. Ruppert, J. Grams, M. Jędrzejczyk, J. Matras-Michalska, N. Keller, K. Ostojska, P. Sautet, ChemSusChem. 2015, 8, 1538.
[232] J.A. Rard, Chem. Rev. 1985, 85,1.
[233] H.H. Cady, R.E. Connick, J.A.C.S. 1958, 80, 2646.
[234] R.E. Connick, Advances in the Chemistry of the Coordination Compounds. Ed. S. Kirschner, Mac Millan, 1961.
[235] D.A. Fine, Thesis. University of California at Berkeley, 1958.

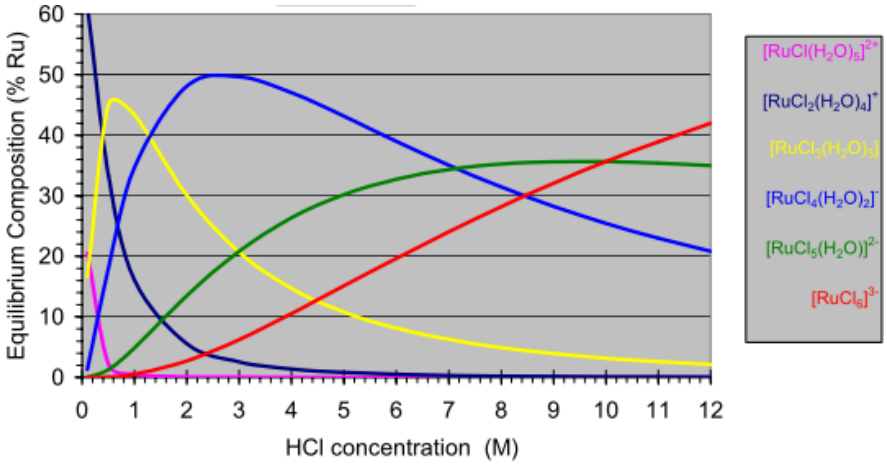

Figure 38. Distribution diagram for $[RuCl_{6-n}(H_2O)_n]_{n-3}$.[233]

As a result, at low pH, the adsorption of Ru species on the positively-charged TiO_2 surface was unfavored due to electrostatic repulsion, while by contrast the increase in the pH of the solution above the isoelectrical point strongly enhanced the adsorption of Ru species on the positively-charged TiO_2 surface.

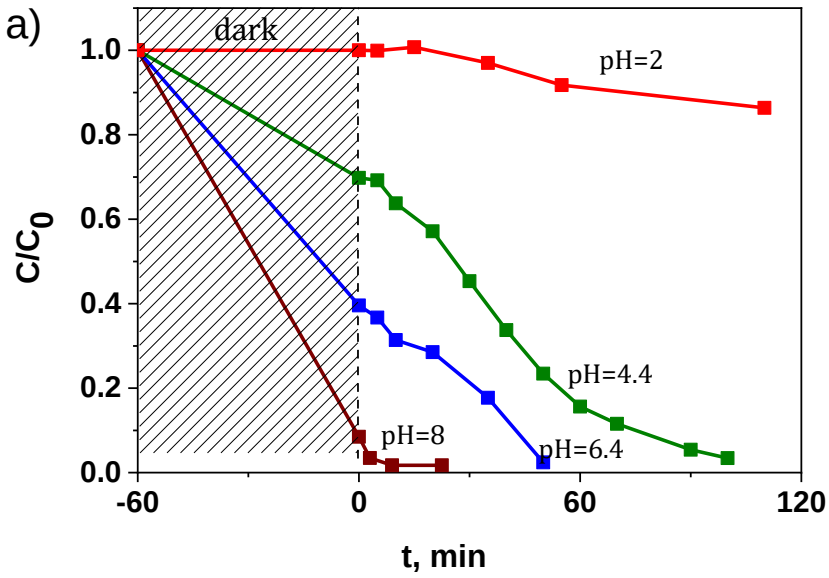

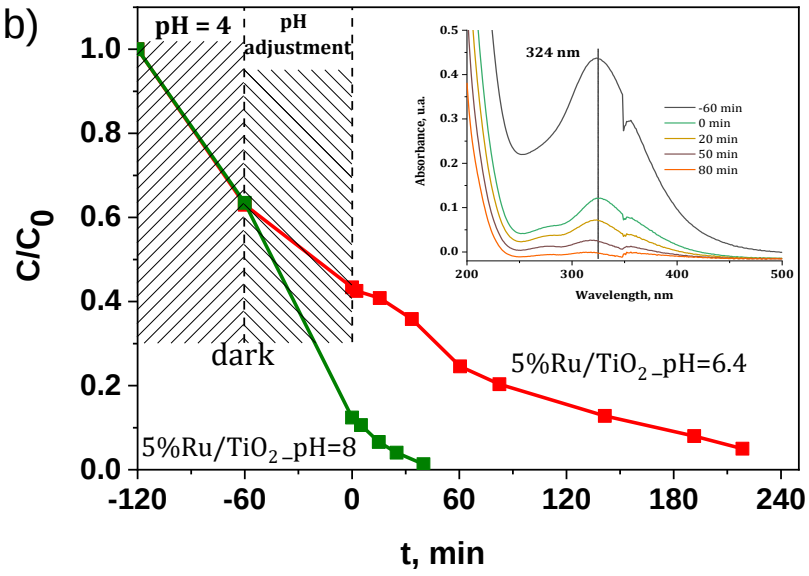

Figure 39. a) Influence of the pH of the precursor solution on the disappearance of the $RuCl_3$ precursor in the presence of TiO_2-P25 as a function of the illumination time for a Ru content of 0.5 wt. %; b) Disappearance of the $RuCl_3$ precursor in the presence of TiO_2-P25 as a function of the illumination time at pH 6.4 and pH 8.0, with a Ru content of 5 wt. %. Inset: UV-vis absorbance spectra evolution as a function of the illumination time during the photo-assisted synthesis of Ru(5 wt. %)/TiO_2 at pH 8.

The strong influence of the pH on the adsorption behavior and consequently on the photodeposition kinetics opened the possibility of preparing Ru/TiO_2 catalysts with a high Ru metal loading of 5 wt. %, as shown in Figure 39b. At a higher Ru loading, a similar C/C_0 profile was obtained, with a higher adsorption on the TiO_2 support at pH 8 compared to that observed at pH 6.4, so that a reaction time greater than 200 min was needed for achieving the complete disappearance of the Ru precursor at pH 6.4, while less than 60 min was necessary at pH 8.

4.6. Characterization of the Ru(5 wt. %)/TiO_2 P25 catalyst

Table 4 shows the real metal content of the materials after the photo-assisted deposition. An excellent agreement was obtained between the measured Ru content and the theoretical one derived from the evolution of the UV-vis absorption signal, with a relative difference being at the maximum of about 4%.

Table 4. Ru content in Ru/TiO_2 P25 materials analyzed by ICP-OES.

Sample name	Ru content, wt.%
5%Ru/TiO_2_Cl_pH 6.4	4.8 ± 0.1
5%Ru/TiO_2_Cl_pH 8	4.9 ± 0.1

Figure 40 shows the TEM images with the corresponding histograms of the Ru nanoparticle size distribution for the Ru(5 wt.%)/TiO_2-P25 catalyst prepared at pH 8.0 and pH 6.4. First, in both cases the supported nanoparticles were homogeneously dispersed and no ruthenium aggregates were observed. Small and sharp nanoparticle size distributions were obtained, centered on 0.8 nm (FWHM= 0.34 nm) and 1.0 nm (FWHM= 0.70 nm) at pH 8.0 and pH 6.4, respectively. The slightly smaller and sharper particle size distribution achieved at pH 8.0 was attributed to the higher pre-adsorption of the aqueous Ru chloro-complexes with the negatively-charged TiO_2 surface at this pH that led to maintain a higher and narrower dispersion at the support surface. When performing the reaction at pH 8, it is remarkable that increasing the Ru content by an order of magnitude (from 0.5 wt.% to 5 wt.%) did not result neither in a strong increase in the mean particle size, nor in its broadening.

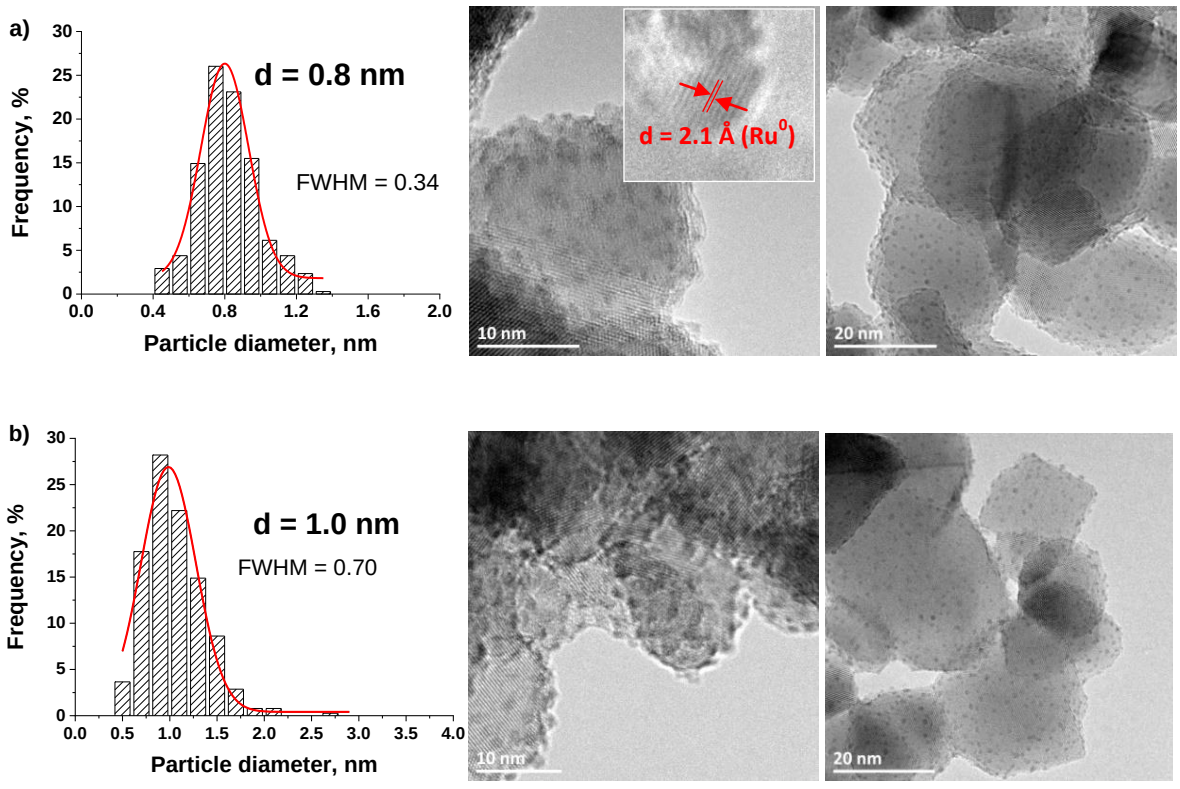

Figure 40. TEM image and the corresponding Ru nanoparticle size distribution for the Ru(5 wt.%)/TiO$_2$-P25 catalysts prepared (a) at pH=8 with the measured interplane distance of (101) planes of metallic Ru; and (b) at pH=6.4.

The metallic nature of the supported nanoparticles of the Ru(5 wt.%)/TiO$_2$ catalyst was confirmed by the high resolution TEM image (insert of Figure 40a) that evidenced an interplane distance of 2.1 Å corresponding to the atomic (101) planes of metallic Ru, as well as by XPS surface characterization (Figure 41). The Ru 3p$_{1/2}$ and Ru 3d$_{5/2}$ - Ru 3d$_{3/2}$ orbital XPS spectra exhibited similar patterns than those recorded on the Ru(0.5 wt.%)/TiO$_2$ catalyst. They differed only in terms of Ru/Ti surface atomic ratio, calculated at 0.23 for 5 wt.% of Ru *vs.* 0.02 for 0.5 wt.% of Ru. The higher surface atomic ratio (ie. 10 x higher) characterized the maintenance of a very high dispersion of small size Ru nanoparticles at the surface of the TiO$_2$ support while increasing the Ru loading of an order of magnitude up to 5 wt.%, in agreement with the slight increase in mean particle size from 0.6 nm to 0.8 nm and the slight increase in FHWM from 0.27 nm to 0.34 nm.

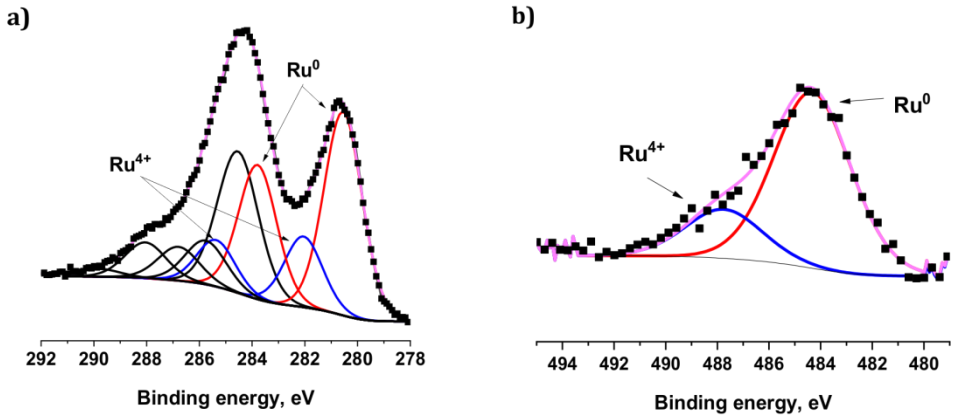

Figure 41. a) Ru 3d + C 1s ; b) Ru 3p XPS profile of the Ru(5 wt.%)/TiO$_2$-P25 catalysts. No presence of any residual chlorine species was observed by XPS at the surface of TiO$_2$ when the chloride precursor was used (Cl 2p XPS spectra not shown).

This highlighted the interest of the synthesis method for preparing Ru/TiO$_2$ catalysts with well-calibrated Ru nanoparticles dispersed at the surface of the TiO$_2$ support.

To conclude, considering the Ru nanoparticle size distribution obtained and the faster synthesis observed at pH 8 compared to that observed at pH 6.4, pH 8 was therefore chosen for preparing the Ru catalysts on TiO_2 P25 as well as on Ca-free and Ca-modified sol-gel TiO_2 supports to be further used in the catalytic tests (Chapters 5 and 6).

4.7. **Influence of the thermal reduction**

The stability of the Ru(5 wt. %)/TiO_2 catalyst has been evaluated by submitting the as-prepared catalysts to further reduction under hydrogen at 200°C for 1 h. Those conditions are classical conditions for getting metallic Ru nanoparticles on supports such as *eg.* titania, activated carbon, alumina or zirconia from acetylacetonate or chloride precursors.[236,237,238] Figure 42 shows the TEM images and the corresponding histograms of the Ru nanoparticle size distribution for the treated Ru/TiO_2-P25 catalyst.

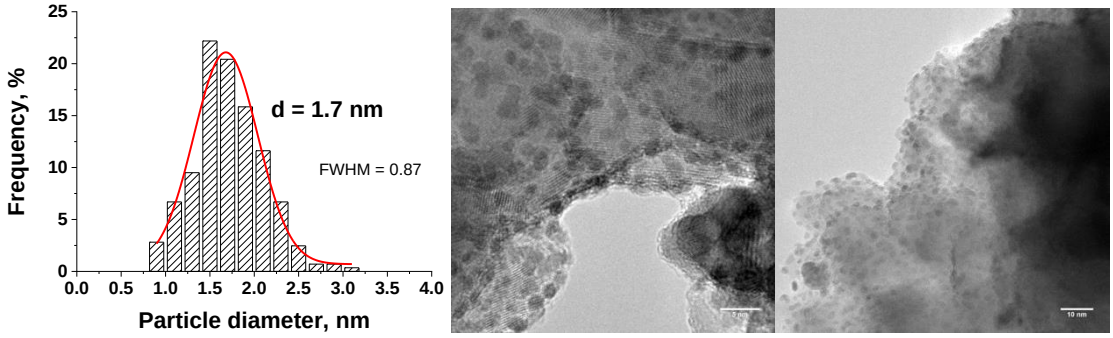

Figure 42. TEM images and the corresponding histogram of the Ru nanoparticle size distribution for the Ru(5 wt.%)/TiO_2-P25 catalyst obtained by the photo-assisted preparation method, after treatment at 200°C under hydrogen for 1 h.

It was worth noting that the Ru(5 wt.%)/TiO_2 catalyst displayed a good resistance to nanoparticle sintering and growth. Indeed, although the mean Ru particle size (slightly) increased from 0.8 nm to 1.7 nm, with a (slight) broadening of the distribution from 0.27 nm to 0.87 nm in terms of FWHM values, the nanoparticles remained homogeneously dispersed on the support, and the characteristic values remained

[236] A.M. Ruppert, M. Jędrzejczyk, O. Sneka-Płatek, N. Keller, A.S. Dumon, C. Michel, P. Sautet, J. Grams, Green Chem. 2016, 18, 2014.
[237] A.M. Ruppert, J. Grams, M. Jędrzejczyk, J. Matras-Michalska, N. Keller, K. Ostojska, P. Sautet, ChemSusChem. 2015, 8, 1538.
[238] M. Wachala, J. Grams, W. Kwapinski, A.M. Ruppert, Int J Hydrogen Energy, 2016, 41, 8688.

far smaller than those obtained *via* a wet impregnation method with thermal reduction in hydrogen (mean particle size of 2.9 nm with a FWHM of 1.86, cf. Figure 47a).

4.8. Scale-up of the Ru(5 wt. %)/TiO$_2$ catalyst preparation

So far, all the materials were prepared at relatively small scale by irradiating 100 mL dispersion at 1 g/L of support for producing only 100 mg of the catalysts per reaction batch. It means that the preparation of higher amounts of samples would require performing several photodeposition runs (at least 10 times) to achieve the desired amount of catalysts necessary for performing the catalytic investigation. This approach is much more time consuming, not justified economically and would require additional extended characterization of samples. Therefore, the preparation of higher amounts of the catalysts is crucial and the photodeposition was subsequently performed using 1 L of the solvent at 1 g/L concentration of catalyst for producing 1 g of the catalyst per synthesis batch. All other process parameters remained unchanged (see Chapter 2.2.2.).

Figure 43 shows the comparison of the C/C$_0$ curves for the preparation of 5%Ru/TiO$_2$ at small (100 mg) and large scale (1.0 g) and the influence of the scale on the photodeposition duration.

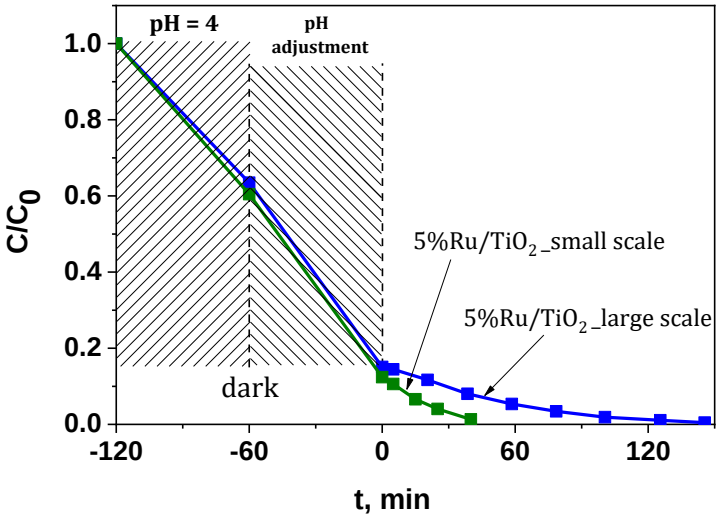

Figure 43. Disappearance of the RuCl$_3$ in the presence of TiO$_2$ (P25) as a function of the illumination time for 5%Ru/TiO$_2$ prepared at pH 8 a) at small scale (100 mL, 100 mg) and b) at large scale (1 L, 1 g).

Although the photodeposition process carried out in a large scale requires a higher volume of the dispersion and a longer irradiation time, the characterization data showed that both processes led to the preparation of the same materials. The longer irradiation time might be related most probably to a worse illumination at the bottom part of the beaker due to the higher thickness of the dispersion volume or a less homogenous stirring.

Figure 44 shows the TEM images of the 5%Ru/TiO_2 P25 prepared at large scale. It can be concluded that the process scale does affect neither the Ru particle size nor their distribution. The only difference is a slight increase in the FWHM value from 0.34 nm to 0.46 nm that might result from the longer irradiation time.

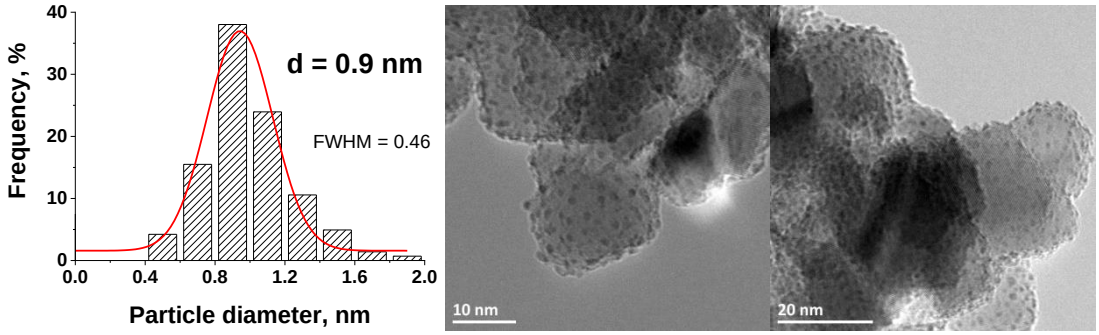

Figure 44. TEM images and the corresponding histogram of the Ru nanoparticle size distribution for the Ru(5 wt.%)/TiO_2-P25 catalyst obtained by the photdeposition method at the large scale at pH 8.

Therefore the final set of the 5%Ru/TiO_2 catalysts prepared with the different TiO_2 and Ca-modified TiO_2 sol-gel supports was obtained by implementing the photo-assisted synthesis at a large scale at pH 8 (Figure 33). Whatever the catalyst prepared, the C/C_0 disappearance curves showed similar profiles, although some differences in the adsorption step were observed. With the increasing amount of calcium the sample become more negative due to the increased number of unsaturated O^{2-} ions and therefore positively charged Ru species could be much easier and faster adsorbed on the surface of the nanoparticles.

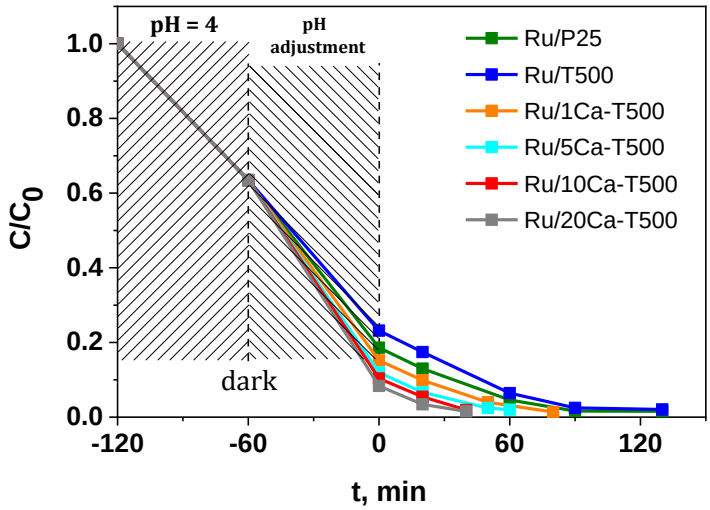

Figure 45. Disappearance of the $RuCl_3$ in the presence of TiO_2 – based supports as a function of the illumination time for 5%Ru/TiO_2 prepared at pH 8 at large scale (1 L, 1 g).

Table 5 presents the real Ru in the catalysts and as could be observed exactly the same amount of 5% of metal was achieved in each case.

Table 5. Ru content in Ru/TiO_2 materials prepared at large scale at pH 8 analysed by ICP-OES.

Sample name	Ru content, wt.%
5%Ru/TiO_2_Cl_pH 8	4.9 ± 0.1
5%Ru/T500_Cl_pH 8	5.1 ± 0.2
5%Ru/1Ca-T500_Cl_pH 8	5.0 ± 0.1
5%Ru/5Ca-T500_Cl_pH 8	5.1 ± 0.2
5%Ru/10Ca-T500_Cl_pH 8	4.9 ± 0.1
5%Ru/20Ca-T500_Cl_pH 8	4.9 ± 0.1

The TEM images of the Ru/TiO_2 catalysts together with the corresponding Ru nanoparticle size distributions are presented in Figure 46.

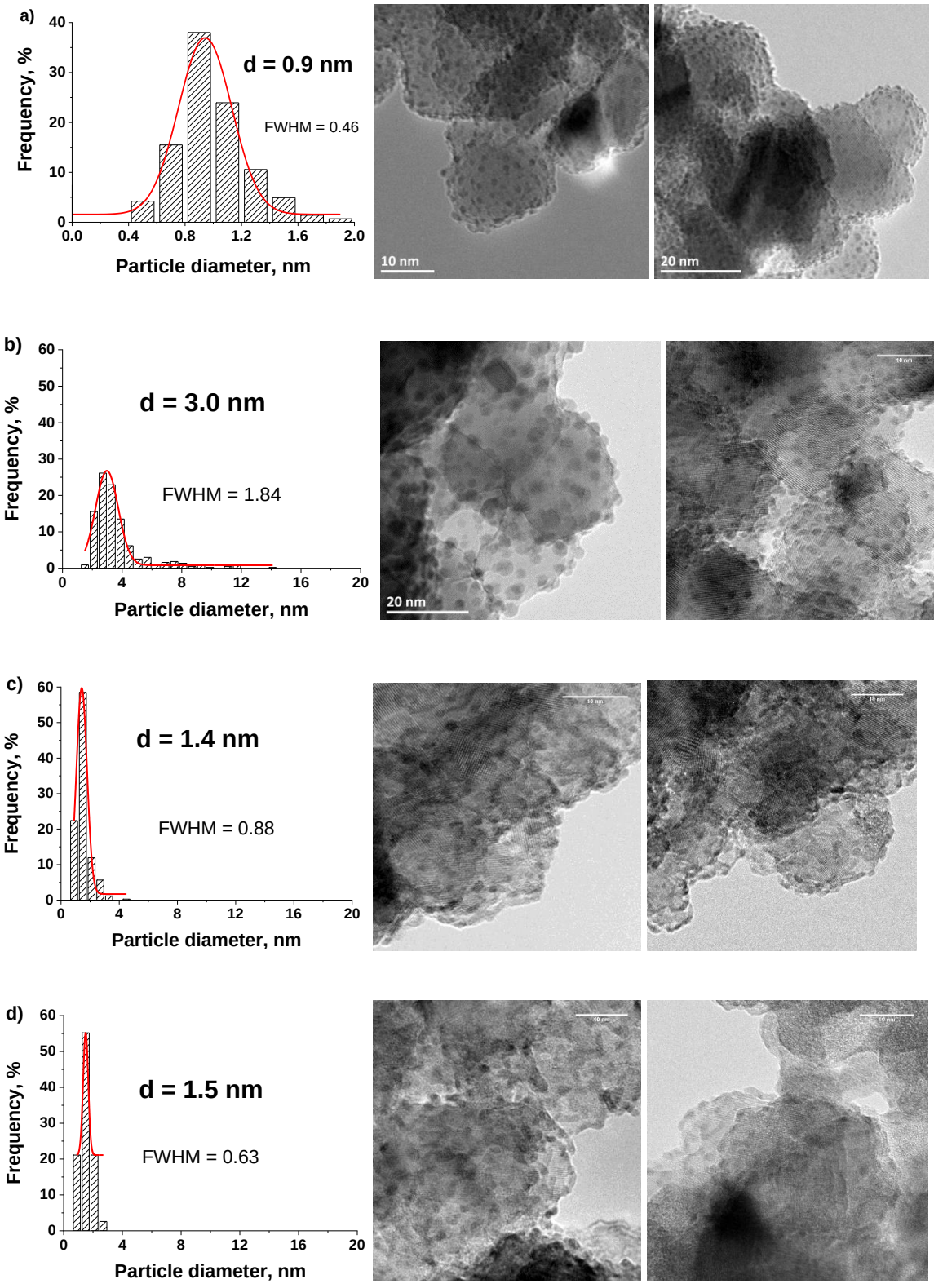
a)
Frequency, %
d = 0.9 nm
FWHM = 0.46
Particle diameter, nm
10 nm
20 nm
b)
Frequency, %
d = 3.0 nm
FWHM = 1.84
Particle diameter, nm
20 nm
c)
Frequency, %
d = 1.4 nm
FWHM = 0.88
Particle diameter, nm
d)
Frequency, %
d = 1.5 nm
FWHM = 0.63
Particle diameter, nm

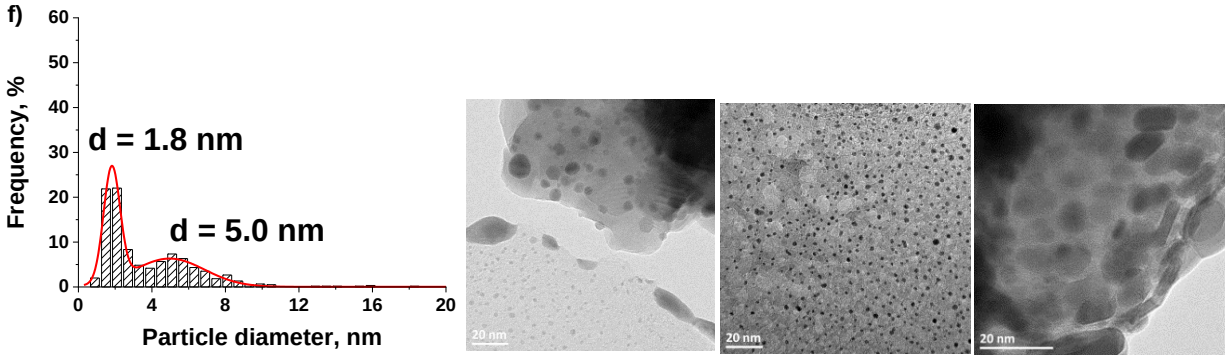

Figure 46. *TEM images and the corresponding histograms of the Ru nanoparticle size distribution for the catalysts prepared via the photo-assisted synthesis approach: a) Ru/P25; b) Ru/T500; c) Ru/1Ca-T500; d) Ru/5Ca-T500; e) Ru/10Ca-T500.*

The supported nanoparticles were homogeneously dispersed and no large ruthenium nanoparticle aggregates were observed. Small Ru nanoparticles were synthesized on the supports, with sharp nanoparticle size distributions centered on small particle sizes. The smallest and sharpest Ru nanoparticle size distribution was obtained on the Ru/P25 catalyst with a sub-nanometric mean size of 0.9 nm and a very small FWHM of 0.46 nm, while the Ru/T500 catalyst displayed the largest particle size centered on 3 nm with the largest FWHM of 1.8 nm. Globally, the presence of Ca in the support decreased the mean Ru particle size. Modifying the TiO_2 support with 1-5 wt.% of Ca led to reduce the mean Ru particle size down to 1.4-1.5 nm with a much sharper size distribution (FWHM=0.6-0.8 nm) when compared to that obtained on the sol-gel TiO_2 reference. Only in the case of the Ru/10Ca-T500 catalyst, a bimodal distribution was identified, with the significant contribution of larger particles centered on 5 nm in size in parallel to the well-calibrated small size particles at 1.8 nm. Detailed hypothesis would require additional experiments. The bimodal distribution might result from the increased amount of amorphous phase in the material when increasing the Ca content or from different bulk and surface charge recombination rates between both $CaTiO_3$ and TiO_2 semiconductor phases, which in both cases might impact the photogenerated charge dynamics at the support surface during the UV-A light-assisted preparation method.

The differences in terms of Ru particle size distribution between the samples could be explained by differences in terms of adsorption behavior resulting from BET surface area and surface chemistry differences as well as by differences in terms of photo-redox ability of the TiO_2-based supports.

When it comes to the interaction of Ru nanoparticles with the support composed of two different phases (anatase and calcium titanate), no selective location of the metal nanoparticles has been observed. Further, in the case of the catalysts prepared by the photo-assisted synthesis method, $CaTiO_3$ is a well-known titanium-based perovskite material with a wide band gap of ca. 3.3-3.5 eV that can be activated by UV light in a similar way than anatase TiO_2.[239,240] In addition, the position of both conduction and valence bands of the $CaTiO_3$ phase allows the reduction of the Ru^{3+} ions into metallic Ru.[241] This is in agreement with TEM observations (Figure 30) that revealed the location of Ru nanoparticles on both phases, so that Ru nanoparticles can interact with both $CaTiO_3$ and TiO_2 phases from the support. However, it was not possible to determine two different particle size distributions depending on the location of Ru nanoparticles on $CaTiO_3$ or TiO_2 phases, so that all the particle size distributions are global distributions.

4.9. Comparison with the Ru(5 wt. %)/TiO_2 prepared by the wet impregnation method

A series of 5%Ru/TiO_2 catalysts were prepared as well *via* classical incipient wetness impregnation followed by the reduction in H_2 flow for 1h at 200°C. Figure 47 shows the TEM images with the Ru particle size distributions of selected samples to compare with the ones prepared by the photochemical reduction method.

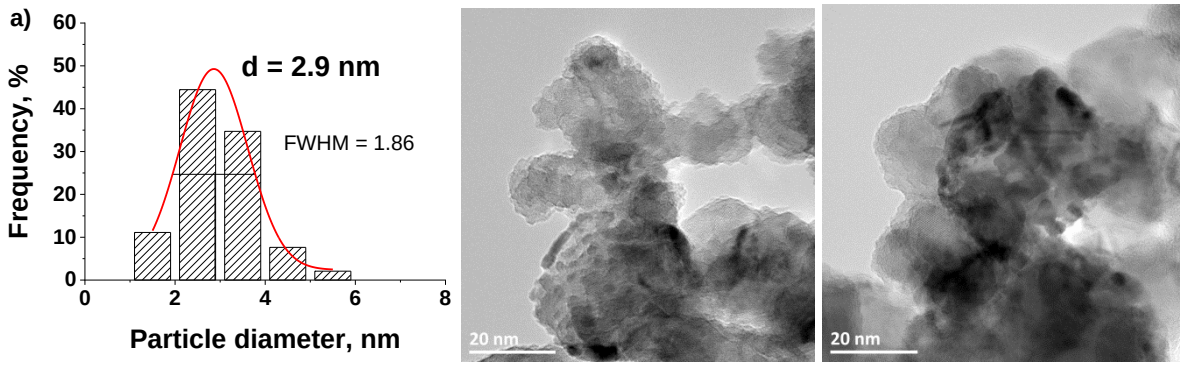

[239] J. Beilstein, Nanotechnol. 2018, 9, 671
[240] H. Zhang, G. Chen, Y. Li, Y. Teng, Int. J. Hydrogen Energy 2010, 35, 2713.
[241] J.S. Jang, P.H. Borse, J.S. Lee, K.T. Lim, O.S. Jung, E.D. Jeong, J.S. Bae, H.G. Kim, Bull. Korean Chem. Soc. 2011, 32(1) 95

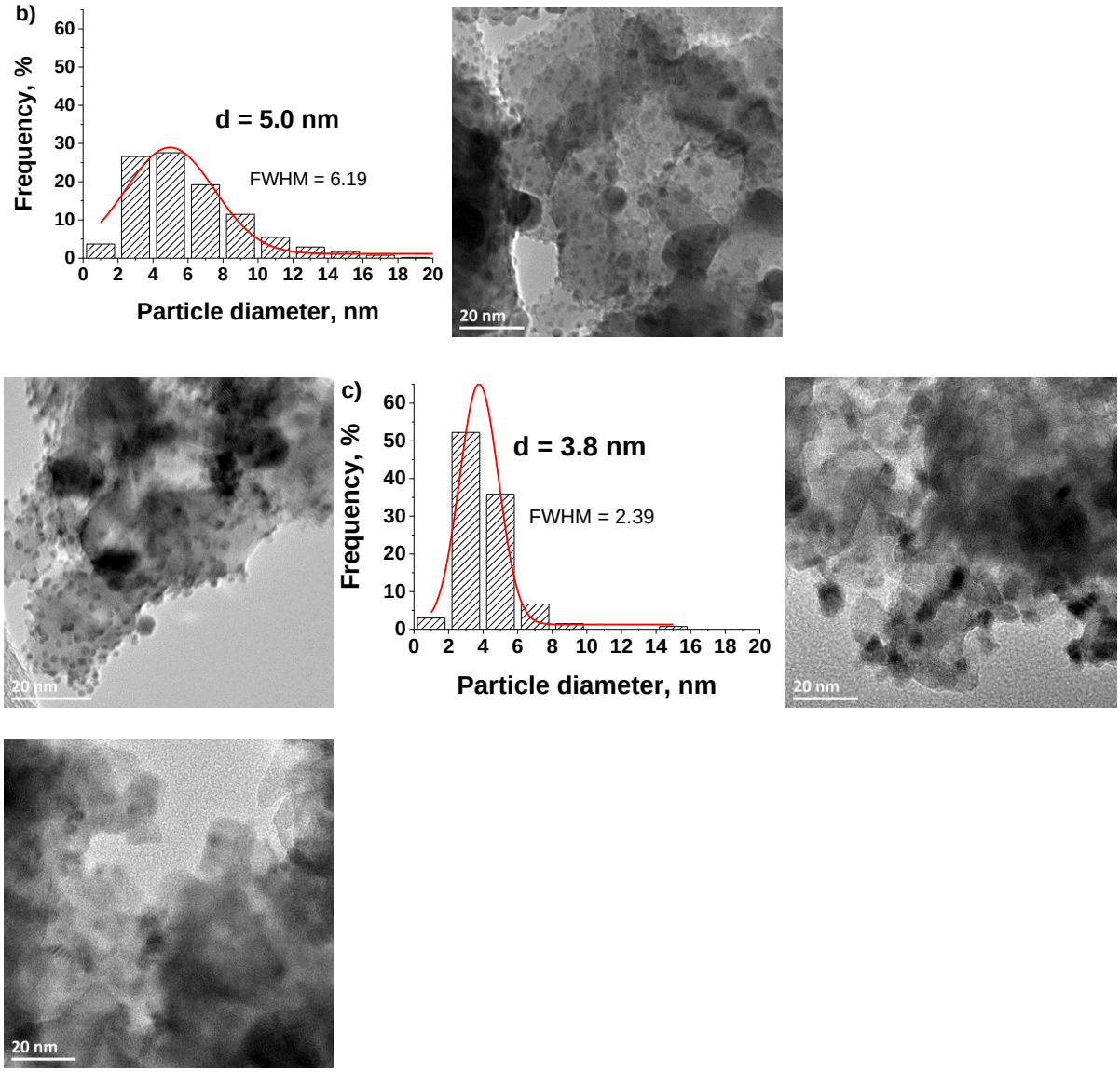

Figure 47. TEM images and the corresponding histograms of the Ru nanoparticle size distribution for the catalysts prepared via classical incipient wet impregnation with final thermal treatment under hydrogen: a) 5%Ru/P25-I; b)5%Ru/T500-I; c) 5%Ru/10Ca-T500-I.

As could be seen, the 5%Ru/P25-I sample exhibited the smallest mean particle size of 2.9 nm with the narrowest size distribution (FWHM = 1.9). By contrast, the 5%Ru/T500-I sample was characterized by a broader nanoparticle size distribution (FWHM = 6.2), centered on a much larger mean Ru nanoparticle size at 5 nm, together with the contribution of very large particles, up to 18 nm in size. Modifying the support with 10% of Ca improved the dispersion of the supported nanoparticles, with a reduced mean Ru particle size at 3.8 nm and a more homogeneous size distribution (FWHM = 2.4).

This however contrasted strongly with the catalysts prepared by the photodeposition as it was evidenced that the use of the alternative preparation method allowed Ru/TiO_2 catalysts to be prepared with much smaller Ru nanoparticle size than when using the classical incipient wet impregnation. Moreover it is worth noting that the Ru particle size for the sample prepared by the photodeposition and reduced in H_2 at 200°C remained still far lower, and a particle size distribution still far sharper, than those obtained on the Ru(5 wt.%)/TiO_2 catalyst prepared *via* classical impregnation with final reduction in hydrogen at 200°C.

4.10. Concluding remarks

An elegant low-temperature one-step photo-assisted method has been developed as sustainable alternative to the classical wet impregnation of the support, for synthesizing highly dispersed metallic Ru nanoparticles on TiO_2, using the redox photoactivity developed by the TiO_2 support under solar light. Considering the 3.2 eV band gap of TiO_2 material, the UV-A light photon from the solar light spectra allows the promotions of electrons from the valence band to the conduction band of the semi-conductor, further able to directly reduce at room temperature highly dispersed pre-adsorbed metal ions at the surface of the support. Whether the Ru chloride or the Ru acetylacetonate precursor precursor was used, sub-nanometric metallic Ru nanoparticles were synthesized on the TiO_2 support with a sharp size distribution. TEM and XPS characterizations evidenced the high dispersion and the metallic nature of the Ru nanoparticles on TiO_2. The chloride precursor was proposed to be more suitable than the acetylacetonate one for preparing Ru/TiO_2 catalysts, due to the lower photodeposition efficiency observed with acetylacetonate, that did not allow to synthesize Ru nanoparticles with a loading higher than 1 wt.% in contrary to the chloride precursor.

It has been proposed that different reaction mechanisms take place at the TiO_2 surface depending on the Ru precursor used. The photo-assisted synthesis mechanism has been discussed to involve the sole photogenerated electrons in the case of the chloride, while both photogenerated holes and electrons would be involved in oxidation and reduction steps, respectively, in the case of the acetylacetonate precursor, the first necessary step being the photocatalytic oxidation of the acetylacetonate ligand.

Further, it was demonstrated that a fine monitoring of the metal Ru nanoparticle size on the TiO_2 support was possible *via* a controlled growth of the Ru nanoclusters under irradiation, allowing the synthesis of well-calibrated metallic nanoparticles to be achieved.[242]

It was shown that increasing the pH led to significantly enhanced adsorption of the Ru precursor species on the TiO_2 support in the dark, allowing further for the preparation of Ru/TiO_2 catalysts with higher Ru contents. The size distribution of the supported sub-nanometric size Ru nanoparticles was not strongly influenced by the Ru content within a large 0.5-5 wt. % range.

Far smaller Ru nanoparticles with sharper size distribution were synthesized *via* photodeposition when compared to the catalysts prepared *via* incipient wet impregnation with final thermal reduction in hydrogen.

[242] J. Wojciechowska, E. Gitzhofer, J. Grams, A. M. Ruppert, N.Keller, Catalysis Today, 2018, 10.1016/j.cattod.2018.07.013.

CHAPTER 5

5. Ru/TiO_2-BASED CATALYSTS IN THE LEVULINIC ACID HYDROGENATION WITH FORMIC ACID AS INTERNAL H_2 SOURCE

This chapter is devoted to the evaluation and the understanding of the catalytic behavior of 5%Ru/TiO_2-based catalysts prepared by wet impregnation and photodeposition methods in the levulinic hydrogenation using formic acid as internal source of hydrogen.

So, this chapter will first present some specific surface characterizations of the supported Ru catalysts (temperature programmed reduction, CO-FTIR, ToF-SIMS analysis) before to report on the catalytic performances of the catalysts in the one-pot simultaneous formic acid decomposition and levulinic acid hydrogenation (FALA reaction). The catalysts were further tested in both FA dehydrogenation and LA hydrogenation separated reactions for evidencing the influence of the catalyst modification on each single reaction, and for getting insight on the catalyst features playing a role in the achievement of enhanced performances in the process.

The detailed preparation of the supports and the catalysts can be found in Chapters 2.1 and 2.2, and the detailed experimental protocols and reaction conditions can be found in Chapter 2.4.

5.1. **Temperature programed reduction (TPR) measurements**

To study the reducibility of the Ru/TiO_2 catalysts prepared by impregnation as well as to understand the influence of the Ca modification on the physicochemical properties of the catalysts, temperature programed reduction (TPR) measurements were performed. TPR profiles are only shown for Ru catalysts prepared by impregnation, since the photodeposition method led to directly synthesize metallic Ru nanoparticles on the support. TPR profiles were recorded after performing a slight in-situ oxidative treatment in air (200°C for 30 min) on the impregnated supports after a drying step, allowing the decomposition of the chloride precursor. This temperature of pretreatment was chosen for preventing the occurrence of nanoparticle sintering, and only allows to clean the surface before the TPR

measurement. This has been confirmed by comparing the TPR profiles of catalysts pretreated at 120°C and at 200°C. As illustrated in the following Figure 48, the similar following TPR profiles (200°C vs. 120°C) indicated that a pretreatment at 200°C does not influence the TPR results, by contrast to a pretreatment at 350°C.

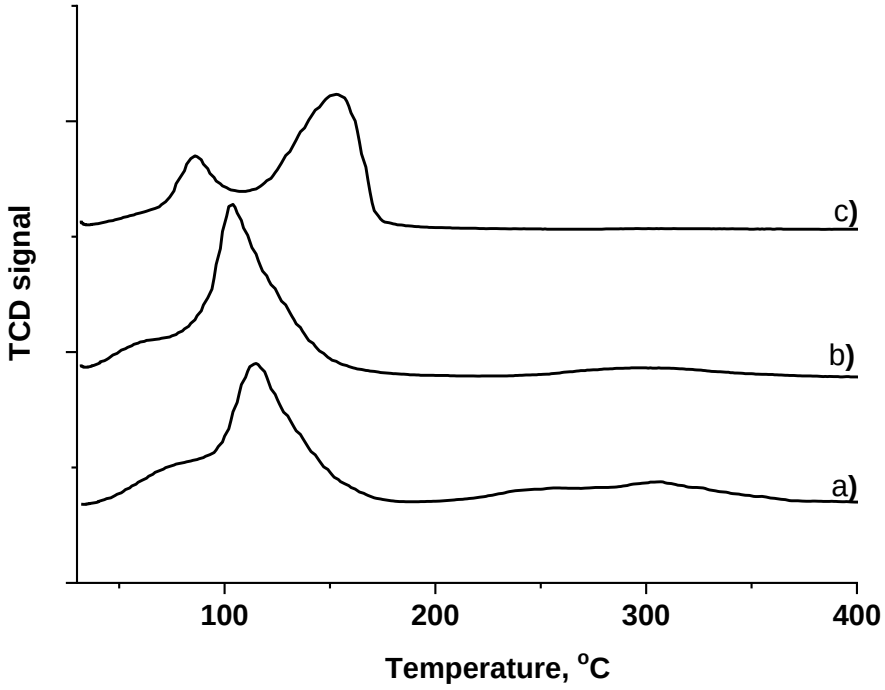

Figure 48. TPR results of 5%Ru/TiO_2 (P25) catalysts after oxidative pre-treatment for 30 min at different temperatures a) 120°C, b) 200°C and c) 350°C; [0.1 g of the dried catalyst, H_2/Ar 5:95 v/v, 20 ml/min, 10°C/min].

Figure 49 shows that all the catalysts prepared by impregnation exhibit one main reduction maximum. On both commercial and sol-gel titania, the profiles look very similar, with a maximum at 110°C that could be most probably attributed to the reduction of well dispersed crystalline RuO_2.[243,244] The very low H_2 consumption with no clear maximum observed at lower temperature before the appearance of the main signal could be assigned to the presence of well dispersed, small and amorphous RuO_2.[245] With the addition of Ca to the support, the reduction maximum is shifted towards higher temperatures, from 140°C for 1%, to 200-210°C for the highest Ca content, indicating stronger

[243] X. Liu, J. Zeng, W. Shi, J. Wang, T. Zhu, Y. Chen, Catal. Sci. Technol. 2017, 7, 213.
[244] D. P. Debecker, B. Farin, E. M. Gaigneaux, C. Sanchez, C. Sassoye, Appl Catal A, 2014, 481, 11
[245] L. Li, L. Qu, J. Cheng, J. Li, Z. Hao, Appl Catal B, 2009, 88, 224.

interactions of RuO_2 with TiO_2. Similar effect of strengthening of the metal–support interaction was observed by Carrero et al. in Mg and Ca-promoted Ni–Cu/SiO_2 catalysts.[246] Moreover in the case of the Ca-modified samples, a third smaller and very broad shoulder is observed between 190°C-300°C, which increases with the Ca loading. This might be associated with RuO_2 with strong interactions with the $CaTiO_3$ phase. Another possible interpretation might be the presence of ruthenium oxychloride species $RuOCl_x$ which are more difficult to reduce.[247] Besides, in our previous work the presence of ruthenium oxychloride was also speculated, although on carbon support.[248] It could be hypothetised that the stabilization of $RuOCl_x$ species might be facilitated by the presence of Ca^{2+} on the surface of the catalyst.

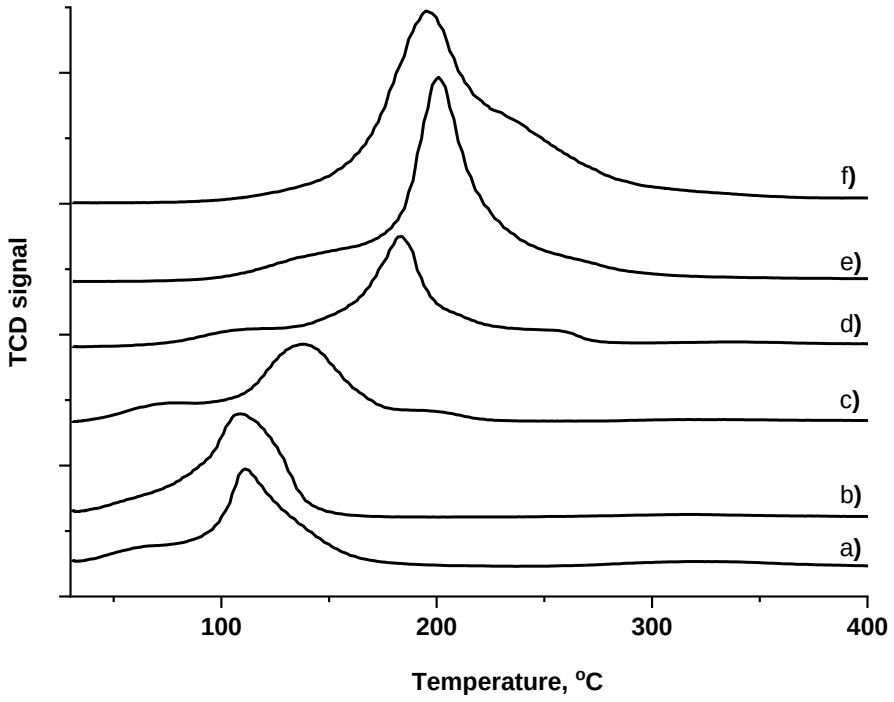

Figure 49. TPR profiles of calcined Ru catalysts prepared by the impregnation method a) Ru/P25-I; b) Ru/T500-I; c) Ru/1Ca-T500-I; d) Ru/5Ca-T500-I; e) Ru/10Ca-T500-I; f) Ru/20Ca-T500-I; [0.1 g of the dried catalyst calcined in-situ. at 200°C for 30 min, H_2/Ar 5:95 v/v, 20 ml/min, 10°C/min].

[246] A. Carrero, J.A. Calles, A.J. Vizcaíno, Chem Eng J. 2010, 163, 395
[247] D. Eliche-Quesada, M.I. Macías-Ortiz, J. Jiménez-Jiménez, E. Rodríguez-Castellón, A. Jiménez-López, J Mol Catal A, 2006, 255, 41.
[248] A.M. Ruppert, M. Jędrzejczyk, O. Sneka-Płatek, N. Keller, A.S. Dumon, C. Michel, P. Sautet, J. Grams, Green Chem. 2016,18, 2014.

5.2. CO-FTIR studies

FTIR spectra of adsorbed CO are presented in Figure 50 for catalysts prepared by impregnation. The spectra show bands at frequencies 2138 cm^{-1}, 2084 cm^{-1} and 2016 cm^{-1} with a shoulder at 1980 cm^{-1} that are attributed to CO adsorbed on Ru crystallites. In addition, in the spectra of samples containing 5%, 10% and 20% of Ca, a band at 1620 cm^{-1} is visible.

It has to be mentioned that in the case of supported Ru catalysts, there is an ongoing discussion on the interpretation of the FTIR spectra and on the peak assignment.[249,250,251,252] Both bands at 2084 cm^{-1} and 2138 cm-^{1} are assigned to the multicoordinated CO adsorption on electron deficient ruthenium particles $Ru^{\delta+}$.[253,254,255] The presence of positively-charged metal particles may result from its strong interaction with the carrier or the presence of chlorine.[252,254,255] Another mechanism involves the oxidation of metallic Ru induced by the reaction of adsorbed CO and hydroxyl groups of the support.[249] The band at 2016 cm^{-1} with a shoulder at 1980 cm^{-1} is attributed to CO linearly adsorbed on Ru sites.[253,254,255] In this region, there are bands which can be ascribed to the linear CO adsorption on faces and steps of Ru crystallites. It is however difficult to clearly differentiate between them as their exact position depends on the CO coverage.

On one hand, according to Blyholder et al., the shoulder at 1980 cm^{-1} represents the CO adsorption on edges, corners or dislocations of Ru particles. CO adsorption on lower coordination sites (like corners or edges) is stronger due to the reduced competition for electrons involved in the back-donation from the central Ru atom to carbon.[256] On another hand, this band was assigned by Elmasides at al. to CO adsorbed on metal sites strongly interacting with the support in Ca-doped Ru/TiO_2 materials.[257]

[249] K. Hadjivanov, J.-C. Lavalley, J. Lamotte, F. Mauge, J. Saint-Just, M.Che, J Catal. 1998, 176, 415-425.
[250] P. Panagiotopoulou, D. I. Kondarides, X. E. Verykios, J. Phys. Chem. 2011, 115, 1220-1230
[251] A. M. Abdel-Mageed, D. Widmann, S.E. Olesen, I. Chorkendorff, J. Biskupek, R.J. Behm, ASC Catal. 2015, 5, 6753
[252] V. Mazzieri, F. Coloma-Pascual, A. Arcoya, P.C. L`Argentiere, N.S. Figoli, Appl Surf Sci. 2003, 210, 222-230.
[253] S. Scirè, C. Crisafulli, R. Maggiore, S. Minicò, S. Galvagno, Catal Lett. 1998, 51, 41-45.
[254] C. Elmasides, D.I. Kondarides, J. Phys. Chem. B. 1999, 103, 5227-5239
[255] E. Guglielminotti, G.C. Bond, J. Chem. Soc. Faraday Trans. 1990, 86, 979-987.
[256] G. Blyholder, J Phys Chem. 1964, 68, 2772-2777.
[257] C. Elmasides, D.I. Kondarides, S.G. Neophytides, X. E. Verykios, J Catal. 2001, 198, 195-207

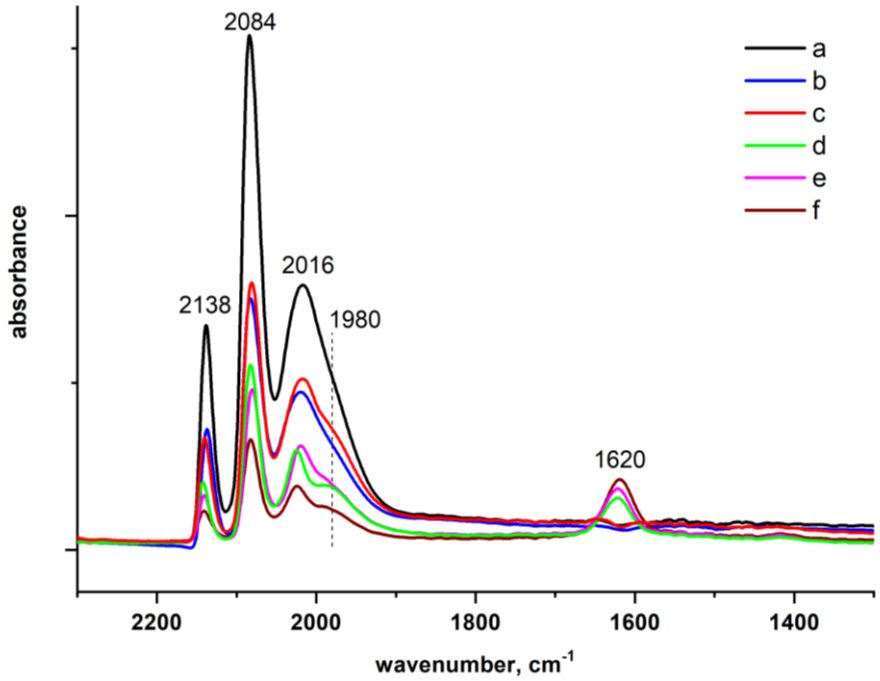

Figure 50. FTIR spectra of adsorbed CO obtained for the catalysts prepared by the impregnation method a) Ru/P25-I; b) Ru/T500-I; c) Ru/1Ca-T500-I; d) Ru/5Ca-T500-I; e) Ru/10Ca-T500-I; f) Ru/20Ca-T500-I; [20 mg of catalyst reduced at 200°C for 1 h in H_2, measurement at 40°C at flow 20 ml/min].

This is in agreement, first with Figure 50, evidencing that the contribution of this shoulder becomes more prominent (in respect of the 2016 cm^{-1} band) for samples containing more Ca, and further with the TPR results, showing that increasing the Ca content in the support facilitates stronger Ru-support interactions. Furthermore, the band located at 1620 cm^{-1}, which can be assigned to the carbonate type species formed on the surface of the available calcium cations, was evidenced in the case of the samples containing 5%, 10% and 20% of Ca.

When it comes to the intensity of different bands, it is necessary to point out that several aspects such as the metal particle size or the metal-support interactions can be responsible for the level of CO adsorbed. For Ru/P25-I, the highest CO adsorption was observed most probably due to the smallest Ru particle size. For Ru/T500-I, larger metal particles caused a drop in the amount of the adsorbed CO. Furthermore, a global trend is observed, CO adsorption globally decreased with increasing the Ca content. Considering that the Ru/10Ca-T500-I catalyst displayed a smaller mean particle size than the Ru/T-500 reference, the influence of the nanoparticle size does not seem to be predominant in the change in the CO

adsorption band intensity. Based on the TPR results, increasing contribution of Ca-modified support cause stronger Ru-support interactions. Therefore, it could be concluded that the CO adsorption on Ru strongly interacting with the support remains limited.

Figure 8 shows CO-FTIR spectra of the samples prepared by the photodeposition method. Analogous bands to those obtained for the materials prepared by impregnation were observed, however with the red shift for each band of about 10-20 cm^{-1}. The red shift could be explained either by the smaller Ru particle size for samples prepared by photodeposition or by a decrease in the dipole-dipole coupling effect of adsorbed CO molecules with decreasing coverage.[258] The band in the region 2000-1990 cm^{-1} is attributed to the linear CO adsorption on Ru, while the two bands at 2063 cm^{-1} and 2126 cm^{-1} represent the multicoordinated CO adsorption on Ru$^{\delta+}$.

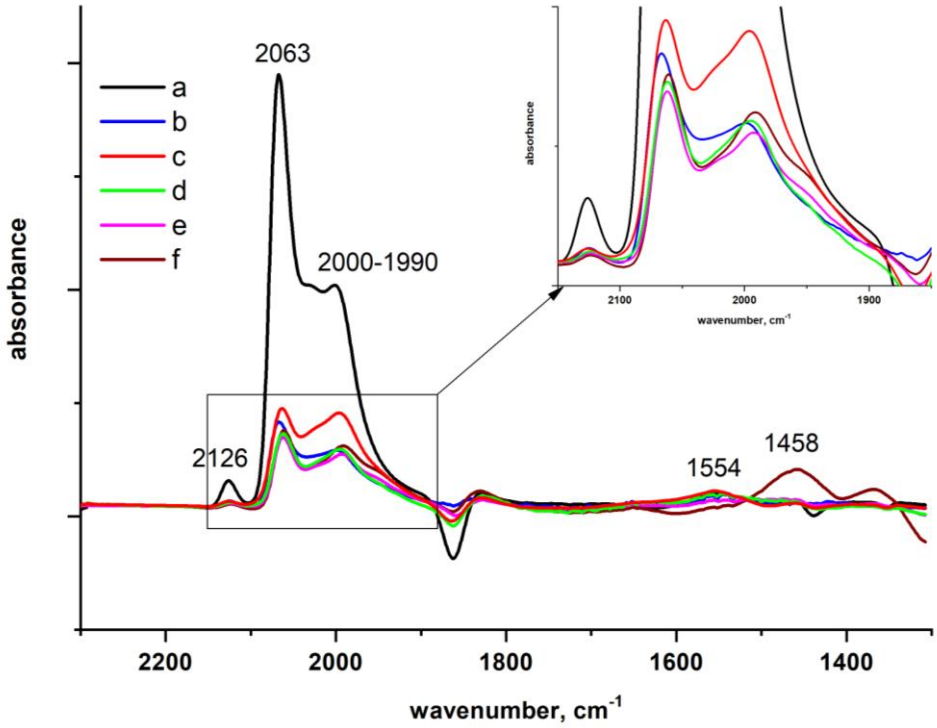

Figure 51. FTIR spectra of adsorbed CO obtained for the catalysts prepared by the photodeposition method a) Ru/P25-P; b) Ru/T500-P; c) Ru/1Ca-T500-P; d) Ru/5Ca-T500-P; e) Ru/10Ca-T500-P; f) Ru/20Ca-T500-P; [20 mg of catalyst reduced at 200^{o}C for 1 h in H$_2$, measurement at 40^{o}C at flow 20 ml/min].

[258] P. Panagiotopoulou, D. I. Kondarides, Appl Catal B. 2011, 101, 738-746.

The relationship between the particle size and the CO adsorption was similar for samples prepared by photodeposition, namely the highest intensity of the bands was identified on smallest particles of Ru/P25-P. A similar CO adsorption was observed whatever the Ca content of the modified TiO_2 materials, in agreement with the TPR analyses, for which it was concluded that all the tested samples exhibited the same type of metal-support interactions. Signals at 1458 cm^{-1} and 1554 cm^{-1} which are especially identified for Ru/20Ca-T500 correspond to the carbonate species adsorbed on the support.

5.3. **Analysis of the catalyst surface by ToF-SIMS analysis**

ToF-SIMS analysis of the catalyst surface was performed in order to understand the effect of the calcium modification and the ruthenium interactions with the support (Table 6).

Table 6. Normalized intensities of ions calculated on the basis of ToF-SIMS spectra collected from the surface of catalysts prepared by the impregnation and photodeposition method.

Sample	**Ions intensities**				
	$Ru^+/total^+ \times 10^{-2}$	$Ru^+/Ti^+ \times 10^{-1}$	$Ca^+/total^+ \times 10^{-2}$	Ca^+/Ti^+	$CaRuO_2^+/total^+ \times 10^{-4}$
Ru/T500-I	1.3	1.8	-	-	-
Ru/1Ca-T500-I	1.2	1.8	3.8	0.58	1.3
Ru/5Ca-T500-I	1.9	6.1	14.0	4.3	3.9
Ru/10Ca-T500-I	2.0	7.1	13.0	4.5	4.4
Ru/20Ca-T500-I	2.1	8.0	18.0	6.9	3.0
Ru/T500-P	2.3	7.7	-	-	-
Ru/1Ca-T500-P	2.2	5.6	2.7	0.69	1.2
Ru/5Ca-T500-P	2.5	11	5.6	2.5	1.8
Ru/10Ca-T500-P	2.6	9.0	7.0	2.5	1.9
Ru/20Ca-T500-P	2.2	6.0	9.1	2.5	2.2

It was observed that the signals from ruthenium and the Ru^+/Ti^+ ratio are the lowest in the case of Ru/T500-I and Ru/1Ca-T500-I among the samples prepared by the impregnation method. Moreover, by comparing the catalysts prepared by the two different methods, a slightly lower Ru intensity is observed

for the ones prepared by impregnation. This can be explained by the partial coverage of Ru by titania migrating during the thermal treatment which occurs to higher extent for samples prepared by impregnation.[259] This suggests also that the modification with Ca could stabilize the support to some extent. The smaller Ru intensity could be also related with the presence of larger crystallites.

It is worth noting that the intensities of Ru signal observed for those samples prepared by photodeposition are similar to each other meaning that metal particles deposited on the surface are within the same size range. Based on the comparison of the Ru^+/Ti^+ ratio, it is possible to say that either Ru is more exposed on the surface of TiO_2 in the case of the catalysts with higher amount of Ca (5, 10 and 20%). This effect is more pronounced in the case of the catalysts prepared by impregnation.

Further, the intensities of the signal originating from Ca^+ ion confirmed that there is more Ca on the surface when a higher amount of Ca was used for the support preparation whatever the synthesis method. It is however important to note that generally the intensity of the signals coming from Ca^+ are lower for the samples prepared by photodeposition, indicating that Ca is less exposed on the catalyst surface. The presence of $CaRuO_2^+$ ion confirms the existence of the interactions between the Ca-based phase and Ru, the intensity of the $CaRuO_2^+$ being globally higher for Ca-rich catalysts whatever the preparation method.

5.4. Catalytic activity

The catalytic activity of the different materials was evaluated in the simultaneous FA decomposition and LA hydrogenation towards GVL (FALA). First it was crucial to determine the proper conditions for reducing the catalysts. Although the standard reduction temperature for Ru catalysts is 200°C it might be suggested based on TPR results (Figure 49) that this temperature is not high enough for reducing entirely the Ru nanoparticles in Ca-modified samples. Therefore, the influence of the reduction temperature was first studied, and preliminary tests were performed with the Ru/10Ca-T500 and Ru/20Ca-T500 catalysts reduced at 200°C or 300°C to select the preparation conditions for the whole catalyst series.

[259] A. M. Ruppert, T. Paryjczak, Appl. Catal. A 2007, 320, 80

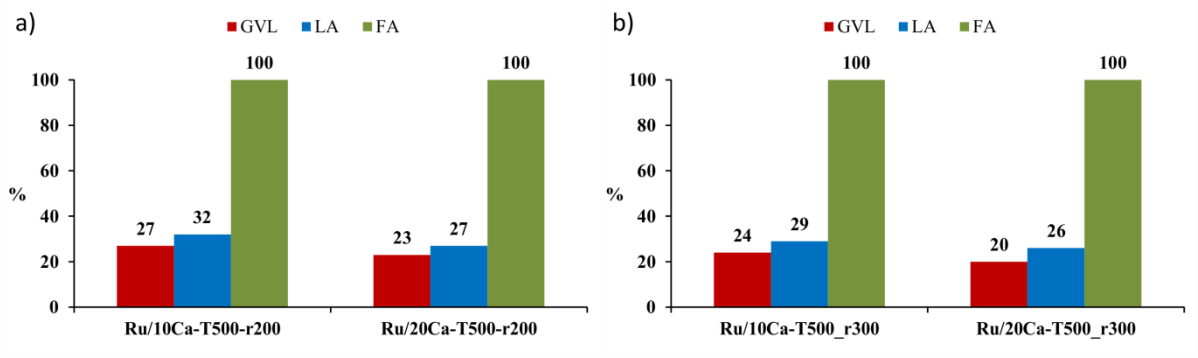

Figure 52. LA hydrogenation, FA decomposition and GVL yield obtained in the FALA reaction on the Ru/Ca-T500 catalysts prepared by the impregnation method reduced at a) 200^{o}C and b) 300^{o}C; [1 g of LA, 0.4 ml of FA, 0.6 g of catalyst, 30 ml of H$_2$O, 190 °C, 5 h].

Based on the results presented in Figure 52, it could be seen that the Ca-based catalysts reduced at two different temperatures gave very similar results in terms of LA conversion and GVL yield, while complete FA decomposition was achieved whatever the reduction temperature. Even slightly higher performances were obtained when the material was reduced at 200^{o}C. Therefore the milder reduction conditions were chosen for reducing the rest of the materials.

Catalytic performances of the catalysts in the one-pot FALA reaction.

Figure 53 shows both liquid and gaseous products formed in the reaction using Ru catalysts prepared by impregnation.

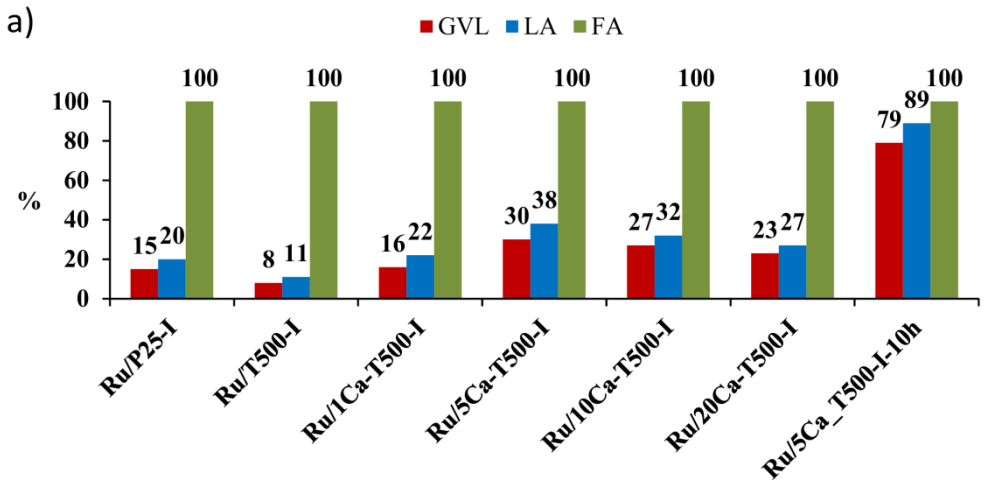

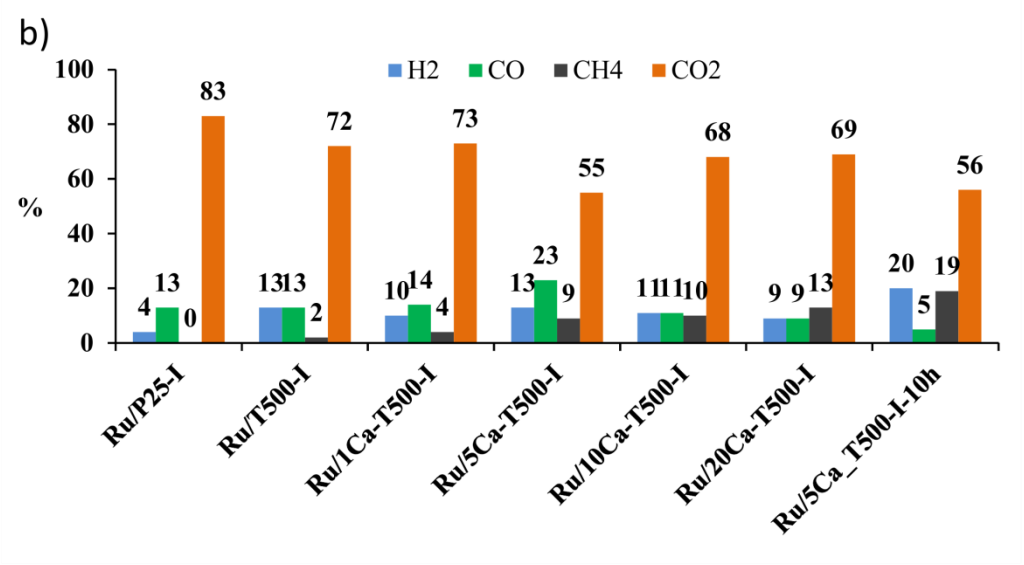

Figure 53. Catalytic activity of the Ru catalysts prepared by the impregnation method in the FALA reaction, in terms of a) LA hydrogenation, FA decomposition and GVL yield; and b) Gaseous product distribution; [1 g of LA, 0.4 ml of FA, 0.6 g of catalyst, 30 ml of H_2O, 190 °C, 5 h].

First, full decomposition of FA was achieved with all catalysts. The reference T500-based catalyst gave lower GVL yield (8%) than the commercial P25-based one (15%) which could be related to the larger Ru particle size (5 nm) supported on T500 than those on P25 (2.9 nm). It was however interesting to notice that the Ca-modified Ru catalysts performed much better than Ru supported on bare sol-gel TiO_2 and commercial P25 showing a positive effect of Ca modification. Initially, with the addition of 1% of Ca the catalytic performance is improved and it is comparable to the one obtained in case of Ru/P25. Further addition of Ca (5%) gives twofold increase in the GVL yield where 30% is produced making this catalyst the most active among this set of materials. Increasing concentration of calcium ions in the sample does not improve the catalytic ability of Ru catalysts and in fact causes a slight decrease in the LA conversion level and GVL yield.

When it comes to the distribution of gaseous products, expressed as vol%, it can be concluded that FA is decomposed most probably *via* two pathways, i.e. dehydration and dehydrogenation, leading to the formation of both CO and CO_2. Methane was also identified in the gas phase as a result of a secondary reaction ($CO + 3H_2 \rightarrow CH_4 + H_2O$). The higher amount of CO detected in the case of Ru/5Ca-T500-I could be most probably explained by the fact that less CO remained adsorbed on the catalyst surface.

The catalysts prepared by the photodeposition method performed much better in the FALA reaction, while they exhibited the same trend in terms of LA conversion and GVL yield as their counterparts prepared by impregnation (Figure 54). The highest yield also occurred for Ru/5Ca-T500-P giving almost 50% of the final product, however this maximum was less pronounced than for the catalysts prepared by impregnation. Further, since the catalysts were used in the reaction without any thermal reduction, it was interesting to check how they behave when additionally reduced in the same conditions than the ones prepared by impregnation. The reduced sample Ru/5Ca-T500-P showed much lower performance and two times lower LA conversion and GVL yield was achieved despite a full decomposition of formic acid. The distributions of gaseous products are quite similar to those obtained on their counterparts prepared by impregnation, meaning that two decomposition pathways of FA also took place. In all cases, formation of CH_4 was evidenced. On one hand, the much higher volume of H_2 recorded for Ru/5Ca-T500-P and Ru/10Ca-T500-P samples as well for Ru/P25-P could mean that a small Ru size improves the selectivity of FA decomposition, while by contrast the hydrogenation reaction was blocked by strongly adsorbed CO in this case.

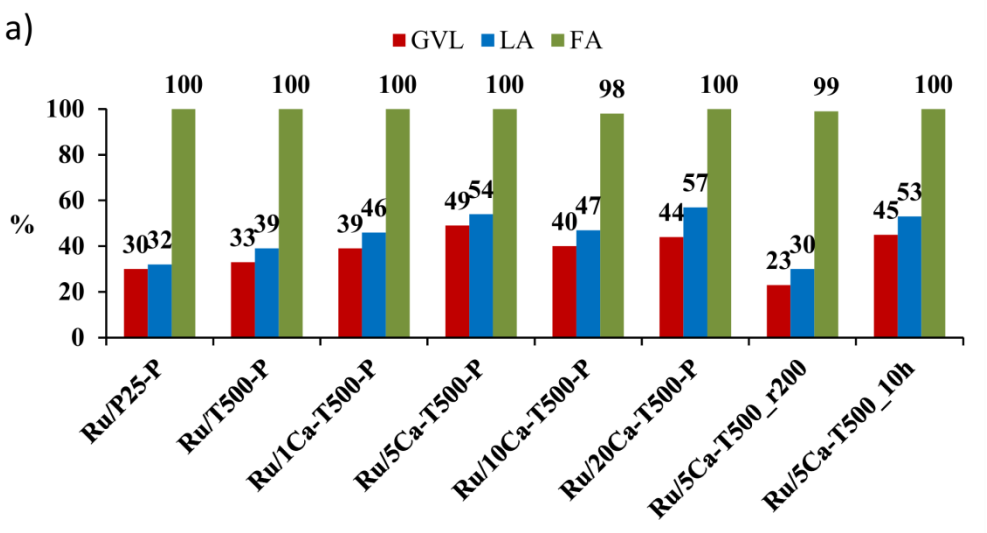

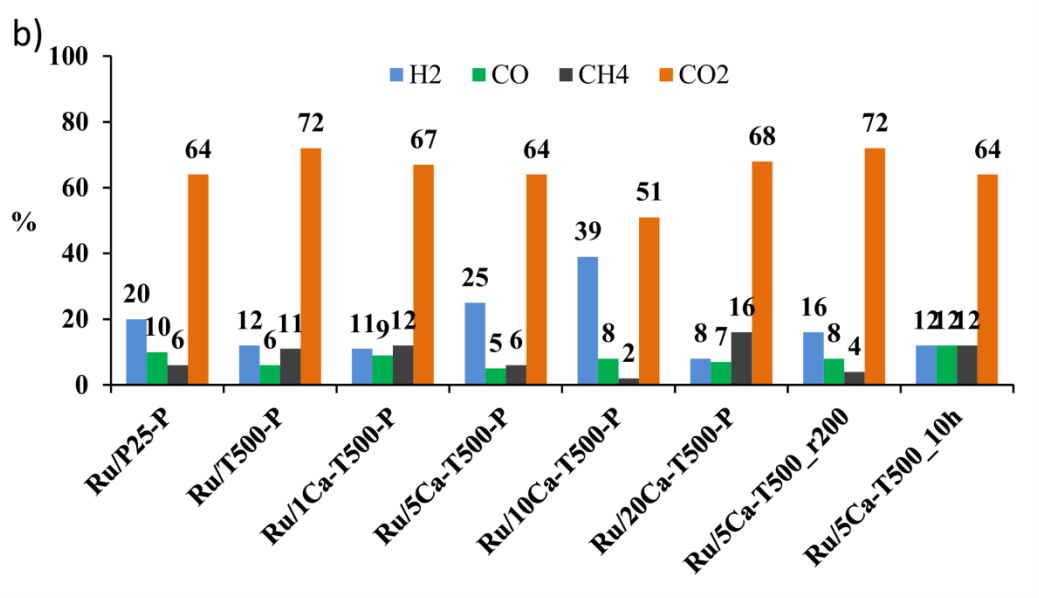

Figure 54. Catalytic activity of the Ru catalysts prepared by the photodeposition method in the FALA reaction, in terms of a) LA hydrogenation, FA decomposition and GVL yield; and b) Gaseous product distribution; [1 g of LA, 0.4 ml of FA, 0.6 g of catalyst, 30 ml of H_2O, 190 °C, 5 h]

As the next step, it was interesting to check the behavior of the most active material, Ru/5Ca-T500 prepared by both methods in the longer reaction run – 10 h. In the case of the sample prepared by impregnation, the LA conversion and GVL yield were boost to reach 89% and 79% respectively (Figure 53). While in the case of photon-assisted preparation method the LA conversion and GVL yield remain at the same level even after 10 h (Figure 54). Further explanation will be provided in the discussion paragraph 5.5.

Catalytic performances in the LA hydrogenation and FA decomposition separate reactions.

The catalysts were also tested separately in both FA decomposition and LA hydrogenation (Figure 55and Figure 56) to evaluate in more details the influence of the Ca modification and of the new preparation method in each step of the GVL synthesis. It is important to mention that in order to be able to compare the catalysts between each other, it was necessary to decrease their performance and therefore the amount of catalysts used in those tests was four times lower than the one in FALA. Compared to FALA reaction, similar trends were observed for both types of materials. The catalysts prepared by photodeposition showed higher catalytic performances than their counterparts prepared by impregnation

in both separated reactions. First, in FA decomposition (Figure 55) it was observed that the modification with Ca^{2+} improved the catalytic performance forming a clear volcano-type profile for both series of Ru catalysts, with Ru/5Ca-T500 as the best materials.

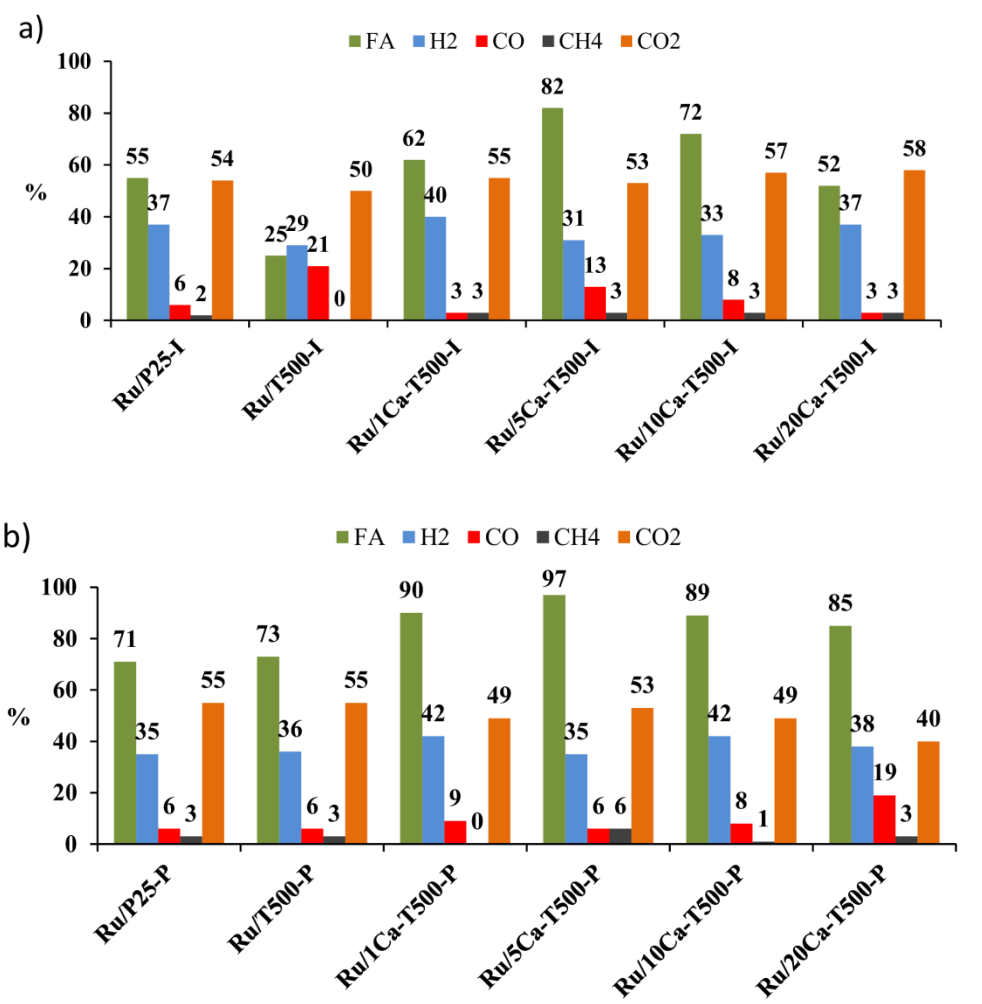

Figure 55. Catalytic activity of the Ru catalysts prepared by a) impregnation and b) photodeposition in the FA decomposition; [0.4 ml of FA, 0.15 g of catalyst, 30 ml of H_2O, 190 °C, 2 h]

Moreover, it was also shown that the selectivity to H_2 of the FA decomposition was improved using Ca-based catalysts prepared by impregnation (with less CO produced) compared to Ru/T500-I. On the other hand, the selectivity was not significantly changed in the case of catalysts prepared by photodeposition and remained similar to the Ca-based impregnated ones except for Ru/20Ca-T500 where quite a lot of CO was recorded.

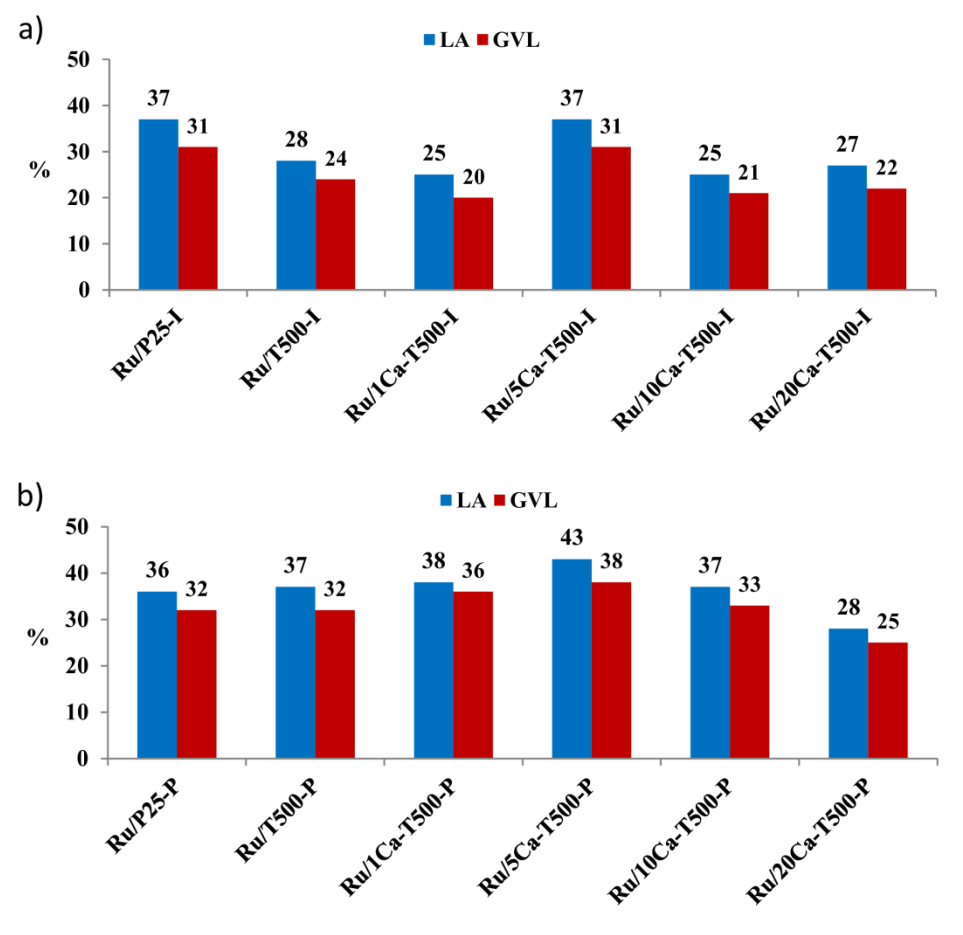

Figure 56. Catalytic activity in terms of LA hydrogenation and GVL yield of the Ru catalysts prepared by a) impregnation and b) photodeposition in the LA hydrogenation with external H_2; [1 g of LA, 0.15 g of catalyst, 30 ml of H_2O, 5 bar H_2, 190 °C, 30 min]

Figure 56 shows the results of LA hydrogenation for both series of catalysts. It is very important to notice that the modification with Ca has a positive effect on the catalytic activity in the hydrogenation reaction as well. Again, the sample containing 5% of Ca allowed reaching the highest conversion of levulinic acid, whatever the material preparation method.

5.5. Discussion of the catalytic results

In this chapter the influence of several factors (Ru particle size, support modification, novel synthesis method) on the hydrogenation of LA into GVL with FA as internal hydrogen source at low temperatures in water was investigated.

Focusing firstly on the Ru particle size effect it can be seen that for both P25 and T500 supported materials the GVL yield is higher when smaller Ru nanoparticles were tested meaning those prepared by the photodeposition method. (Figure 57a) Moreover it is worth noting that small Ru size is beneficial for both processes FA decomposition (Figure 57b) and LA hydrogenation (Figure 57c).

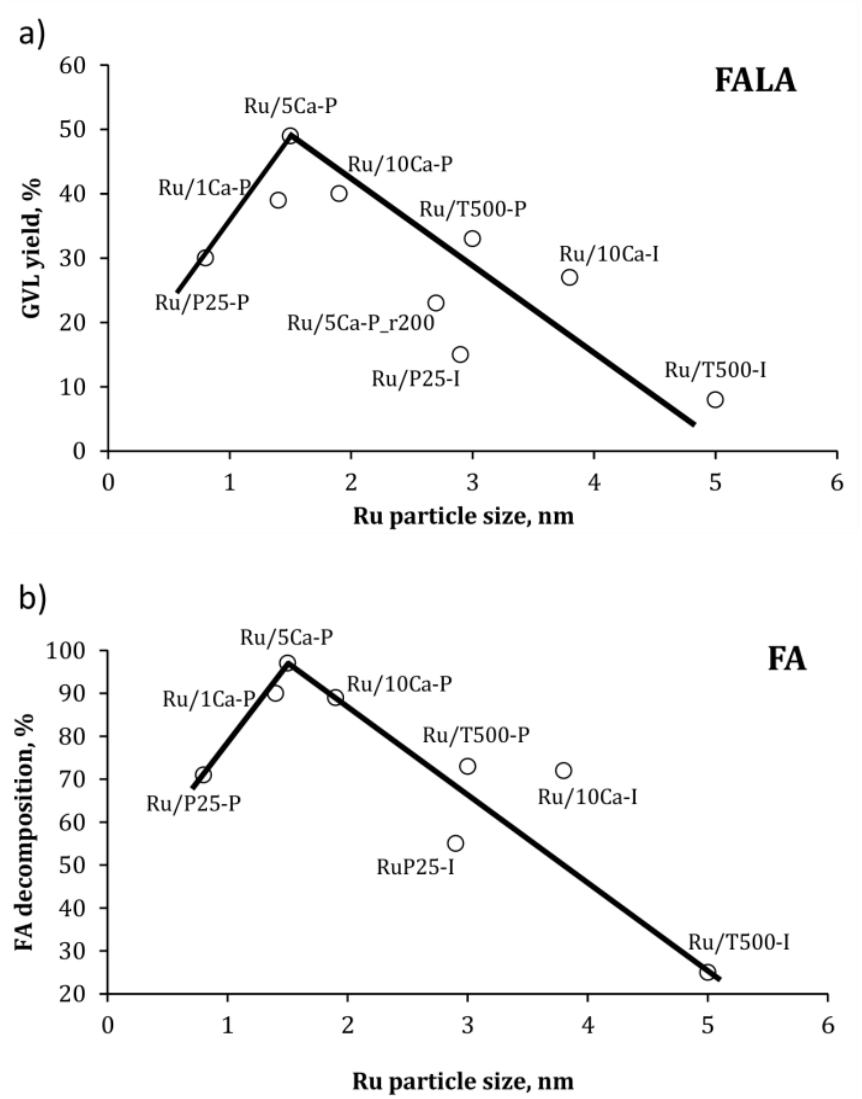

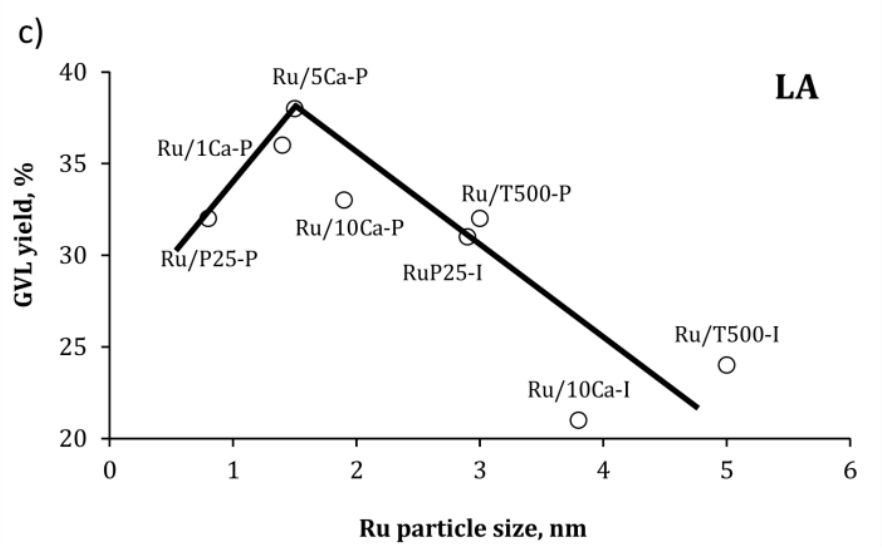

Figure 57. a) Influence of the Ru nanoparticle size on a) the GVL yield in FALA, b) the FA decomposition and c) the GVL yield in LA hydrogenation with external hydrogen, for Ru catalysts prepared by impregnation and photodeposition.

The size effect in FA dehydrogenation was investigated using mainly Pd based catalysts, although the optimum size letting to obtain highest conversion of FA is still under the debate as depends also on the reaction conditions. Generally the smallest particles showed higher activity. However in the work of Navlani-García et al.[260] the volcano type relationship with optimum moderate Pd nanoparticle size of 3.9 nm was associated with the suitable proportion of low-coordinated (small particles) and high-coordinated (large particles) palladium atoms. The mechanism of the FA dehydrogenation on metals and metal oxides was proposed by Mars.[261] In the initial step formic acid is adsorbed on the surface and donates a proton to the catalyst leading to the formation of formate intermediate.[262,263] Then the metal-formate species undergo β-hydride elimination producing CO_2 and the H^- that forms H_2 with previously adsorbed H^+ on the catalyst.[264,265,266] According to the work of Navlani-Garcia et al. regarding the Pd catalysts the adsorption of $HCOO^-$ is favored on the smaller NPs owing its high reactivity to a large number of

[260] M. Navlani-García, K. Mori, A. Nozaki, Y. Kuwahara, H. Yamashita, Chem Select 2016, 1, 1879
[261] P. Mars, J.J.F. Scholten, P. Zwietering, Adv Catal. 1963, 14, 35-113.
[262] A. Masami, K. Kosaku, I.Toshinobu, T. Shiichiro, Bull Chem Soc Japan, 1966, 40, 1290-1292.
[263] a) M. Adachi, T. Imanaka, S. Teranishi, Nippon Kagaku Kaishi. 1968, 89, 446; Nippon Kagaku Kaishi 1969, 90, 348; Nippon Kagaku Kaishi 1970, 91, 400.
[264] M. Ojeda, E. Iglesia, Angew Chem Int Ed 2009, 48, 4800.
[265] S. Fukuzumi, T. Kobayashi, T. Suenobu, ChemSusChem 2008,1, 827.
[266] S. Fukuzumi, T. Kobayashi, T. Suenobu, JACS **2010**, 132, 1496

unsaturated atoms. Therefore in our case it could be said that higher yield of FA decomposition achieved on smaller Ru supported on TiO_2 is due to the larger proportion of unsaturated low coordinated Ru atoms.

In case of LA hydrogenation the higher activity of smaller Ru nanoparticles is most probably attributed to the higher number of metal active sites available.[267,268] When we consider also Ru particles supported on Ca-based supports a clear maximum of catalytic performance was observed with the NP of 1.5 nm being the most active in all reactions. Interestingly for the most active catalyst Ru/5Ca-T500 the GVL yield dropped from ca. 50% to ca. 20% after reducing at 200^{o}C which resulted in an increase in nanoparticle size.

The optimal Ru particles size is however not the only factor responsible for reaching high activity. Comparing two samples Ru/1Ca-T500 and Ru/5Ca-T500 with almost the same Ru particle size (1.4 and 1.5 nm) the catalyst with 5% of Ca exhibited higher activity suggesting that addition of Ca^{2+} has a crucial effect as well. Based on XRD results titania modification with Ca^{2+} resulted in decreased anatase crystallite size which could favor the formation of smaller metal particles on the surface of the support.[269] However the role of calcium cannot be limited to the effect of the nanoparticle size. Ca^{2+} ions are incorporated into the TiO_2 crystal lattice together with the formation of new calcium titanate phase. This in turn has an effect on the supported Ru nanoparticles which are interacting stronger with the support when the calcium content is increasing. This is well evidenced on TPR profiles for the catalysts prepared by the impregnation method as well as on CO-FTIR spectra with the presence of the band at 1980 cm^{-1} assigned to the adsorption of CO on Ru strongly interacting with the support. Another proof of Ru being in direct interactions with the Ca-modified support is given by ToF-SIMS. The presence of $CaRuO_2^+$ ions was identified for catalysts containing more Ca^{2+}. Changes in the metal-support interaction strength resulted in a change of the nature of CO molecule adsorption. Apparently for Ca-based materials the CO adsorption was lower which could be one reason for their generally better performance since CO could act as poison for the active metal centers. Besides the fact that CO and H_2 adsorb on the same sites explains why the catalytic activity does not increase further with increasing amount of Ca. Differences in

[267] M. Nemanashi, J.-H. Noh, R. Meijboom, Appl Catal A 2018, 550, 77-89.
[268] D. R. Jones, S. Iqbal, P. J. Miedziak, D. J. Morgan, J. K. Edwards, Q. He, G. J. Hutchings, Topics in Catal. 2018, 61, 833-843
[269] G. Li, H. Yang, M. Cheng, W. Hu, L. Tian, W. Mao, R. Nie, Mol Catal. 2018, 455, 95-102.

the CO adsorption observed in FTIR studies between catalysts prepared by impregnation and photodeposition might also explain the possibility to boost the performance of impregnated Ru/5Ca-T500 in a 10 h test – adsorbed CO is transformed into methane, since it is apparently not adsorbed very strongly on the impregnated sample and the reaction goes further. For photodeposited samples it is not possible since the CO adsorption is stronger on small Ru particles and blocking the active sites. Therefore a kind of plateau is achieved because the LA conversion and GVL yield remain at the same level even after 10 h.

Generally the better activity of the catalysts prepared by the photodeposition method could be explained by several factors with the smaller Ru nanoparticle size and their more uniform distribution being one of them.

The role of modification with Ca^{2+} is also strongly associated with the formation of new basic sites. It was shown in the literature that doping catalysts with Ca results in a formation of new basic sites by increasing the concentration and strength of the O^{2-} on the surface.[270,271] Indeed the changes in the surface charge were observed by measuring the isoelectric point of the support materials suggesting that with addition of Ca surface becomes more negative. Presence of basic sites explains well the improved catalytic performance of Ca-based catalysts in both reactions FA decomposition and LA hydrogenation despite the catalyst preparation method. Dehydrogenation of FA is facilitated by the presence of basic sites which act as a proton scavenger in O-H bond cleavage step.[272,273,274] On the other hand the mechanism of improved catalytic performance in LA hydrogenation could be related to the activation of the carbonyl compound where basic sites would interact with π* orbital of C=O group.[275,276]

5.6. Concluding remarks

In this chapter, the evaluation of the catalytic behavior of 5%Ru/TiO_2-based catalysts prepared by wet impregnation and photodeposition methods in the one-pot simultaneous formic acid decomposition and levulinic acid hydrogenation was presented. For getting insight on the catalyst features playing a role

[270] S. Scirè, C. Crisafulli, R. Maggiore, S. Minicò, S. Galvagno, Appl Surf Sci. 1998, 136, 311-320.
[271] C. Morterra, G. Magnacca, G. Cerrato, N. Del Favero, F. Filippi, C. V. Folonari, J. Chem. Soc. Faraday Trans. 1993, 89, 135.
[272] Q.-Y. Bi, X.-L. Du, Y.-M. Liu, Y. Cao, H.-Y. He, K.-N. Fan, J. Am. Chem. Soc. 2012, 134, 8926.
[273] K. Mori, M. Dojo, H. Yamashita, ACS Catal. 2013, 3, 1114.
[274] M. Ai, J. Catal. 1977, 50(2) 291-300.
[275] H. Liu, Q. Hu, G. Fan, L. Yang, F. Li, Catal. Sci. Technol. 2015, 5, 3960–3969.
[276] Y. Zhang, S. Zhang, X. Pan, M. Bao, J. Huang, W. Shen, Catal Lett. 2017, 147, 102-109.

in the achievement of enhanced performances in the process, the catalysts were characterized using TPR, CO-FTIR, ToF-SIMS analysis, and they were further tested in both FA dehydrogenation and LA hydrogenation separated reactions.

It was evidenced that the controlled modification of the TiO_2 support by calcium addition improved the catalytic performance in the comined FALA reaction, as a result of enhanced performances in both the FA dehydrogenation step and the LA hydrogenation reaction. Such modification resulted in a decreased anatase crystallite size, together with the formation of a new calcium titanate phase, leading to the stabilization of smaller ruthenium particles on the support. Stronger interaction of ruthenium with the support was observed, which affected the strength of CO adsorption on the surface of the Ca-modified catalyst, thus facilitating the reaction performance.

Then, it was shown that the photon-assisted catalyst preparation method allowed to further enhance the catalytic activity towards GVL production with FA as hydrogen source in comparison to the reference counterparts prepared by impregnation. This was possible owing to the formation of uniform, small and well-dispersed metal crystallites.

A volcano-type relationship was found between the mean Ru nanoparticle size and the catalytic activity, with an optimal Ru size of 1.5 nm resulting in the most active catalyst in all reactions. This volcano-type dependence has been associated with the suitable proportion of low-coordinated (small particles) and high-coordinated (large particles) atoms.

CHAPTER 6

6. ACTIVITY OF Ru/TiO_2-BASED CATALYSTS IN GAS PHASE FORMIC ACID DECOMPOSITION

Formic acid was used in this research as a hydrogen donor for the one-pot levulinic acid hydrogenation. Formic acid however could be used also as a hydrogen storage material[277] or as a source of H_2 for fuel cell applications.[278] Due to the increasing interest in those research topics, it was additionally interesting to evaluate the potential of 5%Ru/TiO_2-based catalysts in the reaction of gas phase formic acid decomposition in a flow reactor mode. Gas phase was chosen since majority of the reports published in the literature have been done in this phase and the flow reactor provide the constant hydrogen supply that is important from an industrial point of view to maintain continuous process.

Therefore, in this chapter the 5%Ru/TiO_2-based catalysts prepared by wet impregnation and photodeposition methods were tested in the gas phase formic acid decomposition. First, the bare support materials were tested in the reaction to examine their influence on the final performance of the catalysts.

Each sample was tested starting from the low temperature of 50^{o}C with subsequent increase towards the final temperature of 190^{o}C (detailed reaction protocol can be found in Chapter 2.4.4.). The detailed preparation of the supports and the catalysts can be found in Chapters 2.1, 2.2 and 2.3.

6.1. Catalytic activity of the supports materials

It was reported in the literature that TiO_2 shows activity towards formic acid dehydration in the gas phase forming CO and H_2O.[279] For that reason therefore, it was crucial to examine the activity of the bare supports (Figure 58) and moreover to evaluate the effect of the Ca modification on the activity of Ru/TiO_2 catalysts in FA decomposition. The materials were reduced at 50^{o}C for 1 h in the H_2 flow before testing in order to clean the surface from the adsorbed impurities. It was observed that both Ca-free TiO_2 supports (TiO_2 P25 and sol-gel TiO_2 reference) showed activity in FA dehydration at 190^{o}C, with a FA conversion of 37% and 21%, respectively. CO was the only reaction product detected, neither H_2 nor CO_2 being

[277] K. Mori, S. Masuda, H. Tanaka, K. Yoshizawa, M. Che, H. Yamashita, Chem Commun. 2017, 53, 4677.
[278] F. Wang, H. Xue, Z. Tian, W. Xing, L. Feng, J Power Sources, 2018, 375, 37.
[279] G. Munuera, J Catal 1970, 18, 19

formed. On the other hand, the FA conversion dropped significantly (below 10% at 190°C) when Ca ions were introduced to the support. For high Ca loading such as 20%, no activity was observed.

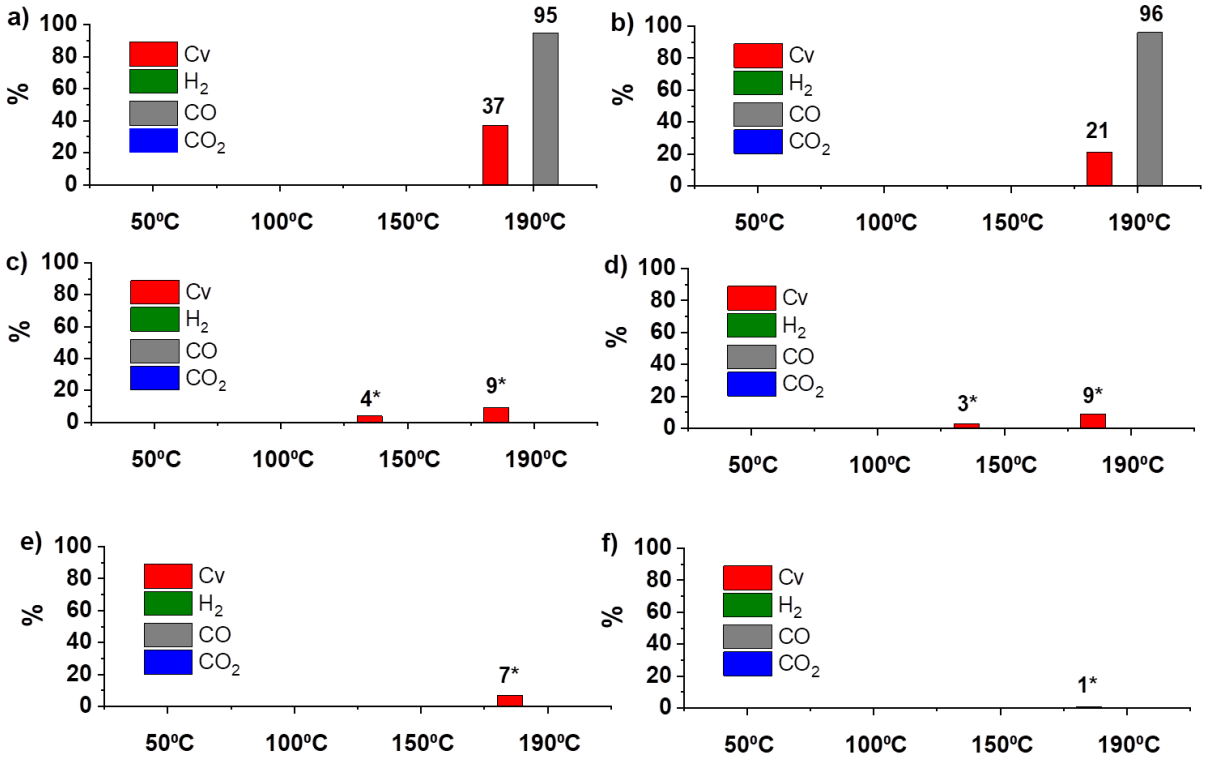

Figure 58. Catalytic activity of the support materials in gas phase formic acid decomposition: a) P25; b) T500; c) 1Ca-T500; d) 5Ca-T500; e) 10Ca-T500; f) 20Ca-T500; [0.02 g of catalyst, 17000 ppm of FA, 1 h at each temperature, Ar flow 30 ml/min].

** means that for conversions <10% the precise measurement of the components distribution was not possible*

Indeed the formic acid decomposition is known to take place as well on metal oxides surfaces and the activity of TiO_2 in the formic acid dehydration has been reported in the literature.[280,281,282] A mechanism of FA dehydration on TiO_2 has been proposed by Henderson who pointed out the complexity of this process.[283] According to this study, formic acid decomposition involves a complex set of chemical reactions. The first step is the formation of water and the creation of oxygen vacancies by the reaction of the acid proton with the oxide lattice (Equations 8 and 9). Further, the formate could decompose to form

[280] K. S. Kimt, A. Barteau, Langmuir 1990, 6, 1485-1488
[281] M. Ai, J Catal. 1977, 50, 201.
[282] J. M. Trillo, G. Munuera, J. M. Criado, Catal Rev. 1972, 7, 51.
[283] M.A. Henderson, J. Phys. Chem. B 1997, 101, 221

CO (Equation 10) or through the interaction with the oxygen vacancies, into a variety of decomposition products in very low amounts (i.e. formaldehyde or CO_2). Those processes could be presented in the following equations:

Formation of water and oxygen vacancies:

$$a)\ 2HCOOH + 2O^{2-}_{lattice} \rightarrow 2HCOO^{-}_{ad} + 2OH^{-}_{lattice} \quad (8)$$

$$b)\ 2OH^{-}_{lattice} \rightarrow \mathbf{H_2O} + O^{2-}_{lattice} + vac \quad (9)$$

Formate decomposition processes:

$$a)\ 2HCOO^{-}_{ad} \rightarrow 2\mathbf{CO} + 2OH^{-}_{ad} \quad (10)$$

$$b)\ 2OH^{-}_{ad} \rightarrow \mathbf{H_2O} + O^{2-}_{ad} \quad (11)$$

$$c)\ O^{2-}_{ad} + vac \rightarrow O^{2-}_{lattice} \quad (12)$$

$$d)\ 2HCOO^{-}_{ad} + vac \rightarrow CO_2 + H_2CO + O^{2-}_{lattice} \quad (13)$$

Bennet et al. also indicated that the dissociative adsorption of formic acid occurred at low temperature to produce formate and adsorbed hydroxyl species.[284]

The reaction is occurring directly at the surface of the support, so that the activity of the TiO_2 support might be directly related to the value of the specific surface area, as it seems to be the case in the TiO_2 P25 / sol-gel TiO_2 comparison. Therefore, the activity of a series of commercially available TiO_2 materials differing notably in terms of mean crystallite size, and therefore covering a large range of BET specific surface area, has been evaluated, and the results are reported in Figure 59, and in Figure 60 as a function of the value of the BET surface area. The results confirmed that on non-modified TiO_2 supports, higher the specific surface area, higher the FA conversion, only *via* the dehydration pathway (formation of CO). Therefore, the specific surface area is definitely one of the parameters directly influencing the activity of the oxide materials in the FA decomposition.

Other effects however play a role when Ca-based samples are considered. The results presented in Figure 58 showed further that the TiO_2 modification with Ca^{2+} significantly reduces the activity of the TiO_2-based support in the FA decomposition. Indeed, whatever the Ca content, the FA conversion dropped significantly down to a near zero-level, the higher the Ca content, the lower the FA conversion.

[284] R.A. Bennett, P. Stone, R.D. Smith, M. Bowker, Surf Sci, 2000, 454-456, 390-395.

At first it was very surprising that the Ca-modified supports gave almost no activity in FA decomposition since they have surface area in the range of that of P25. Although there are no studies available regarding the behavior of formic acid on $CaTiO_3$ surface, there is one example in the literature with $SrTiO_3$.[285] The authors however studied the interaction of FA with the defective and defect-free $SrTiO_3$ surfaces using single crystals at the low temperature of -23^oC. It was reported that FA decomposes through dehydration producing CO and H_2O on both the defective and defect-free $SrTiO_3$ surfaces. Therefore some activity on Ca-based supports which are composed of mixed phases of TiO_2 and $CaTiO_3$ (based on XRD results, Chapter 3) was expected. The activity decrease with the addition of Ca to the TiO_2 structure could be possibly explained as follows. From the dehydration mechanism, it can be seen that the formate is generated on $O^{2-}_{lattice}$ sites (Equation 8) which concentration was proposed to increase in Ca-modified samples based on the decreasing isoelectric point (as described in Chapter 3). The presence of O^{2-} should rather facilitate the decomposition of formic acid, however the obtained results suggest that the presence of Ca^{2+} might block effectively the majority of active sites on bare support material. Indeed, based on Figure 50, the presence of some Ca carbonate species was observed. Moreover it was reported that $HCOO^-$ strongly adsorbs on reduced Ti^{3+} sites blocking the active sites. In addition, it was reported that the chemistry of FA on TiO_2 depends on its surface structure and composition.[285,286]

As a result, modifying the TiO_2 with calcium was thus an interesting way to suppress the intrinsic activity of the support itself, and therefore to inhibit the formation of CO, known to act as potential poison in the case of Ru nanoparticle catalysts.

[285] L-Q. Wang, K. F. Ferris, G. S. Herman, M. H. Engelhard, J. Vac. Sci. Technol. 2000, 18, 1893.
[286] Y. Morikawa, I. Takahashi, M. Aizawa, Y. Namai, T. Sasaki, Y. Iwasawa, J. Phys. Chem. B 2004, 108, 14446.

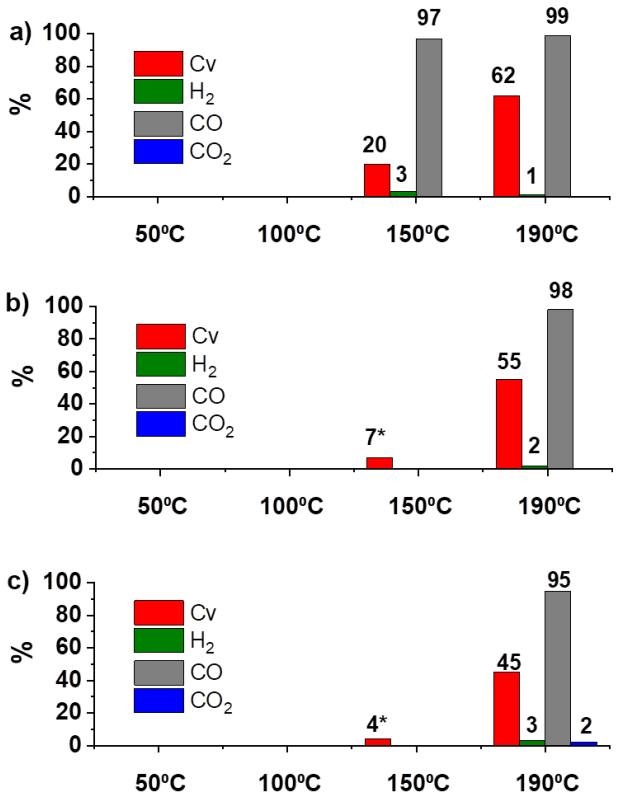

Figure 59. Catalytic activity of different TiO_2 support materials in gas phase formic acid decomposition: decomposition: a) Hombikat UV100 (320 m^2/g); b) ST01 (310 m^2/g); c) Aeroxide P90 (90 m^2/g); [0.02 g of catalyst, 17000 ppm of FA, 1 h at each temperature, Ar flow 30 ml/min].

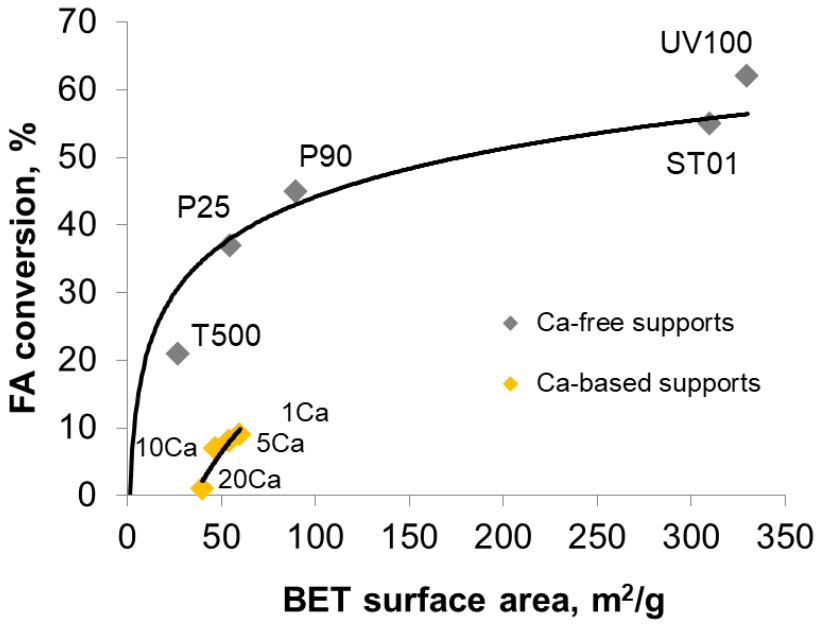

Figure 60. FA conversion obtained on the TiO_2 and the Ca-modified TiO_2 support materials in the gas phase formic acid decomposition at 190^{o}C as a function of the BET specific surface area.

6.2. Catalytic activity of the 5%Ru/TiO$_2$ catalysts prepared by the wet impregnation method

Figure 61 presents the catalytic performance of the 5%Ru/TiO$_2$ catalysts prepared by the wet impregnation method.

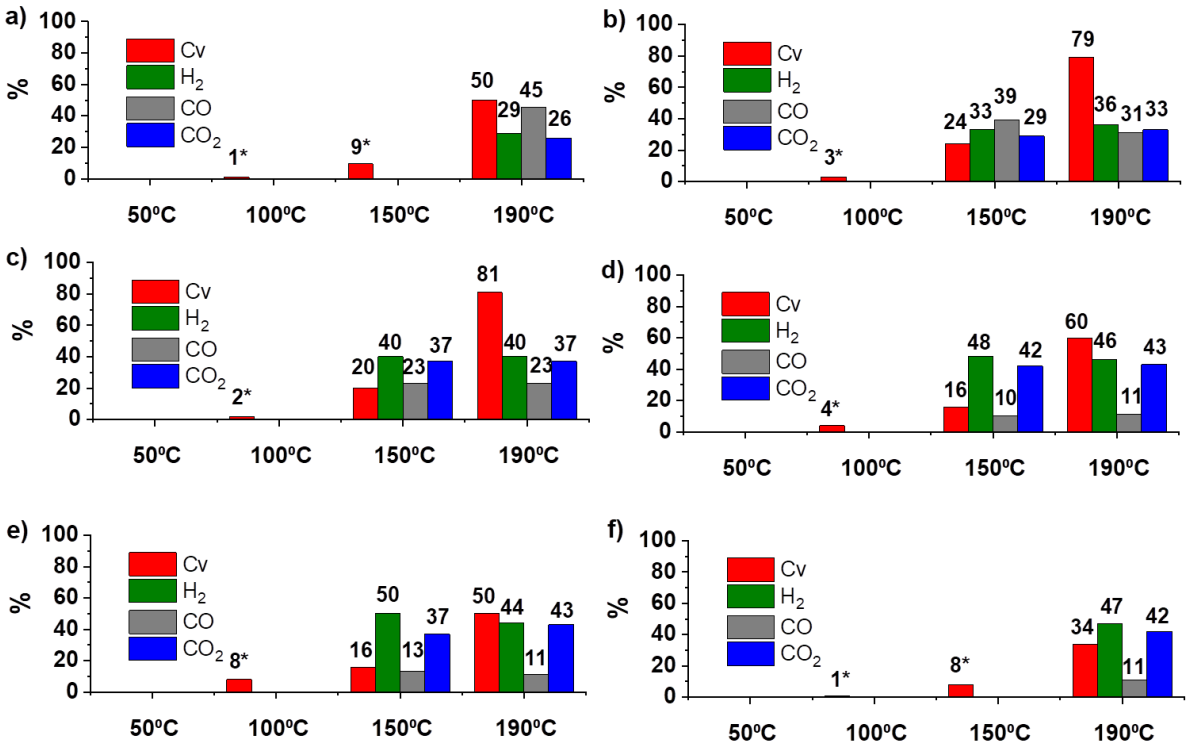

Figure 61. Catalytic activity of Ru/TiO$_2$ catalysts prepared by the wet impregnation method in gas phase formic acid decomposition: a) 5%Ru/P25-I; b)5%Ru/T500-I; c) 5%Ru/1Ca-T500-I; d) 5%Ru/5Ca-T500-I; e) 5%Ru/10Ca-T500-I; f) 5%Ru/20Ca-T500-I; [0.02 g of catalyst reduced at 200^{o}C for 1h 17000 ppm of FA, 1 h at each temperature, Ar flow30 ml/min].

High formic acid conversions (34%-81%) were achieved at 190^{o}C as well as some activity was observed also at lower temperatures such 150^{o}C or even at 100^{o}C in few cases, proving undoubtedly that active sites are located on the metallic ruthenium particles. However, no conversion was observed at 50^{o}C. When it comes to Ca-free catalysts, higher formic acid conversion was reached for 5%Ru/T500-I than for 5%/P25-I (79% compared to 50%). It is surprising, since Ru NPs are larger on T500 than on P25 and therefore is could be speculated that other aspects are responsible for this behavior such as the titania preparation method or difference in Ru particles dispersion on those supports. Besides, although the active sites are located on Ru, there is still a potential contribution of the support activity.

Significant enhancement in the produced amount of H_2 for Ru/P25-I and Ru/T500-I (29% and 36% respectively) compared to the bare TiO_2 supports (Figure 58, 0%) was observed. This could result from the fact that the surface of TiO_2 is partially covered by Ru NPs and therefore less active sites of the support itself are available for the dehydration pathway.

Then, with addition of 1% of Ca to the support, the FA conversion at 190^{o}C is comparable to that obtained on 5%Ru/T500-I but the selectivity is improved in the favor of H_2 formation (from 36% to 40%). It was observed that with the increasing amount of Ca, the distribution of gaseous products is further driven positively towards hydrogen (more H_2 and less CO is produced), particularly when comparing the CO level for 5%Ru/P25-I and 5%Ru/10Ca-T500-I being 45% and 11%, respectively. Improved selectivity with addition of Ca^{2+} comes with the price of decreasing FA conversion from 81% for the most active Ru/1Ca-T500-I to 60%, 50% and eventually 34% for Ru/5Ca-T500-I, Ru/10Ca-T500-I and Ru/20Ca-T500-I, respectively.

6.3. Catalytic activity of the 5%Ru/TiO_2 catalysts prepared by the photodeposition method

Although the photodeposition method yielded the Ru nanoparticles present predominantly in its metallic state, due to the unavoidable air surface oxidation, which was observed during the XPS analysis described in Chapters 4.2 (for 0.5%Ru/TiO_2) and Chapter 4.6 (for 5%Ru/TiO_2), it was necessary to reduce the oxidized external surface of the Ru nanoparticles before testing. For the reason of choosing the proper reducing conditions, the reference sample 5%Ru/T500-P was reduced either at 200^{o}C for 1 h (conditions used for the catalysts prepared by the impregnation method) or at 50^{o}C for 30 min. Based on the results presented in Figure 62, it can be seen that even slightly better FA conversion and selectivity was achieved (75% of FA conversion and 37% of H_2 amount) when using mild reducing conditions (considered only as a "surface cleaning") compared to 200^{o}C (70% of FA conversion and 37% of H_2) and therefore those were used for the reduction of all the catalysts prepared by the photon-assisted method.

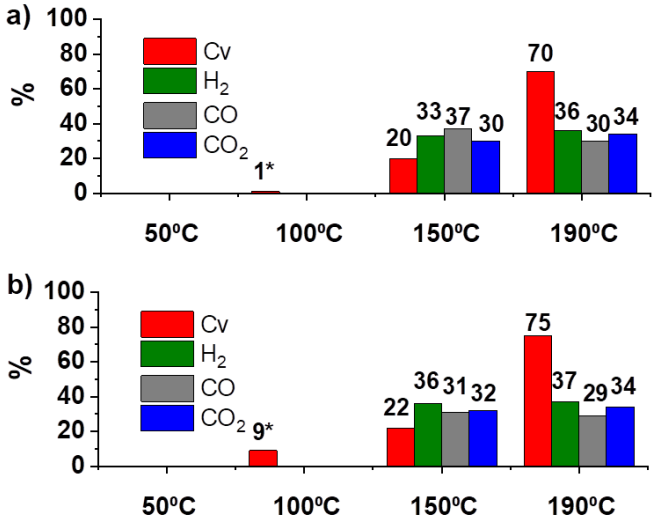

Figure 62. Catalytic activity of 5%Ru/T500 catalysts reduced at a) 200°C for 1 h and b) at 50°C for 30 min in gas phase formic acid decomposition; [0.02 g of catalyst, 17000 ppm of FA, 1 h at each temperature, Ar flow 30 ml/min].

The catalytic activity of the entire series prepared by photodeposition and reduced in situ at 50°C for 30 min is presented inFigure 63. First it can be seen that, similarly to the reactions conducted in the liquid phase reaction, those catalysts exhibited higher FA conversions than the samples prepared by the wet impregnation. It is visible especially by comparing the conversions at the temperature 100°C, at which the samples prepared by the photodeposition gave values in the range of 10%, while their counterparts prepared by wet impregnation exhibited almost no activity. Generally, the activity trend is almost the same as for the samples prepared by the impregnation method. However, unlike in the case of samples prepared by the impregnation method, the reference TiO_2 P25 supported Ru catalyst showed much higher FA conversion values at 150°C and 190°C (35% and 96%) than the Ru/T500-P (22% and 75% of conversion). This result could be most probably attributed to the extremely small Ru nanoparticles (average size of 0.9 nm) compared to T500 (2.9 nm).

The support modification with 1% of Ca causes an improvement in both the conversion and the selectivity mainly at 190°C, where this difference is the most prominent (conversion raised from 75% to 86%). Further increasing of Ca content caused a drop in the FA conversions: 63%, 68% and 67% for Ru/5Ca-T500-P, Ru/10Ca-T500-P and Ru/20Ca-T500-P, respectively. Although it is difficult to compare selectivity at different conversion levels, a reliable comparison could be made based on the results of

sample Ru/T500 and Ru/10Ca-T500. At very similar conversions, much less CO was recorded at 150°C and 190°C for Ca-based catalyst and therefore it could be seen that the presence of Ca improves the selectivity towards hydrogen of the Ru catalysts in gas phase formic acid decomposition.

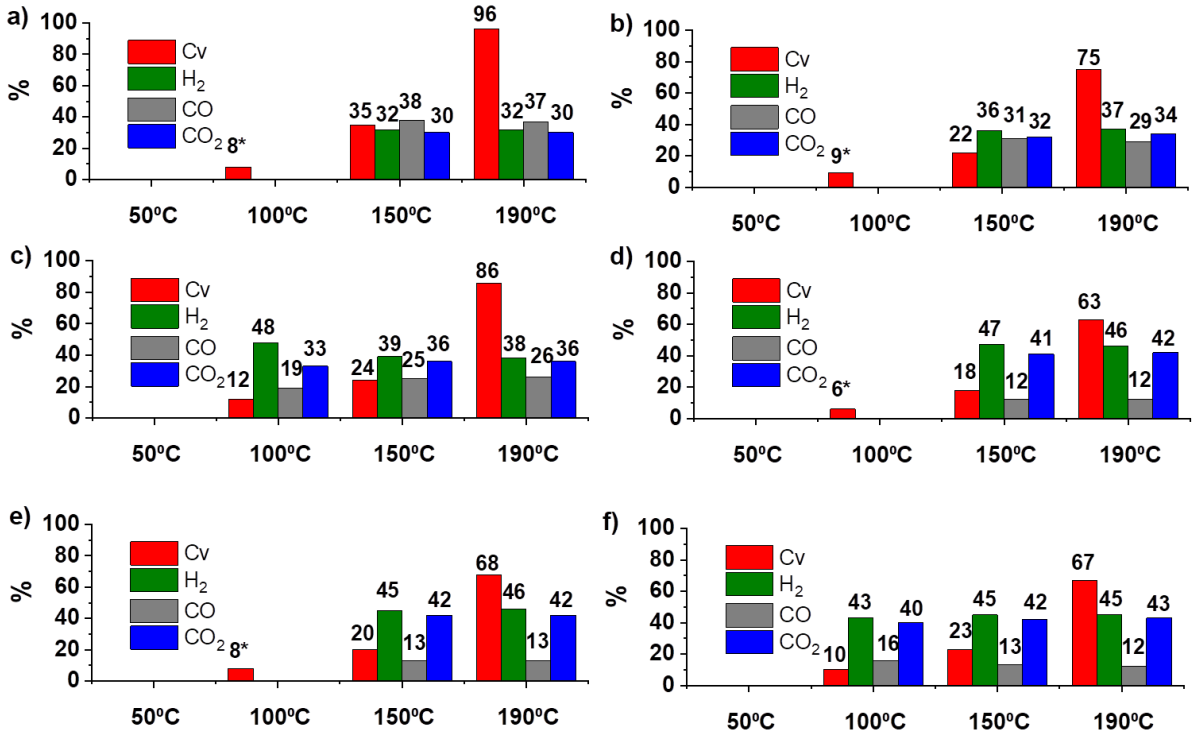

Figure 63. Catalytic activity of Ru/TiO$_2$ catalysts prepared by the photodeposition method in gas phase formic acid decomposition: a) 5%Ru/P25-P; b)5%Ru/T500-P; c) 5%Ru/1Ca-T500-P; d) 5%Ru/5Ca-T500-P; e) 5%Ru/10Ca-T500-P; f) 5%Ru/20Ca-T500-P; [0.02 g of catalyst treated at 50°C under H$_2$ for 30 min,17000 ppm of FA, 1 h at each temperature, Ar flow 30 ml/min].

Further, in order to check the performance of the catalysts in the extended reaction run, one sample, 5%Ru/1Ca-T500-P, was chosen for the test over the 8 h. The reaction was carried out under the same conditions until 190°C followed by the additional 4 h at this temperature. The reaction products were analyzed after each hour (Figure 64).

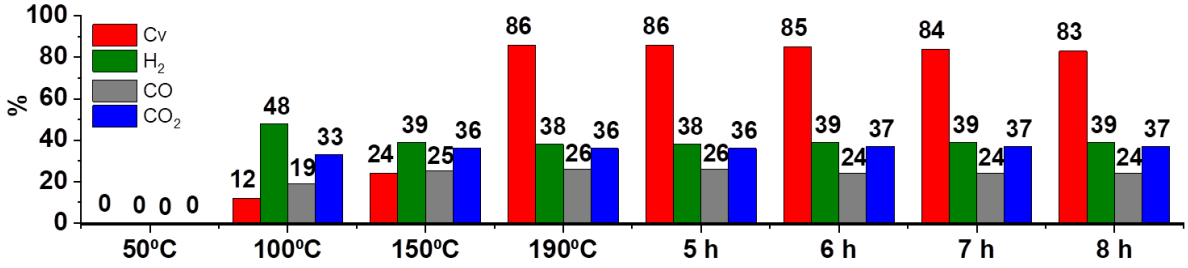

Figure 64. Catalytic activity of 5%Ru/1Ca-T500-P in the extended reaction run of gas phase formic acid decomposition; [0.02 g of catalyst treated under H_2 at 50°C for 30 min, 17000 ppm of FA, 1 h at each temperature + 4 additional hours at 190°C, Ar flow 30 ml/min].

As seen in Figure 56 the catalyst is stable for another 4 h of the reaction as the formic acid conversion level and the distribution of gaseous products remains basically without change. This shows the promising potential of using the material for even longer reaction runs which of course is very attractive from the industrial point of view and could provide the continuous supply of the gas products.

6.4. Discussion of the catalytic results

In this chapter the catalytic activity of the catalysts prepared by two different methods was evaluated in the gas phase formic acid decomposition at increasing reaction temperature. The influence of the support modification, the Ru particle size and the preparation method was investigated. Since a detailed discussion on the aspects influencing the catalytic activity in FA decomposition has already been presented in the Chapter 5.5, here a summary of the results with short explanation will be presented.

It was observed that the catalysts prepared by the photodeposition method gave a higher formic acid conversion level which is attributed to the generally smaller Ru nanoparticles size produced with the photo-reduction method as compared to that of the samples prepared by the impregnation. The correlation of conversion and H_2 selectivity with the metal nanoparticle size of all tested materials is presented in Figure 65. The overall profile might indicate that the conversion decreases with the increasing Ru particle size, which could be due to the lower proportion of highly active low coordinated Ru atoms on which the adsorption of $HCOO^-$ is favored. However, the samples Ru/T500-I and Ru/T500-P with Ru particles of 5 nm and 3 nm, respectively clearly deviates from this trend, suggesting that probably other parameters play

a role, such as the presence of Ca^{2+} in the support. In terms of H_2 formation, similarly, no clear trend could be distinguished as a function of the Ru particle size.

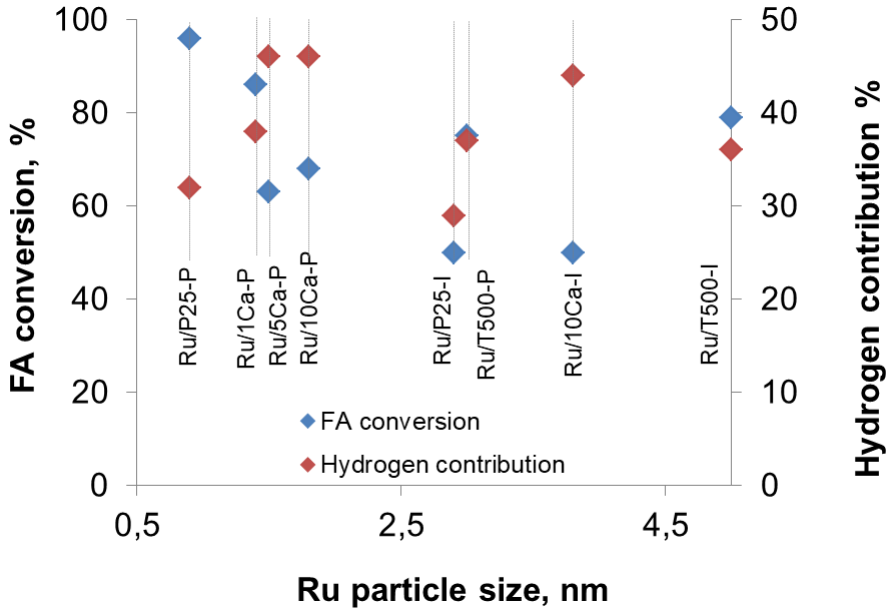

Figure 65. Formic acid conversion and hydrogen selectivity results as a function of Ru particle size.

Therefore the FA conversion and the H_2 selectivity results were plotted against the amount of Ca and presented in Figure 66. As already discussed in Chapter 5.5, several factors are responsible for the improved activity in the FA decomposition reaction, such as smaller metal particles on Ca-modified supports or lower CO adsorption as compared to the Ca-free catalysts. Those aspects were discussed in detail in Chapter 5 as the improved FA conversion was observed in liquid phase.

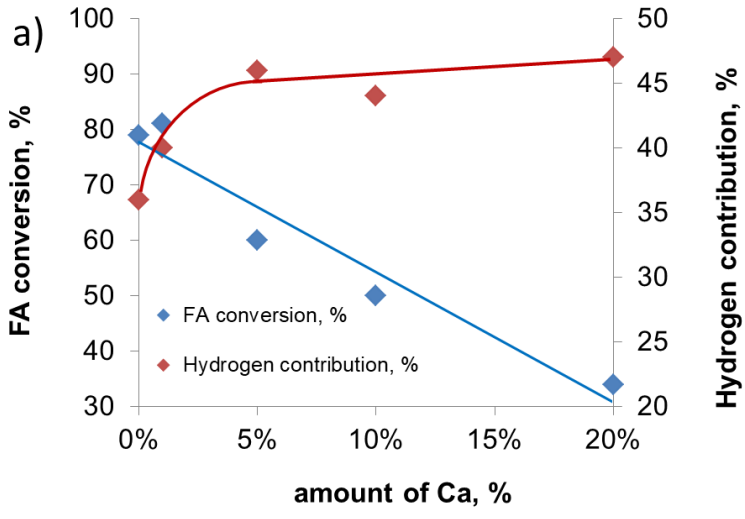

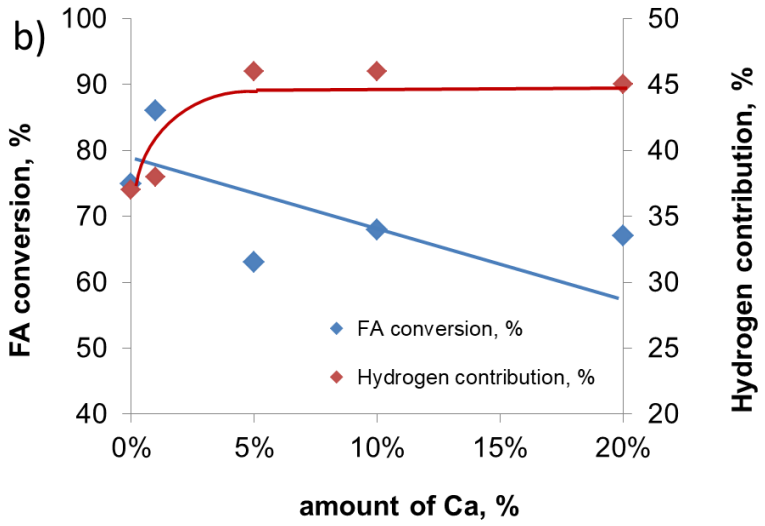

Figure 66. Influence of the Ca content on the FA conversion and the selectivity to H_2 obtained on 5%Ru/TiO_2 catalysts prepared by a) the wet impregnation method and b) the photodeposition method, in gas phase formic acid decomposition at 190°C.

However in this case when the reaction was carried out in as phase, a different trend was observed. Indeed, for a very low Ca content (1%), no clear improvement in the activity was observed on the Ru/1Ca-T500 catalyst (81% vs. 79%), while the improvement was significant when the catalyst was prepared by the photodeposition (85% vs. 75%). Increasing further the amount of Ca in the support, resulted in a decrease in the FA conversion which could be explained as follows.

It can be seen from Figure 61 and Figure 63 that the decomposition of formic acid proceeds *via* two pathways (dehydration and dehydrogenation) since the products of both pathways were recorded. Since non-negligible activity for dehydration pathway was observed on the surface of P25 and T500 (37% and 21%) it can be concluded that the overall activity of Ru catalysts supported on those materials could come from the activity of support itself (towards CO and H_2O) and from Ru active sites. As it was already discussed in a previous paragraph, the addition of Ca^{2+} ions to the support deactivates its activity towards FA dehydration due to the hypothetical blocking the active sites. Therefore the drop in conversion and better selectivity towards H_2 for Ca-modified catalysts could be explained by the fact that the contribution of the dehydration pathway is considerably reduced. Improved selectivity for Ca-based catalysts was also observed for the reaction of FA decomposition in a liquid phase (Chapter 5.4, Figure 55). Indeed, the

improvement of the selectivity towards H_2 production from formic acid using catalysts with basic sites has been observed in the literature. Yadav et al. used gold nanoparticles encapsulated in amine-functionalized silica nanospheres at 90^{o}C and obtained 100% selectivity towards H_2 which they accounted for the strong interactions between amine-functionalized support and the metal.[287]

In addition the basicity of the materials plays crucial role in the improvement of the selectivity. Dehydrogenation of FA is facilitated by the presence of basic sites which act as a proton scavenger in O-H bond cleavage step. [272,273,274]

6.5. Concluding remarks

In this chapter, 5%Ru/TiO_2-based catalysts prepared by wet impregnation and photodeposition methods were tested in the gas phase formic acid decomposition and the influence of the support modification, the Ru particle size and the preparation method was investigated.

First, the bare supports were tested and activity towards formic acid dehydration was observed on the surface of pure TiO_2 materials (P25 and T500), with a direct relationship with the surface area of the support, the higher the specific surface area, the higher the FA dehydration yield. Further, it was shown that modifying the TiO_2 with calcium is an interesting way to suppress the intrinsic activity of the support itself, and therefore to inhibit the formation of CO. This effect was speculated to be attributed to the blocking of the majority of O_{2-} active sites on TiO_2 by calcium.

Further, it was found that the better performance of the Ru catalysts prepared by the photodeposition method was attributed to the smaller Ru nanoparticles compared to the ones obtained on the catalysts prepared by the impregnation. The support modification with 1% of Ca causes an improvement in both the conversion and the selectivity to H_2 mainly at 190^{o}C in the case of both sets of samples. However, further drop in the activity (with simultaneous improvement in selectivity towards H_2) was attributed to the fact that the contribution of the dehydration pathway originating from non-modified TiO_2 is considerably reduced on Ca-based materials.

[287] M.Yadav, T. Akita, N. Tsumoria, Q. Xu, J. Mater. Chem., 2012, 22, 12582

CHAPTER 7

7. CONCLUSIONS AND PERSPECTIVES

The objective of the PhD work consisted in the design of efficient TiO_2 supported Ru (5 wt.%) catalysts for the one-pot combined hydrogenation of levulinic acid towards γ-valerolactone using formic acid as internal source.

Compared to the Ru/TiO_2 reference catalysts traditionally prepared by incipient wet impregnation, **we successfully improved the production of γ-valerolactone by combining two complementary synthetic strategies** playing on both the support material and the supported active phase:

1. **At the support level**, the controlled modification of a TiO_2 sol-gel synthesis by calcium ions resulted in **the formation of a new Ca-modified TiO_2 support**. While it displayed modified bulk and surface properties compared to the pristine TiO_2, it contained intimate association of both $CaTiO_3$ calcium titanate and TiO_2 anatase phases. The TiO_2 anatase is proposed to incorporate Ca ions into the crystal lattice, this latter being proposed to limit the anatase crystallite growth during the synthesis, while the newly formed $CaTiO_3$ calcium titanate phase is all the more evidenced as the Ca content was increasing. In comparison to non-modified TiO_2 support, the Ca-modified TiO_2 support provides the following new features:
   - **This support modification improved the catalytic performance of the Ru-based catalysts** in the combined hydrogenation of levulinic acid towards γ-valerolactone using formic acid as internal hydrogen source. This improvement resulted from enhanced performances in both the formic acid decomposition step and the hydrogenation of levulinic acid independently.
   - Smaller ruthenium particles were stabilized on the support. **Stronger interaction of ruthenium with the support was observed, which affected the strength of CO adsorption** on the surface of the Ca-modified catalyst, thus facilitating the reaction performance.

- Further, the addition of Ca was proposed to result in an increased basicity of the materials due to the presence of coordinatively unsaturated oxygen ions O^{2-}. The presence of basic sites might facilitate the dehydrogenation of formic acid, and improve the hydrogenation step as well by helping in the activation of the carbonyl function.

2. **We developed an elegant low-temperature one step photo-assisted synthesis method** as sustainable alternative to the classical incipient wet impregnation one for synthesizing highly dispersed metal Ru nanoparticles on TiO_2 and Ca-modified TiO_2 supports. This method takes advantage of the redox photoactivity developed by the TiO_2-based supports under solar light. Whether Ru (III) acetylacetonate or Ru (III) chloride hydrate was used as precursors, s**ub-nanometric metallic Ru nanoparticles were successfully synthesized on the support with a sharp (uniform) size distribution**. Far smaller Ru nanoparticles with sharper size distribution were synthesized *via* the photo-assisted synthesis method when compared to the counterpart catalysts prepared *via* incipient wetness impregnation with final thermal reduction in hydrogen.
    - A mechanism of photodeposition was proposed depending on the precursor used, involving the sole photogenerated electrons in the case of the chloride, while both photogenerated holes and electrons would be involved in oxidation and reduction steps in the case of acetylacetonate. In addition, we showed that the chloride precursor had to be preferred to the acetylacetonate one due to strong kinetics limitation in the case of acetyacetonate, and that basic pH have to be maintained for increasing the process kinetics.
    - Further, it was demonstrated that **a fine monitoring of the metal Ru nanoparticle size on the TiO_2 support was possible** *via* a controlled growth of the Ru nanoclusters under irradiation.

Therefore, **the enhancement of the catalytic performances in both separated reactions allowed to enhance as well the production of γ-valerolactone in the one-pot combined reaction** in comparison to those achieved on the counterparts catalysts prepared by classical wet impregnation. **They were further exalted thanks to the controlled support modification *via* the calcium introduction into the titania support**. A volcano-type relationship was obtained with the Ru nanoparticle size, **with a 1.5 nm optimal Ru size**.

When it comes to the decomposition of formic acid in the gas phase, we showed that **modifying the TiO_2 support with calcium was a way to suppress the negative dehydration activity into CO of the support itself**, that would further play against the implementation of TiO_2-based supports in this reaction.

This PhD work opens several perspectives for further studies:

- After having demonstrated the enhanced performances of the Ca-modified TiO_2 supported Ru catalysts compared to the reference Ru/TiO_2 counterparts, the stability aspect of the catalysts should be also addressed and re-usability studies should be performed. This concerns the supported ruthenium nanoparticles as well as the calcium heteroatom introduced to the support. Preliminary results were encouraging, since no ruthenium leaching to the solution was evidenced over the first five runs in the FALA reaction.

- The interest of modifying the TiO_2 support by calcium ions could be extended to other heteroatoms able to be incorporated into the TiO_2 lattice or to form new surface phase with titanium. Preliminary tests with Mg and Ba have been performed. The further replacement of calcium by other elements able to provide the strong interaction with the supported ruthenium metal could be a way to improve the re-use stability of the Ca-modified catalyst, if any. In addition, associating TiO_2 to another support material already used in FALA or in hydrogenation reaction with external hydrogen could be also an elegant way to benefit from the advantage of both support natures in terms of activity, time-stability or resistance to impurities, while

minimizing their intrinsic drawbacks. The flexibility of the sol-gel synthesis is clearly an advantage in this frame.

- Indeed, the behavior of the most efficient catalytic systems should subsequently be evaluated in the presence of impurities in the levulinic acid, and further should be tested on real biomass-feedstocks. In this frame, the combination of new synthetic strategies at both the metal phase and the support material levels is of high importance for getting closer the real operating conditions. Further, it could be interesting to investigate how the catalytic behavior or the catalysts are influenced by the way of implementing the FALA reaction, *i.e.* in a flow mode for the continuous production of γ-valerolactone compared to the discontinuous batch mode used in the present study. This discontinuous mode is of clear interest for industrial purposes.

- In terms of supported metallic phase, it will be interesting to replace monometallic by bimetallic systems, for taking advantage on the versatility of the supported bimetallic catalysts for tuning their properties to a large extent. Both reactivity and adsorption properties of bimetallic particles are different than those of each metal considered separately. This could be also a promising way for lowering the load of noble metals in the catalyst, by substituting part of the noble metal by low cost and abundant non-noble metal element. In this frame, the flexibility of the photo-assisted synthesis method could be also of great help for preparing bi-metallic systems with different structures (core/shell structure, surface alloys, separated nanoparticles, etc…). Especially, such a method has been evidence to provide the possibility to prepare bimetallic nanoparticles with specific properties, since the low temperature does not give the atoms the energy to re-organize for minimizing the surface energy of the particles.

LIST OF PUBLICATIONS AND CONFERENCES:

Publications:

Light-driven synthesis of sub-nanometric metallic Ru catalysts on TiO_2, J. Wojciechowska, E. Gitzhofer, J. Grams, A. M. Ruppert, N. Keller, Catalysis Today, 2018, doi.org/10.1016/j.cattod.2018.07.013

Enhanced production of γ-valerolactone with internal source of hydrogen on Ca-modified TiO_2 supported Ru catalysts, J. Wojciechowska, M. Jędrzejczyk, J. Grams, N. Keller, A. M. Ruppert, ChemSusChem 2018 – https://doi.org/10.1002/cssc.201801974

Solar light induced photon-assisted synthesis of TiO_2 supported highly dispersed Ru nanoparticles catalysts, J. Wojciechowska , E. Gitzhofer , J. Grams , A. Ruppert , N. Keller, Materials 2018 - Submitted

Conferences:

XLVII Polish Conference on Catalysis and Surface Chemistry, flash-oral and poster presentation, *Novel catalysts prepared via the alginate route for the levulinic acid hydrogenation towards biofuel additives*, Krakow, Poland, 16-18.03.2015.

XXXII Meeting of Polish Chemical Society – Student Section, oral presentation, *Nośnik katalizatora – czy to w ogóle istotne?* Dobieszków, Poland, 22-26.04.2015.

III Lodz Symposium of Doctoral Students in Chemistry, poster presentation, *Innowacyjne katalizatory przygotowane z wykorzystaniem alg jako biomasy trzeciej generacji*, Łódź, Poland, 27-28.04.2015.

XLXIX Polish Conference on Catalysis and Surface Chemistry, flash-oral and poster presentation, *High efficiency titania-based catalysts for converting biomass into fuels*, Krakow, Poland, 15-18.04.2017.

Journée Des Doctorants En Chimie, oral presentation, *Light-driven synthesis of sub-nanometric metallic Ru catalysts on TiO_2*, Strasbourg, France, 10.11.2017.

Photocatalytic and Superhydrophilic Surfaces Workshop 2017, oral presentation, *Light-driven synthesis of sub-nanometric metallic Ru catalysts on TiO_2*, Manchester, UK, 7-8.12.2017.

4th International Congress on Catalysis for Biorefineries, Catbior 2017, poster presentation, *High efficiency calcium modified titania-based catalysts for γ-valerolactone formation*, Lyon, France, 11-15.12.2017.